From trees to cloud seeds: Modelling the climate influence of biogenic volatile organic compounds with the Norwegian Earth System Model

Sara Marie Blichner

Dissertation for the degree of Philosophiae Doctor (PhD)

Section for Meteorology and Oceanography

Department of Geosciences

University of Oslo

December 2020

Series of dissertations submitted to the
Faculty of Mathematics and Natural Sciences, University of Oslo
No. 2382

ISSN 1501-7710

Cover: Hanne Baadsgaard Utigard.
Print production: Reprosentralen, University of Oslo.

:Preface

This synthesis and collection of papers are submitted for the degree of pilosophiae doctor (PhD) in atmospheric physics and chemistry at the Section for Meteorology and Oceanography (MetOs), Department of Geosciences, University of Oslo. The work has been conducted in the period from September 2016 until December 2020. The research has been conducted under the supervision of Terje Koren Berntsen (MetOs), Moa Sporre (previously MetOs, now Lund University), Frode Stordal (MetOs), Ander Bryn (Natural History Museum) and Hui Tang (MetOs). The funding for this research is from the interdisciplinary initiative LATICE (Land-ATmosphere Interactions in Cold Environments), which is recognized as a strategic research area by the Faculty of Mathematics and Natural Sciences at the University of Oslo. The thesis consists of a the introduction part (Part I) and a part consisting of the papers listed below (Part II). Part I includes an introduction to the topics covered and summarizes and discusses the research in the thesis. A summary of all four papers, including author contributions, is found in Chapter 4.2.

Paper I Moa K. Sporre, **Sara M. Blichner**, Inger H. H. Karset , Risto Makkonen, and Terje K. Berntsen (2019), "BVOC–aerosol–climate feedbacks investigated using NorESM", Atmospheric Chemistry and Physics, doi:10.5194/acp-19-4763-2019

Paper II: Moa K. Sporre, **Sara M. Blichner**, Roland Schrödner, Inger H. H. Karset, Terje K. Berntsen, Twan van Noije, Tommi Bergman, Declan O'Donnell, and Risto Makkonen (2020), "Large difference in aerosol radiative effects from BVOC-SOA treatment in three Earth system models", Atmospheric Chemistry and Physics, doi:10.5194/acp-20-8953-2020

Paper III: **Sara M. Blichner**, Moa K. Sporre, Risto Makkonen, and Terje K. Berntsen (2020), "Implementing a sectional scheme for early aerosol growth from new particle formation in the Norwegian Earth System Model v2: comparison to observations and climate impacts", Geoscientific Model Development Discussions, doi:doi.org/10.5194/gmd-2020-357

Paper VI: **Sara M. Blichner**, Moa K. Sporre, and Terje K. Berntsen , "Reduced effective radiative forcing from cloud-aerosol interactions (ERF_{aci}) with improved treatment of early aerosol growth in an Earth System Model", Submitted to Atmospheric Chemistry and Physics

:Acknowledgements

First and foremost, I would like to thank all my supervisors for guidance and support: Terje Koren Berntsen for guiding me, letting me go with my own ideas, supporting me even when I get off track and teaching me to block out academic noise and keep my eye on the scientific questions. I feel very privileged to have had you as a supervisor. Moa Sporre for being the best scientific older sister anyone could ask for – writing and working closely with you has been a true highlight of my time as a PhD student. Frode Stordal and Anders Bryn for all the good discussions and support. Hui Tang, for de-mystifying land modelling for me.

Furthermore, I would like to thank Jón Egill Kristjánsson, who was supposed to be my supervisors but who passed away right before I started my PhD. I feel lucky to have gotten to know you, your enthusiasm and support.

I would also like to thank Trude Storelvmo, who, though not formally my advisor, has let me join in her group, made me feel very welcome and has been a great scientific support.

Thanks to LATICE (Land-ATmosphere Interactions in Cold Environments) both for funding me and many excellent interdisciplinary meetings. Thanks to the Kristine Bonnevie scholarship for funding my research stay abroad in Helsinki. Thanks to Risto Makkonen for hosting me at INAR and for many good discussions – some of them sparking the idea for two of the papers in this thesis.

I would also like to thank my colleagues at MetOs: Inger Helene who is much cleverer than me and was my NorESM guru when I started. Tim and Rob both for keeping me sane (sometimes driving me crazy) and scientific discussions and writing help. Thanks to Kine for giving my thesis text a good beating. Also thanks to all the other colleagues and friends at work for the coffee breaks, discussions, encouragement and for generally being great people.

Thanks to my brother Jonas, both for checking my writing and, together with Tanja, feeding and watering me with semi-regular intervals (of course including the conversation that often comes with that). Thanks also to the rest of my family for all the encouragement and support.

Special thanks to Eirik and also great thanks to Ingrid, Anna, Ida, Andrea, Ingvild, Mikkel, Olga, Fede, Jon, Vera and many more. I highly suspect I would have failed at everything were it not for these people. A huge thanks to Diego for being the best support team anyone could ask for.

Oslo, December 2020
Sara Marie Blichner

Contents

Part I

Thesis

Chapter 1

:Introduction

1.1 Motivation

Changes in the climate system originate from a complicated interplay between a myriad of factors: green house gas emissions, solar activity, volcanic activity, the Milankovitch cycles, changes in vegetation and tiny invisible particles in the air are just some. Lately though, the most important ones can be traced back to intelligent lifeforms within the climate system itself.

The various factors influencing the climate system are difficult to dissect – cause and effect are easily confused in a system with many co-existing factors and strong feedback mechanisms[1]. If we are to draw conclusions about how much temperature change to expect from human activities like greenhouse gas emissions, we must be able to separate other radiative forcing [2] agents that have affected the climate during the historical period. The largest contribution to the anthropogenic radiative forcing, apart from green house gases, originate from changes in aerosols and aerosol pre-cursors, particularly through the interactions with clouds (*Boucher et al.*, 2013).

A cloud droplet in the atmosphere will always form around a pre-existing aerosol. The consequence of this is that the number and qualities of particles in the atmosphere will strongly influence the number of cloud droplets a cloud contains, and therefore how reflective the cloud is – a cloud with more numerous, but smaller droplets will have more surface area and thus also be whiter/have higher albedo (*Twomey*, 1974). Aerosols may also affect the lifetime of clouds , e.g. by suppressing the precipitation (*Albrecht*, 1989). Since the industrial revolution, sulphur emissions have greatly increased, leading to more reflective and therefore cooling clouds, through such mechanisms. However, the radiative forcing from aerosols is very uncertain – in fact it is the main contributor to the overall uncertainty in anthropogenic radiative forcing during the historical period. An important reason why this forcing is so uncertain, is that the effect of the anthropogenic perturbation of the aerosols and thus the clouds, is highly dependent on what the atmosphere was like in pre-industrial times. In an atmosphere with many particles that cloud droplets can form around, adding more aerosol will not

[1] A climate feedback is a mechanism which is initiated by a temperature change and ends up enhancing (positive) or dampening (negative) the initial temperature change

[2] A radiative forcing is a perturbation of the earth system, e.g. the increase in CO_2 concentrations, which changes the radiative balance at the top of the atmosphere, either trapping more energy within the system or letting more energy escape to space.

make much difference to the clouds. However, in a very clean atmosphere, adding more aerosols will have a very large impact on the reflectivity of the clouds (see Chapter 2.4). The cloud response to added aerosol is thus highly non-linear (*Twomey*, 1991).

In other words, we must improve our understanding of natural aerosol in the pre-industrial environment to improve estimates of the aerosol radiative forcing. Since we cannot measure the pre-industrial atmosphere, the best option is to put our knowledge of aerosol processes and emissions into models.

Biogenic volatile organic compounds (BVOCs) are one important source of such natural aerosols. These are gas species which are emitted from vegetation and through oxidization produce vapors that may condense and form aerosol. Despite their importance, there are still substantial uncertainties in terms of emissions, how much aerosol is formed and their properties, both in the past, present and future.

BVOCs are important both because they impact the pre-industrial aerosol state, and because their emissions have changed over time and will change in the future. Though not the focus in this thesis, BVOCs also play an important part in the atmospheric chemistry in general and, more specifically, in the formation of ozone (e.g. *Heald and Geddes*, 2016; *Scott et al.*, 2017; *Unger*, 2014a). BVOC emissions change both due to land use change, e.g. deforestation, and because the emissions are highly dependent on temperature and other environmental factors like CO_2 concentrations,radiation, soil moisture and different kinds of stress on the plant. The dependency on temperature in particular, gives rise to BVOC related climate feedbacks. A climate feedback is a process that dampens or enhances a temperature change. An example of such a BVOC feedback is the following: if the temperature increases, then the BVOC missions increase. This leads to more aerosol forming. The added aerosol cool the surface due to their effect on radiation directly and their effect on the reflectivity of the clouds. This dampens the initial temperature change.

Over recent years, much progress has been made in our understanding of the climatic effects of BVOCs, especially regarding the contribution their oxidation products can have on the formation of new particles in the atmosphere (*Bianchi et al.*, 2016; *Gordon et al.*, 2016; *Kirkby et al.*, 2016; *Riccobono et al.*, 2014; *Riipinen et al.*, 2011; *Tröstl et al.*, 2016). This is important because the cloud–albedo effect mentioned above is dependent on the *number* of particles which droplets can form around – the number of cloud condensation nuclei (CCN). If the formation of new particles is very low without anthropogenic emissions, then as a consequence, the pre-industrial atmosphere will have had very few CCN. If oxidation products from BVOCs can contribute significantly to new particle formation alone, then there will have been much more CCN in the pre-industrial atmosphere (see e.g. *Riccobono et al.*, 2014; *Scott et al.*, 2014). As mentioned above, this would result in a large impact from adding anthropogenic aerosols and thus a large cooling effect.

The effect that BVOCs have on new particle formation (NPF) depends on what kind of oxidation products the BVOCs form in the atmosphere. Some products have very low volatility, while others are so-called semi-volatile and yet another subset has properties that will stabilize and enhance the formation of new tiny clusters in the atmosphere. NPF has two barriers: 1) the formation of a tiny critical cluster which can grow spontaneously in the atmosphere, and 2) the survival of these particles as they grow by condensation and are scavenged by coagulation with larger particles. Organic vapors can contribute to both steps, but in this thesis we have focused mainly on the

contribution to the early growth. Due to the Kelvin effect, only the oxidation products with very low volatility will contribute to the early growth of particles: The Kelvin effect is that the equilibrium vapor pressure with respect to a surface is dependent on the curvature of the surface, such that the vapor pressure needed to sustain a small aerosol is higher than the vapor pressure needed to sustain a larger particle.

Modelling aerosols involves modelling particles on a scale from nanometers (0.000 001 mm) to approximately 10 micrometers (0.01 mm) within a model which has a grid, in the case of many climate models, on the scale of kilometers. In climate models, this is usually done by using some number of log-normal modes to represent the size distribution of the aerosols. Sectional schemes on the other hand, where the distribution is represented by bins, are usually computationally too expensive for climate models, but are considered closer to first principles because they do not assume a shape to the size distribution.

The focus of this thesis is to improve understanding of the climate impacts of BVOCs through working with the Norwegian Earth System Model (NorESM). Earth System Models (ESMs) are global climate models which include as many climate relevant interactions as possible (*Flato et al.*, 2013). To be useful, these models must be able to simulate hundreds or even thousands of years with reasonable computing resources, and computational efficiency is therefore necessary. This means that we have to make efforts to simplify the processes represented in the models, but not make them so simple that they loose relevance or fail to capture important features.

1.2 Objectives and scope

Overall the goal of this work is to **improve modelling and understanding how BVOC emissions impact climate, especially focusing on the formation and early growth of new particles in the atmosphere.** Throughout the thesis, NorESM is applied and developed for this purpose. The overall objective of the thesis is met by addressing a series of sub objectives.

- Assess the strength of the BVOC feedbacks through temperature and CO_2 changes with NorESM (*Sporre et al.*, 2019)
  - Technical development: Develop method for assessing the BVOC feedback strength.
- Unveil and discuss uncertainties in BVOC-to-aerosol modelling by comparing differences and sensitivities in thee current state-of-the-art ESMs (*Sporre et al.*, 2020).
- Improve the understanding of how formation of new particles in the atmosphere influences climate and radiative forcing (*Blichner et al.*, 2020a,b)
- Improve the understanding of how new particle formation and early growth influences cloud condensation nuclei and the activation of aerosols in clouds (*Blichner et al.*, 2020a)
  - Technical development: Develop and evaluate a sectional scheme for treating the early stages of particle growth in NorESM (*Blichner et al.*, 2020a)

  - Technical development: Improve the coagulation sink for newly formed particles in NorESM (*Sporre et al.*, 2019)

- Improve the understanding of the effect of the organics through early growth

- Quantify the effect of implementing a sectional scheme for early particle growth on ERF_{aci} (*Blichner et al.*, 2020b, submitted to ACP)

Paper I presents an investigation into the strength of the BVOC feedbacks through the formation of aerosols, also including the effect of increased CO_2 concentrations. We find both to be considerable. In Paper II we investigated the uncertainty in modelling secondary organic aerosol (SOA) in ESMs through comparing a series of sensitivity tests for 3 different ESMs. The study demonstrated that the ESMs respond very differently to perturbations depending on their particle size distribution and the balance between contributing to the formation of new particles and the growth of the pre-existing ones. Through the work on the first two papers, it became clear that NorESM has a much coarser treatment of newly formed particles than many other ESMs. Where the other ESMs have nucleation modes (from 3 or 5 nm in diameter) which treat the growth of newly formed particles explicitly, NorESM skips this size range and puts the particles directly into a mode with number median diameter 23.6 nm. This growth takes hours to days in most atmospheric conditions, while it is parameterized in one time step (0.5 hours) in NorESM. Thus the aerosol scheme in NorESM omits potentially important factors, like atmospheric transport, mixing and changes to the aerosol and chemistry. This has been shown to lead to overestimation of particle formation rates (*Lee et al.*, 2013; *Olenius and Riipinen*, 2017). Furthermore, parameterizing the growth as done in NorESM does not allow for representing the fact that growth by organics is dependent on both volatility of the species and particle size: some organic species will condense on even the smallest particles due to their extremely low volatility, while others will only condense on the larger particles due to the Kelvin effect. These factors motivated the model development which constitutes a major part of the work in this thesis: the implementation of a sectional scheme to treat the early growth of particles which thereafter inputs the grown particles into the pre-existing modal scheme. We chose a sectional scheme because it represents the growth and coagulation of the growing particles with higher resolution and without a priori assuming a shape to the distribution. The major draw back of a sectional scheme versus a modal scheme is the increase in computational cost. However, when implementing the sectional scheme only for the smallest particles, this limits the cost due to the limiting of the number of bins (we use 5 or less), and the number of condensing species we need to track (currently 2). This means that we can add precision in this range, while limiting the increase in computational cost.

In Paper III, we find that the new scheme improves the aerosol concentrations with diameter above 50 nm compared to observations and find that the scheme reduces the number of particles in polluted regions while increasing the number of particles in the remote regions and that it increases the role of SOA in early growth of particles. In Paper IV, motivated by these results, we compare the estimated aerosol cooling from pre-industrial to present day with the new scheme and the old scheme and find a significant reduction in the estimated cooling.

Because of the large number of open questions and fast development within the field of biogenic secondary organic aerosol, there are many questions that this thesis could potentially have covered. The chemistry of SOA formation, SOA volatility, ion induced biogenic nucleation and are just some. Some of these factors require a different model setup than NorESM currently has in order to investigate, and sometimes a setup that would be challenging to implement in the framework of an ESM due to the added computational cost. I have therefore rather focused on applying and investigating uncertanties in the default model version and then developing the feature which seemed to hold the most potential for improvement, namely the early growth of particles.

1.3 Thesis outline

In Chapter 2, I present an overview over the relevant scientific background needed to understand the scientific work in this thesis. In Chapter 3, I will describe the NorESM model and further the sectional scheme for early growth developed in this thesis. Thereafter in Chapter 4 I, summarize the scientific findings from each of the four papers and relate these to the objectives listed above. Finally in Chapter 5, I discuss the results and potential further research. Part II of the thesis contains the scientific papers.

Chapter 2

:Background

This chapter presents an overview of the scientific background for the work in this thesis, and attempts to put the work in context. Since the range of topics touched upon in this thesis are quite wide, it is not possible to go into detail on all topics, so my objective will be to introduce the most important concepts and questions. I start by separating radiative forcing from feedback in Chapter 2.1, before introducing the most important processes and concepts concerning atmospheric aerosols in Chapter 2.2. In Chapter 2.3, I discuss the influence of BVOCs on climate, focusing on the formation of secondary organic aerosol. In Chapter 2.4, I cover cloud aerosol interactions, which play an important part in the thesis. Finally, I discuss earth system modelling (Chapter 2.5) and aerosol modelling (Chapter 2.6).

2.1 Forcing and feedback

In analyzing changes to the climate system, we usually distinguish between radiative forcing and feedback mechanisms. A radiative forcing is a human or naturally induced change to the top of the atmosphere radiative balance (*Myhre et al.*, 2013), usually expressed in Wm^{-2}. It is calculated as the radiative effect of the change in a forcing agent over some time period, normally from the pre-industrial atmosphere (year 1750 or 1850) to present day (*Myhre et al.*, 2013). An example of a forcing is the effect of changes in atmospheric concentrations of CO_2 since pre-industrial times, which is estimated to be approximately $1.7\,\mathrm{Wm}^{-2}$ (*Myhre et al.*, 2013). A climate feedback on the other hand, is a process that is initiated by a temperature change in itself and which either enhances (positive feedback) or suppresses (negative feedback) the initial temperature change. An example of a climate feedback mechanism is the effect of increasing temperatures on sea ice: when the temperature increases, sea ice melts and thus the dark ocean surface absorbs more incoming radiation from the sun than would the bright sea ice. This further increases the initial temperature increase and is therefore a positive feedback.

The net radiative balance R of the atmosphere when a radiative forcing F is introduced, can be expressed as

$$R = F - \alpha \Delta T \tag{2.1}$$

where α is the feedback parameter and ΔT is the change in surface temperature (*Gregory et al.*, 2004), assuming the feedback parameter of the system to be invariant. The

final equilibrium response to a forcing can then be calculated by setting $R = 0$,

$$\Delta T = \frac{F}{\alpha}. \tag{2.2}$$

Note that this equation is a simplification, since it is known that the feedback parameter is in fact not invariant to the forcing agent or even to the size of the temperature change (e.g. *Bjordal et al.*, 2020). It is however, a useful simplification and is widely used for comparing the strengths of different feedbacks and forcings on a global scale.

Different radiative forcing agents will entail different short timescale changes to the troposphere, which may either enhance or suppress the initial radiative perturbation – so called rapid adjustments. Rapid adjustment includes all changes in the atmospheric column caused by the forcing agent, except the change in surface temperature. For example, increasing emissions of absorbing aerosols will change the temperature profile of the troposphere and hence the stability which may further change cloud formation etc (*Myhre et al.*, 2013). Perturbing another forcing agent, CO_2 for example, will not have the same effect. Therefore, the concept of effective radiative forcing (ERF) is introduced, which includes these rapid adjustments in the troposphere, but excludes or limits changes to the surface temperature (*Myhre et al.*, 2013). In a climate model, ERF is often estimated by keeping the sea surface temperatures fixed and calculating the top of the atmosphere energy balance with and without the perturbation of the forcing agent (*Hansen et al.*, 2005). This is the method used to calculate ERF in this thesis. Other methods for estimating ERF, include the *Gregory et al.* (2004) method.

2.2 Aerosol

By definition, an aerosol is a tiny solid particle or liquid droplet suspended in the air. We distinguish between anthropogenic and natural aerosol dependent on whether the emission of the particles is caused by human activities or not. Two common examples of natural aerosol are dust and sea salt particles, which would be emitted whether humans existed or not. An example of a very important anthropogenic aerosol is sulphate aerosol originating from industry emissions of SO_2.

We further distinguish between primary and secondary aerosol. Primary aerosols are emitted into the atmosphere as fully formed particles, while secondary aerosol originate from precursor gases which undergo chemical reactions before condensing and forming aerosol in the atmosphere (*Boucher et al.*, 2013). Examples of primary aerosol are mineral dust, sea salt particles and primary organic aerosol (*Boucher et al.*, 2013). An example of secondary aerosol is again sulphate, of which most originates from emitted SO_2, which is oxidized in the atmosphere by OH or forms within cloud droplets by reactions with O_3 or H_2O_2(chapter 6.13 and 7.5 *Seinfeld and Pandis*, 2016). Another important secondary aerosol species which will be discussed in detail in Chapter 2.3.2, is secondary organic aerosol originating from BVOCs.

Though water droplets in the atmosphere formally fall inside the definition of aerosols, they are usually referred to as cloud droplets once the particle has activated with respect to water.

Aerosols play a role in the climate system due to their interaction with radiation, either directly by absorbing or scattering short wave radiation, or indirectly through interacting with clouds (see Chapter 2.4) (*Boucher et al.*, 2013; *Twomey*, 1991). This

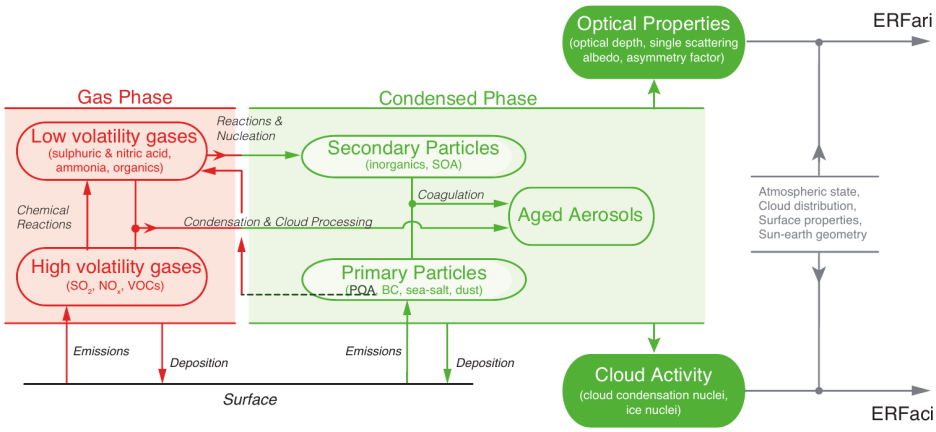

Figure 2.1: *Illustration of climate impacts through changes in aerosol and aerosol precursor emissions. Figure 7.12 from Boucher et al. (2013).*

is illustrated in Figure 2.1, showing a schematic of aerosol proesses and their impact on climate. These interactions are highly dependent on the size and properties of the aerosols. Particles that are comparable in size to incoming solar radiation (380 to 750 nm), can scatter incoming radiation efficiently and by this act to cool the surface by reflecting short wave radiation back to space. On the other hand, some aerosol species will absorb incoming radiation and in this way affect the radiative forcing directly, and furthermore indirectly, through effects on clouds and precipitation (*Samset et al.*, 2018). Furthermore, hygroscopic aerosols influence clouds and their properties through acting as cloud condensation nuclei (CCN) – i.e. particles around which a cloud droplet can form (see Chapter 2.4). Depending on the environment (clean or polluted, high or low updraft velocity), the particles can become relevant as CCN from around 50 nm. Finally, some species may act as ice nuclei and contribute to ice formation and subsequent precipitation in supercooled clouds (*Boucher et al.*, 2013). In this thesis, the main focus will be on the cloud aerosol interactions in warm clouds, through acting as CCN.

2.2.1 Aerosol dynamics

Aerosols exist and interact over a wide diameter size range, approximately from 1 nm to 10 μm. In terms of mass or volume, the range is even wider, spanning 12 orders of magnitude. A typical example of the size distribution of an atmospheric aerosol population is illustrated in Figure 2.2. The size distribution will change over time.In addition to changing due to primary emissions and various loss processes, the size distribution is altered by (1) condensation/evaporation of low or semi-volatile species onto the existing particles, thus increasing their diameter, (2) coagulation between particles in the size distribution and (3) new particle formation (NPF) in the atmosphere. The importance and relevance of each process will vary in different size ranges.

Loss process: wet and dry deposition

Aerosols mass is removed from the atmosphere by dry or wet deposition. Dry deposition refers to when particles depose directly on the earth surface. This loss process

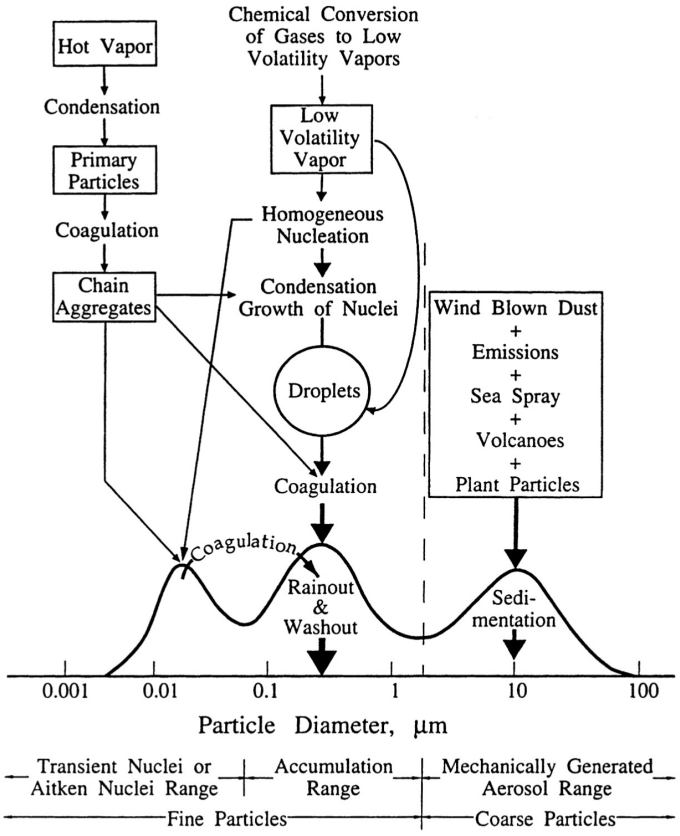

Figure 2.2: *Illustration of a typical aerosol number distribution with the main processes for each size included. Source: Seinfeld and Pandis (Figure 2.7 2016).*

is more efficient for larger particles both due to gravitational settling and because their inertia makes it easier to cross the airflow streamlines and thus the barrier of the quasilaminar sublayer right above the surface (millimeters in thickness). On the other hand, the ultrafine particles (below 100 nm) are more affected by brownian motion, which also improves the efficiency by which they cross the quasilaminar sublayer and depose on the surface (ch. 19 *Seinfeld and Pandis*, 2016). Thus dry deposition is most efficient for the largest and the smallest particles.

Wet deposition refers to when particles are scavenged by cloud, rain, fog or snow and removed from the atmosphere via precipitation (ch. 20 *Seinfeld and Pandis*, 2016). We distinguish between nucleation scavenging, when particles act as CCN for cloud droplets, and in-cloud or below-cloud scavenging. Following a similar logic as for dry deposition, below cloud scavenging is most efficient for larger particles and for the smallest particles. This leaves a minima for both dry deposition and below-cloud wet deposition around 0.1 μm–1 μm and originating the name accumulation mode particles (see Figure 2.2).

Condensation

Condensation or evaporation onto an aerosol particle is driven by the difference between the vapor pressure of the condensing species, p_i, and the equilibrium vapor pressure of the same species above the surface of the aerosol, $p_{eq,i}$. The mass flux of a

species i onto a particle with diameter D_p, must be described differently dependent on how large the diameter of the particle is compared to the mean free path of the condensing vapor molecules, λ. This ratio, $K_n = 2\lambda/D_p$, is called the Knudsen number. There are three regimes,

- the continuum regime, where the particle is large enough that the surrounding air can be treated as a continuum because the particle is much larger than λ ($K_n \sim 0$)
- the kinetic regime, where the particle is so small that the molecules colliding with it must be treated discrete because the particle is much smaller than λ ($K_n \gg 1$)
- the transition regime between the two above ($K_n \sim 1$)

The mass flux of species i onto a particle with diameter D_p can usually be described well by

$$\frac{dm}{dt} = \frac{2\pi D_p D_i M_i}{RT} f(K_n, \alpha)(p_i - p_{eq,i}) \tag{2.3}$$

(eq. 13.3, *Seinfeld and Pandis*, 2016), where D_i is the diffusion coefficient of species i, M_i is its molecular weight and $f(Kn, \alpha)$ is a correction factor due to non–continuum effects and surface accommodation factors (α is the mass accommodation coefficient). The equilibrium vapor pressure, $p_{eq,i}$, will depend on the diameter of the particle due to the Kelvin effect (see Chapter 2.4) (*Seinfeld and Pandis*, 2016). For very low- or non-volatile species, however, it is reasonable to neglect the Kelvin effect. Then for the continuum regime, since $K_n = 0$, we may assume that $f(K_n, \alpha)$ is constant. Thus, we can use that $\frac{dD_p}{dt} \propto \frac{1}{D_p^2}\frac{dm}{dt}$ to show that eq. 2.3 show that small particles will grow faster in diameter than larger particle, because $\frac{dD_p}{dt} \propto \frac{1}{D_p}$. In the kinetic regime, $f(Kn, \alpha)$ will be approximately proportional to $1/K_n \propto D_p$, meaning that in total the growth rate of the particle is independent of size. However, for the very smallest particles, typically sub-10 nm, some assumptions used to derive the equation above break down: 1) the assumption that the condensing vapor molecules have negligible size compared to the particle and 2) the assumption that the particles mobility can be neglected compared to the vapour molecule (see e.g. *Nieminen et al.*, 2010). If these are taken into account, it can be shown that the the growth rate again decreases with the diameter of the particle (*Nieminen et al.*, 2010).

Coagulation

While condensation is adding mass to the aerosol population, but conserving the number of particles, coagulation is reducing the number but conserving mass. Coagulation efficiency between particles of different sizes is described by a coagulation coefficient, K_{12}, which describes how likely these two particles are to collide and stick together (sec. 13.3 *Seinfeld and Pandis*, 2016). The frequency of which the coagulation happens, can then be expressed as $K_{12}N_1N_2$ (*Seinfeld and Pandis*, 2016). Coefficients are in general much higher for large particles coagulating with small particles, than for particles of the same size. This is due to the combination of the large particle providing a large surface area target for the small particle, while the small particle moves faster (Brownian motion) and is thus more likely to hit the target.

New particle formation (NPF)

New particle formation is the clustering and nucleation (at around 1–3 nm) of low volatile vapors and the subsequent early growth of these particles in the atmosphere up to a reasonable size (e.g. 10 nm). Figure 2.3 shows a schematic of this process. Even though the scientific understanding of NPF has greatly improved over recent years, much due to advances in measurement techniques, there is still a lot of uncertainty about the species involved in NPF, when it is likely to occur and what factors are most important. Observed NPF mechanisms in one environment are not necessarily transferable to a different environment which makes the modelling of NPF on a global scale, challenging (*Kerminen et al.*, 2018).

Sulphuric acid is known to be the most important species for nucleation in most environments due to its low vapor pressure, while stabilizing bases such as ammonia and amines may greatly enhance the nucleation rate (*Semeniuk and Dastoor*, 2018). Furthermore, very low volatility organics or highly oxygenated organic molecules (HOMs) make substantial contributions to nucleation – both alone (pure biogenic nucleation) and in combination with sulphuric acid (*Bianchi et al.*, 2016; *Dunne et al.*, 2016; *Gordon et al.*, 2016; *Kirkby et al.*, 2016; *Paasonen et al.*, 2010; *Riccobono et al.*, 2014). Ion-induced nucleation may play a role, especially in the free troposphere and is of particular importance for pure biogenic nucleation (*Kirkby et al.*, 2016; *Semeniuk and Dastoor*, 2018). Assessing the importance of organics for nucleation rates, either in the pre-industrial or the present day atmosphere, is made difficult due to the complex chemistry involved in the production HOMs and other low volatile products and their dependence on the atmospheric composition and state (see Chapter 2.3.1) (*Heinritzi et al.*, 2020; *McFiggans et al.*, 2019; *Yan et al.*, 2020).

Because the coagulation sink is very high for the smallest particles, the newly formed particles will quickly be lost if they do not grow fast enough to larger sizes (where the coagulation sink is lower) (*Kerminen et al.*, 2018; *Yli-Juuti et al.*, 2020). This makes early particle growth an equally important phase as nucleation, when considering the potential impacts on climate through the formation of CCN from NPF (see e.g. *Riipinen et al.*, 2011; *Semeniuk and Dastoor*, 2018). In this stage of NPF, organics contribute significantly and often dominate the mass growth (*Yli-Juuti et al.*, 2020). We will discuss this further in Chapter 2.3.2. Figure 2.3 shows a schematic of the process.

The formation of new particles is quite tightly constrained by negative feedbacks. For one, if NPF is high, this results in an increase in surface area for condensation, thus decreasing the concentration of the vapors responsible for nucleation. Secondly, high NPF will lead to higher coagulation sink for the newly forming particles, thus limiting the fraction that survive to larger sizes. The result is a suppression of further NPF (*Carslaw et al.*, 2013a; *Kerminen et al.*, 2018; *Schutgens and Stier*, 2014; *Semeniuk and Dastoor*, 2018; *Westervelt et al.*, 2013, 2014, etc.). Some model studies have shown a stronger sensitivity to model changes which affect the loss of newly formed particles through coagulation sink, than to the actual nucleation parameterization in itself (*Carslaw et al.*, 2013a,b).

Other potentially important aerosol processes include cloud processing, which is changes to the aerosol in a cloud droplet before re-evaporation and release of the aerosol, and chemical aging which changes the chemical properties of the aerosol (*Se-*

infeld and Pandis, 2016). These are important, but fall outside of the scope of this thesis.

2.3 Vegetation aerosol interactions: Biogenic volatile organic compounds and secondary organic aerosol

Biogenic volatile organic compound (BVOCs) are emitted by all vegetation and constitute a large flux of reactive carbon from the biosphere to the atmosphere, rivaling methane in size (*Heald and Spracklen*, 2015). The most important compounds in terms of emitted mass are isoprene, monoterpene and sesquiterpenes (*Kulmala et al.*, 2013). Once in the atmosphere, they are quickly oxidized and can influence the climate through both through chemistry, influencing the ozone production and the methane lifetime – and through producing secondary organic aerosol (SOA) (*Glasius and Goldstein*, 2016; *Heald and Spracklen*, 2015; *Peñuelas and Staudt*, 2010). In fact, most of the SOA on a global scale is believed to originate from BVOCs, although anthropogenic emissions can be equally important in some regions (*Boucher et al.*, 2013). Since this thesis does not consider the chemical implications of changing BVOC emissions, we will focus here on the climate effects of BVOCs through the formation of SOA.

Because BVOC emissions can change both due to land use change and altered environmental factors (temperature, radiation etc.) (*Peñuelas and Staudt*, 2010), they will both initiate climate forcings and climate feedback mechanisms (*Kulmala et al.*, 2004; *Makkonen et al.*, 2012; *Paasonen et al.*, 2013; *Rap et al.*, 2018; *Scott et al.*, 2014, 2018a; *Sporre et al.*, 2019). Changes in emissions can result from the direct effect of environmental factors on the plant, but also from the effects that these factors have through the change in gross primary production (GPP) and thus leaf area index (LAI). E.g. CO_2 is known to inhibit isoprene emissions (*Arneth et al.*, 2007) directly, but through CO_2 fertilization it may increase the density of the vegetation and LAI which increases emissions (*Peñuelas and Staudt*, 2010).

The IPCC special report on Climate Change and Land (*Jia et al.*, 2019) assess with low confidence that the land use change since pre-industrial time has exerted a positive aerosol forcing through decrease in BVOC emissions. This uncertainty originates from both large uncertainty in the past and future emissions of BVOCs (*Makkonen et al.*, 2012) and on the uncertainty in processes after emission: oxidation mechanisms, SOA yields, volatility and hygroscopicity of the products (*Heald and Spracklen*, 2015). *Scott et al.* (2014) show that the radiative effect exerted by biogenic SOA (BSOA) has a high dependency on the extent to which the organic oxidation products participate in forming new particles and how early in the particle growth they can contribute. In their simulations, the radiative effect of cloud albedo changes from BVOCs was $-0.12\,\mathrm{W\,m^{-2}}$, but this was strengthened to between $-0.22\,\mathrm{W\,m^{-2}}$ and $-0.77\,\mathrm{W\,m^{-2}}$ when they included organics in the the formation of the smallest particles (the nucleation rate). *Unger* (2014a) use another model and find the cloud aerosol radiative effect from BVOCs to be $-0.17\,\mathrm{Wm^{-2}}$.

2.3.1 Oxidation and yields

BVOCs have a short lifetime in the atmosphere ($\sim$ 1.5 hour or less) and are quickly oxidized, mainly by OH, O_3 and NO_3 (*Shrivastava et al.*, 2017). While isoprene is more abundant in the atmosphere than monoterpenes, monoterpenes tend to have higher SOA yields with lower volatilities, especially from reactions with ozone (*Ehn et al.*, 2014; *Jokinen et al.*, 2015). However, laboratory experiments often calculate yields with mixing only e.g. two vapors, and the yields of low volatility products from ozonolysis of monoterpenes can be significantly reduced by the presence of isoprene in the mix (*Heinritzi et al.*, 2020; *McFiggans et al.*, 2019).

Due to BVOCs short lifetime, uncertainties in SOA yields in models may arise not only from uncertainties concerning the chemical oxidation pathways, but also due to anti-correlations in BVOCs and oxidants on a sub-grid level (*Shrivastava et al.*, 2017) The concentration of nitrogen oxides (NO_x) are also known to affect the yields (*Shrivastava et al.*, 2017) either positively or negatively depending on the environment. Most of the factors mentioned above are not considered in Earth System Models, which more often than not represent the yields as fixed numbers for each reaction (see e.g. *Sporre et al.*, 2020).

2.3.2 Participation in NPF and early growth

As mentioned above, organic vapors, especially originating from BVOCs, have been shown to be important both for nucleation and particularly for the subsequent early growth of particles. Figure 2.3 shows a schematic of the process of NPF and where contributions from organic vapors factor in (*Shrivastava et al.*, 2017). It was previously thought that organics would only play a role in nucleation by acting as a stabilizer for sulphuric acid, (*Riccobono et al.*, 2014; *Zhang et al.*, 2012). In recent years, evidence of so called "pure" biogenic nucleation driven by HOMs, has emerged (*Bianchi et al.*, 2016; *Kirkby et al.*, 2016) and it has been hypothesised that this could be a major source of particles in a cleaner pre-industrial atmosphere (*Gordon et al.*, 2016, 2017). In fact, *Gordon et al.* (2016) find that including this nucleation pathway in their model, results in a 27 % reduction in cloud albedo forcing.

During the early stages of growth of newly formed particles, only gases with extremely low volatilities can participate, due to a strong Kelvin effect (*Kerminen et al.*, 2018). As the particle grows larger, the coagulation sink is reduced, and the growth rate may increase due to the contribution of less volatile vapours (*Ehn et al.*, 2014). There has been much research over the past years on the role of oxidation products from BVOCs in early growth (*Ehn et al.*, 2014; *Jokinen et al.*, 2015; *Mohr et al.*, 2019; *Riipinen et al.*, 2011; *Stolzenburg et al.*, 2018; *Tröstl et al.*, 2016). While there is still a great deal of uncertainty about the yield (*Shrivastava et al.*, 2017), there is strong evidence that organics do play a very important role in growing the particles, especially in pristine environments (*Mohr et al.*, 2019; *Yli-Juuti et al.*, 2020).

2.3.3 The role of biogenic SOA in forcing

BVOC emissions and subsequent SOA formation are important for the aerosol forcing uncertainty for two main reasons:

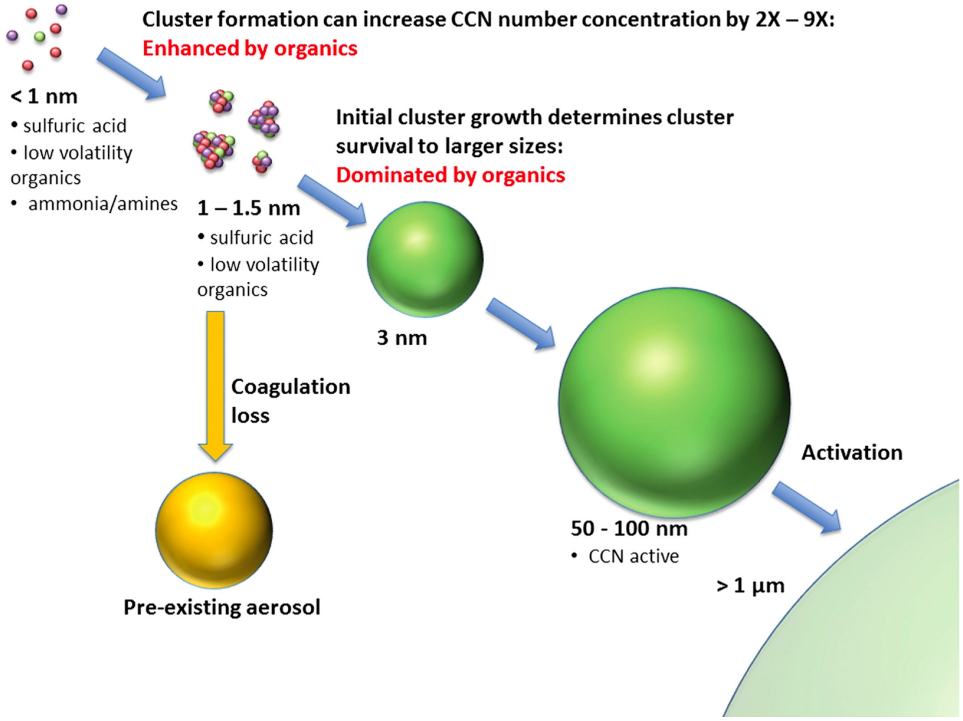

Figure 2.3: *Schematic showing the governing processes of NPF and the formation of CCN. Source: Shrivastava et al. (2017).*

(1) As mentioned above, the emissions of BVOCs change due to land use change and changes in CO_2 and thus emissions have changed in the past and will change in the future. Note that emissions in BVOC also change due to temperature and climate change, but these changes falls under feedbacks, which is covered in the next section. The direct radiative forcing due to changes in biogenic SOA changes from land use change has been estimated in some model studies to be positive and 0.017–0.09 Wm^{-2} (*Heald and Geddes*, 2016; *Scott et al.*, 2017; *Unger*, 2014b). However, *Unger* (2014a) get a negative value of $-0.12\,\mathrm{Wm}^{-2}$ when she includes the effect of changing anthropogenic emissions, meaning that the co-emission of BVOCs with anthropogenic emissions enhances the negative radiative effect of BSOA, even when emissions are reduced. These studies, however, do not include the effect of CO_2 fertilization which could be considered a forcing in the same way as land use change.

(2) BVOCs are natural emissions, meaning that they constitute part of the pre-industrial aerosol "base state". Since aerosol-cloud interactions are highly nonlinear, this base state has a large impact on the estimated forcing from anthropogenic aerosol (*Carslaw et al.*, 2013b). Firstly, the effect of adding CCN is dependent on whether or not these CCN actually end up activating and forming cloud droplets. When there are many CCN, the maximum supersaturation may decrease due to supersaturation adjustment (see Chapter 2.4) and thus a lower fraction of the added CCN will activate. Secondly, the cloud albedo, A, changes with the cloud droplet number concentration (CDNC), roughly as $dA/dCDNC = A(1-A)/(3CDNC)$, meaning that the higher the baseline CDNC is, the lower the increase in albedo will be *Carslaw et al.* (2013b); *Twomey* (1991). In conclusion, the extent to which oxidation products of BVOC participate in the production of pre-industrial CCN, has a large impact on the estimated radiative forcing. An illustration of this is the previously mentioned study

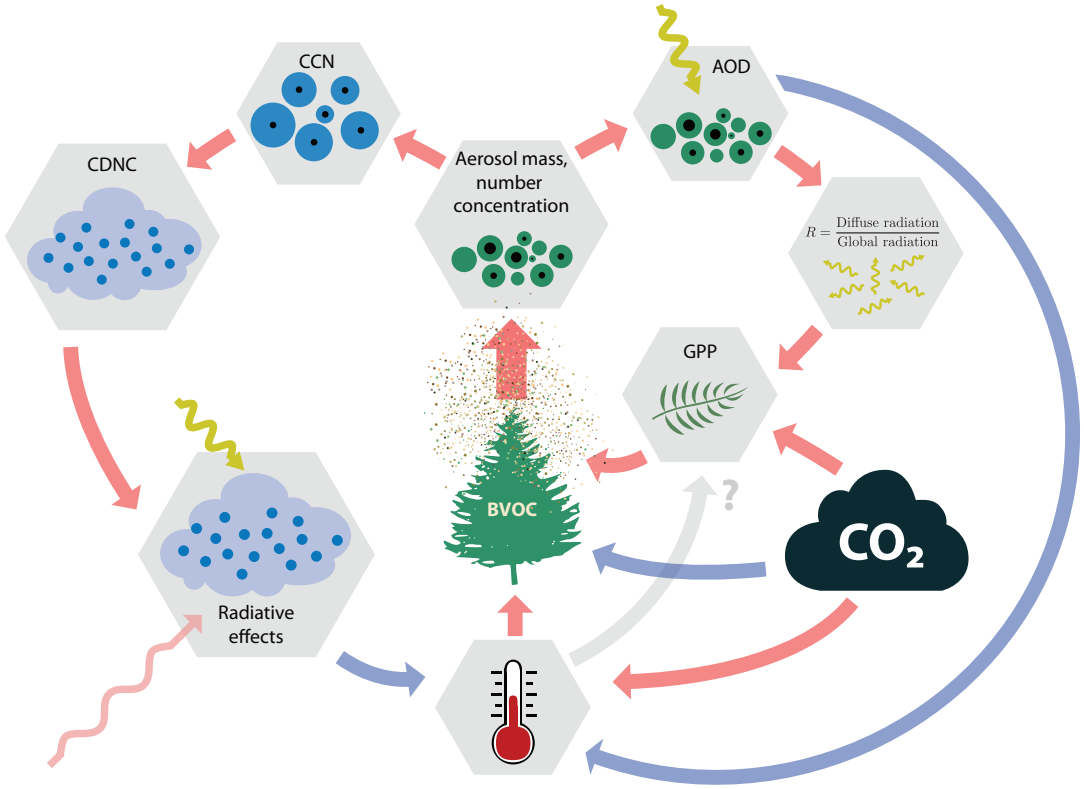

Figure 2.4: *Illustration of BVOC related feedbacks and forcing mechanisms. Red arrows indicate a positive relationship (increase in A leads to increase in B), while blue arrows indicate a negative relationship (increase in A leads to a decrease in B). Made by Diego Aliaga.*

by (*Gordon et al.*, 2016), showing a greatly reduced forcing from cloud albedo when including a pure biogenic nucleation parameterization. Another example is our results in paper IV.

2.3.4 BVOC feedbacks

BVOC emissions are highly dependent on temperature (*Guenther et al.*, 2012) as well as other environmental factors (*Heald and Spracklen*, 2015; *Peñuelas and Staudt*, 2010). This opens the path for several possible feedback mechanisms. I will here focus on those involving the formation of SOA. Figure 2.4 illustrates some important proposed feedbacks (*Kulmala et al.*, 2004, 2013). Let us start with the feedbacks involving temperature and the direct and indirect effect. Temperature increase leads to an increase in BVOC emissions (e.g. *Guenther et al.*, 2012), which further increases the SOA mass that is formed. The increase in SOA increases (1) CCN concentrations which leads to a cooling through changing cloud properties (*Albrecht*, 1989; *Twomey*, 1974) and (2) increasing aerosol optical depth (AOD) and scattering of short wave incoming radiation (direct effect) and thus cooling the surface. Furthermore, a second feedback involving the increase in AOD has been proposed (*Kulmala et al.*, 2013): when AOD increases, this increases the scattering and thus increases the diffuse (non-direct) radiation to total (global) radiation ratio (R). This has been found to increase gross primary production (GPP) in plants (*Roderick et al.*, 2001), which can potentially produce more BVOC emissions. This thus constitutes a positive feedback on BVOC emissions, and a

negative feedback on temperature via the two feedbacks mentioned before.

Studies find different values for the strength of these feedbacks. *Paasonen et al.* (2013) use measurements to show a relationship between boundary layer burden of CCN and temperature and make an order-of-magnitude estimate of the feedback strength of $-0.01\,\mathrm{Wm^{-2}K^{-1}}$. *Scott et al.* (2018b) find $-0.013\,\mathrm{Wm^{-2}K^{-1}}$ for the cloud-aerosol interaction branch and a stronger feedback from the direct effect branch of approximately $-0.05\,\mathrm{Wm^{-2}K^{-1}}$. *Kulmala et al.* (2014) investigate the diffuse radiation feedback with measurement data from SMEAR II in Hyytiälä (1996-2011) and find a gain of 1.3 (1.02-1.5), which is considerable.

2.4 Cloud-aerosol interactions

In addition to being an enjoyable, free ever changing spectacle above, clouds also play a crucial role in climate. Clouds are highly important both in the short wave and long wave radiation budget and can be cooling in one region while warming in others, depending on which process dominates (*Boucher et al.*, 2013). Clouds consist of either ice, liquid water, or a mix of the two (mixed phase clouds). Since this thesis concerns itself mainly with cloud-aerosol interactions where aerosol act as CCN, I will only discuss liquid clouds in this section.

In earth's atmosphere, each cloud droplet that forms needs a pre-existing particle to form around in order to overcome the Kelvin effect – the effect of the surface curvature. Such a particle is called a cloud condensation nuclei (CCN). The activation of an aerosol particle is described by Köhler theory (*Köhler*, 1936) and combines the Kelvin effect (curvature effect) with the effect that in a soluble particle, the solute will suppress evaporation from the droplet and thus lower the supersaturation required for equilibrium – Raoult's effect. The Kelvin effect, which requires a higher supersaturation to maintain small droplets than larger droplets, will decrease as the particle takes up water and grows. Raoult's effect on the other hand, will diminish with size since the solute is diluted, and higher supersaturations will be required as the particle grows. At a certain critical radius, the Kelvin effect dominates, and the supersaturation required to maintain the droplet decreases with size. At this point we say that the particle is activated and we call it a cloud droplet. An illustration of this is shown in Figure 2.5.

Because of this dependency on aerosols during cloud formation, enhanced aerosol concentrations may lead to more droplets activating and thus more numerous, but smaller droplets. Given the same amount of liquid water, a cloud with many small droplets will have more droplet surface area than a cloud with few but larger droplets. Due to the increase in surface area of the cloud, this will increase the reflectiveness – the albedo – of the cloud and exert a cooling effect on the surface (*Twomey*, 1974). This is referred to as the cloud-albedo effect or the first indirect aerosol effect (*Boucher et al.*, 2013). As the name "first indirect effect" alludes to, these changes in cloud properties, especially the reduction in droplet size, may entail several rapid adjustments of the clouds (*Boucher et al.*, 2013). Maybe most well known is the suppression of onset of precipitation proposed by *Albrecht* (1989), leading to a longer lifetime for the cloud and increased average liquid water path. However, this effect is partly offset by processes involving entrainment and increased evaporation (more surface area $\rightarrow$ stronger evaporation) (*Boucher et al.*, 2013). In case studies, climate models have been shown

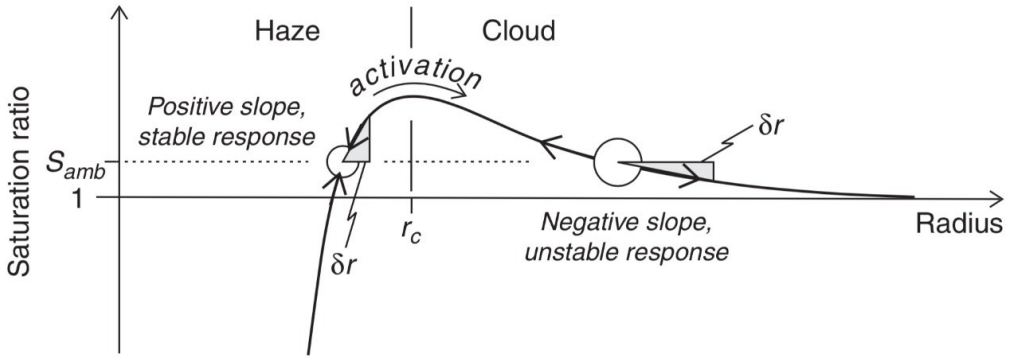

Figure 2.5: *Illustration of the activation of an aerosol into a cloud droplet. From Lamb and Verlinde (2011).*

to overestimate the lifetime effect, possibly due to a limited treatment of processes that would decrease lifetimes of clouds (*Malavelle et al.*, 2017).

Note that, as mentioned earlier, the effect of adding aerosols is highly dependent on the baseline aerosol state. First, the change in albedo of a cloud by a change in CDNC is higher when the base state has a low CDNC than a high ($dA/dCDNC = A(1-A)/(3CDNC)$) *Carslaw et al.* (2013b); *Twomey* (1991). Secondly, during lifting and cloud formation, the number of CCN which will activate and become cloud droplets is decided by the maximum supersaturation which is achieved (*Köhler*, 1936). If there are many CCN however, some CCN will quickly activate and act as a water vapor sink during lifting, thus decreasing the maximum supersaturation. Since the maximum supersaturation is lower, less of the added CCN will activate (assuming the added CCN have approximately the same size distribution) (*Bellouin et al.*, 2020). This effect is discussed further in Paper IV .

2.5 Earth System Modelling

While weather models try to project the weather in the days or weeks ahead, climate models try to project the average weather in the coming tens or hundreds of years. Though involving many of the same physical laws and being similar in form, these are two very different kinds of problems. The first, projecting the weather, is a so-called initial value problem, meaning that assuming we have represented the physical laws well enough, the success of our projection of the future relies on having the initial conditions (the winds, the pressure, the temperature) right. Due to the chaotic nature of weather, small errors in initial conditions will magnify over time and this is why weather forecasts are usually very uncertain even just a week into the future. Climate modelling, on the other hand, does not attempt to get the weather patters on any particular day correct, but rather tries to model the climate – the statistical distribution of the weather. This is a boundary condition problem, rather than an initial condition, i.e. it depends on how much energy goes in and out of the system.

Fundamentally, climate models split the earth surface and atmosphere into grid-boxes within which quantities like temperature, wind and chemical concentrations are

assumed to be the invariant. We call a climate model an Earth System Model (ESM) if it not only represents the atmosphere and ocean circulation and their response to forcings, but also biogeochemical cycles like the carbon cycle (*Flato et al.*, 2013). Climate models are required to be run for hundreds to thousands of years, which puts constraints on how high the resolution can be – usually 1–2 $^\circ$ in current generation models (*Flato et al.*, 2013).

ESMs are used both to make climate projections and assess future scenarios, but also to quantify and distinguish between the various factors in the climate system. For example we might perturb only BVOC emissions to quantify it's radiative effect on climate. When doing the latter, the ESMs are often run with constraints on one or more components in the Earth System. For example, when estimating the ERF of aerosols ($ERF_{aci+ari}$) with the fixed SST method (*Hansen et al.*, 2005), we use fixed sea surface temperatures and sea ice (the ocean and sea ice component is turned off), and run one simulation with pre-industrial aerosol emissions and one with present day emissions. We can then find the $ERF_{aci+ari}$ by taking the change in radiative effect of aerosols with present day emissions and pre-industrial emissions. In these simulations, the active components are the atmosphere and the land model.

2.6 Aerosol modelling

Adequately representing aerosol processes in ESMs is challenging, due to the fine scale compared to the grid-box (nanometers versus hundreds of kilometer) and due to the constrain of computational cost. For this reason, it is most common to use some number of log-normal modes to represent the size distribution of the aerosols (e.g. *Liu et al.*, 2005; *Mann et al.*, 2010; *Stier et al.*, 2005; *Vignati et al.*, 2004). Another, more computationally expensive alternative, is to use sectional schemes where the size distribution is split up into bins and the model keeps track of the concentration in each bin (e.g. *Kokkola et al.*, 2008; *Spracklen et al.*, 2005). While the modal approach makes assumptions about the shape the size distribution can take, the sectional scheme is closer to first principles, but requires more bins than the number of modes in the modal scheme. The constraining factor is that the model needs to keep track of tracers for each aerosol species in each bin or mode, so the total number is the number of aerosol species $\times$ the number of bins or modes. We discuss aerosol modelling in further detail in paper III.

Chapter 3

:Methods

The development of Earth System Models is important for projecting future climate scenarios and assessing the consequences of our actions as a society. Additionally, because ESMs try to include all important drivers of global change, they can serve as a test ground to check the relevance of some process and where important knowledge may be missing. In this way the conversation between modelling and measurements/-experiments can go both ways, each informing the other.

The main tool used in this thesis is the Norwegian Earth System Model, which is both applied as is (paper I), compared to other ESMs with respect to SOA formation (paper II) and further developed and compared against observations (paper III and IV). A considerable amount of work has gone into developing a sectional scheme which handles the early growth of newly formed particles in the model, feeds the particle into the original semi-modal scheme. While the model description is described in paper III, I will describe the fundamental idea and key features here as well.

Note that two versions of NorESM are used in this thesis. In papers I and II a development version of NorESMv1 is used, while in papers III and IV NorESM2 is used and developed.

In this chapter, I will first give an overview of the general features of NorESM, before going more in detail on the aerosol scheme, OsloAero. Next, I will describe the development of the aerosol scheme, OsloAeroSec.

3.1 NorESM

3.1.1 General information

NorESM (*Bentsen et al.*, 2013; *Iversen et al.*, 2013; *Kirkevåg et al.*, 2013, 2018a; *Seland et al.*, 2020) is a branch of the Community Earth System Model (CESM) (*Danabasoglu et al.*, 2020; *Hurrell et al.*, 2013) and the two models thus share many characteristics. The land model, the Community Land Model (CLM) and the sea ice model are the same as CESM with only minor changes. The ocean model in CESM is exchanged completely with the Bergen Layered Ocean Model (BLOM) in NorESM2 and Miami Isopycnic Coordinate Ocean Model (MICOM) in NorESM1. The atmospheric component, the Community Atmosphere Model (CAM) (*Bogenschutz et al.*, 2018; *Liu et al.*, 2016; *Neale et al.*, 2012), is also used in NorESM, but with some changes and a

completely different aerosol scheme, namely OsloAero (described below). The atmospheric model in NorESM is called CAM-Oslo or CAM-Nor, depending on the version.

In the work in this thesis, all simulations are done with fixed sea surface temperatures, meaning the ocean model is not active. I will therefore only describe the land and atmosphere model.

Note that paper I and II were done using CAM5.3-Oslo (*Kirkevåg et al.*, 2018a) coupled with CLM4.5 (*Oleson et al.*, 2013), while papers III and IV are done using NorESM2, and thus CAM6-Nor (*Seland et al.*, 2020) and CLM5 (*Lawrence et al.*, 2019).

3.1.2 The Community Land Model

CLM is used in several global and regional models and treats the cycling of energy, water, momentum in the land surface. It also includes a carbon and nitrogen cycle, which allows for the vegetation to respond to perturbations in the climate with increased GPP and increases in biomass. Furthermore, CLM includes the Model of Emissions of Gases and Aerosols from Nature version 2.1 (MEGAN2.1) *Guenther et al.* (2012) which handles the emissions of BVOCs and their dependence on vegetation and environment. Thus, the model is well suited for the purpose of this thesis.

3.1.3 The Community Atmosphere Model - Nor/Oslo

In both CAM6-Nor and CAM5.3-Nor the CAM aerosol scheme has been replaced by OsloAero (see next section).

CAM5.3-Oslo (*Kirkevåg et al.*, 2018b): Cloud droplet activation is done with *Abdul-Razzak and Ghan* (2000) and droplets and ice in stratiform clouds are modelled with the double moment bulk microphysics scheme MG1.5 (*Gettelman et al.*, 2008; *Morrison and Gettelman*, 2008), which includes prognostic calculations of mass and number. For deep and shallow convective clouds on the other hand, are tracked only with mass and fixed sizes are used (*Bretherton and Park*, 2009; *Zhang and McFarlane*, 1995). This means that aerosols only influence activation and cloud droplet number concentration in stratiform clouds. The deep convection microphysics are treated with a simplified single–moment representation based on *Zhang and McFarlane* (1995).

CAM6-Nor *Seland et al.* (2020): In CAM6, and thus also CAM6-Nor, The Cloud Layers Unified by Binormals (CLUBB *Bogenschutz et al.*, 2013; *Golaz et al.*, 2002) replaces the schemes for boundary layer turbulence, shallow convection and cloud macrophysics. MG1.5 is replaced by the improved version, MG2 (*Gettelman and Morrison*, 2015). Furthermore, compared to CAM6, CAM6-Nor contains a correction to the zonal wind increments implemented to enforce conservation of angular momentum, described in *Toniazzo et al.* (2020) and some modifications to the deep convection scheme to reduce the resolution dependence of the scheme (*Seland et al.*, 2020).

3.1.4 OsloAero

The most notable difference in OsloAero from other aerosol models, is that it divides the aerosol into "background tracers" and "process tracers". The background tracers are

primary emissions or particles from NPF, while the process tracers track mass resulting from condensation, coagulation or cloud processing. The background tracers form log-normal modes and these decide the number concentration. The process tracers are then added to the background modes and alter the initial size distribution, forming mixtures of the background and tracer modes. Finally, the optical properties and the best log-normal fit to the final distribution is produced by interpolating a look-up table based on offline simulations with the size-resolving model AeroTab. AeroTab has 44 bins ranging from 0.001 –20 μm and produces the size distribution by solving the discrete form of the process relevant continuity equation (*Kirkevåg et al.*, 2013). The optical properties are then used in the radiation calculations, while the log-normal fit is used in the cloud activation scheme which is (*Abdul-Razzak and Ghan*, 2000).

In total there are 12 background modes representing the formation of NPF, the primary emissions of dust, sea salt (SS), black carbon (BC) and organic matter (OM). There are 15 background tracers in total, since some tracers combine to form the same mode. The process tracers consist of condensate (SO_4 and SOA), coagulate (SO_4, SOA/OM and BC) and production in cloud droplets (SO_4).

The version of OsloAero used in this thesis contains a simplified chemistry scheme for the oxidation of sulphur and BVOCs, making use of the chemical pre-processor MOZART (*Emmons et al.*, 2010) and pre-calculated mean fields for the oxidants, OH, O_3, NO_3 and HO_2 (for further detail see *Karset*, 2020). There are three tracers that contribute to condensation in OsloAero, H_2SO_4, low volatile SOA gas ($SOAG_{LV}$) and semi-volatile SOA gas ($SOAG_{SV}$). Note that all these are considered essentially non-volatile during condensation, so the separation between low volatile and semi-volatile is done through which processes the tracers can partake in – only $SOAG_{LV}$ can participate in NPF and growth up to the smallest mode (23.6 nm in diameter). All of these are formed from oxidation in the gas phase. The process for forming SOAG in NorESM is as illustrated in figure 3.1: MEGAN2.1 calculates BVOC emissions online which are then lumped into two tracers in the OsloAero, isoprene and monoterpene. These are then oxidized in reaction with O_3, NO_3 and OH. Monoterpene has yields of 15 %, while isoprene has yields of 5 %. Only the ozonolysis of monoterpenes produces $SOAG_{LV}$, the other reactions produce $SOAG_{SV}$. The monoterpene yield of 15 % has been used in many global models (*Tsigaridis et al.*, 2014, see e.g.) and originates from AeroCom emissions inventory presented in *Dentener et al.* (2006), where 15 % of all terpene emissions are assumed to form SOA. The isoprene yield of 5 % is similar to that used in other models (*Sporre et al.*, 2020). The uncertainties are large for both yields (*Shrivastava et al.*, 2017).

For nucleation, OsloAero uses *Vehkamäki et al.* (2002) for the whole atmosphere and *Paasonen et al.* (eq.18 2010) to account for boundary layer nucleation. While *Vehkamäki et al.* (2002) includes only sulphuric acid and water, *Paasonen et al.* (2010) includes a linear relationship with both sulphuric acid and low volatile organics:

$$J_2 = A_{s1}[H_2SO_4] + A_{s2}[SOAG_{LV}] \tag{3.1}$$

The smallest background mode in OsloAero has a number median diameter of 23.6 nm, which is a considerable jump from the size at which the particles are formed (approximately 2 nm). To estimate the number of particles that survive growth up to this diameter, OsloAero uses the parameterization from *Lehtinen et al.* (2007), which estimates

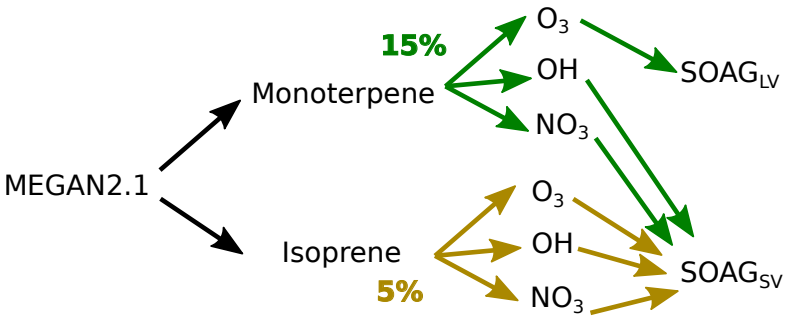

Figure 3.1: *Formation of low volatile and semi-volatile SOA in gas phase (SOAG) in NorESM. MEGAN2.1 calculates emissions online, these are lumped into two tracers in the OsloAero, isoprene and monoterpene, which are subsequently oxidized.*

the survival percentage mainly based on the ratio of the growth rate and the coagulation sink. This is illustrated in the top panel of figure 3.2. For further information on OsloAero, see Paper III which includes a quite detailed model description.

3.2 OsloAeroSec: Development of a new module in OsloAero

An important part of this thesis has been to develop a new scheme for the treatment of early growth of particles in OsloAero. The implementation is motivated by the fact that the smallest mode in OsloAero which holds the NPF particles, is already at 23.6 nm (before condensational growth) and that this is a rather large jump to parameterize with *Lehtinen et al.* (2007). In fact in reality, this growth will take considerable time (hours to even days, depending on the growth rate) and go over many time steps (0.5 hour).

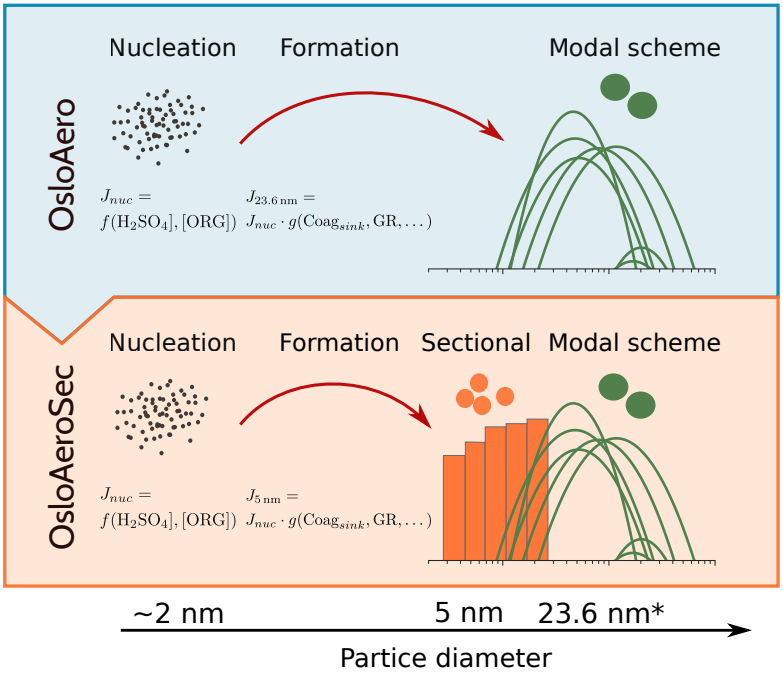

Figure 3.2: *Illustration of the difference between OsloAero and OsloAeroSec.*

As is discussed in depth in paper III, this runs the risk of excluding important processes which may change the result *Lee et al.* (2013); *Olenius and Riipinen* (2017). For

one, the assumption that the growth rate and coagulation rate (which go into the *Lehtinen et al.* (2007) parameterization), are the same throughout the growth will normally fail. This is because nucleation usually happens at the diurnal peak concentration of condensing vapors, and the growth happens after this while the growth rate is diminishing. Secondly, it neglects the effect of mixing and transport, possibly letting particles form at a different location from where they would form in reality. In paper II we show that NPF parameterization is of high importance for the effects of BVOCs and SOA on the climate, and this further motivated us to improve the early growth treatment in the aerosol model. Inserting a nucleation mode in this range, would better some of the concerns mentioned above, but a modal representation has drawbacks in that it assumes an a priori shape to the distribution in a range where e.g. coagulation is highly size sensitive. We therefore opted for including a sectional scheme in this range of the models.

The sectional scheme consists of 5 bins from 5 nm and up to 39.6 nm (the volume median diameter of the background mode for NPF particles). Two condensing vapors are included, H_2SO_4 and $SOAG_{LV}$ and these are both treated as non-volatile during condensation. The particle growth, moving particles from one bin to the next, is done using a quasi-stationary structure *Jacobson* (1997, 2005).

Coagulation losses are calculated for coagulation between the sectional particles and the modal particles, while coagulation between the particles in the sectional scheme may also contribute to growth of the combined particle.

When the particles grow out of the sectional scheme, they are added to the background tracer/mode which keeps the NPF particles. Since the sectional scheme only treats the growth up to the modal scheme and are thus very small particles, it does not interact with radiation or the cloud microphysics.

3.2.1 Oxidant improvement and NPF parameterization

During the development of the sectional scheme, we also updated the NPF parameterization from *Paasonen et al.* (2010) (eq. 3.1) to *Riccobono et al.* (2014) which is on the form:

$$J_2 = A[\mathrm{H_2SO_4}]^2[\mathrm{ELVOC}]. \tag{3.2}$$

The oxidant values are interpolated from pre-calculated monthly mean files in OsloAero. We found that, especially when using a super-linear parameterization for the nucleation, the diurnal variation in oxidants were important because they controlled the diurnal variation in sulphuric acid and organics. In the default version of OsloAero, OH has a step function: on during the day, and off during the night. This lead to a similar step function like shape in the diurnal sulphuric acid concentration, diminishing the peak. Since this had lead to to lower nucleation rates (super-linear nucleation equation) and longer lasting events, we decided to implement a simple sine shape to the diurnal OH concentrations instead.

Chapter 4

:Presentation of findings

In this chapter I will present the main findings in this thesis and how they relate to the objectives given in Chapter 1. Before giving a summary of each of the individual papers included in the model, I will present an improvement to the coagulation treatment of newly formed particles which is used in papers II,II and IV, but is not presented properly in either.

4.1 Coagulation treatment

When I started working with NPF in NorESM, it quickly became clear that in the default version of the model, almost all particles that nucleated survived the growth to the first mode (see left panel of figure 4.1), much in contrast with what happens in reality (e.g. *Lehtinen et al.*, 2007).

This survival percentage from nucleation ($\sim 2\,\text{nm}$) to the smallest mode (23.6 nm) in OsloAero, is parameterized with *Lehtinen et al.* (2007), namely

$$J_{d_{\text{mode}}} = J_{\text{nuc}} \exp\left(-\gamma d_{\text{nuc}} \frac{CoagS(d_{\text{nuc}})}{GR} \right) \tag{4.1}$$

where $J_{d_{\text{mode}}}$ is the formation rate at d_{mode}, d_{nuc} is the diameter of the nucleated particle, $CoagS(d_{\text{nuc}})$ is the coagulation sink of the particles [h^{-1}], GR is the growth rate

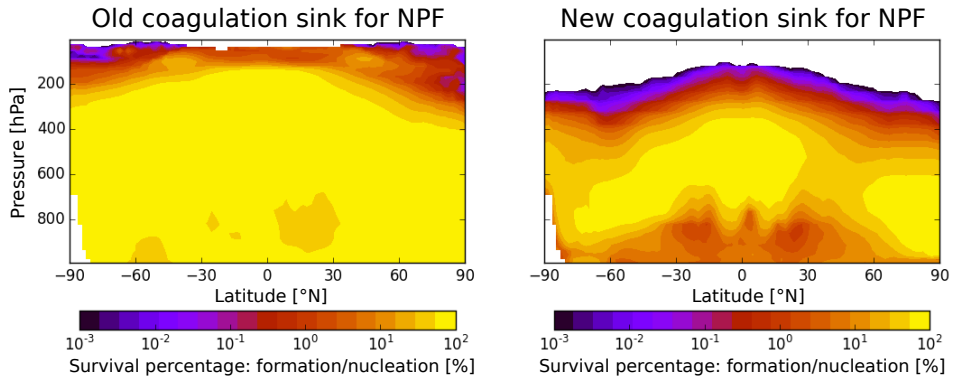

Figure 4.1: *The zonally averaged survival percentage between nucleation and formation at* 23.6 nm *for the old version of the coagulation sink (left) and the new (right).*

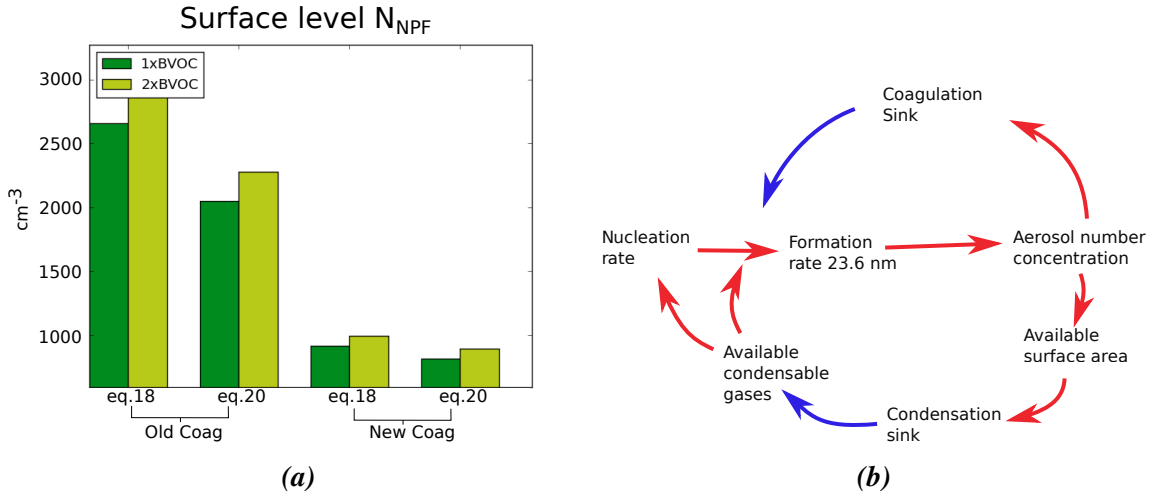

Figure 4.2: ***(a)*** *The globally averaged number concentration of particles from NPF with the old coagulation sink and the new. Tests are done with changing the nucleation parameterization and the BVOC emissions with both schemes (single BVOC emissions in dark green and double BVOC emissions in light green). The nucleation parameterization is changes between the default eq. 18 from (Paasonen et al., 2010) and equation 20 from the same paper. Eq.18 is on the form* $J_2 = A_{s1}[H_2SO_4] + A_{s2}[SOAG_{LV}]$*, while eq.20 is on the form* $J_2 = K_{s1}[H_2SO_4]^2 + K_{s2}[SOAG_{LV}][H_2SO_4] + K_{s3}[SOAG_{LV}]$ *.* ***(b)*** *Schematic showing the feedbacks working to constrain NPF.*

$[\mathrm{nmh}^{-1}]$ of the particle and γ is a function of d_{form} and d_{nuc}:

$$\gamma = \frac{1}{m+1}\left[\left(\frac{d_{\mathrm{form}}}{d_{\mathrm{nuc}}}\right)^{(m+1)} - 1\right], \; m = -1.6. \tag{4.2}$$

The problem in the default version, was that coagulation with the smaller modes was considered negligible. These smaller modes included the mode that held the NPF particles, which meant that the number of particles could increase without impacting the survival percentage at all. In other words, not only was the coagulation sink too low, additionally an important feedback loop constraining NPF was removed.

We fixed this issue by including all pre-existing aerosol in the coagulation sink used in *Lehtinen et al.* (2007). Figure 4.1 shows zonally averaged survival percentage (nucleation rate divided by formation rate) with the old coagulation sink (left) and the new coagulation sink (right) from a two year simulation with OsloAero5.3-Oslo. While with the old coagulation sink, almost all the particles survived everywhere, the new one shows a much more realistic behaviour. Each simulation consists of two years and is nudged to the same model meteorologic data. The method for the nudging is described in paper I (*Sporre et al.*, 2019).

As expected, this resulted in a drastic decrease in number concentration, particularly in the lower levels of the model. This can be seen in Figure 4.2a, which shows some sensitivity tests run with the old and the new coagulation sink. I used two different nucleation rate equations, equation 18 (the default) and equation 20 from *Paasonen et al.* (2010) and default and doubled BVOC emissions. The results are for two year simulations nudged to the same model meteorology. The number concentration is more than halved, and interestingly the difference between the different sensitivity runs is less with the new coagulation sink. This is natural, considering we have included a missing negative feedback on the formation of new particles. Figure 4.2b shows the feedbacks

constraining new particle formation. With the old coagulation sink treatment, the top loop via increasing coagulation sink was missing.

In sum the new treatment is more physically correct and shows improvement in the results.

4.2 Summary of papers

4.2.1 Paper I: "BVOC–aerosol–climate feedbacks investigated using NorESM"

Objective

Assess the strength of the BVOC feedbacks through temperature and CO_2 changes with NorESM.

- *Technical development: Develop method for assessing the BVOC feedback strength.*

Summary

In this study, we used NorESM with active atmosphere (CAM5.3-Oslo) and land (CLM4.5) components, to investigate the strength of the climate feedback through increase in BVOC emissions with higher temperatures and the feedback on gross primary production (GPP) via increase in diffuse radiation with SOA increase (see description in Chapter2.3).

We use CLM4.5 in BGC mode in which the vegetation distribution is fixed (no dynamic vegetation), but the vegetation density is allowed to respond to the environment. We run two different forcing scenarios: (1) increase in sea surface temperatures corresponding to a doubling of CO_2 and (2) a doubling of CO_2. Furthermore, we also investigated the combined forcing scenario of CO_2 *and* temperature increase. We developed a method for quantifying the BVOC feedbacks by saving emission fields from A) a control simulation and B) a simulation where the temperature and/or the CO_2 concentration was perturbed. This made it possible to run and compare simulations with the feedback on BVOC emissions turned on (emissions from B) and off (emissions from A).

Main findings

- The annual mean emissions of BVOCs were 63 % higher with the feedbacks on, i.e. the vegetation was allowed to response to increase in temperature and CO_2 concentrations. This leads to a 53 % increase in SOA mass.

- The increase in SOA leads to a considerable strengthening of the negative cloud radiative effect, which is $-0.43\,\mathrm{Wm}^{-2}$ stronger with the feedback on.

- We also found that with lower aerosol emissions, which is expected in the future, the strength of the feedback increased significantly (50 % with pre-industrial (1850) aerosol emissions).

- We do not manage to find that the increase in aerosol boosts GPP significantly on a global scheme, mainly because the BVOC effect on clouds seem to dominate the change in GPP.

- A small enhancement to the aerosol direct effect ($-0.06\,\mathrm{Wm}^{-2}$) is found

Main conclusion

The model estimated total aerosol effect (direct and indirect) associated with this feedback from a doubling of CO_2 is $-0.49\,\mathrm{Wm}^{-2}$. This is considerable, in fact it is enough to offset about 13 % of the forcing associated with a doubling of CO_2.

Author contribution

I was involved in the planning and discussions on the design of the project. Furthermore, I was involved in discussions on the analysis and result, as well as providing feedback and suggestions on the manuscript. Lastly, the model simulations (performed by Moa Sporre) used an improvement to the code concerning coagulation sink for newly formed particles, which I developed.

4.2.2 Paper II: "Large difference in aerosol radiative effects from BVOC-SOA treatment in three Earth system models"

Objective

Unveil and discuss uncertainties in BVOC-to-aerosol modelling by comparing differences and sensitivities in thee current state-of-the-art ESMs.

Summary

In this study, we compare three ESMs with respect to their treatment and climate effect of SOA: NorESM, ECHAM and EC-Earth. We do this by running a series of sensitivity experiments where we perturb common parameters or emissions in the same way in all three models. The experiments are:

Yield higher	Increase the SOA yields from BVOC oxidation by 50 %
Yield lower	Decrease the SOA yields from BVOC oxidation by 50 %
No ELVOCs	No ELVOCs are formed, i.e. no organics participate in NPF, but the same mass is converted to semi-/low volatile VOCs.
No isoprene	Isoprene emissions are set to zero.
No monoterpene	Monoterpene emissions are set to zero.

These are all compared against a control simulation for each model.

Main findings

- Changes in the direct radiative effect (DRE) is linked directly and positively to the changes in SOA production in each model, though the magnitude is varies quite a bit. EC-Earth has the strongest response with a change of $0.15\,\mathrm{Wm}^{-2}$.
- The results in terms of cloud radiative effect (CRE) differ strongly amongst the models. The *Yield higher/Yield lower/No monoterpene* sensitivity tests show a quite symmetric response, with NorESM being the most sensitive model, followed by EC-Earth, while ECHAM has an insignificant response. However, in the *No isoprene* run, NorESM shows a strong warming ($0.5\,\mathrm{Wm}^{-2}$), while EC-Earth shows an even stronger cooling ($-0.82\,\mathrm{Wm}^{-2}$).
- We find that the differences in response from the models are related to where in the size distribution the SOA changes occurs as well as the baseline aerosol concentration and distribution in the models.
- We find that in EC-Earth, the response to higher/lower yields is opposite in areas that are close to and far away from sources. E.g. in *Yield lower*, the CDNC is reduced close to the emission sources, but increases in remote ocean areas which partly compensates in the global average. We attribute this to increased NPF in these remote regions due to reduced coagulation/condensation sink.

- We further find that differences in NPF parameterization play a role, particularly in response to the *No ELVOCs* test, which sets to zero organic participation in NPF.

Main conclusion

We conclude that the treatment of SOA in current ESMs has a considerable impact on the modelled climate, but the difference in model response to sensitivity tests, indicate large uncertanties. These results imply uncertainty to model estimates of both aerosol forcing and feedbacks.

Author contribution

I analysed model output from all three models, specifically focusing on the chemistry and aerosol size distributions (figures 3, 4 and 9 in the paper) and contributed to discussions concerning model design and results. I co-wrote the paper together with Moa Sporre.

4.2.3 Paper III: "Implementing a sectional scheme for early aerosol growth from new particle formation in the Norwegian Earth System Model v2: comparison to observations and climate impacts"

Objective

To develop and evaluate a sectional scheme for treating the early stages of particle growth in NorESM. Improve the understanding of how new particle formation and early growth influences cloud condensation nuclei and the activation of aerosols in clouds.

Summary

In order to improve the representation of early aerosol growth in NorESM, we implement a sectional scheme which grows the smallest particles from formation at 5 nm and up to the smallest mode in OsloAero, with a number median diameter of 23.6 nm. Traditionally, aerosol schemes would use either a modal or a sectional approach. To our knowledge, this is the first time this kind of combination has been tried.

The sectional scheme includes 2 condensing species, low volatile organics and H_2SO_4 and 5 bins. It includes loss by coagulation (both with particles in the modal and sectional scheme) and growth through condensation. Since the particles are so small, they do not interact with other parts of the code, like radiation or cloud activation. In addition to implementing the sectional scheme, we also update the nucleation parameterization and improve the diurnal variation of oxidants. We compare simulations with the new scheme, which we refer to as OsloAeroSec, to two versions of the original OsloAero scheme: the default version, OsloAero$_{def}$ and a version with the same improvements to oxidants and nucleation parameterization as OsloAeroSec, OsloAero$_{imp}$.

We compare CCN relevant particle number concentrations (N_{50-100}, N_{50-500}, $N_{100-500}$) to observations from 24 stations on Europe from the EUSAAR database presented in *Asmi et al.* (2011).

Main findings

- We find that OsloAeroSec performs better against observations than the original scheme, especially in N_{50-100}. The improvement is particularly large in summer, when NPF is high most places.

- We find that OsloAeroSec over-predicts number concentrations in the smallest bins in the sectional scheme and that this is related to too frequent and too long lasting NPF events.

- Comparing the model versions in the whole atmosphere, we find that OsloAeroSec in general produces much less particles (excluding the particles still in the sectional scheme) than OsloAero$_{def}$ (almost half at the surface). However, compared to OsloAero$_{imp}$, OsloAeroSec produces less particles in polluted regions but more in remote regions of the atmosphere. In particular, OsloAeroSec often produces more particles than the other model versions higher up in the atmosphere.

Main conclusion

Explicitly treating the early growth of particles with a sectional scheme improves the performance of the model compared to observations. The implementation of the sectional scheme also changes not only the amount of particles that survive to larger sizes, but also where this happens, with more surviving in remote regions and less in polluted.

Author contribution

I initiated this project after coming up with the idea together with Risto Makkonen. I did the coding of the model development, ran all simulations and performed the data analysis. Finally, I wrote the paper with help from the co-authors.

4.2.4 Paper IV: "Reduced ERF_{aci} with combining a sectional scheme for early growth with a model scheme in Earth System Model"

Objective

Improve the understanding of how formation of new particles in the atmosphere influences climate and radiative forcing. Quantify the effect of implementing a sectional scheme for early particle growth on effective radiative forcing from aerosol cloud interactions (ERF_{aci}). Improve the understanding of the effect of the organics through early growth

Summary

Motivated in particular by the improvement shown with the sectional scheme, OsloAeroSec in paper III, and in particular the increase in particle number in cleaner parts of the atmosphere, we investigate the implications for ERF_{aci} and ERF_{ari}. We use a standard fixed SST method for estimating ERF, comparing simulations with pre-industrial (1850) and present day (2014) aerosol emissions. We do this both for OsloAeroSec and for two versions of the default model, the default $OsloAero_{def}$ and a version which includes updates to the nucleation parameterization and oxidants which are also part of OsloAeroSec.

Main findings

- We find that the ERF_{aci} decreases in magnitude with OsloAeroSec by 0.13 and $0.14\,Wm^{-2}$ compared to $OsloAero_{def}$ and $OsloAero_{imp}$ respectively.

- OsloAeroSec produces more particles than $OsloAero_{def}$ in much of the pre-industrial atmosphere, while producing less in most of the present day atmosphere. In sum this means OsloAeroSec has approximately half the increase in number concentration over the historical period to $OsloAero_{imp}$.

- It is often assumed that more new particle formation automatically leads to increase in CCN and CDNC. By comparing model versions with different NPF efficiency (amount of particles formed per emissions), we also discover that in fact higher NPF efficiency leads to lower cloud activation and lower CDNC in many environments. The reason is that the increase in number concentration decreases the available condensate and thus the number median diameter of the modes. In these environments, which are especially polluted environments, this effect is stronger than the increase in total number concentration.

- We find that overall OsloAeroSec has a tendency to have higher NPF efficiency where more NPF leads to higher cloud droplet activation and CDNC, while having lower NPF efficiency where NPF leads to less cloud droplet activation and CDNC. The sum is that, compared to OsloAero, OsloAeroSec has a higher CDNC concentration both in the pre-industrial and the present day atmosphere, but the change over the historical period is less.

Main conclusion

The explicit treatment of NPF in a sectional scheme has a considerable impact on the estimated ERF_{aci} and omitting the dynamics in the early growth runs the risk of overestimating the forcing from aerosol-cloud interactions.

Author contribution

I initiated and designed the study and performed the model simulations. Furthermore, I did the data analysis and made the figures for the paper. Finally, I wrote the paper with help from the co-authors.

Chapter 5

:Discussion, future outlook and concluding remarks

The overall goal of this thesis is to improve modelling and understanding how BVOC emissions impact climate, especially focusing on the formation and early growth of new particles in the atmosphere. With this goal, I have worked on quantifying BVOC feedbacks, revealing uncertainties in SOA modelling through comparing different ESMs, improved the NPF and early growth modelling in NorESM and quantified it's impact on radiative forcing.

In this chapter I will start by discussing the scientific results in this thesis compared to the objectives presented in Chapter 1.2. After this I will discuss potential future research regarding the effects of BVOCs on climate, both historically and in a policy assessment perspective.

5.1 SOA treatment in ESMs

Objectives

- *Assess the strength of the BVOC feedbacks through related to temperature and CO_2 changes (Sporre et al., 2019)*
- *Unveil and discuss uncertainties in BVOC-to-aerosol modelling by comparing differences and sensitivities in thee current state-of-the-art ESMs (Sporre et al., 2020).*

Paper I establishes that BVOC feedbacks via SOA formation are of considerable size, at least in NorESM. However, in Paper II, we also show that different ESMs respond quite differently to changes in both emissions and SOA yields. For example, in Paper I we find that when temperatures and CO_2 concentrations were perturbed to roughly match a 2xCO_2 scenario, the subsequent changes in BVOC emissions (+63 %) led to a $-0.43\,\mathrm{Wm}^{-2}$ stronger net cloud radiative effect. Meanwhile in Paper II, we show that NorESM has a considerably stronger response in cloud radiative effect to changes in SOA production, than the other two models . The *Yield higher* (+50 %) and *Yield lower* (-50 %) sensitivity runs reveal that NorESM responds with $-0.27\,\mathrm{Wm}^{-2}$ (*Yield higher*) and $0.35\,\mathrm{Wm}^{-2}$ (*Yield lower*). EC-Earth on the other hand has a much

lower response ($-0.11\,\mathrm{Wm}^{-2}$ and $0.076\,\mathrm{Wm}^{-2}$) and ECHAM has an insignificant response. This could of course mean that NorESM is on the rather high end in sensitivity to the production of SOA, possibly due simply to higher SOA production than the other two. However, the estimates of SOA production have a large range (*Tsigaridis et al.*, 2014), and it may equally well be that the other models are underestimating SOA. Furthermore, the globally averaged cloud effects in EC-Earth the product of compensating local effects: a cooling close to the SOA sources are compensated by a warming over remote ocean regions (or opposite). Lastly, EC-Earth shows a much larger change in the direct aerosol effect in the same sensitivity tests, almost double that of NorESM. In sum, we find that most of the differences between the model have to do with the size distribution and where in it the SOA is added. In a way, this is somewhat disheartening, because it may mean that correctly estimating the forcings and feedback from BSOA may be highly dependent on getting the size distribution *without* BSOA right.

Furthermore, in Paper III, we found that implementing an explicit treatment of the growth up to the modal scheme globally almost doubled the estimated fraction of the early growth which originates from SOA in the model. The reason is that in the original model, the growth from nucleation to the modal scheme (23.6 nm) is parameterized within one time step, which means that most new particles will form when sulphuric acid concentrations peak. In reality the growth may very well happen during a time of day when sulphuric acid is decreasing and thus organics may contribute more. This effect is captured by the sectional scheme. When the original scheme was updated with the super-linear nucleation parameterization ($k[\mathrm{H_2SO_4^2}]\times[\mathrm{ELVOC}]$) from *Riccobono et al.* (2014), the difference to the sectional scheme became even larger, because the production of new particles was then even more confined to the daily peak in sulphuric acid.

It is hard to draw one single conclusion from these studies, but in general they all indicate that a) biogenic SOA matters for climate (Paper I) b) It matters how it is implemented, both in terms of added mass and in terms of where in the size distribution SOA contributes and c) if the BVOC influence on early growth is to be captured, then the growth of newly formed particles must be explicitly modelled.

5.2 NPF and ERF: what is needed for models to be "good enough"?

Objectives:

- *Improve the understanding of how formation of new particles in the atmosphere influences climate and radiative forcing (Blichner et al., 2020a,b)*
- *Improve the understanding of how new particle formation and early growth influences cloud condensation nuclei and the activation of aerosols in clouds (Blichner et al., 2020a)*
- *Improve the understanding of the effect of the organics through early growth*
- *Quantify the effect of implementing a sectional scheme for early particle growth on ERF_{aci} (Blichner et al., 2020b, submitted to ACP)*

A major part of this thesis is that I have merged a sectional scheme with a semi–modal scheme in an earth system model. This approach was chosen for several reasons. Firstly, the treatment of early growth was clearly very coarse in NorESM and more so than other ESMs. This meant that improving this part was potentially large improvement. Secondly, through working on the coagulation sink for new particles (see Chapter 4.1), I saw the importance of of including feedbacks which constrain the formation of new particles.Before this improvement, the formation rate of new particles did not impact the coagulation sink for newly forming particles at all, thus omitting an important constraint. Seeing how sensitive the NPF rate was to the coagulation sink made it clear that including the dynamics in the range below 23.6 nm diameter was important. This due to both the effect newly formed particles (below 23.6 nm) can have on formation rate through acting as a sink for vapors and the effects from changing conditions due to mixing/transport/chemistry during the growth time up to 23.6 nm. Thirdly, through the work with Paper II, we experienced that rather small differences in the implementation of the nucleation mode between ECHAM and EC-Earth seemed to make a large difference to how many particles were transferred to the larger mode. This is related to the diameter at which the particles are added versus how much the particles need to grow to be moved to the next mode. Because a nucleation mode does not explicitly treat the growth and is sensitive to implementation choices, this seemed like a less attractive option. Finally, implementing a sectional scheme for early growth in combination with a modal scheme, is, to our knowledge, a new approach and the development can thus serve as example for other models.

Including a sectional scheme significantly reduced the model's ERF_{aci}, as is discussed in Paper IV. This effect is due to the sectional scheme producing less particles in regions with high aerosol concentrations together with producing more particles in regions with low aerosol concentration. Related to this we also found that in the model, independently of the sectional scheme, NPF may both inhibit and enhance cloud droplet activation, depending on the environment. This has been noted before (*Sullivan et al.*, 2018), but not to my knowledge in the context of estimating ERF. The basic concept of NPF inhibiting cloud activation is that increase in NPF increases the condensation sink and thus reduces the growth of the larger particles which might otherwise activate. In regions where the NPF particles activate, on the other hand, NPF will enhance activation. While the concept of NPF inhibiting activation is physically sound and intuitive, we cannot exclude that this is a product of either our model specifically or common model setups.

In Paper II, we show that in EC-Earth, CDNC in remote regions goes up when SOA yield are reduced. This is due to higher NPF when coagulation and condensation sink is lower due to less SOA. Because EC-Earth is so clean, even very small particles can activate, and hence the clouds become more cooling. Had there been more larger particles in EC-Earth the effect may well have been different.

In sum these factors point to the importance of capturing remote NPF well in models for the estimated ERF_{aci}. Secondly, it shows that the effect of NPF on CCN depends on the non-NPF particles. The sectional scheme reduces the magnitude of ERF_{aci} by 0.13–0.14 Wm^{-2} (Paper IV), which is approximately half of the intra model standard deviation in ERF_{aci} between the CMIP6 models (0.3 Wm^{-2}, *Smith et al.*, 2020) and brings the estimate in NorESM closer to the multi model mean.

5.3 Further research

Let us take a step back: BVOCs can influence the climate both via inducing radiative forcing and through climate feedbacks. We therefore care about them for a couple of different reasons:

1. To understand and untangle processes in the historical climate change. In this regard, understanding the base line aerosol state, of which oxidation products from BVOCs are very important, but also how BVOC emissions have changed in response to temperature and climate change, AND in response to land use change.

2. To be able to make assessments about future climate scenarios. Changing BVOC emissions with changes in climate (feedbacks) and land use (forcing) will affect the overall temperature change.

3. To assess policy options for example with regards to widespread roll outs of Bio-energy with carbon capture and storage (BECCS), afforestation or reforestation. These would definitely have the potential to significantly impact BVOC emissions.

In all of the above, an important uncertainty is the amount of SOA and to what degree this SOA contributes to NPF. In our research, the contribution of SOA to early growth almost doubles with including the sectional scheme, but is still only a little above 20 %. This might well be very different if we were to change the assumed SOA yields in the model. A fruitful endeavor therefore, would be to compare observations of early growth from SOA with the model. This could firstly potentially give us an idea of whether we have chosen appropriate yields for the task. Secondly, by comparing different environments, it could potentially give us an idea of which factors must be included to adequately capture the behaviour and which factors are insignificant. For example, it may be that effects of NO_x on yields simply cannot be ignored or that we need more tracers or a volatility basis set to capture the contribution to early growth. But it may also happen that these factors are nice-to-have's but are dominated by other effects in a climate perspective. Here, it may be fruitful to compare both more complex and ESM type models.

Additionally, more comparisons to observations are needed in general. One planned study like this, is to compare SOA and other organic aerosols in NorESM to a the dataset from Hyytiälä presented in *Heikkinen et al.* (2020) which constitutes the longest online time series on sub-micron aerosol chemical composition in a boreal environment.

In terms of understanding the role of BVOCs in historical climate change, an interesting project which we are planning to investigate further, is the effect of CO_2 fertilization on BVOC emissions over the historical period. This is seldom, to my knowledge, considered when calculating the forcing from BVOCs over the historical period, which usually just considers land use change and thus a reduction in BVOC emissions. Including CO_2 fertilization may largely counteract the reduction in BVOC emissions from land use change, even without the effect of temperature increase.

In this research we find that NPF in some regions and at least in excess, inhibits cloud droplet activation and reduces CDNC. While this effect has a physically sound

explanation and also has been seen in other models, we cannot know for sure whether it is exaggerated in NorESM. This effect does not seem to show up in the research by *Scott et al.* (2014), *Riccobono et al.* (2014) or *Merikanto et al.* (2009) for example, but these all use GLOMAP, which has a limited treatment of activation (e.g. assumes one updraft for ocean and one for land) and does not have prognostic clouds. Because there is a good chance that the distribution of the primary particles are of great importance for whether or not NPF enhances or inhibits cloud activation of aerosols, a good approach might be to use e.g. a more detailed box model and investigate with which primary emissions and which updrafts or hygroscopicities we would end up in which regime (NPF enhances/NPF inhibits cloud droplet activation).

Additionally comes factors that have been outside the scope of this thesis, but which may be very important in terms of assessing policy and future climates (point 2 and 3 above). The most prominent example of this is the effect of interactive chemistry – both on the SOA formation and on the concentration of tropospheric ozone (a green house gas) and the lifetime of methane.

With regards to point 3 above, concerning policy assessment, a very relevant question would be the climate impacts of a massive roll out of afforestation/reforestation/BECCS (*Shukla et al.*, 2019). This is part of all 1.5 ° target pathways presented in *IPCC* (2018) and policy decisions on these topics are imminent. In addition to the factors we have already mentioned, the forcing from chemical effect on ozone production and possibly methane lifetimes must also be considered. Since increased BVOC emissions increase the ozone concentrations in areas with sufficient NO_x (*Jia et al.*, 2019), this should be considered. With better overview over the different climate effects of BVOCs, one might for example opt for afforestation with trees which emit less BVOCs in total, but more monoterpene. Less BVOCs would entail less ozone, while monoterpenes have higher SOA yields which could increase the aerosol cooling.

5.3.1 Aerosol modelling development

While the process understanding of SOA is improving rapidly, there seems to be little convergence of the effects in ESMs. One may ask why this is. In future modelling developments, we must ask ourselves 1) which processes are best understood which are not included in models 2) can these be simplified enough to be inserted into ESMs? 3) are there processes which we can prove to be non-important?

5.3.2 Interactive chemistry

The oxidant chemistry is an example of a process which is well understood, but currently not treated interactively in most ESMs. The limit here is computational cost, so the argument must be made that interactive chemistry is important enough to be included. In the work with Papers III and IV we saw that adding a improved diurnal variation to the oxidant fields has a considerable impact of the NPF when also considering a super-linear nucleation parameterization. While our diurnal variation is an improvement (replacing a step function with a sine function during daylight hours), it will of course repeat the same pattern every day, while in reality it would change with both radiation and air mass origin. Additionally, in paper II, the EC-Earth is the only model with interactive chemistry. When isoprene is removed, this reduces the lifetime

of monoterpenes and thus the geographical distribution of the SOA formation. Though we do not try to assess the importance of these changes in Paper II, Paper IV illustrates that the geographical distribution is indeed important. Interactive chemistry would also allow for including the climate impacts of BVOCs through ozone chemistry and lifetimes of CH_4.

5.3.3 Limitations and potential developments of aerosol dynamics in NorESM

A possible weakness of NorESM is the way particles from nucleation cannot grow beyond the initial NPF mode. One might imagine that this exaggerates the relationship between CCN and NMR, because no particle gets to escape the mode. A potential future research project would therefore be to investigate if this simplification in NorESM is justified or not. If it is not, there are several ways this might be improved. One option would be to extend the sectional scheme to include the whole Aitken mode and e.g. rather add the particles to the modal scheme in the accumulation mode. This would of course require more processes to be included in the sectional scheme (cloud droplet activation, deposition etc). Another option would be to just add an accumulation mode to which the particles could grow.

5.4 Concluding remarks

The scientific knowledge of how BVOCs influence climate has dramatically increased in recent years. However, rather than decreasing the uncertainties, it has uncovered new ones. This thesis attempts to reduce these uncertainties by improving the modelling of early growth in NorESM and including feedback mechanisms which constrain NPF. It also, however, to a large extent concerns itself with distinguishing which processes are uncertain and why. This last point is perhaps more important than it might seem. In an ideal dream world of an ESM modeller, results from these kinds of studies would inform both lab experiments, observations and simulations with more detailed models to verify or falsify the effects seen in the models.

Acronyms

BSOA biogenic secondary organic aerosol. 15, 17, 42

BVOC niogenic volatile organic compounds. 5, 30, 32

CCN cloud condensation nuclei. 4, 11, 12, 14, 17–20, 36, 38, 46

CDNC cloud droplet number concentration. 17, 20, 38, 43, 44

CRE cloud radiative effect. 34

ERF effective radiative forcing. 10, 21, 38, 43

ERF$_{aci}$ effective radiative forcing from aerosol cloud interactions. 6, 38, 39, 42, 43

ERF$_{ari}$ effective radiative forcing from aerosol radiation interactions. 38

ESM earth system model. 5–7, 21, 23, 34, 35, 41, 43–46

GPP gross primary production. 15, 18, 24, 32

HOMs highly oxygenated organic molecules. 14, 16

LAI leaf area index. 15

NorESM Norwegian Earth System Model. 6

NPF new particle formation. 4, 11, 14, 25–27, 29, 30, 34–36, 38, 39, 41, 43–46

SOA secondary organic aerosol. i, 6, 7, 15–18, 23, 25, 35, 41–46

Bibliography

Abdul-Razzak, H., and S. J. Ghan (2000), A parameterization of aerosol activation: 2. Multiple aerosol types, *J. Geophys. Res.*, *105*(D5), 6837–6844, doi:10.1029/1999JD901161. 3.1.3, 3.1.4

Albrecht, B. A. (1989), Aerosols, Cloud Microphysics, and Fractional Cloudiness, *Science*, *245*(4923), 1227–1230, doi:10.1126/science.245.4923.1227. 1.1, 2.3.4, 2.4

Arneth, A., Ü. Niinemets, S. Pressley, J. Bäck, P. Hari, T. Karl, S. Noe, I. C. Prentice, D. Serça, T. Hickler, A. Wolf, and B. Smith (2007), Process-based estimates of terrestrial ecosystem isoprene emissions: Incorporating the effects of a direct CO_2-isoprene interaction, *Atmospheric Chemistry and Physics*, *7*(1), 31–53, doi:10.5194/acp-7-31-2007. 2.3

Asmi, A., A. Wiedensohler, P. Laj, A.-M. Fjaeraa, K. Sellegri, W. Birmili, E. Weingartner, U. Baltensperger, V. Zdimal, N. Zikova, J.-P. Putaud, A. Marinoni, P. Tunved, H.-C. Hansson, M. Fiebig, N. Kivekäs, H. Lihavainen, E. Asmi, V. Ulevicius, P. P. Aalto, E. Swietlicki, A. Kristensson, N. Mihalopoulos, N. Kalivitis, I. Kalapov, G. Kiss, G. de Leeuw, B. Henzing, R. M. Harrison, D. Beddows, C. O'Dowd, S. G. Jennings, H. Flentje, K. Weinhold, F. Meinhardt, L. Ries, and M. Kulmala (2011), Number size distributions and seasonality of submicron particles in Europe 2008–2009, *Atmospheric Chemistry and Physics*, *11*(11), 5505–5538, doi:10.5194/acp-11-5505-2011. 4.2.3

Bellouin, N., J. Quaas, E. Gryspeerdt, S. Kinne, P. Stier, D. Watson-Parris, O. Boucher, K. S. Carslaw, M. Christensen, A.-L. Daniau, J.-L. Dufresne, G. Feingold, S. Fiedler, P. Forster, A. Gettelman, J. M. Haywood, U. Lohmann, F. Malavelle, T. Mauritsen, D. T. McCoy, G. Myhre, J. Mülmenstädt, D. Neubauer, A. Possner, M. Rugenstein, Y. Sato, M. Schulz, S. E. Schwartz, O. Sourdeval, T. Storelvmo, V. Toll, D. Winker, and B. Stevens (2020), Bounding Global Aerosol Radiative Forcing of Climate Change, *Reviews of Geophysics*, *58*(1), e2019RG000,660, doi:10.1029/2019RG000660. 2.4

Bentsen, M., I. Bethke, J. B. Debernard, T. Iversen, A. Kirkevåg, Ø. Seland, H. Drange, C. Roelandt, I. A. Seierstad, C. Hoose, and J. E. Kristjánsson (2013), The Norwegian Earth System Model, NorESM1-M – Part 1: Description and basic evaluation of the physical climate, *Geoscientific Model Development*, *6*(3), 687–720, doi:10.5194/gmd-6-687-2013. 3.1.1

Bianchi, F., J. Tröstl, H. Junninen, C. Frege, S. Henne, C. R. Hoyle, U. Molteni, E. Herrmann, A. Adamov, N. Bukowiecki, X. Chen, J. Duplissy, M. Gysel, M. Hutterli,

J. Kangasluoma, J. Kontkanen, A. Kürten, H. E. Manninen, S. Münch, O. Peräkylä, T. Petäjä, L. Rondo, C. Williamson, E. Weingartner, J. Curtius, D. R. Worsnop, M. Kulmala, J. Dommen, and U. Baltensperger (2016), New particle formation in the free troposphere: A question of chemistry and timing, *Science*, p. aad5456, doi: 10.1126/science.aad5456. 1.1, 2.2.1, 2.3.2

Bjordal, J., T. Storelvmo, K. Alterskjær, and T. Carlsen (2020), Equilibrium climate sensitivity above 5 °C plausible due to state-dependent cloud feedback, *Nature Geoscience*, *13*(11), 718–721, doi:10.1038/s41561-020-00649-1. 2.1

Blichner, S. M., M. K. Sporre, R. Makkonen, and T. K. Berntsen (2020a), Implementing a sectional scheme for early aerosol growth from new particle formation in the Norwegian Earth System Model v2: Comparison to observations and climate impacts, *Geoscientific Model Development Discussions*, pp. 1–45, doi: 10.5194/gmd-2020-357. 1.2, 5.2

Blichner, S. M., M. K. Sporre, and T. K. Berntsen (2020b), Reduced ERF_{aci} with combining a sectional scheme for early growth with a model scheme in earth system model, *To be submitted to Atmospheric Chemistry and Physics*. 1.2, 5.2

Bogenschutz, P. A., A. Gettelman, H. Morrison, V. E. Larson, C. Craig, and D. P. Schanen (2013), Higher-Order Turbulence Closure and Its Impact on Climate Simulations in the Community Atmosphere Model, *Journal of Climate*, *26*(23), 9655–9676, doi: 10.1175/JCLI-D-13-00075.1. 3.1.3

Bogenschutz, P. A., A. Gettelman, C. Hannay, V. E. Larson, R. B. Neale, C. Craig, and C.-C. Chen (2018), The path to CAM6: Coupled simulations with CAM5.4 and CAM5.5, *Geoscientific Model Development*, *11*(1), 235–255, doi:10.5194/gmd-11-235-2018. 3.1.1

Boucher, O., D. Randall, P. Artaxo, C. Bretherton, G. Feingold, P. Forster, V.-M. Kerminen, Y. Kondo, H. Liao, U. Lohmann, P. Rasch, S. Satheesh, S. Sherwood, B. Stevens, and X. Zhang (2013), Clouds and Aerosols, in *Climate Change 2013: The Physical Science Basis. Contribution of Working Group I to the Fifth Assessment Report of the Intergovernmental Panel on Climate Change*, edited by T. Stocker, D. Qin, G.-K. Plattner, M. Tignor, S. Allen, J. Boschung, A. Nauels, Y. Xia, V. Bex, and P. Midgley, pp. 571–658, Cambridge University Press, Cambridge, United Kingdom and New York, NY, USA. 1.1, 2.2, 2.2, 2.1, 2.3, 2.4, 2.4

Bretherton, C. S., and S. Park (2009), A New Moist Turbulence Parameterization in the Community Atmosphere Model, *Journal of Climate*, *22*(12), 3422–3448, doi: 10.1175/2008JCLI2556.1. 3.1.3

Carslaw, K. S., L. A. Lee, C. L. Reddington, G. W. Mann, and K. J. Pringle (2013a), The magnitude and sources of uncertainty in global aerosol, *Faraday Discuss.*, *165*(0), 495–512, doi:10.1039/C3FD00043E. 2.2.1

Carslaw, K. S., L. A. Lee, C. L. Reddington, K. J. Pringle, A. Rap, P. M. Forster, G. W. Mann, D. V. Spracklen, M. T. Woodhouse, L. A. Regayre, and J. R. Pierce (2013b), Large contribution of natural aerosols to uncertainty in indirect forcing, *Nature*, *503*(7474), 67–71, doi:10.1038/nature12674. 2.2.1, 2.3.3, 2.4

Danabasoglu, G., J.-F. Lamarque, J. Bacmeister, D. A. Bailey, A. K. DuVivier, J. Edwards, L. K. Emmons, J. Fasullo, R. Garcia, A. Gettelman, C. Hannay, M. M. Holland, W. G. Large, P. H. Lauritzen, D. M. Lawrence, J. T. M. Lenaerts, K. Lindsay, W. H. Lipscomb, M. J. Mills, R. Neale, K. W. Oleson, B. Otto-Bliesner, A. S. Phillips, W. Sacks, S. Tilmes, L. van Kampenhout, M. Vertenstein, A. Bertini, J. Dennis, C. Deser, C. Fischer, B. Fox-Kemper, J. E. Kay, D. Kinnison, P. J. Kushner, V. E. Larson, M. C. Long, S. Mickelson, J. K. Moore, E. Nienhouse, L. Polvani, P. J. Rasch, and W. G. Strand (2020), The Community Earth System Model Version 2 (CESM2), *Journal of Advances in Modeling Earth Systems*, *12*(2), e2019MS001,916, doi:10.1029/2019MS001916. 3.1.1

Dentener, F., S. Kinne, T. Bond, O. Boucher, J. Cofala, S. Generoso, P. Ginoux, S. Gong, J. J. Hoelzemann, A. Ito, L. Marelli, J. E. Penner, J.-P. Putaud, C. Textor, M. Schulz, G. R. van der Werf, and J. Wilson (2006), Emissions of primary aerosol and precursor gases in the years 2000 and 1750 prescribed datasets for AeroCom, *Atmospheric Chemistry and Physics*, *6*(12), 4321–4344, doi: 10.5194/acp-6-4321-2006. 3.1.4

Dunne, E. M., H. Gordon, A. Kürten, J. Almeida, J. Duplissy, C. Williamson, I. K. Ortega, K. J. Pringle, A. Adamov, U. Baltensperger, P. Barmet, F. Benduhn, F. Bianchi, M. Breitenlechner, A. Clarke, J. Curtius, J. Dommen, N. M. Donahue, S. Ehrhart, R. C. Flagan, A. Franchin, R. Guida, J. Hakala, A. Hansel, M. Heinritzi, T. Jokinen, J. Kangasluoma, J. Kirkby, M. Kulmala, A. Kupc, M. J. Lawler, K. Lehtipalo, V. Makhmutov, G. Mann, S. Mathot, J. Merikanto, P. Miettinen, A. Nenes, A. Onnela, A. Rap, C. L. S. Reddington, F. Riccobono, N. A. D. Richards, M. P. Rissanen, L. Rondo, N. Sarnela, S. Schobesberger, K. Sengupta, M. Simon, M. Sipilä, J. N. Smith, Y. Stozkhov, A. Tomé, J. Tröstl, P. E. Wagner, D. Wimmer, P. M. Winkler, D. R. Worsnop, and K. S. Carslaw (2016), Global atmospheric particle formation from CERN CLOUD measurements, *Science*, *354*(6316), 1119–1124, doi: 10.1126/science.aaf2649. 2.2.1

Ehn, M., J. A. Thornton, E. Kleist, M. Sipilä, H. Junninen, I. Pullinen, M. Springer, F. Rubach, R. Tillmann, B. Lee, F. Lopez-Hilfiker, S. Andres, I.-H. Acir, M. Rissanen, T. Jokinen, S. Schobesberger, J. Kangasluoma, J. Kontkanen, T. Nieminen, T. Kurtén, L. B. Nielsen, S. Jørgensen, H. G. Kjaergaard, M. Canagaratna, M. D. Maso, T. Berndt, T. Petäjä, A. Wahner, V.-M. Kerminen, M. Kulmala, D. R. Worsnop, J. Wildt, and T. F. Mentel (2014), A large source of low-volatility secondary organic aerosol, *Nature*, *506*(7489), 476–479, doi:10.1038/nature13032. 2.3.1, 2.3.2

Emmons, L. K., S. Walters, P. G. Hess, J.-F. Lamarque, G. G. Pfister, D. Fillmore, C. Granier, A. Guenther, D. Kinnison, T. Laepple, J. Orlando, X. Tie, G. Tyndall, C. Wiedinmyer, S. L. Baughcum, and S. Kloster (2010), Description and evaluation of the Model for Ozone and Related chemical Tracers, version 4 (MOZART-4), *Geoscientific Model Development*, *3*(1), 43–67, doi:10.5194/gmd-3-43-2010. 3.1.4

Flato, G., J. Marotzke, B. Abiodun, P. Braconnot, S. Chou, W. Collins, P. Cox, F. Driouech, S. Emori, V. Eyring, C. Forest, P. Gleckler, E. Guilyardi, C. Jakob, V. Kattsov, C. Reason, and M. Rummukainen (2013), Evaluation of Climate Models, in *Climate Change 2013: The Physical Science Basis. Contribution of Work-*

ing Group I to the Fifth Assessment Report of the Intergovernmental Panel on Climate Change, edited by T. Stocker, D. Qin, G.-K. Plattner, M. Tignor, S. Allen, J. Boschung, A. Nauels, Y. Xia, V. Bex, and P. Midgley, pp. 741–866, Cambridge University Press, Cambridge, United Kingdom and New York, NY, USA, doi:10.1017/CBO9781107415324.020. 1.1, 2.5

Gettelman, A., and H. Morrison (2015), Advanced Two-Moment Bulk Microphysics for Global Models. Part I: Off-Line Tests and Comparison with Other Schemes, *J. Climate*, *28*(3), 1268–1287, doi:10.1175/JCLI-D-14-00102.1. 3.1.3

Gettelman, A., H. Morrison, and S. J. Ghan (2008), A New Two-Moment Bulk Stratiform Cloud Microphysics Scheme in the Community Atmosphere Model, Version 3 (CAM3). Part II: Single-Column and Global Results, *Journal of Climate*, *21*(15), 3660–3679, doi:10.1175/2008JCLI2116.1. 3.1.3

Glasius, M., and A. H. Goldstein (2016), Recent Discoveries and Future Challenges in Atmospheric Organic Chemistry, *Environ. Sci. Technol.*, *50*(6), 2754–2764, doi:10.1021/acs.est.5b05105. 2.3

Golaz, J.-C., V. E. Larson, and W. R. Cotton (2002), A PDF-Based Model for Boundary Layer Clouds. Part I: Method and Model Description, *Journal of Atmospheric Sciences*, *59*(24), 3540–3551, doi:10.1175/1520-0469(2002)059<3540:APBMFB>2.0.CO;2. 3.1.3

Gordon, H., K. Sengupta, A. Rap, J. Duplissy, C. Frege, C. Williamson, M. Heinritzi, M. Simon, C. Yan, J. Almeida, J. Tröstl, T. Nieminen, I. K. Ortega, R. Wagner, E. M. Dunne, A. Adamov, A. Amorim, A.-K. Bernhammer, F. Bianchi, M. Breitenlechner, S. Brilke, X. Chen, J. S. Craven, A. Dias, S. Ehrhart, L. Fischer, R. C. Flagan, A. Franchin, C. Fuchs, R. Guida, J. Hakala, C. R. Hoyle, T. Jokinen, H. Junninen, J. Kangasluoma, J. Kim, J. Kirkby, M. Krapf, A. Kürten, A. Laaksonen, K. Lehtipalo, V. Makhmutov, S. Mathot, U. Molteni, S. A. Monks, A. Onnela, O. Peräkylä, F. Piel, T. Petäjä, A. P. Praplan, K. J. Pringle, N. A. D. Richards, M. P. Rissanen, L. Rondo, N. Sarnela, S. Schobesberger, C. E. Scott, J. H. Seinfeld, S. Sharma, M. Sipilä, G. Steiner, Y. Stozhkov, F. Stratmann, A. Tomé, A. Virtanen, A. L. Vogel, A. C. Wagner, P. E. Wagner, E. Weingartner, D. Wimmer, P. M. Winkler, P. Ye, X. Zhang, A. Hansel, J. Dommen, N. M. Donahue, D. R. Worsnop, U. Baltensperger, M. Kulmala, J. Curtius, and K. S. Carslaw (2016), Reduced anthropogenic aerosol radiative forcing caused by biogenic new particle formation, *Proceedings of the National Academy of Sciences*, *113*(43), 12,053–12,058, doi:10.1073/pnas.1602360113. 1.1, 2.2.1, 2.3.2, 2.3.3

Gordon, H., J. Kirkby, U. Baltensperger, F. Bianchi, M. Breitenlechner, J. Curtius, A. Dias, J. Dommen, N. M. Donahue, E. M. Dunne, J. Duplissy, S. Ehrhart, R. C. Flagan, C. Frege, C. Fuchs, A. Hansel, C. R. Hoyle, M. Kulmala, A. Kürten, K. Lehtipalo, V. Makhmutov, U. Molteni, M. P. Rissanen, Y. Stozkhov, J. Tröstl, G. Tsagkogeorgas, R. Wagner, C. Williamson, D. Wimmer, P. M. Winkler, C. Yan, and K. S. Carslaw (2017), Causes and importance of new particle formation in the present-day

and preindustrial atmospheres: CAUSES AND ROLE OF NEW PARTICLE FORMATION, *Journal of Geophysical Research: Atmospheres*, *122*(16), 8739–8760, doi:10.1002/2017JD026844. 2.3.2

Gregory, J. M., W. J. Ingram, M. A. Palmer, G. S. Jones, P. A. Stott, R. B. Thorpe, J. A. Lowe, T. C. Johns, and K. D. Williams (2004), A new method for diagnosing radiative forcing and climate sensitivity, *Geophys. Res. Lett.*, *31*(3), L03,205, doi: 10.1029/2003GL018747. 2.1, 2.1

Guenther, A. B., X. Jiang, C. L. Heald, T. Sakulyanontvittaya, T. Duhl, L. K. Emmons, and X. Wang (2012), The Model of Emissions of Gases and Aerosols from Nature version 2.1 (MEGAN2.1): An extended and updated framework for modeling biogenic emissions, *Geoscientific Model Development*, *5*(6), 1471–1492, doi: 10.5194/gmd-5-1471-2012. 2.3.4, 3.1.2

Hansen, J., M. Sato, R. Ruedy, L. Nazarenko, A. Lacis, G. A. Schmidt, G. Russell, I. Aleinov, M. Bauer, S. Bauer, N. Bell, B. Cairns, V. Canuto, M. Chandler, Y. Cheng, A. D. Genio, G. Faluvegi, E. Fleming, A. Friend, T. Hall, C. Jackman, M. Kelley, N. Kiang, D. Koch, J. Lean, J. Lerner, K. Lo, S. Menon, R. Miller, P. Minnis, T. Novakov, V. Oinas, J. Perlwitz, J. Perlwitz, D. Rind, A. Romanou, D. Shindell, P. Stone, S. Sun, N. Tausnev, D. Thresher, B. Wielicki, T. Wong, M. Yao, and S. Zhang (2005), Efficacy of climate forcings, *Journal of Geophysical Research: Atmospheres*, *110*(D18), doi:10.1029/2005JD005776. 2.1, 2.5

Heald, C. L., and J. A. Geddes (2016), The impact of historical land use change from 1850 to 2000 on secondary particulate matter and ozone, *Atmos. Chem. Phys.*, *16*(23), 14,997–15,010, doi:10.5194/acp-16-14997-2016. 1.1, 2.3.3

Heald, C. L., and D. V. Spracklen (2015), Land Use Change Impacts on Air Quality and Climate, *Chemical Reviews*, *115*(10), 4476–4496, doi:10.1021/cr500446g. 2.3, 2.3.4

Heikkinen, L., M. Äijälä, M. Riva, K. Luoma, K. Dällenbach, J. Aalto, P. Aalto, D. Aliaga, M. Aurela, H. Keskinen, U. Makkonen, P. Rantala, M. Kulmala, T. Petäjä, D. Worsnop, and M. Ehn (2020), Long-term sub-micrometer aerosol chemical composition in the boreal forest: Inter- and intra-annual variability, *Atmospheric Chemistry and Physics*, *20*(5), 3151–3180, doi:10.5194/acp-20-3151-2020. 5.3

Heinritzi, M., L. Dada, M. Simon, D. Stolzenburg, A. C. Wagner, L. Fischer, L. R. Ahonen, S. Amanatidis, R. Baalbaki, A. Baccarini, P. S. Bauer, B. Baumgartner, F. Bianchi, S. Brilke, D. Chen, R. Chiu, A. Dias, J. Dommen, J. Duplissy, H. Finkenzeller, C. Frege, C. Fuchs, O. Garmash, H. Gordon, M. Granzin, I. El Haddad, X. He, J. Helm, V. Hofbauer, C. R. Hoyle, J. Kangasluoma, T. Keber, C. Kim, A. Kürten, H. Lamkaddam, T. M. Laurila, J. Lampilahti, C. P. Lee, K. Lehtipalo, M. Leiminger, H. Mai, V. Makhmutov, H. E. Manninen, R. Marten, S. Mathot, R. L. Mauldin, B. Mentler, U. Molteni, T. Müller, W. Nie, T. Nieminen, A. Onnela, E. Partoll, M. Passananti, T. Petäjä, J. Pfeifer, V. Pospisilova, L. L. J. Quéléver, M. P. Rissanen, C. Rose, S. Schobesberger, W. Scholz, K. Scholze, M. Sipilä, G. Steiner, Y. Stozhkov, C. Tauber, Y. J. Tham, M. Vazquez-Pufleau, A. Virtanen, A. L. Vogel, R. Volkamer,

R. Wagner, M. Wang, L. Weitz, D. Wimmer, M. Xiao, C. Yan, P. Ye, Q. Zha, X. Zhou, A. Amorim, U. Baltensperger, A. Hansel, M. Kulmala, A. Tomé, P. M. Winkler, D. R. Worsnop, N. M. Donahue, J. Kirkby, and J. Curtius (2020), Molecular understanding of the suppression of new-particle formation by isoprene, *Atmospheric Chemistry and Physics*, *20*(20), 11,809–11,821, doi:10.5194/acp-20-11809-2020. 2.2.1, 2.3.1

Hurrell, J. W., M. M. Holland, P. R. Gent, S. Ghan, J. E. Kay, P. J. Kushner, J.-F. Lamarque, W. G. Large, D. Lawrence, K. Lindsay, W. H. Lipscomb, M. C. Long, N. Mahowald, D. R. Marsh, R. B. Neale, P. Rasch, S. Vavrus, M. Vertenstein, D. Bader, W. D. Collins, J. J. Hack, J. Kiehl, and S. Marshall (2013), The Community Earth System Model: A Framework for Collaborative Research, *Bull. Amer. Meteor. Soc.*, *94*(9), 1339–1360, doi:10.1175/BAMS-D-12-00121.1. 3.1.1

IPCC (2018), Summary for policymakers. in:, in *Global Warming of 1.5°C. An IPCC Special Report on the impacts of global warming of 1.5°C above pre-industrial levels and related global greenhouse gas emission pathways, in the context of strengthening the global response to the threat of climate change, sustainable development, and efforts to eradicate poverty*, edited by V. Masson-Delmotte, P. Zhai, H.-O. Pörtner, D. Roberts, J. Skea, P. Shukla, A. Pirani, W. Moufouma-Okia, C. Péan, R. Pidcock, S. Connors, J. Matthews, Y. Chen, X. Zhou, M. Gomis, E. Lonnoy, T. Maycock, M. Tignor, and T. Waterfield, In Press. 5.3

Iversen, T., M. Bentsen, I. Bethke, J. B. Debernard, A. Kirkevåg, Ø. Seland, H. Drange, J. E. Kristjansson, I. Medhaug, M. Sand, and I. A. Seierstad (2013), The Norwegian Earth System Model, NorESM1-M – Part 2: Climate response and scenario projections, *Geoscientific Model Development*, *6*(2), 389–415, doi:10.5194/gmd-6-389-2013. 3.1.1

Jacobson, M. Z. (1997), Development and application of a new air pollution modeling system — Part III. Aerosol-phase simulations, *Atmospheric Environment*, *31*(4), 587–608, doi:10.1016/S1352-2310(96)00201-4. 3.2

Jacobson, M. Z. (2005), *Fundamentals of Atmospheric Modeling: Second Edition*, second ed., Cambridge University Press, Cambridge, doi:10.1017/CBO9781139165389. 3.2

Jia, G., E. Shevliakova, P. Artaxo, N. De Noblet-Ducoudré, R. Houghton, J. House, K. Kitajima, C. Lennard, A. Popp, A. Sirin, R. Sukumar, and L. Verchot (2019), Land–climate interactions., in *Climate Change and Land: An IPCC Special Report on Climate Change, Desertification, Land Degradation, Sustainable Land Management, Food Security, and Greenhouse Gas Fluxes in Terrestrial Ecosystems*, In press. 2.3, 5.3

Jokinen, T., T. Berndt, R. Makkonen, V.-M. Kerminen, H. Junninen, P. Paasonen, F. Stratmann, H. Herrmann, A. B. Guenther, D. R. Worsnop, M. Kulmala, M. Ehn, and M. Sipilä (2015), Production of extremely low volatile organic compounds from biogenic emissions: Measured yields and atmospheric implications, *PNAS*, *112*(23), 7123–7128, doi:10.1073/pnas.1423977112. 2.3.1, 2.3.2

Karset, I. H. H. (2020), Enhancing the confidence in estimates of effective radiative forcing by aerosol through improved global modelling, Ph.D. thesis, University of Oslo, Oslo. 3.1.4

Kerminen, V.-M., X. Chen, V. Vakkari, T. Petäjä, M. Kulmala, and F. Bianchi (2018), Atmospheric new particle formation and growth: Review of field observations, *Environ. Res. Lett.*, *13*(10), 103,003, doi:10.1088/1748-9326/aadf3c. 2.2.1, 2.3.2

Kirkby, J., J. Duplissy, K. Sengupta, C. Frege, C. Gordon, H. Williamson, M. Heinritzi, M. Simon, C. Yan, J. Almeida, J. Tröstl, T. Nieminen, Ortega, R. Wagner, A. Adamov, A. Amorim, A. Bernhammer, F. Bianchi, M. Breitenlechner, S. Brilke, X. Chen, J. Craven, A. Dias, S. Ehrhart, R. C. Flagan, A. Franchin, C. Fuchs, R. Guida, J. Hakala, C. R. Hoyle, T. Jokinen, J. Junninen, H. Kangasluoma, J. Kim, A. Krapf, M. Kürten, A. Laaksonen, K. Lehtipalo, V. Makhmutov, S. Mathot, U. Molteni, A. Onnela, O. Peräkylä, F. Piel, T. Petäjä, A. P. Praplan, K. Pringle, A. Rap, N. Richards, I. Riipinen, M. P. Rissanen, L. Rondo, N. Sarnela, S. Schobesberger, C. Scott, J. H. Seinfeld, M. Sipilä, G. Steiner, Y. Stozhkov, F. Stratmann, A. Tomé, A. Virtanen, A. Vogel, A. Wagner, P. Wagner, E. Weingartner, D. Wimmer, P. Winkler, P. Ye, X. Zhang, A. Hansel, J. Dommen, N. M. Donahue, D. Worsnop, U. Baltensperger, M. Kulmala, K. S. Carslaw, and J. Curtius (2016), Ion-induced nucleation of pure biogenic particles, *Nature*, doi:10.1038/nature17953. 1.1, 2.2.1, 2.3.2

Kirkevåg, A., T. Iversen, Ø. Seland, C. Hoose, J. E. Kristjánsson, H. Struthers, A. M. L. Ekman, S. Ghan, J. Griesfeller, E. D. Nilsson, and M. Schulz (2013), Aerosol–climate interactions in the Norwegian Earth System Model – NorESM1-M, *Geosci. Model Dev.*, *6*(1), 207–244, doi:10.5194/gmd-6-207-2013. 3.1.1, 3.1.4

Kirkevåg, A., A. Grini, D. Olivié, Ø. Seland, K. Alterskjær, M. Hummel, I. H. H. Karset, A. Lewinschal, X. Liu, R. Makkonen, I. Bethke, J. Griesfeller, M. Schulz, and T. Iversen (2018a), A production-tagged aerosol module for earth system models, OsloAero5.3 – extensions and updates for CAM5.3-Oslo, *Geoscientific Model Development Discussions*, pp. 1–72, doi:10.5194/gmd-2018-46. 3.1.1

Kirkevåg, A., A. Grini, D. Olivié, Ø. Seland, K. Alterskjær, M. Hummel, I. H. H. Karset, A. Lewinschal, X. Liu, R. Makkonen, I. Bethke, J. Griesfeller, M. Schulz, and T. Iversen (2018b), A production-tagged aerosol module for Earth system models, OsloAero5.3 – extensions and updates for CAM5.3-Oslo, *Geoscientific Model Development*, *11*(10), 3945–3982, doi:10.5194/gmd-11-3945-2018. 3.1.3

Köhler, H. (1936), The nucleus in and the growth of hygroscopic droplets, *Transactions of the Faraday Society*, *32*(0), 1152–1161, doi:10.1039/TF9363201152. 2.4, 2.4

Kokkola, H., H. Korhonen, K. E. J. Lehtinen, R. Makkonen, A. Asmi, S. Järvenoja, T. Anttila, A.-I. Partanen, M. Kulmala, H. Järvinen, A. Laaksonen, and V.-M. Kerminen (2008), SALSA – a Sectional Aerosol module for Large Scale Applications, *Atmospheric Chemistry and Physics*, *8*(9), 2469–2483, doi:10.5194/acp-8-2469-2008. 2.6

Kulmala, M., T. Suni, K. E. J. Lehtinen, M. Dal Maso, M. Boy, A. Reissell, Ü. Rannik, P. Aalto, P. Keronen, H. Hakola, J. Bäck, T. Hoffmann, T. Vesala, and P. Hari (2004), A new feedback mechanism linking forests, aerosols, and climate, *Atmos. Chem. Phys.*, *4*(2), 557–562, doi:10.5194/acp-4-557-2004. 2.3, 2.3.4

Kulmala, M., T. Nieminen, R. Chellapermal, R. Makkonen, J. Bäck, and V.-M. Kerminen (2013), Climate Feedbacks Linking the Increasing Atmospheric CO2 Concentration, BVOC Emissions, Aerosols and Clouds in Forest Ecosystems, in *Biology, Controls and Models of Tree Volatile Organic Compound Emissions*, edited by Ü. Niinemets and R. K. Monson, pp. 489–508, Springer Netherlands, Dordrecht. 2.3, 2.3.4

Kulmala, M., T. Nieminen, A. Nikandrova, K. Lehtipalo, H. E. Manninen, M. K. Kajos, P. Kolari, A. Lauri, T. Petäjä, R. Krejci, T. Vesala, V. M. Kerminen, T. Nieminen, P. Kolari, P. Hari, J. Bäck, R. Krejci, H. C. Hansson, E. Swietlicki, A. Lindroth, T. R. Christensen, and A. Arneth (2014), CO2-induced terrestrial climate feedback mechanism: From carbon sink to aerosol source and back, *Boreal Environment Research*, *19*, 122–131. 2.3.4

Lamb, D., and J. Verlinde (2011), *Physics and Chemistry of Clouds*, Cambridge University Press, Cambridge, doi:10.1017/CBO9780511976377. 2.5

Lawrence, D. M., R. A. Fisher, C. D. Koven, K. W. Oleson, S. C. Swenson, G. Bonan, N. Collier, B. Ghimire, L. van Kampenhout, D. Kennedy, E. Kluzek, P. J. Lawrence, F. Li, H. Li, D. Lombardozzi, W. J. Riley, W. J. Sacks, M. Shi, M. Vertenstein, W. R. Wieder, C. Xu, A. A. Ali, A. M. Badger, G. Bisht, M. van den Broeke, M. A. Brunke, S. P. Burns, J. Buzan, M. Clark, A. Craig, K. Dahlin, B. Drewniak, J. B. Fisher, M. Flanner, A. M. Fox, P. Gentine, F. Hoffman, G. Keppel-Aleks, R. Knox, S. Kumar, J. Lenaerts, L. R. Leung, W. H. Lipscomb, Y. Lu, A. Pandey, J. D. Pelletier, J. Perket, J. T. Randerson, D. M. Ricciuto, B. M. Sanderson, A. Slater, Z. M. Subin, J. Tang, R. Q. Thomas, M. V. Martin, and X. Zeng (2019), The Community Land Model Version 5: Description of New Features, Benchmarking, and Impact of Forcing Uncertainty, *Journal of Advances in Modeling Earth Systems*, *11*(12), 4245–4287, doi:10.1029/2018MS001583. 3.1.1

Lee, Y. H., J. R. Pierce, and P. J. Adams (2013), Representation of nucleation mode microphysics in a global aerosol model with sectional microphysics, *Geoscientific Model Development*, *6*(4), 1221–1232, doi:10.5194/gmd-6-1221-2013. 1.2, 3.2

Lehtinen, K. E. J., M. Dal Maso, M. Kulmala, and V.-M. Kerminen (2007), Estimating nucleation rates from apparent particle formation rates and vice versa: Revised formulation of the Kerminen–Kulmala equation, *Journal of Aerosol Science*, *38*(9), 988–994, doi:10.1016/j.jaerosci.2007.06.009. 3.1.4, 3.2, 3.2, 4.1, 4.1

Liu, X., J. E. Penner, and M. Herzog (2005), Global modeling of aerosol dynamics: Model description, evaluation, and interactions between sulfate and nonsulfate aerosols, *Journal of Geophysical Research: Atmospheres*, *110*(D18), doi:10.1029/2004JD005674. 2.6

Liu, X., P.-L. Ma, H. Wang, S. Tilmes, B. Singh, R. C. Easter, S. J. Ghan, and P. J. Rasch (2016), Description and evaluation of a new four-mode version of the Modal Aerosol Module (MAM4) within version 5.3 of the Community Atmosphere Model, *Geosci. Model Dev.*, *9*(2), 505–522, doi:10.5194/gmd-9-505-2016. 3.1.1

Makkonen, R., A. Asmi, V.-M. Kerminen, M. Boy, A. Arneth, A. Guenther, and M. Kulmala (2012), BVOC-aerosol-climate interactions in the global aerosol-climate model ECHAM5.5-HAM2, *Atmos. Chem. Phys.*, *12*(21), 10,077–10,096, doi:10.5194/acp-12-10077-2012. 2.3

Malavelle, F. F., J. M. Haywood, A. Jones, A. Gettelman, L. Clarisse, S. Bauduin, R. P. Allan, I. H. H. Karset, J. E. Kristjánsson, L. Oreopoulos, N. Cho, D. Lee, N. Bellouin, O. Boucher, D. P. Grosvenor, K. S. Carslaw, S. Dhomse, G. W. Mann, A. Schmidt, H. Coe, M. E. Hartley, M. Dalvi, A. A. Hill, B. T. Johnson, C. E. Johnson, J. R. Knight, F. M. O'Connor, D. G. Partridge, P. Stier, G. Myhre, S. Platnick, G. L. Stephens, H. Takahashi, and T. Thordarson (2017), Strong constraints on aerosol–cloud interactions from volcanic eruptions, *Nature*, *546*(7659), 485–491, doi:10.1038/nature22974. 2.4

Mann, G. W., K. S. Carslaw, D. V. Spracklen, D. A. Ridley, P. T. Manktelow, M. P. Chipperfield, S. J. Pickering, and C. E. Johnson (2010), Description and evaluation of GLOMAP-mode: A modal global aerosol microphysics model for the UKCA composition-climate model, *Geoscientific Model Development*, *3*(2), 519–551, doi:10.5194/gmd-3-519-2010. 2.6

McFiggans, G., T. F. Mentel, J. Wildt, I. Pullinen, S. Kang, E. Kleist, S. Schmitt, M. Springer, R. Tillmann, C. Wu, D. Zhao, M. Hallquist, C. Faxon, M. L. Breton, Å. M. Hallquist, D. Simpson, R. Bergström, M. E. Jenkin, M. Ehn, J. A. Thornton, M. R. Alfarra, T. J. Bannan, C. J. Percival, M. Priestley, D. Topping, and A. Kiendler-Scharr (2019), Secondary organic aerosol reduced by mixture of atmospheric vapours, *Nature*, *565*(7741), 587, doi:10.1038/s41586-018-0871-y. 2.2.1, 2.3.1

Merikanto, J., D. V. Spracklen, G. W. Mann, S. J. Pickering, and K. S. Carslaw (2009), Impact of nucleation on global CCN, *Atmos. Chem. Phys.*, *9*(21), 8601–8616, doi:10.5194/acp-9-8601-2009. 5.3

Mohr, C., J. A. Thornton, A. Heitto, F. D. Lopez-Hilfiker, A. Lutz, I. Riipinen, J. Hong, N. M. Donahue, M. Hallquist, T. Petäjä, M. Kulmala, and T. Yli-Juuti (2019), Molecular identification of organic vapors driving atmospheric nanoparticle growth, *Nature Communications*, *10*(1), 4442, doi:10.1038/s41467-019-12473-2. 2.3.2

Morrison, H., and A. Gettelman (2008), A New Two-Moment Bulk Stratiform Cloud Microphysics Scheme in the Community Atmosphere Model, Version 3 (CAM3). Part I: Description and Numerical Tests, *Journal of Climate*, *21*(15), 3642–3659, doi:10.1175/2008JCLI2105.1. 3.1.3

Myhre, G., D. Shindell, F.-M. Bréon, W. Collins, J. Fuglestvedt, J. Huang, D. Koch, J.-F. Lamarque, D. Lee, B. Mendoza, T. Nakajima, A. Robock, G. Stephens, T. Takemura, and H. Zhang (2013), Anthropogenic and Natural Radiative Forcing, in *Cli-*

mate Change 2013: The Physical Science Basis. Contribution of Working Group I to the Fifth Assessment Report of the Intergovernmental Panel on Climate Change, edited by T. Stocker, D. Qin, G.-K. Plattner, M. Tignor, S. Allen, J. Boschung, A. Nauels, Y. Xia, V. Bex, and P. Midgley, pp. 659–740, Cambridge University Press, Cambridge, United Kingdom and New York, NY, USA. 2.1, 2.1

Neale, R. B., A. Gettelman, S. Park, C.-c. Chen, P. H. Lauritzen, D. L. Williamson, A. J. Conley, D. Kinnison, D. Marsh, A. K. Smith, F. Vitt, R. Garcia, J.-f. Lamarque, M. Mills, S. Tilmes, H. Morrison, P. Cameron-smith, W. D. Collins, M. J. Iacono, R. C. Easter, X. Liu, S. J. Ghan, P. J. Rasch, and M. a Taylor (2012), Description of the NCAR Community Atmosphere Model (CAM 5.0). NCAR Technical Notes., *Ncar/Tn-464+Str*, p. 214, doi:10.5065/D6N877R0. 3.1.1

Nieminen, T., K. E. J. Lehtinen, and M. Kulmala (2010), Sub-10 nm particle growth by vapor condensation – effects of vapor molecule size and particle thermal speed, *Atmospheric Chemistry and Physics*, *10*(20), 9773–9779, doi:10.5194/acp-10-9773-2010. 2.2.1

Olenius, T., and I. Riipinen (2017), Molecular-resolution simulations of new particle formation: Evaluation of common assumptions made in describing nucleation in aerosol dynamics models, *Aerosol Science and Technology*, *51*(4), 397–408, doi:10.1080/02786826.2016.1262530. 1.2, 3.2

Oleson, K., M. Lawrence, B. Bonan, B. Drewniak, M. Huang, D. Koven, S. Levis, F. Li, J. Riley, M. Subin, S. Swenson, E. Thornton, A. Bozbiyik, R. Fisher, L. Heald, E. Kluzek, J.-F. Lamarque, J. Lawrence, R. Leung, W. Lipscomb, P. Muszala, M. Ricciuto, J. Sacks, Y. Sun, J. Tang, and Z.-L. Yang (2013), Technical description of version 4.5 of the Community Land Model (CLM), doi:10.5065/D6RR1W7M. 3.1.1

Paasonen, P., T. Nieminen, E. Asmi, H. E. Manninen, T. Petäjä, C. Plass-Dülmer, H. Flentje, W. Birmili, A. Wiedensohler, U. Hõrrak, A. Metzger, A. Hamed, A. Laaksonen, M. C. Facchini, V.-M. Kerminen, and M. Kulmala (2010), On the roles of sulphuric acid and low-volatility organic vapours in the initial steps of atmospheric new particle formation, *Atmos. Chem. Phys.*, *10*(22), 11,223–11,242, doi:10.5194/acp-10-11223-2010. 2.2.1, 3.1.4, 3.2.1, 4.2, 4.1

Paasonen, P., A. Asmi, T. Petäjä, M. K. Kajos, M. Äijälä, H. Junninen, T. Holst, J. P. D. Abbatt, A. Arneth, W. Birmili, H. D. van der Gon, A. Hamed, A. Hoffer, L. Laakso, A. Laaksonen, W. R. Leaitch, C. Plass-Dülmer, S. C. Pryor, P. Räisänen, E. Swietlicki, A. Wiedensohler, D. R. Worsnop, V.-M. Kerminen, and M. Kulmala (2013), Warming-induced increase in aerosol number concentration likely to moderate climate change, *Nature Geoscience*, *6*(6), 438, doi:10.1038/ngeo1800. 2.3, 2.3.4

Peñuelas, J., and M. Staudt (2010), BVOCs and global change, *Trends in Plant Science*, *15*(3), 133–144, doi:10.1016/j.tplants.2009.12.005. 2.3, 2.3.4

Rap, A., C. E. Scott, C. L. Reddington, L. Mercado, R. J. Ellis, S. Garraway, M. J. Evans, D. J. Beerling, A. R. MacKenzie, C. N. Hewitt, and D. V. Spracklen (2018), Enhanced global primary production by biogenic aerosol via diffuse radiation fertilization, *Nature Geoscience*, p. 1, doi:10.1038/s41561-018-0208-3. 2.3

Riccobono, F., S. Schobesberger, C. E. Scott, J. Dommen, I. K. Ortega, L. Rondo, J. Almeida, A. Amorim, F. Bianchi, M. Breitenlechner, A. David, A. Downard, E. M. Dunne, J. Duplissy, S. Ehrhart, R. C. Flagan, A. Franchin, A. Hansel, H. Junninen, M. Kajos, H. Keskinen, A. Kupc, A. Kürten, A. N. Kvashin, A. Laaksonen, K. Lehtipalo, V. Makhmutov, S. Mathot, T. Nieminen, A. Onnela, T. Petäjä, A. P. Praplan, F. D. Santos, S. Schallhart, J. H. Seinfeld, M. Sipilä, D. V. Spracklen, Y. Stozhkov, F. Stratmann, A. Tomé, G. Tsagkogeorgas, P. Vaattovaara, Y. Viisanen, A. Vrtala, P. E. Wagner, E. Weingartner, H. Wex, D. Wimmer, K. S. Carslaw, J. Curtius, N. M. Donahue, J. Kirkby, M. Kulmala, D. R. Worsnop, and U. Baltensperger (2014), Oxidation Products of Biogenic Emissions Contribute to Nucleation of Atmospheric Particles, *Science*, *344*(6185), 717–721, doi:10.1126/science.1243527. 1.1, 2.2.1, 2.3.2, 3.2.1, 5.1, 5.3

Riipinen, I., J. R. Pierce, T. Yli-Juuti, T. Nieminen, S. Häkkinen, M. Ehn, H. Junninen, K. Lehtipalo, T. Petäjä, J. Slowik, R. Chang, N. C. Shantz, J. Abbatt, W. R. Leaitch, V.-M. Kerminen, D. R. Worsnop, S. N. Pandis, N. M. Donahue, and M. Kulmala (2011), Organic condensation: A vital link connecting aerosol formation to cloud condensation nuclei (CCN) concentrations, *Atmospheric Chemistry and Physics*, *11*(8), 3865–3878, doi:10.5194/acp-11-3865-2011. 1.1, 2.2.1, 2.3.2

Roderick, M. L., G. D. Farquhar, S. L. Berry, and I. R. Noble (2001), On the direct effect of clouds and atmospheric particles on the productivity and structure of vegetation, *Oecologia*, *129*(1), 21–30, doi:10.1007/s004420100760. 2.3.4

Samset, B. H., C. W. Stjern, E. Andrews, R. A. Kahn, G. Myhre, M. Schulz, and G. L. Schuster (2018), Aerosol Absorption: Progress Towards Global and Regional Constraints, *Curr Clim Change Rep*, pp. 1–19, doi:10.1007/s40641-018-0091-4. 2.2

Schutgens, N. a. J., and P. Stier (2014), A pathway analysis of global aerosol processes, *Atmospheric Chemistry and Physics*, *14*(21), 11,657–11,686, doi:10.5194/acp-14-11657-2014. 2.2.1

Scott, C. E., A. Rap, D. V. Spracklen, P. M. Forster, K. S. Carslaw, G. W. Mann, K. J. Pringle, N. Kivekäs, M. Kulmala, H. Lihavainen, and P. Tunved (2014), The direct and indirect radiative effects of biogenic secondary organic aerosol, *Atmospheric Chemistry and Physics*, *14*(1), 447–470, doi:10.5194/acp-14-447-2014. 1.1, 2.3, 5.3

Scott, C. E., S. A. Monks, D. V. Spracklen, S. R. Arnold, P. M. Forster, A. Rap, K. S. Carslaw, M. P. Chipperfield, C. L. S. Reddington, and C. Wilson (2017), Impact on short-lived climate forcers (SLCFs) from a realistic land-use change scenario via changes in biogenic emissions, *Faraday Discuss.*, *200*(0), 101–120, doi:10.1039/C7FD00028F. 1.1, 2.3.3

Scott, C. E., S. A. Monks, D. V. Spracklen, S. R. Arnold, P. M. Forster, A. Rap, M. Äijälä, P. Artaxo, K. S. Carslaw, M. P. Chipperfield, M. Ehn, S. Gilardoni, L. Heikkinen, M. Kulmala, T. Petäjä, C. L. S. Reddington, L. V. Rizzo, E. Swietlicki, E. Vignati, and C. Wilson (2018a), Impact on short-lived climate forcers increases projected warming due to deforestation, *Nature Communications*, *9*(1), 157, doi:10.1038/s41467-017-02412-4. 2.3

Scott, C. E., S. R. Arnold, S. A. Monks, A. Asmi, P. Paasonen, and D. V. Spracklen (2018b), Substantial large-scale feedbacks between natural aerosols and climate, *Nature Geoscience*, *11*(1), 44–48, doi:10.1038/s41561-017-0020-5. 2.3.4

Seinfeld, J. H., and S. N. Pandis (2016), *Atmospheric Chemistry and Physics*, third ed., John Wiley & Sons, New Jersey. 2.2, 2.2, 2.2.1, 2.2.1, 2.2.1, 2.2.1

Seland, Ø., M. Bentsen, L. Seland Graff, D. Olivié, T. Toniazzo, A. Gjermundsen, J. B. Debernard, A. K. Gupta, Y. He, A. Kirkevåg, J. Schwinger, J. Tjiputra, K. Schancke Aas, I. Bethke, Y. Fan, J. Griesfeller, A. Grini, C. Guo, M. Ilicak, I. H. Hafsahl Karset, O. Landgren, J. Liakka, K. Onsum Moseid, A. Nummelin, C. Spensberger, H. Tang, Z. Zhang, C. Heinze, T. Iverson, and M. Schulz (2020), The Norwegian Earth System Model, NorESM2 – Evaluation of theCMIP6 DECK and historical simulations, *Geoscientific Model Development Discussions*, pp. 1–68, doi:10.5194/gmd-2019-378. 3.1.1, 3.1.3

Semeniuk, K., and A. Dastoor (2018), Current state of aerosol nucleation parameterizations for air-quality and climate modeling, *Atmospheric Environment*, *179*, 77–106, doi:10.1016/j.atmosenv.2018.01.039. 2.2.1

Shrivastava, M., C. D. Cappa, J. Fan, A. H. Goldstein, A. B. Guenther, J. L. Jimenez, C. Kuang, A. Laskin, S. T. Martin, N. L. Ng, T. Petaja, J. R. Pierce, P. J. Rasch, P. Roldin, J. H. Seinfeld, J. Shilling, J. N. Smith, J. A. Thornton, R. Volkamer, J. Wang, D. R. Worsnop, R. A. Zaveri, A. Zelenyuk, and Q. Zhang (2017), Recent advances in understanding secondary organic aerosol: Implications for global climate forcing, *Rev. Geophys.*, *55*(2), 2016RG000,540, doi:10.1002/2016RG000540. 2.3.1, 2.3.2, 2.3, 3.1.4

Shukla, P., J. Skea, R. Slade, R. Diemen, E. Haughey, J. Malley, M. Pathak, and J. Pereira (2019), Technical summary, in *Climate Change and Land: An IPCC Special Report on Climate Change, Desertification, Land Degradation, Sustainable Land Management, Food Security, and Greenhouse Gas Fluxes in Terrestrial Ecosystems*, In Press. 5.3

Smith, C. J., R. J. Kramer, G. Myhre, K. Alterskjær, W. Collins, A. Sima, O. Boucher, J.-L. Dufresne, P. Nabat, M. Michou, S. Yukimoto, J. Cole, D. Paynter, H. Shiogama, F. M. O'Connor, E. Robertson, A. Wiltshire, T. Andrews, C. Hannay, R. Miller, L. Nazarenko, A. Kirkevåg, D. Olivié, S. Fiedler, A. Lewinschal, C. Mackallah, M. Dix, R. Pincus, and P. M. Forster (2020), Effective radiative forcing and adjustments in CMIP6 models, *Atmospheric Chemistry and Physics*, *20*(16), 9591–9618, doi:10.5194/acp-20-9591-2020. 5.2

Sporre, M. K., S. M. Blichner, I. H. H. Karset, R. Makkonen, and T. K. Berntsen (2019), BVOC–aerosol–climate feedbacks investigated using NorESM, *Atmospheric Chemistry and Physics*, *19*(7), 4763–4782, doi:10.5194/acp-19-4763-2019. 1.2, 2.3, 4.1, 5.1

Sporre, M. K., S. M. Blichner, R. Schrödner, I. H. H. Karset, T. K. Berntsen, T. van Noije, T. Bergman, D. O'Donnell, and R. Makkonen (2020), Large difference in aerosol radiative effects from BVOC-SOA treatment in three Earth sys-

tem models, *Atmospheric Chemistry and Physics*, *20*(14), 8953–8973, doi:10.5194/acp-20-8953-2020. 1.2, 2.3.1, 3.1.4, 5.1

Spracklen, D. V., K. J. Pringle, K. S. Carslaw, M. P. Chipperfield, and G. W. Mann (2005), A global off-line model of size-resolved aerosol microphysics: I. Model development and prediction of aerosol properties, *Atmospheric Chemistry and Physics*, *5*(8), 2227–2252, doi:10.5194/acp-5-2227-2005. 2.6

Stier, P., J. Feichter, S. Kinne, S. Kloster, E. Vignati, J. Wilson, L. Ganzeveld, I. Tegen, M. Werner, Y. Balkanski, M. Schulz, O. Boucher, A. Minikin, and A. Petzold (2005), The aerosol-climate model ECHAM5-HAM, *Atmospheric Chemistry and Physics*, *5*(4), 1125–1156, doi:10.5194/acp-5-1125-2005. 2.6

Stolzenburg, D., L. Fischer, A. L. Vogel, M. Heinritzi, M. Schervish, M. Simon, A. C. Wagner, L. Dada, L. R. Ahonen, A. Amorim, A. Baccarini, P. S. Bauer, B. Baumgartner, A. Bergen, F. Bianchi, M. Breitenlechner, S. Brilke, S. B. Mazon, D. Chen, A. Dias, D. C. Draper, J. Duplissy, I. E. Haddad, H. Finkenzeller, C. Frege, C. Fuchs, O. Garmash, H. Gordon, X. He, J. Helm, V. Hofbauer, C. R. Hoyle, C. Kim, J. Kirkby, J. Kontkanen, A. Kürten, J. Lampilahti, M. Lawler, K. Lehtipalo, M. Leiminger, H. Mai, S. Mathot, B. Mentler, U. Molteni, W. Nie, T. Nieminen, J. B. Nowak, A. Ojdanic, A. Onnela, M. Passananti, T. Petäjä, L. L. J. Quéléver, M. P. Rissanen, N. Sarnela, S. Schallhart, C. Tauber, A. Tomé, R. Wagner, M. Wang, L. Weitz, D. Wimmer, M. Xiao, C. Yan, P. Ye, Q. Zha, U. Baltensperger, J. Curtius, J. Dommen, R. C. Flagan, M. Kulmala, J. N. Smith, D. R. Worsnop, A. Hansel, N. M. Donahue, and P. M. Winkler (2018), Rapid growth of organic aerosol nanoparticles over a wide tropospheric temperature range, *PNAS*, p. 201807604, doi:10.1073/pnas.1807604115. 2.3.2

Sullivan, R. C., P. Crippa, H. Matsui, L. R. Leung, C. Zhao, A. Thota, and S. C. Pryor (2018), New particle formation leads to cloud dimming, *npj Climate and Atmospheric Science*, *1*(1), 1–9, doi:10.1038/s41612-018-0019-7. 5.2

Toniazzo, T., M. Bentsen, C. Craig, B. E. Eaton, J. Edwards, S. Goldhaber, C. Jablonowski, and P. H. Lauritzen (2020), Enforcing conservation of axial angular momentum in the atmospheric general circulation model CAM6, *Geoscientific Model Development*, *13*(2), 685–705, doi:10.5194/gmd-13-685-2020. 3.1.3

Tröstl, J., W. K. Chuang, H. Gordon, M. Heinritzi, C. Yan, U. Molteni, L. Ahlm, C. Frege, F. Bianchi, R. Wagner, M. Simon, K. Lehtipalo, C. Williamson, J. S. Craven, J. Duplissy, A. Adamov, J. Almeida, A.-K. Bernhammer, M. Breitenlechner, S. Brilke, A. Dias, S. Ehrhart, R. C. Flagan, A. Franchin, C. Fuchs, R. Guida, M. Gysel, A. Hansel, C. R. Hoyle, T. Jokinen, H. Junninen, J. Kangasluoma, H. Keskinen, J. Kim, M. Krapf, A. Kürten, A. Laaksonen, M. Lawler, M. Leiminger, S. Mathot, O. Möhler, T. Nieminen, A. Onnela, T. Petäjä, F. M. Piel, P. Miettinen, M. P. Rissanen, L. Rondo, N. Sarnela, S. Schobesberger, K. Sengupta, M. Sipilä, J. N. Smith, G. Steiner, A. Tomè, A. Virtanen, A. C. Wagner, E. Weingartner, D. Wimmer, P. M. Winkler, P. Ye, K. S. Carslaw, J. Curtius, J. Dommen, J. Kirkby, M. Kulmala, I. Riipinen, D. R. Worsnop, N. M. Donahue, and U. Baltensperger (2016), The role of

low-volatility organic compounds in initial particle growth in the atmosphere, *Nature*, *533*(7604), 527–531, doi:10.1038/nature18271. 1.1, 2.3.2

Tsigaridis, K., N. Daskalakis, M. Kanakidou, P. J. Adams, P. Artaxo, R. Bahadur, Y. Balkanski, S. E. Bauer, N. Bellouin, A. Benedetti, T. Bergman, T. K. Berntsen, J. P. Beukes, H. Bian, K. S. Carslaw, M. Chin, G. Curci, T. Diehl, R. C. Easter, S. J. Ghan, S. L. Gong, A. Hodzic, C. R. Hoyle, T. Iversen, S. Jathar, J. L. Jimenez, J. W. Kaiser, A. Kirkevåg, D. Koch, H. Kokkola, Y. H. Lee, G. Lin, X. Liu, G. Luo, X. Ma, G. W. Mann, N. Mihalopoulos, J.-J. Morcrette, J.-F. Müller, G. Myhre, S. Myriokefalitakis, N. L. Ng, D. O'Donnell, J. E. Penner, L. Pozzoli, K. J. Pringle, L. M. Russell, M. Schulz, J. Sciare, Ø. Seland, D. T. Shindell, S. Sillman, R. B. Skeie, D. Spracklen, T. Stavrakou, S. D. Steenrod, T. Takemura, P. Tiitta, S. Tilmes, H. Tost, T. van Noije, P. G. van Zyl, K. von Salzen, F. Yu, Z. Wang, Z. Wang, R. A. Zaveri, H. Zhang, K. Zhang, Q. Zhang, and X. Zhang (2014), The AeroCom evaluation and intercomparison of organic aerosol in global models, *Atmos. Chem. Phys.*, *14*(19), 10,845–10,895, doi:10.5194/acp-14-10845-2014. 3.1.4, 5.1

Twomey, S. (1974), Pollution and the planetary albedo, *Atmospheric Environment (1967)*, *8*(12), 1251–1256, doi:10.1016/0004-6981(74)90004-3. 1.1, 2.3.4, 2.4

Twomey, S. (1991), Aerosols, clouds and radiation, *Atmospheric Environment. Part A. General Topics*, *25*(11), 2435–2442, doi:10.1016/0960-1686(91)90159-5. 1.1, 2.2, 2.3.3, 2.4

Unger, N. (2014a), On the role of plant volatiles in anthropogenic global climate change, *Geophysical Research Letters*, *41*(23), 8563–8569, doi:10.1002/2014GL061616. 1.1, 2.3, 2.3.3

Unger, N. (2014b), Human land-use-driven reduction of forest volatiles cools global climate, *Nature Climate Change*, *4*(10), 907–910, doi:10.1038/nclimate2347. 2.3.3

Vehkamäki, H., M. Kulmala, I. Napari, K. E. J. Lehtinen, C. Timmreck, M. Noppel, and A. Laaksonen (2002), An improved parameterization for sulfuric acid–water nucleation rates for tropospheric and stratospheric conditions, *J.-Geophys.-Res.*, *107*(D22), 4622, doi:10.1029/2002JD002184. 3.1.4

Vignati, E., J. Wilson, and P. Stier (2004), M7: An efficient size-resolved aerosol microphysics module for large-scale aerosol transport models: AEROSOL MICROPHYSICS MODULE, *Journal of Geophysical Research: Atmospheres*, *109*(D22), n/a–n/a, doi:10.1029/2003JD004485. 2.6

Westervelt, D. M., J. R. Pierce, I. Riipinen, W. Trivitayanurak, A. Hamed, M. Kulmala, A. Laaksonen, S. Decesari, and P. J. Adams (2013), Formation and growth of nucleated particles into cloud condensation nuclei: Model–measurement comparison, *Atmospheric Chemistry and Physics*, *13*(15), 7645–7663, doi:10.5194/acp-13-7645-2013. 2.2.1

Westervelt, D. M., J. R. Pierce, and P. J. Adams (2014), Analysis of feedbacks between nucleation rate, survival probability and cloud condensation nuclei formation, *Atmospheric Chemistry and Physics*, *14*(11), 5577–5597, doi:10.5194/acp-14-5577-2014. 2.2.1

Yan, C., W. Nie, A. L. Vogel, L. Dada, K. Lehtipalo, D. Stolzenburg, R. Wagner, M. P. Rissanen, M. Xiao, L. Ahonen, L. Fischer, C. Rose, F. Bianchi, H. Gordon, M. Simon, M. Heinritzi, O. Garmash, P. Roldin, A. Dias, P. Ye, V. Hofbauer, A. Amorim, P. S. Bauer, A. Bergen, A.-K. Bernhammer, M. Breitenlechner, S. Brilke, A. Buchholz, S. B. Mazon, M. R. Canagaratna, X. Chen, A. Ding, J. Dommen, D. C. Draper, J. Duplissy, C. Frege, C. Heyn, R. Guida, J. Hakala, L. Heikkinen, C. R. Hoyle, T. Jokinen, J. Kangasluoma, J. Kirkby, J. Kontkanen, A. Kürten, M. J. Lawler, H. Mai, S. Mathot, R. L. Mauldin, U. Molteni, L. Nichman, T. Nieminen, J. Nowak, A. Ojdanic, A. Onnela, A. Pajunoja, T. Petäjä, F. Piel, L. L. J. Quéléver, N. Sarnela, S. Schallhart, K. Sengupta, M. Sipilä, A. Tomé, J. Tröstl, O. Väisänen, A. C. Wagner, A. Ylisirniö, Q. Zha, U. Baltensperger, K. S. Carslaw, J. Curtius, R. C. Flagan, A. Hansel, I. Riipinen, J. N. Smith, A. Virtanen, P. M. Winkler, N. M. Donahue, V.-M. Kerminen, M. Kulmala, M. Ehn, and D. R. Worsnop (2020), Size-dependent influence of NOx on the growth rates of organic aerosol particles, *Science Advances*, *6*(22), eaay4945, doi:10.1126/sciadv.aay4945. 2.2.1

Yli-Juuti, T., C. Mohr, and I. Riipinen (2020), Open questions on atmospheric nanoparticle growth, *Communications Chemistry*, *3*(1), 1–4, doi:10.1038/s42004-020-00339-4. 2.2.1, 2.3.2

Zhang, G. J., and N. A. McFarlane (1995), Sensitivity of climate simulations to the parameterization of cumulus convection in the Canadian climate centre general circulation model, *Atmosphere-Ocean*, *33*(3), 407–446, doi:10.1080/07055900.1995.9649539. 3.1.3

Zhang, R., A. Khalizov, L. Wang, M. Hu, and W. Xu (2012), Nucleation and Growth of Nanoparticles in the Atmosphere, *Chemical Reviews*, *112*(3), 1957–2011, doi:10.1021/cr2001756. 2.3.2

Part II

Papers

I

Paper I

BVOC–aerosol–climate feedbacks investigated using NorESM

Moa K. Sporre, **Sara M. Blichner**, Inger H. H. Karset , Risto Makkonen, and Terje K. Berntsen

Atmospheric Chemistry and Physics, 2019

doi:10.5194/acp-19-4763-2019

Atmos. Chem. Phys., 19, 4763–4782, 2019
https://doi.org/10.5194/acp-19-4763-2019

Atmospheric Chemistry and Physics
Open Access
EGU

BVOC–aerosol–climate feedbacks investigated using NorESM

Moa K. Sporre[1], **Sara M. Blichner**[1], **Inger H. H. Karset**[1], **Risto Makkonen**[2,3], **and Terje K. Berntsen**[1,4]

[1]Department of Geosciences, University of Oslo, Oslo, Norway
[2]Climate System Research, Finnish Meteorological Institute, P.O. Box 503, Helsinki, Finland
[3]Institute for Atmospheric and Earth System Research/Physics, Faculty of Science, P.O. Box 64, 00014, University of Helsinki, Helsinki, Finland
[4]CICERO Center for International Climate Research, Oslo, Norway

Correspondence: Moa K. Sporre (m.k.sporre@geo.uio.no)

Received: 4 September 2018 – Discussion started: 10 October 2018
Revised: 22 February 2019 – Accepted: 14 March 2019 – Published: 9 April 2019

Abstract. Both higher temperatures and increased CO_2 concentrations are (separately) expected to increase the emissions of biogenic volatile organic compounds (BVOCs). This has been proposed to initiate negative climate feedback mechanisms through increased formation of secondary organic aerosol (SOA). More SOA can make the clouds more reflective, which can provide a cooling. Furthermore, the increase in SOA formation has also been proposed to lead to increased aerosol scattering, resulting in an increase in diffuse radiation. This could boost gross primary production (GPP) and further increase BVOC emissions. In this study, we have used the Norwegian Earth System Model (NorESM) to investigate both these feedback mechanisms. Three sets of experiments were set up to quantify the feedback with respect to (1) doubling the CO_2, (2) increasing temperatures corresponding to a doubling of CO_2 and (3) the combined effect of both doubling CO_2 and a warmer climate. For each of these experiments, we ran two simulations, with identical setups, except for the BVOC emissions. One simulation was run with interactive BVOC emissions, allowing the BVOC emissions to respond to changes in CO_2 and/or climate. In the other simulation, the BVOC emissions were fixed at present-day conditions, essentially turning the feedback off. The comparison of these two simulations enables us to investigate each step along the feedback as well as estimate their overall relevance for the future climate.

We find that the BVOC feedback can have a significant impact on the climate. The annual global BVOC emissions are up to 63 % higher when the feedback is turned on compared to when the feedback is turned off, with the largest response when both CO_2 and climate are changed. The higher BVOC levels lead to the formation of more SOA mass (max 53 %) and result in more particles through increased new particle formation as well as larger particles through increased condensation. The corresponding changes in the cloud properties lead to a $-0.43\,\mathrm{W\,m^{-2}}$ stronger net cloud forcing. This effect becomes about 50 % stronger when the model is run with reduced anthropogenic aerosol emissions, indicating that the feedback will become even more important as we decrease aerosol and precursor emissions. We do not find a boost in GPP due to increased aerosol scattering on a global scale. Instead, the fate of the GPP seems to be controlled by the BVOC effects on the clouds. However, the higher aerosol scattering associated with the higher BVOC emissions is found to also contribute with a potentially important enhanced negative direct forcing ($-0.06\,\mathrm{W\,m^{-2}}$). The global total aerosol forcing associated with the feedback is $-0.49\,\mathrm{W\,m^{-2}}$, indicating that it has the potential to offset about 13 % of the forcing associated with a doubling of CO_2.

1 Introduction

Our climate is warming due to rising atmospheric levels of greenhouse gases originating from human activities (IPCC, 2013). Feedback mechanisms that arise from increasing temperatures and/or greenhouse gas concentrations can enhance or dampen the temperature increase, and contribute to the overall uncertainty in predicting the future climate. Increased emissions of biogenic volatile organic compounds (BVOCs) from terrestrial vegetation caused by increasing temperature and CO_2 levels have been proposed to induce a negative cli-

mate feedback (Kulmala et al., 2004, 2013). Higher BVOC concentrations result in higher aerosol number and mass concentration, which cool the climate by inducing changes in cloud properties (Twomey, 1974; Albrecht, 1989). Aerosol particles and their interactions with clouds and climate constitute one of the largest uncertainties in assessing our future climate (IPCC, 2013).

BVOCs are important sources of aerosol particles (Glasius and Goldstein, 2016), especially in pristine forest regions (Tunved et al., 2006). The most important BVOC compounds for aerosol formation are isoprene, monoterpenes and sesquiterpenes (Kulmala et al., 2013), and their emissions have been estimated to be 700–1000 Tg C annually (Laothawornkitkul et al., 2009). Through oxidation in the atmosphere, these compounds become less volatile and may contribute to aerosol formation. The main oxidation agents are OH, O_3 and NO_3 radicals (Shrivastava et al., 2017). The oxidation products from monoterpenes have been found to be particularly important for new particle formation, while the oxidation products from isoprene have been found to predominantly participate in condensation onto pre-existing aerosols (Jokinen et al., 2015). How sensitive the aerosol number concentration is to changes in BVOC emissions depends on the anthropogenic and natural aerosol load. It has been shown that the BVOCs had greater influence on the number and mass concentration in the pre-industrial (PI) atmosphere (Gordon et al., 2017). The importance of new particle formation and condensation from organic vapours to the global aerosol load, cloud formation and climate has been getting increasing attention over the past 10 years (Glasius and Goldstein, 2016). However, there are still large uncertainties associated with these processes and this contributes to the overall uncertainty of aerosol particles' impact on climate (Kulmala et al., 2013).

In this paper, we investigate the potential climate feedback associated with increasing BVOC emissions due to rising CO_2 concentrations and temperature, shown in Fig. 1. Note that the word "feedback" is used somewhat differently in this paper compared to traditional climate science, since not only temperature but also the CO_2 concentration is directly involved in the change in BVOC emissions. The increase in atmospheric CO_2 results in increasing temperature but also gross primary production (GPP) through CO_2 fertilisation (Morison and Lawlor, 1999). Higher GPP results in more vegetation that can produce BVOCs (Guenther et al., 1995). Increasing temperature also has a positive effect on the emissions of BVOCs because of the exponential relationship between BVOC volatility and temperature (Kulmala et al., 2013). Additionally, rising levels of CO_2 may have a direct impact on the BVOC emissions, as isoprene emissions have been found to decrease with increasing CO_2 levels (e.g. Wilkinson et al., 2009), but whether the same is true for monoterpenes is not yet clear (Arneth et al., 2016). Higher concentrations of BVOCs give an increase in aerosol number concentration (N_a) since oxidation products of BVOCs contribute to new particle formation and early particle growth, as well as more secondary organic aerosol (SOA) mass due to increased condensation. The feedback loop then divides into two different branches.

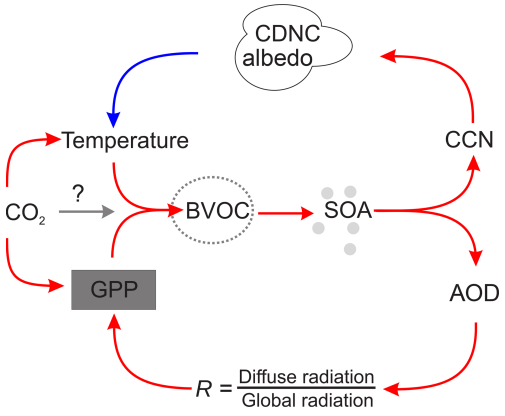

Figure 1. The BVOC feedback driven by increasing CO_2 and temperature. The upper branch of the feedback is the T branch, while the lower part is the GPP branch. The red arrows in the figure indicate that if the variable at the start of the arrow increases, then the variable at the end of the arrow is also expected to increase. A blue arrow on the other hand means that an increase in the variable at the start of the arrow is expected to result in a decrease in the variable at the end of the arrow. The figure is modified after Kulmala et al. (2014).

The upper branch of the feedback loop involves aerosol effects on clouds, radiation and temperature (the T branch). The increase in SOA contributes to more cloud condensation nuclei (CCN), both through the formation of more aerosol particles and through increased condensation, which increases the diameter of existing particles and makes them large enough to act as seeds for cloud droplets (Kulmala et al., 2004). The increase in CCN will result in clouds with a higher cloud droplet number concentration (CDNC) and smaller droplets leading to a higher cloud albedo (Twomey, 1974). Smaller cloud droplets can also lead to a delay in the onset of precipitation, which leads to a longer cloud lifetime (Albrecht, 1989). Higher cloud albedo and longer cloud lifetime lead to decreasing temperature, giving rise to a negative climate feedback.

The lower branch of the feedback involves the impact of aerosol particle scattering on GPP (the GPP branch). More particles and more aerosol mass mean more scattering by aerosol particles in the atmosphere, which increases the fraction of diffuse radiation to global radiation (R). Increased fraction of diffuse radiation, at relatively stable levels of total radiation, has been found to boost photosynthesis through increased photosynthetically active radiation in shaded regions (Roderick et al., 2001). More photosynthesis increases the GPP, which results in larger emissions of BVOCs and a positive feedback on BVOC emissions. Increased BVOC emissions have also been proposed to have other indirect forcing

effects, e.g. on methane lifetime and ozone concentrations, but these effects will not be investigated in this study.

Both measurement and modelling studies have previously investigated parts of the BVOC feedback shown in Fig. 1. Using long-term data of aerosol properties from 11 measurement stations, Paasonen et al. (2013) estimated the feedback associated with the T loop to globally be about $-0.01\,\mathrm{W\,m^2\,K^{-1}}$. Scott et al. (2018a) found a similar number ($-0.013\,\mathrm{W\,m^2\,K^{-1}}$) using a global aerosol model together with an offline radiative transfer model. In Kulmala et al. (2014), the T branch of the feedback was estimated with an atmospheric model by doubling monoterpene emissions. This resulted in a global cloud radiative forcing of approximately $-0.2\,\mathrm{W\,m^2}$. Makkonen et al. (2012) found this number to be $-0.5\,\mathrm{W\,m^2}$ at lower anthropogenic aerosol emissions, using emissions from 2100 according to RCP4.5. The GPP branch has been investigated using measurement data from a station in central Finland, which supported a statistically significant correlation between an increase in diffuse radiation ratio and higher aerosol loading during cloud-free conditions, as well as a resulting increase in GPP (Kulmala et al., 2013, 2014). Rap et al. (2018) combined a global aerosol model, a radiation model and a land surface scheme and found the GPP branch to contribute with a gain in global BVOC emissions by 1.07. To our knowledge, no study has so far used an Earth system model to investigate both branches of the BVOC feedback.

This study provides a comprehensive global investigation of the BVOC feedback using an Earth system model. The model setup enables the vegetation and emissions in the land model to respond to changes in climate, CO_2 and radiation, capturing diurnal as well as seasonal variations in the emissions of BVOCs. Both emissions of isoprene and monoterpenes are calculated interactively by the land model and are included in the SOA formation in the atmospheric model. The scientific objectives of the study are to investigate the impact of CO_2 and temperature on the BVOC feedback separately and combined. We aim to determine the importance of each step along the BVOC-feedback loop globally and regionally. Moreover, we want to determine the relative importance of the two branches of the feedback loop, as well as the overall relevance of the BVOC-feedback loop for estimating the future climate.

2 Method

2.1 Model description

In this study, the Norwegian Earth System Model (NorESM) (Bentsen et al., 2013; Kirkevåg et al., 2013; Iversen et al., 2013) has been used to investigate the feedback loop described in the previous section. NorESM is based on the Community Earth System Model (CESM) but uses a different ocean model and a different aerosol module in the Community Atmosphere Model (CAM). The atmospheric model in NorESM is therefore called CAM-Oslo (Kirkevåg et al., 2013). We used CAM5.3-Oslo (Kirkevåg et al., 2018) coupled to the Community Land Model version 4.5 (CLM4.5) (Oleson et al., 2013). CLM4.5 was run in the BGC (biogeochemistry) mode, which includes active carbon and nitrogen biogeochemical cycling. In this mode, the plants respond to changes in environmental conditions by enhanced or reduced growth, but the geographical vegetation distribution does not change. Included in CLM4.5 is the Model of Emissions of Gases and Aerosols from Nature (MEGAN) version 2.1 (Guenther et al., 2012) that provides emissions of BVOC from the plant functional types in CLM4.5. The BVOCs include isoprene and the following compounds which are lumped together as monoterpenes in CAM-Oslo; myrcene, sabinene, limonene, 3-carene, t-B-ocimene, β-pinene, α-pinene. Both the vegetation and the emissions respond to changes in diffuse radiation, CO_2 and other climate variables. CO_2 inhibition is included in MEGAN for isoprene (Guenther et al., 2012).

The aerosol scheme in CAM5.3-Oslo is called OsloAero (Kirkevåg et al., 2018) and has been developed at the Meteorological Institute of Norway and the University of Oslo. OsloAero can be described as a "production-tagged" aerosol scheme where the aerosol tracers are defined according to their formation mechanism. The tracers include 15 lognormal background modes, which are modified by condensation, coagulation and cloud processing. CAM5.3-Oslo also includes some changes to the gas-phase chemistry compared to CAM5.3. In CAM5.3-Oslo, isoprene and monoterpene can react with O_3, OH and NO_3. The reaction between monoterpene and O_3 yields low volatile SOA (LVSOA), while the other five reactions between BVOCs and the oxidants yield semi-volatile SOA (SVSOA). The yields for the isoprene reactions are 0.05 and the yields for the monoterpene reactions are 0.15, which reflects the findings in, e.g. Jokinen et al. (2015). LVSOA and SVSOA can also be formed from dimethyl sulfide as a proxy for methane sulfonic acid (MSA). Only the LVSOA takes part in the nucleation in the model, while the SVSOA condenses onto already formed aerosol particles (Makkonen et al., 2014). In NorESM, both LVSOA and SVSOA are treated as non-volatile with condensation being kinetically limited.

The nucleation scheme was introduced into CAM-Oslo in Makkonen et al. (2014) but has since then been further developed (Kirkevåg et al., 2018). The nucleation scheme includes binary homogeneous sulfuric acid–water nucleation (Vehkamäki et al., 2002), as well as an activation-type nucleation in the boundary layer. The activation-type nucleation rate is calculated from the concentrations of H_2SO_4 and LVSOA available for nucleation according to Eq. (18) ($J = 6.1\times10^{-7}[H_2SO_4]+0.39\times10^{-7}[\mathrm{LVSOA}]$) from Paasonen et al. (2010). The subsequent growth and survival to the smallest mode (median radius 23.6 nm) is modelled by a parameterisation from Lehtinen et al. (2007), depending

mainly on the ratio between coagulation sink and growth rate (from LVSOA and H_2SO_4). The treatment of early growth of aerosols has been adjusted in this version of the model due to too-high concentrations of particles from new particle formation. This was due to the survival percentage from nucleation (radius 2 nm) to the smallest mode being unrealistically high. In OsloAero, coagulation is calculated only between small modes and larger modes, while autocoagulation and coagulation between smaller modes are considered negligible. In order to improve this, we added coagulation onto all pre-existing particles to the coagulation sink used in the survival calculation (Lehtinen et al., 2007).

The hygroscopicity of aerosol particles in NorESM is calculated for each "mixture", which is what the background modes are called after they have changed composition and shape through condensation, coagulation and cloud processing. The hygroscopicity is a mass-weighted average of all components in the mixtures if the particles are uncoated or have thin coating. If the particles have a thick coating (> 2 nm), the hygroscopicity is instead a mass-weighted average of the coating itself (Kirkevåg et al., 2018). Both the size and hygroscopicity of the aerosol particles are used in the calculations of CCN and the activation of aerosols to cloud droplets.

The cloud schemes in CAM5.3-Oslo include a deep convection scheme (Zhang and McFarlane, 1995), a shallow convection scheme (Park and Bretherton, 2009) and the microphysical two-moment scheme MG1.5 (Morrison and Gettelman, 2008; Gettelman and Morrison, 2015) for stratiform clouds. The microphysical scheme includes aerosol activation according to Abdul-Razzak and Ghan (2000), which depends on updraft velocity and the properties of the different aerosol modes. For both liquid and ice, the mass and number are prognostic and the autoconversion scheme (Khairoutdinov and Kogan, 2000) includes subgrid variability of cloud water (Morrison and Gettelman, 2008). In this paper, the methods from Ghan (2013) are used to calculate the forcing from clouds and aerosols. The net direct forcing (NDF_{Ghan}) is calculated as the difference between the net top-of-the-atmosphere radiative flux and the radiative flux, neglecting the scattering and absorption of solar radiation by the aerosols (F_{clean}). This is calculated in a separate call to the radiation code. Similarly, the net cloud forcing (NCF_{Ghan}) is calculated as the difference between F_{clean} and the flux neglecting the scattering and absorption by both clouds and aerosols ($F_{clear,clean}$). In the model, the forcings are calculated separately for the short-wave and long-wave radiation, which we have used to calculate the net forcing.

2.2 Experimental setup

In order to investigate the feedback loop presented above, three different sets of experiments were performed with NorESM. The first experiment was set up to simulate impacts of the change in BVOC emissions when plants respond to enhanced CO_2 concentrations. The CO_2 was doubled with respect to year 2000 level (denoted $2\times CO_2$), but note that the fixed SSTs highly restricted the temperature increase from the radiative forcing associated with doubling the CO_2. The second experiment simulated the impact of a warmer climate driven by a change in the sea surface temperature (SST) and sea ice to year 2080 conditions according to the RCP8.5 scenario (denoted $+\Delta$SST) but with fixed CO_2 concentrations at the year 2000. The year 2080 was chosen because the CO_2 levels at this time are approximately equal to the $2\times CO_2$ experiment. The temperature difference over land resulting from the increase in SST is shown in Fig. S1. In the last experiment, we doubled both the CO_2 and changed the SSTs and sea ice as described previously ($2\times CO_2+\Delta$SST). The experiments enable us to investigate the response of the BVOC feedback to increased CO_2 and temperature separately and then to see their combined effect in the last experiment. Because the aerosol loading is expected to decrease in the future (Smith et al., 2016), we also ran a simulation identical to the $2\times CO_2+\Delta$SST but where we changed the emissions of aerosol and precursor gases to PI levels (1850), denoted $2\times CO_2+\Delta$SST LA (low aerosol). This simulation was done in order to investigate whether the importance of the BVOC feedback will be larger if the aerosol loading is smaller in the future. The doubling of CO_2, the SST increase and the reduction in aerosol emissions are all at the top end of possible future scenarios and are not the most likely future.

To be able to determine the importance of each step along the BVOC-feedback loop, each of the experiments described were run with the feedback loop turned on (FB-ON) and turned off (FB-OFF). In the FB-OFF simulations, we did not want changes in CO_2, temperature or GPP to affect the BVOC emissions, essentially keeping concentrations constant at present-day (PD) levels. This was done by generating emission fields from a control simulation and using these as input into the FB-OFF simulations; see Fig. 2 and Table 1. We found that reproducing the diurnal variations in the BVOC emissions in the FB-OFF simulations was important in order to get the BVOC concentrations in the model representative of those in the control simulation. The column burdens of isoprene and monoterpene became much higher when no diurnal variation in the BVOC emissions was included, since the BVOC emissions were high also when the oxidant concentrations were low. Moreover, the reaction rates between the BVOCs and the oxidants are temperature dependent and thus lower during the nights. In order to produce emission fields for the FB-OFF simulations with correct diurnal variations, 6 years of control run emission data at half an hour time resolution were averaged to create a yearly input file with half an hour time resolution (the time step used in the model). Thus, the FB-ON simulations and the FB-OFF simulations are set up exactly the same way, except that the FB-ON simulations are run with interactive BVOC emissions, while in the FB-OFF simulations the BVOC emissions are fixed at PD conditions; see Table 1.

Table 1. Specifications of the CO_2 levels, year of the SSTs, BVOC emissions and which meteorology was used for the nudging for each of the simulations. "Met" stands for meteorology and refers to the simulations denoted by met in Fig. 2.

Experiment	CO_2	SSTs and sea ice	BVOC emissions	Aerosol emissions	Meteorology
CTRL	$1 \times CO_2$	PD	Interactive	PD	CTRL met
$2 \times CO_2$ FB ON	$2 \times CO_2$	PD	Interactive	PD	$2 \times CO_2$ met
$2 \times CO_2$ FB OFF	$2 \times CO_2$	PD	Fixed (CTRL)	PD	$2 \times CO_2$ met
$+\Delta$SST FB ON	$1 \times CO_2$	2080	Interactive	PD	$+\Delta$SST met
$+\Delta$SST FB OFF	$1 \times CO_2$	2080	Fixed (CTRL)	PD	$+\Delta$SST met
$2 \times CO_2 + \Delta$SST FB ON	$2 \times CO_2$	2080	Interactive	PD	$2 \times CO_2 + \Delta$SST met
$2 \times CO_2 + \Delta$SST FB OFF	$2 \times CO_2$	2080	Fixed (CTRL)	PD	$2 \times CO_2$,$+\Delta$SST met
$2 \times CO_2 + \Delta$SST FB ON LA	$2 \times CO_2$	2080	Interactive	PI	$2 \times CO_2 + \Delta$SST met LA
$2 \times CO_2 + \Delta$SST FB OFF LA	$2 \times CO_2$	2080	Fixed (CTRL)	PI	$2 \times CO_2 + \Delta$SST met LA

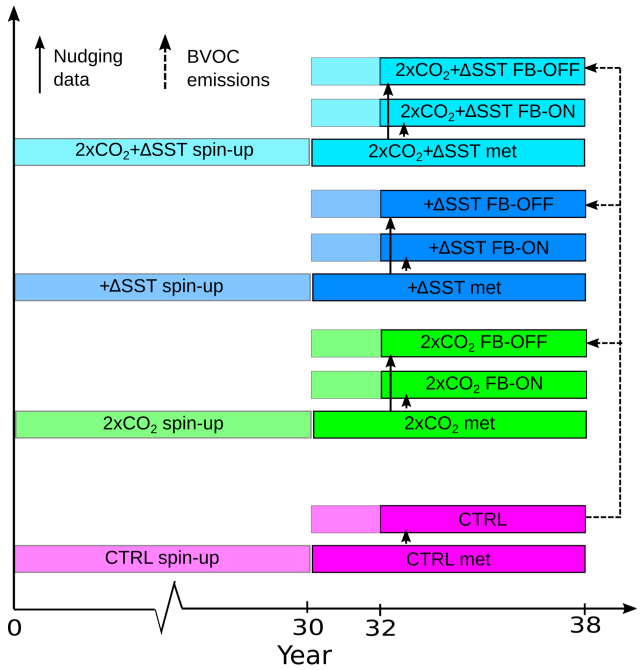

Figure 2. The simulation setup. The CTRL simulation has CO_2 and SSTs at present-day (PD) levels. The $2 \times CO_2$ simulations have doubled CO_2 with respect to the year 2000. In the $+\Delta$SST simulations, the SST and sea ice are increased to the year 2080 levels. In the $2 \times CO_2 + \Delta$SST simulation, the CO_2 is doubled and the SST and sea ice are changed to the year 2080 levels. The CTRL, as well as all FB-ON and FB-OFF simulations, is nudged to their respective met simulation. All FB-ON simulations have interactive emissions, while the FB-OFF simulations have fixed emissions from the CTRL simulation.

Furthermore, to not have changes in weather patterns between the FB-ON and FB-OFF simulations mask the effects of the different BVOC emissions, we have used nudging (Kooperman et al., 2012) of horizontal winds and surface pressure (Zhang et al., 2014). Since meteorological conditions change significantly with doubling of CO_2 and temperature increase, the FB-ON/FB-OFF simulations for each experiment are nudged to separate NorESM runs with the corresponding temperature/CO_2 changes (see Fig. 2 and Table 1). The nudging changes some of the meteorological variables in the model slightly and therefore also the control simulation (CTRL), from which the fixed BVOC emission fields are generated, was nudged to another CTRL simulation (see Fig. 2).

NorESM was run with a $1.9 \times 2.5°$ horizontal resolution, 30 vertical levels and fixed sea ice and SSTs. The emissions of aerosols and precursor gases were set to the year 2000, except for the simulations where we decrease the aerosol loading to PI levels, where the emissions from 1850 are used. Prescribed oxidant fields and land use at PD conditions are used for all simulations. CTRL and the other four experiments described above were run for 30 years as a spin-up (see Fig. 2). After this, another 8 years were run to create the meteorological data for nudging for each experiment. The FB-ON simulations were initialised from the spin-up simulations and run for 8 years using nudging with a relaxation time of 6 h. The FB-OFF simulations were run in the same manner, except that the BVOC emissions were read from file (as described above). The first 2 years of the FB-ON and FB-OFF simulations are considered a spin-up, due to the nudging and the change in the emissions in the FB-OFF simulations. Thus, the last 6 years of the simulations are used for the analysis.

3 Results and discussions

3.1 BVOC emissions and SOA

We will start by discussing the part of the BVOC feedback common to the two branches and then discuss each branch of the feedback separately.

3.1.1 BVOC emissions

The BVOC emissions calculated by NorESM are in line with previous studies. In the CTRL run, the BVOC emissions are $366\,\mathrm{Tg\,yr^{-1}}$ for isoprene and $115\,\mathrm{Tg\,yr^{-1}}$ for monoterpenes. These values are in the range of those in

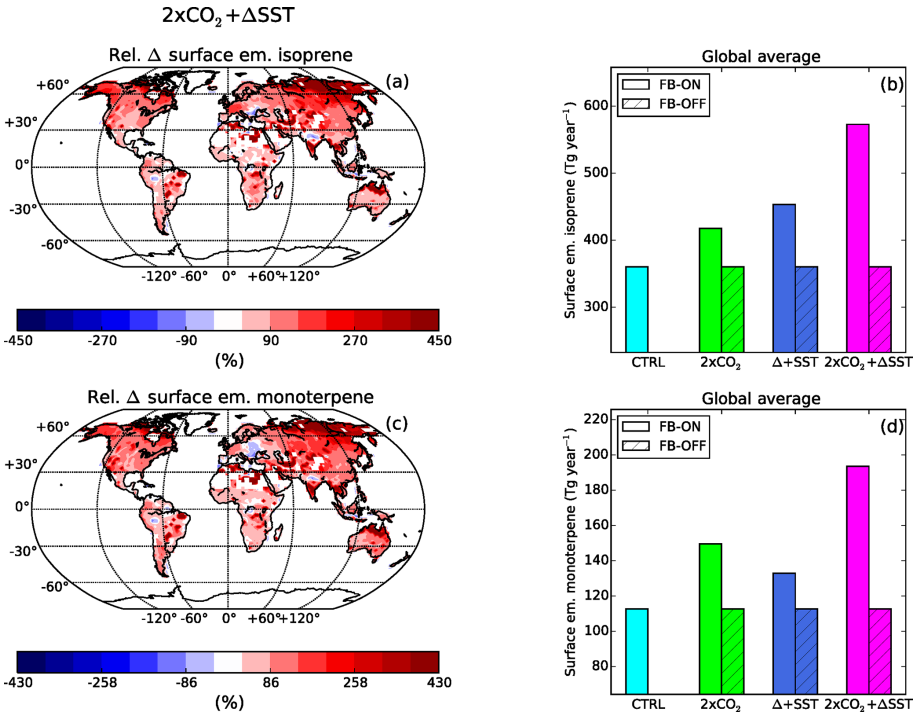

Figure 3. The relative difference between the FB-ON and FB-OFF simulations of the annual average surface emissions of isoprene **(a)** and monoterpenes **(c)** for the $2 \times CO_2 + \Delta SST$ experiment. The relative difference is defined as the (FB-ON − FB-OFF) / FB-OFF. In the bar plots, the yearly global surface emissions of isoprene **(b)** and monoterpenes **(d)** for the CTRL simulation as well as the three experiments (both FB-ON and FB-OFF simulations) are shown.

Guenther et al. (2012) for monoterpenes but on the lower end for isoprene. For the $2 \times CO_2 + \Delta SST$ FB-ON simulation, the emissions are 586 Tg yr^{-1} (+60 %) for isoprene and 198 Tg yr^{-1} (+73 %) for monoterpenes. The emissions are somewhat lower than estimated for the future climate in previous studies (Laothawornkitkul et al., 2009) but the relative increases are on the high end (Carslaw et al., 2010). The isoprene emissions increase more when the temperature is increased ($+\Delta SST$) than when the CO_2 is doubled, but the opposite is true for monoterpenes; see Fig. 3c and d.

The emissions of isoprene and monoterpenes are higher almost everywhere in the FB-ON simulations with $2 \times CO_2$, $+\Delta SST$ and $2 \times CO_2 + \Delta SST$ than in the FB-OFF simulations with the same setup (see Figs. 3 and S2), in line with the BVOC feedback. The absolute increase in the emissions is largest over the tropical forests, while the relative increase in emissions is greatest over the boreal forests in the Northern Hemisphere (NH). Generally, the CO_2 inhibition of isoprene is masked by the CO_2 and temperature boosts of the vegetation, which leads to a higher leaf area index (LAI) and GPP. In the experiment with only increased CO_2, there are a few areas in Africa and India that seem to have lower isoprene emissions due to CO_2 inhibition. This can be seen as lower isoprene emissions and higher monoterpene emissions in the same place (Fig. S2a and c). This does not occur in the experiments where also the SSTs are increased. Over some regions in the tropics (parts of Africa and the Amazon), especially in the $+\Delta SST$ experiment, both monoterpene and isoprene emissions decrease. This is caused by a decrease in the LAI associated with plant mortality that seems to occur because of heat stress. The decrease in LAI leads to a lower albedo in these forest regions, which further increases the temperature, causing more heat stress and creating a feedback mechanism on the vegetation. Nevertheless, the vegetation has had time to adapt to the new temperatures and stabilise by the end of the 30-year spin-up period. The decreases in LAI are smaller in the $2 \times CO_2 + \Delta SST$ experiments as the vegetation is seeded by CO_2 (Fig. 3a).

3.1.2 SOA

The higher BVOC emissions in the FB-ON simulations lead to larger SOA production (see Fig. 4b), as expected from the BVOC feedback. The SOA production in the CTRL simulation is 75 Tg yr^{-1}, which is in the range previously estimated by global models (Tsigaridis et al., 2014; Glasius and Goldstein, 2016). The SOA production in the FB-ON simulations is similar for the $2 \times CO_2$ and $+\Delta SST$ experiments (90 and 92 Tg yr^{-1}) while the combined effect of higher CO_2 and temperature gives a higher SOA production, with values of 115 Tg yr^{-1}. The column burden of SOA is higher over the entire globe when the BVOC feedback is on compared to

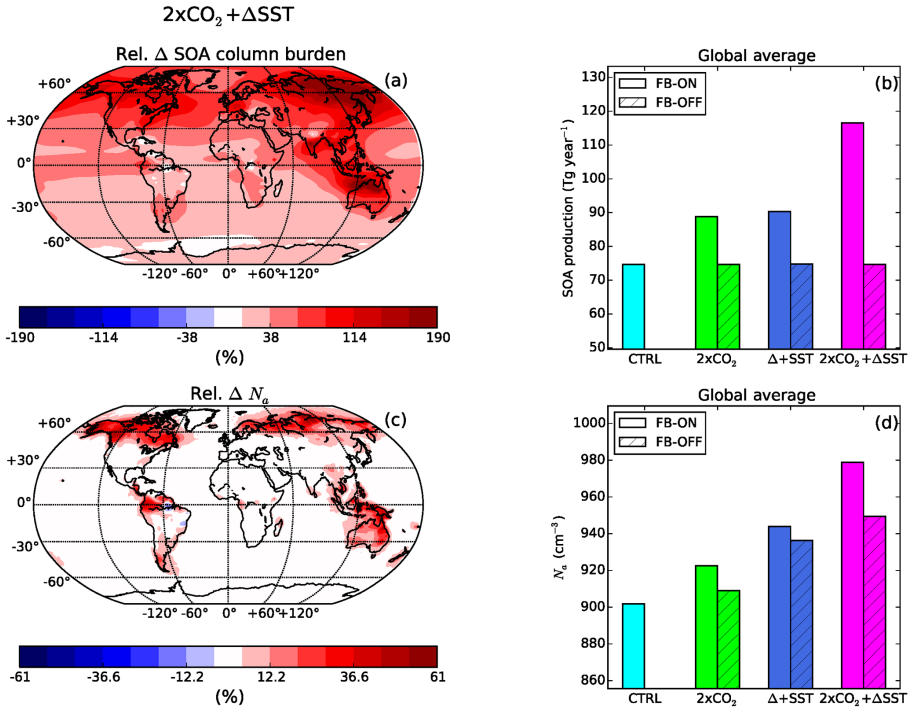

Figure 4. The relative difference between the FB-ON and FB-OFF simulations in the annual average column burden SOA **(a)** and N_a in the boundary layer **(c)** for the $2 \times CO_2 + \Delta SST$ experiment. In the bar plots, the average yearly global production of SOA **(b)** and the global average N_a in the boundary layer **(d)** are shown for the CTRL simulation as well as the three experiments (both FB-ON and FB-OFF simulations).

when it is turned off, except in the $+\Delta SST$ experiment over and downwind of the regions where the BVOC emissions decrease; see Figs. 4a and S3b. The largest absolute increase of column burden SOA is over the tropical forests, while the largest relative increases are over the Arctic and sub-Arctic. The fraction of SOA in the aerosol particles is also higher when the feedback is turned on, which leads to a reduction in the hygroscopicity of the particles (not shown).

3.1.3 Aerosol number and size

Not only is the mass of the aerosol particles affected by higher levels of BVOCs but also the number concentration of aerosol particles and their sizes. The changes in the number concentration and size of the particles vary with region. The largest difference in N_a between the FB-ON and FB-OFF simulations occurs over, and downwind of, the tropical rain forests, as well as over the boreal forests in the NH (see Fig. 4c). The relative difference is largest over the boreal forests in the NH where the particle number concentrations are generally low. The largest absolute differences on the other hand occur in the tropics. Over regions where the emissions decrease (in the $+\Delta SST$ experiment), the N_a decreases (Fig. S3d).

In order to investigate the effect on the sizes of the particles, we analysed the averaged boundary layer aerosol size distributions for two of the regions most affected by the feedback: the boreal forests and the tropical islands in southeast Asia. The size distributions are created from the number median radius and standard deviations of the 12 particle mixtures in OsloAero (Kirkevåg et al., 2018). Over the boreal forests, the higher BVOC emissions result in more particles in the Aitken mode (Fig. 5a and b). The enhanced growth of the particles also results in more particles in the accumulation mode and in a shift to larger sizes of the Aitken mode, which results in a small decrease in the number of particles below 25 nm. In the tropics, there is a larger (smaller) absolute (relative) increase in Aitken-mode particles. The shift in the size distribution due to more condensing vapours is larger here than over the boreal forests and results in decreasing particle concentrations up to 70 nm. The biggest changes in both number and shift in size distribution are seen in the $2 \times CO_2 + \Delta SST$ experiment. The changes in particle sizes occur further downwind from the sources than the changes in aerosol number concentrations which are more restricted to areas close to the sources, in particular in the tropics.

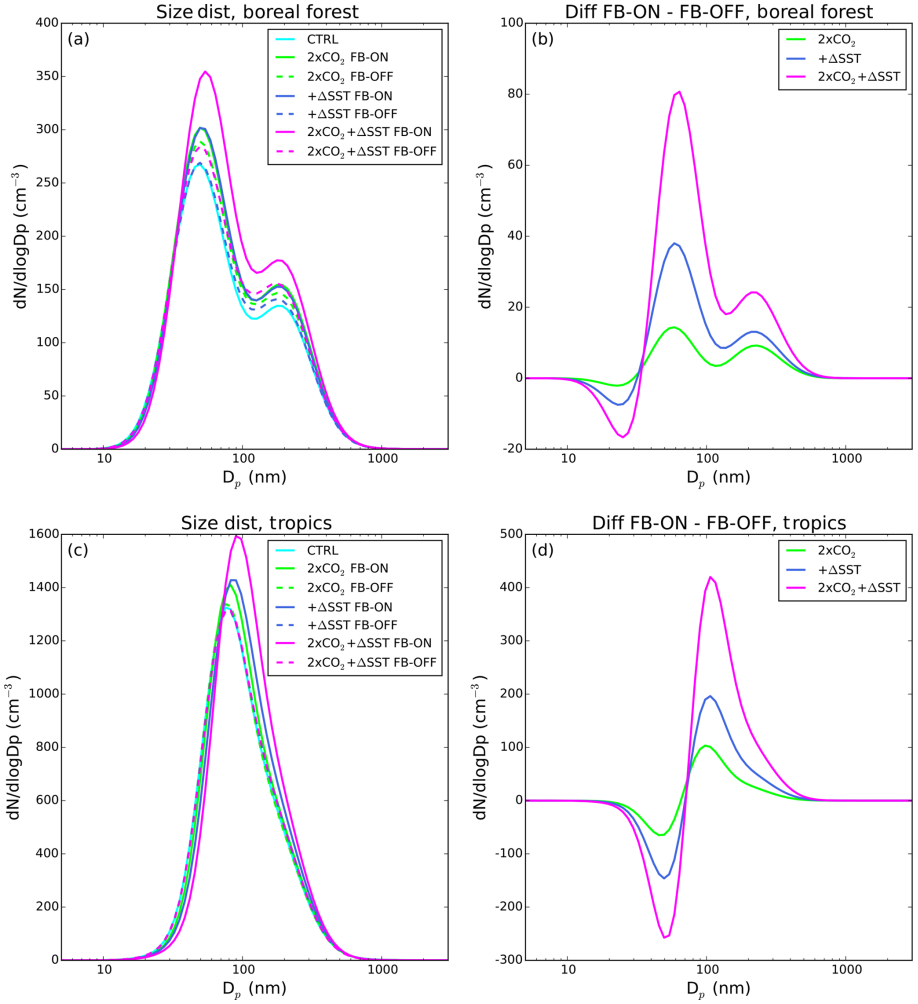

Figure 5. Annually averaged aerosol number size distributions in the boundary layer for the boreal forest region (lat.: 55 to 70° N, long.: 180° W to 180° E) and the region around the tropical islands in southeast Asia (lat.: 20° S to 20° N, long.: 90–130° E). In panels **(a)** and **(c)**, the distributions from the CTRL and the three experiments are plotted, while in panels **(b)** and **(d)**, the differences between the FB-ON and FB-OFF simulations are plotted.

3.2 The T-feedback branch

3.2.1 CCN

The CCN response of the feedback is a combination of the changes in N_a, particle sizes and hygroscopicity. The CCN concentrations are generally higher when the feedback is turned on, as is expected from the feedback (Fig. 1). However, at low supersaturations (0.2 %), the CCN concentration over some regions (in particular over the boreal forests), is lower in the simulations with the feedback turned on (Fig. 6a). The cause for this is the large amount of Aitken-mode particles formed through new particle formation. The smaller particles compete with the larger particles for the water vapour, which reduces the number of aerosol particles that can activate into cloud droplets at low supersaturations. The concentrations of CCN in these regions are very low and the absolute decrease in CCN is small. Moreover, it should be noted that the CCN concentration in the model is calculated only for the cloud-free areas in the grid boxes. Thus, the particles that are activated into cloud droplets are not included in the CCN concentrations. At higher supersaturations (1 %), also particles at smaller sizes can be activated, and thus the feedback results in more CCN almost everywhere (Fig. 6c). The areas downwind of the tropics, where the feedback mainly results in an increase in particle size, have higher CCN at both levels of supersaturation. The effect of increasing particle sizes and number generally dominates the effect of decreased particle hygroscopicity since the feedback contributes with increasing number of CCN.

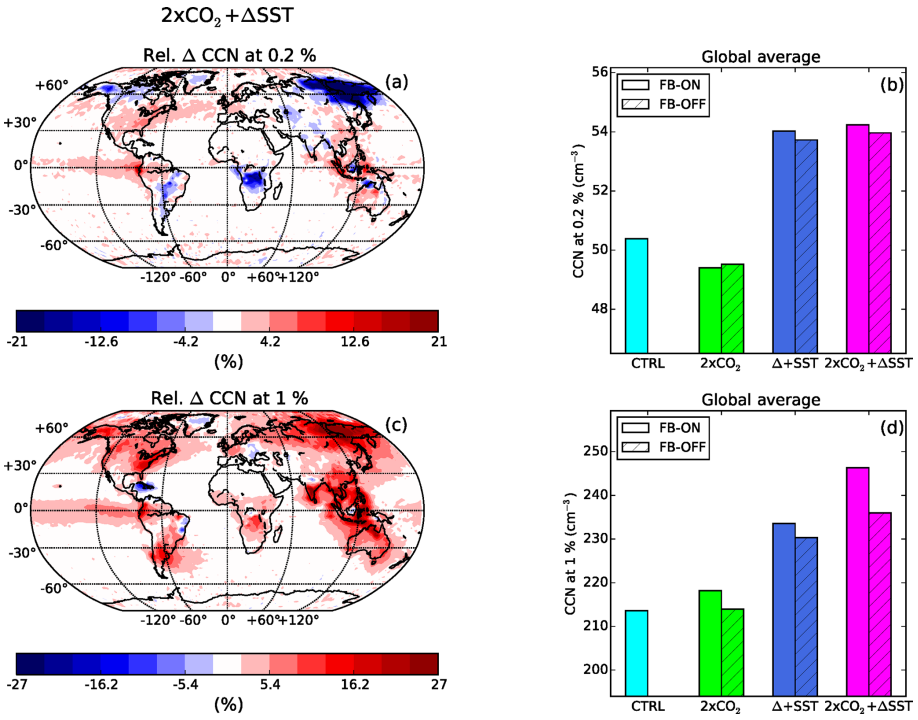

Figure 6. The relative difference between the FB-ON and FB-OFF simulations in the annual average CCN at 0.2 % **(a)** and 1 % **(c)** in the boundary layer, for the $2 \times CO_2 + \Delta SST$ experiment. In the bar plots, the globally averaged CCN at 0.2 % **(b)** and 1 % **(d)** in the boundary layer are shown for the CTRL simulation as well as the three experiments (both FB-ON and FB-OFF simulations).

3.2.2 Cloud properties

The effect from the BVOC feedback on the clouds is mainly seen over and downwind of the regions where the BVOC emissions change the most. The vertically averaged CDNC generally increase (as is expected from the BVOC feedback), mainly north of 45° N and in the tropics Fig. 7a. The weakest response of the CDNC to the feedback occurs in the experiment where only CO_2 has been changed (Figs. 7b and S5). In the experiment with only increased SST, the CDNC is higher mainly in the Northern Hemisphere since the BVOC emissions in parts of the tropics decrease (Fig. S5b). The higher levels of CDNC occur predominantly during the local summer when the BVOC emissions are the highest.

The increasing CDNC associated with the feedback is accompanied by a decrease in cloud droplet effective radius (r_e) and an increasing cloud water path (CWP) (Fig. 7c and e). The total cloud fraction (CF) does however not seem to be impacted to the same extent (see Fig. 7g and h), which may be an effect of the nudging. There is an increase in the CF over the boreal forests, mainly during winter, by up to 4 %. In summer, there is an increase in low- and mid-level clouds over the Arctic and NH midlatitudes. This is accompanied by a decrease in the high-level clouds and therefore does not show up clearly in Fig. 7g. In the tropics, there are no systematic changes in the cloud fraction as a result of the feedback.

The strongest and most widespread difference in the cloud microphysical effects occurs in the NH midlatitudes and high latitudes. One cause for this is the cloud cover and cloud types present close to the emission regions. The clouds in the midlatitudes and high latitudes are commonly stratiform, for which the model includes N_a in the calculations of CDNC (through the Abdul-Razzak and Ghan, 2000 scheme for activation). The differences in CDNC are not as widespread in the tropics, since shallow and deep convection (which aerosols generally do not affect in ESMs) are the dominant cloud types here. Another cause for the more widespread cloud changes in the NH is the larger land areas here, i.e. larger areas where the emissions differ.

3.2.3 Cloud forcing

The potential of the BVOC feedback to affect future climate will now be evaluated by investigating the changes in cloud forcing between the FB-ON and FB-OFF simulations. Since we cannot determine the full temperature response of the feedback, the differences in forcing between the FB-ON and FB-OFF simulations will be used to estimate the potential climate impact of the changed cloud properties. The patterns of the difference in the cloud forcing between the simulations with the FB turned on and the FB turned off (Fig. 8a and c) resemble the patterns of the difference in CDNC (Fig. 7a). The higher CDNC in the high latitudes and midlatitudes as-

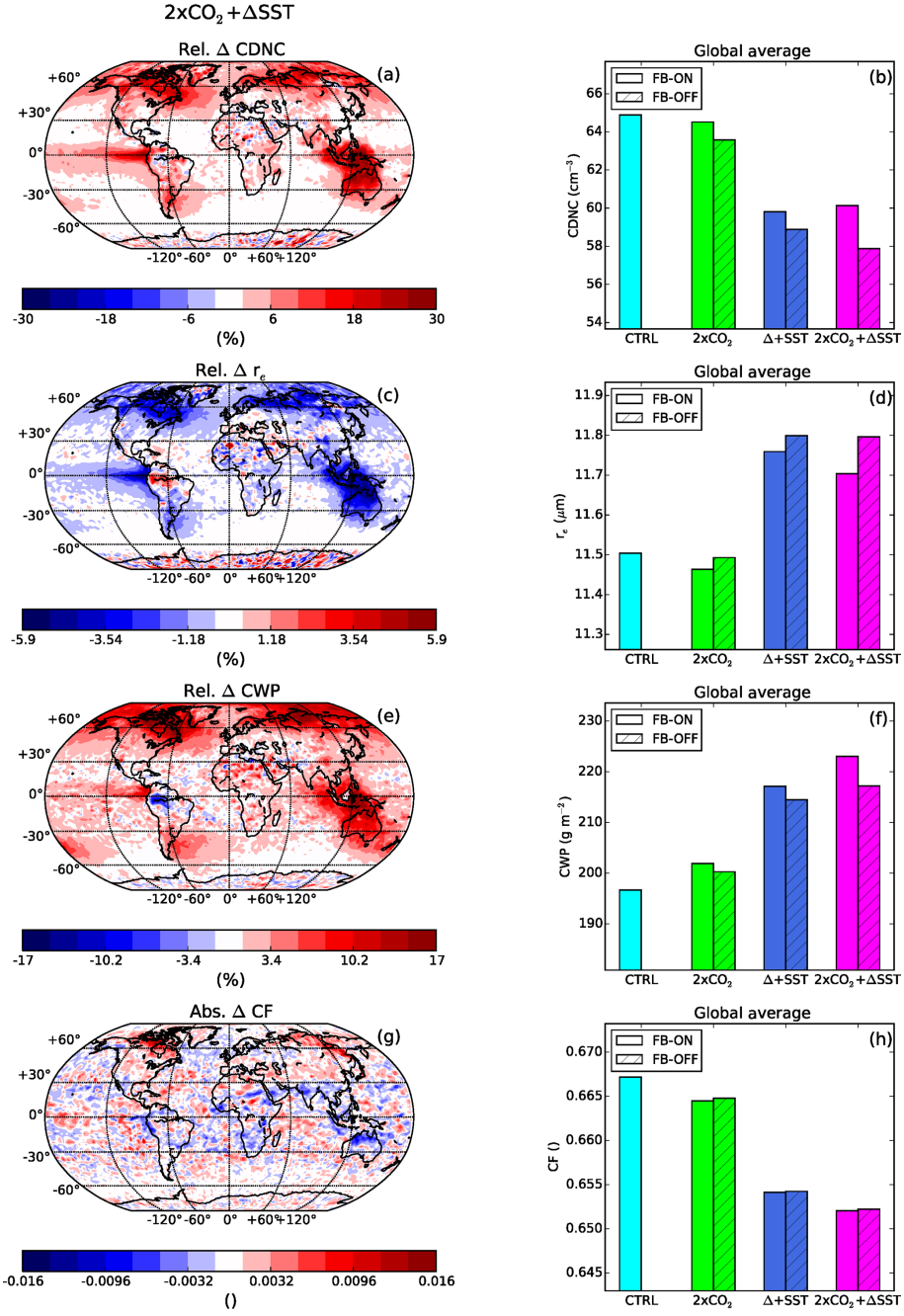

Figure 7. The relative/absolute difference between the FB-ON and FB-OFF simulations in the annual vertically averaged CDNC **(a)**, the vertically averaged r_e **(c)**, the CWP **(e)** and the total CF **(g)** for the $2 \times CO_2 + \Delta SST$ experiment. In the bar plots **(b, d, f, h)**, the globally averaged values of the same variables are shown for the CTRL simulation as well as the three experiments (both FB-ON and FB-OFF simulations). For the CDNC, r_e and CWP, the in-cloud values are used.

sociated with the FB is accompanied by a decrease in the NCF_{Ghan} by up to $-11\ W\ m^{-2}$ during the 3 summer months; see Fig. 8a. The effect of the feedback is seen mainly during the local summer when the BVOC emissions are the highest. The differences in NCF_{Ghan} are smallest in the $2 \times CO_2$ experiment and strongest in the $2 \times CO_2 + \Delta SST$ experiment (Figs. 8 and S6).

The feedback does not only contribute with an enhanced negative cloud forcing though. The difference in NCF at the surface ($\Delta\ NCF_S$) between the FB-ON and FB-OFF simulations is positive over the NH boreal forests during winter in the experiments with increased SST (Figs. 8e and S6f). The changes in microphysical properties as well as cloud cover lead to an increase in the positive long-wave cloud forcing

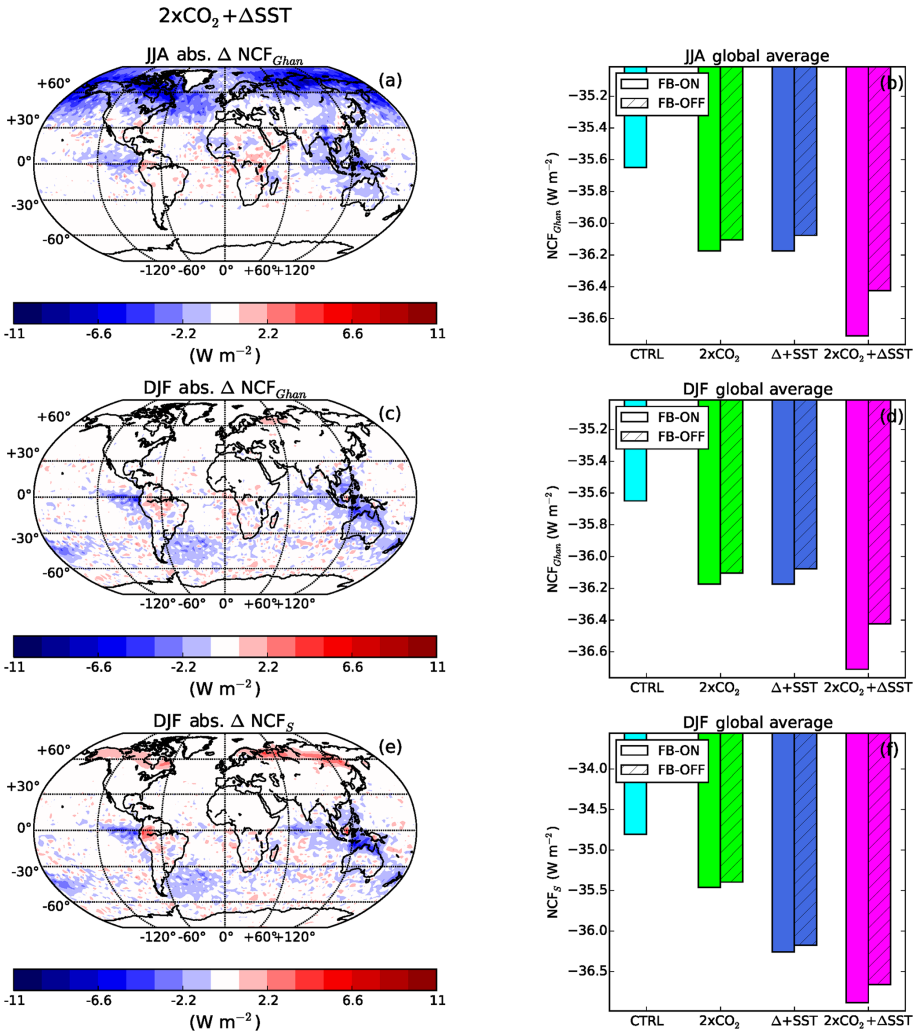

Figure 8. The absolute difference between the FB-ON and FB-OFF simulations for the NCF_{Ghan} during June, July and August **(a)**, December January and February **(c)**, as well as the NCF_S during December, January and February **(e)** for the $2 \times CO_2 + \Delta SST$ experiment. In the bar plots **(b, d, f)**, the globally averaged values of the same variables are shown for the CTRL simulation as well as the three experiments (both FB-ON and FB-OFF simulations).

(LWCF) at the surface, which is larger than the corresponding increase in negative short-wave cloud forcing (SWCF). It can be concluded that the BVOC feedback can contribute to both enhanced and reduced negative cloud forcing depending on region and season. Nevertheless, the difference in yearly global average NCF_{Ghan} is $-0.43\,W\,m^{-2}$ ($SWCF_{Ghan}$ $-0.45\,W\,m^{-2}$, $LWCF_{Ghan}$ $0.02\,W\,m^{-2}$) between the FB-ON and FB-OFF simulations in the $2 \times CO_2 + \Delta SST$ experiment, indicating that the feedback can contribute with a potentially important impact on the future climate on a global scale.

The strongest and most widespread negative cloud forcing associated with the feedback is seen in the Arctic during summer. This is interesting since the Arctic is currently, and is expected to continue, experiencing the largest warming in response to the increasing atmospheric concentrations of greenhouse gases (IPCC, 2013). The strong impact of the BVOC feedback in the Arctic during summer could possibly counteract part of this Arctic amplification. The large impact of the feedback in the NH midlatitudes and high latitudes also results in a quite large difference in the effect of the feedback between the hemispheres. The difference in the NCF_{Ghan}, between the FB-ON and FB-OFF simulations for the $2 \times CO_2 + \Delta SST$ experiments, is $-0.56\,W\,m^{-2}$ in the NH, while in the SH it is $-0.30\,W\,m^{-2}$.

3.3 The GPP-feedback branch

3.3.1 AOD

The higher aerosol loading associated with the feedback also results in higher values for the aerosol optical depth (AOD), in line with the feedback in Fig. 1. The largest relative differences between the FB-ON and FB-OFF simulations oc-

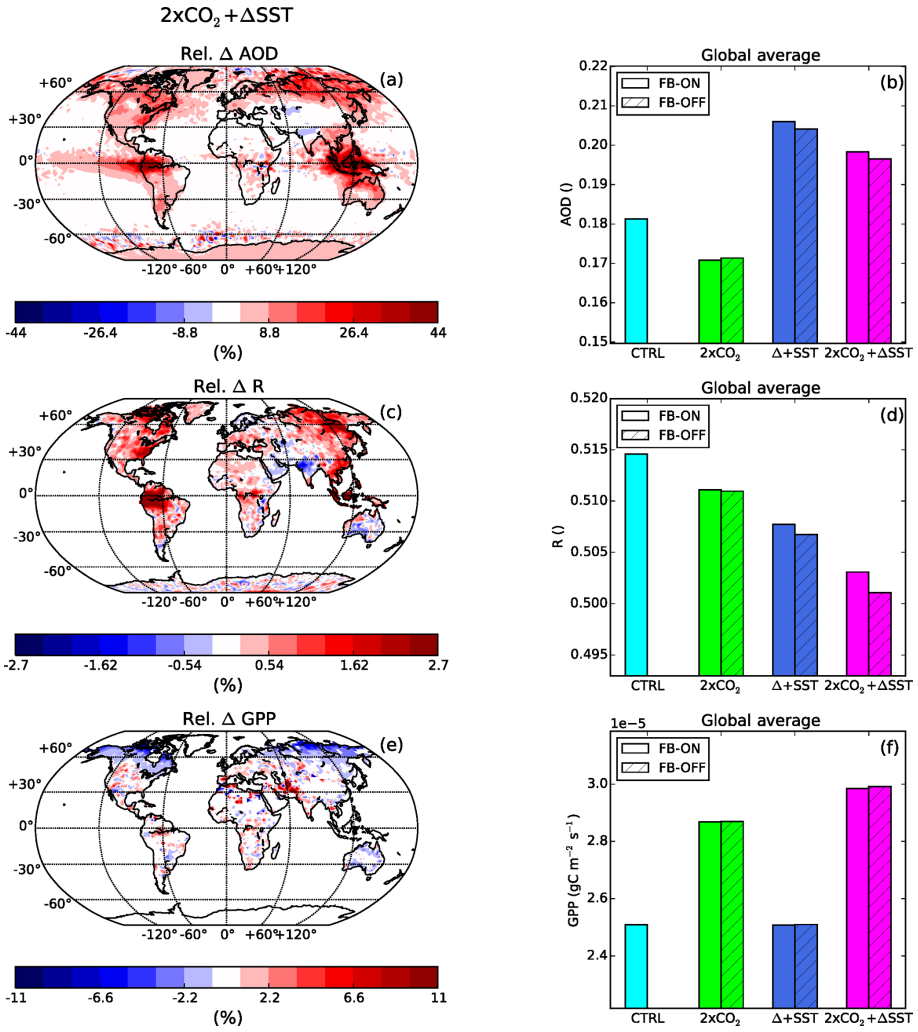

Figure 9. The relative difference between the FB-ON and FB-OFF simulations in the annually average AOD **(a)**, R **(c)** and GPP **(e)** for the $2\times CO_2 + \Delta SST$ experiment. In the bar plots **(b, d, f)**, the globally averaged values of the same variables are shown for the CTRL simulation as well as the three experiments (both FB-ON and FB-OFF simulations).

cur over, and downwind of, the tropical forest and the boreal forests in the NH; see Fig. 9a. The AOD effects are largest in the local summer when the emissions are the highest.

3.3.2 Diffuse radiation

The ratio between the diffuse radiation and the global radiation is, according the BVOC-feedback hypotheses, expected to increase with higher aerosol scattering. Our model simulations show only a small relative difference in R (maximum 5 %) between the FB-ON and FB-OFF simulations (Fig. 9c). The regions where there is a strong difference in R between the FB-ON and FB-OFF simulations correspond to the regions with the largest change in AOD. However, a statistical analysis of the differences between the monthly means from the FB-ON and FB-OFF simulations shows that the correlation coefficient between the difference in R and the difference in total cloud cover (0.53) is higher than between the difference in R and the difference in AOD (0.08); see Fig. 10a and b. Small changes in the cloud cover can offset the AOD effects on R. Changes in cloud cover can therefore explain the decreases in R over, e.g. Scandinavia (Fig. 9), even though the AOD increases there. The increase in R is expected from the BVOC feedback but the larger dependency in R on cloud fraction than AOD was not expected.

3.3.3 GPP

Next, we will investigate the relationship between R and GPP. Neither in the maps nor in the statistical analyses do we find any strong relationship between R and GPP; see Figs. 9e and 10c. The positive effect of diffuse radiation on vegetation growth is included in CLM (Oleson et al., 2013) but it seems like other factors perturbed by the T branch are affecting the

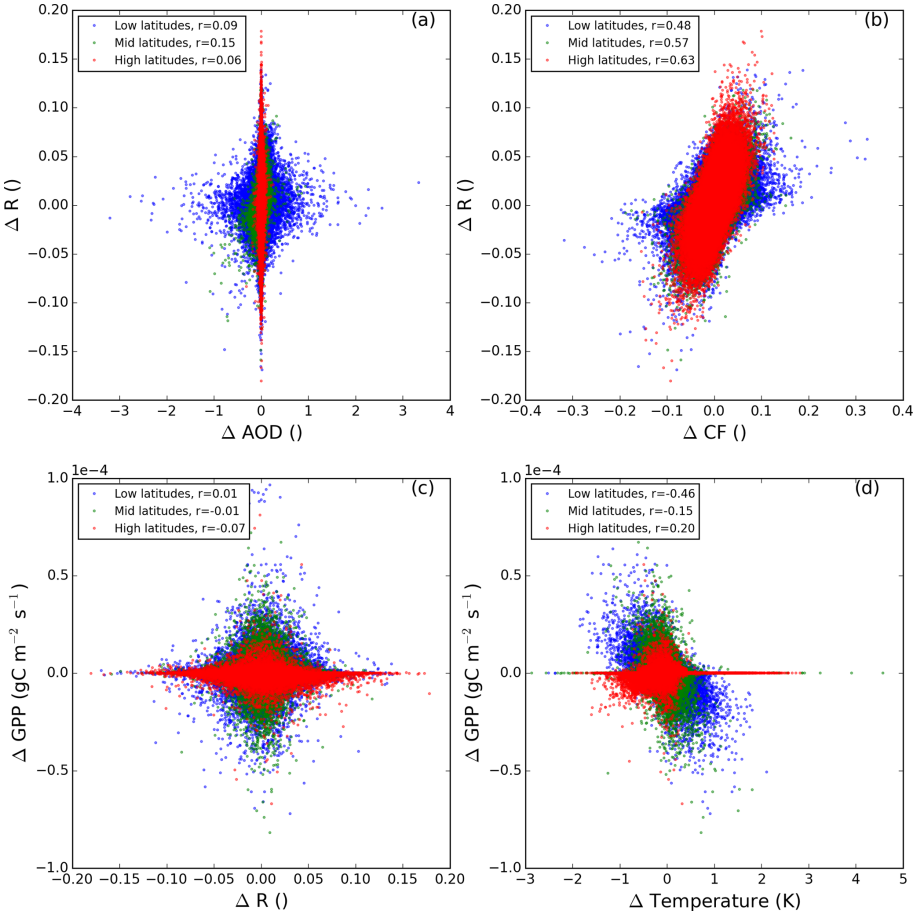

Figure 10. Scatter plots of the absolute differences (FB-ON − FB-OFF) in AOD and R in panel **(a)**, CF and R in panel **(b)**, GPP and R in panel **(c)** and GPP and temperature in the lowest model layer in panel **(d)**. Data from all three experiments ($2 \times CO_2$, $+\Delta$SST and $2 \times CO_2 + \Delta$SST) are included. Each dot is a monthly average for one grid box. Only grid boxes with a land fraction of 1 and GPP greater than zero are included. The dots are coloured according to latitude bands (high latitudes: 90–55° S and 55–90° N, midlatitudes: 55–30° S and 30–55° N, low latitudes: 30° S–30° N) and the correlations coefficient r for each region is shown in the legend. Based on the model output, AOD does not drive diffuse radiation fraction, but cloud fraction does; and diffuse radiation does not drive gross primary product, but temperature does.

vegetation more. Moreover, the difference in R between the FB-ON and FB-OFF simulations was quite small. The relationship between R and GPP is also affected by changes in the total amount of radiation. If the total radiation decreases sufficiently, an increase in R will not boost GPP (Knohl and Baldocchi, 2008). There is a negative correlation between the change in R and the change in the total visible radiation in our experiments, and the total visible radiation is generally lower in the feedback on simulations (see Fig. S8a). The hypothesised boost of GPP by R might therefore be masked by the change in the total visible radiation. Since the focus of this study is the effect of the feedback on a global scale, we have chosen not to look into if we can find the effect of R on GPP in certain conditions or locations.

The GPP instead seems to respond to changes associated with the T-feedback branch (Fig. 10d). In particular, there is a decrease of GPP in the sub-Arctic during the summer months associated with lower temperatures caused by the enhanced negative NCF_{Ghan}. Even though we are running with fixed SSTs, the temperatures over land can change somewhat in response to the changed forcing. In addition, a decrease in total visible radiation reaching the vegetation, associated with the increase in low-cloud cover in this region, can contribute to the decrease in GPP. Overall, the GPP is slightly lower in the simulations where we include the feedback, which is opposite to what is expected from the feedback in Fig. 1. These results are in contrast to the results by Rap et al. (2018), which did not include the effects from the T branch in their study. In our study, it seems that the effects from the T branch of the BVOC-feedback loop is dominating over the GPP branch. The GPP branch may however be important on local scales ot resolvable by NorESM.

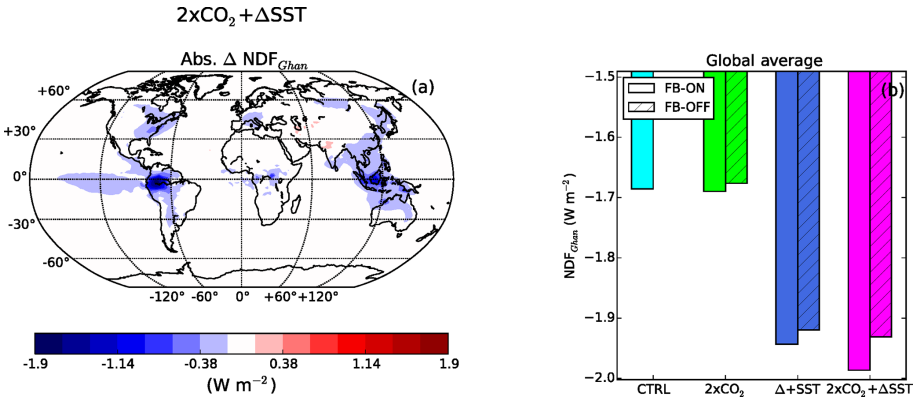

Figure 11. The absolute difference between the FB-ON and FB-OFF simulations in the annual average NDF_{Ghan} **(a)** for the $2\times CO_2+\Delta SST$ experiment. In panel **(b)**, the globally averaged NDF_{Ghan} for the CTRL simulation as well as the three experiments (both FB-ON and FB-OFF simulations) are shown.

3.4 Direct aerosol forcing

The scattering of radiation from aerosols in the atmosphere did not seem to impact the GPP significantly in our experiments, but we do find a direct impact on climate. The annual average NDF_{Ghan} is locally down to $-2.2\,W\,m^{-2}$ when the feedback is turned on; see Fig. 11a. The largest differences in NDF_{Ghan} between the FB-ON and FB-OFF simulations is seen close to the sources and over the regions that have large absolute changes in the emissions, i.e. the tropics. Globally averaged, the difference in NDF_{Ghan} is $-0.06\,W\,m^{-2}$ for the $2\times CO_2+\Delta SST$ experiment. This is approximately 15 % of the difference in forcing from the clouds. The magnitude of the differences in the NDF_{Ghan} indicates that the BVOC feedback can provide an, at least regionally, enhanced negative forcing also through the direct aerosol forcing.

3.5 Future lower aerosol loading

In order to investigate how the impact of the feedback changes if the aerosol emissions decrease in the future, we also ran the $2\times CO_2+\Delta SST$ experiment with lower anthropogenic aerosol emissions. The BVOC emissions in $2\times CO_2+\Delta SST$ LA FB-ON simulation are almost the same as those in the $2\times CO_2+\Delta SST$ FB-ON simulation (4 % and 3 % higher for isoprene and monoterpenes). The response to the feedback is however larger in the experiment with lower anthropogenic emissions. The relative differences in N_a are larger, especially over regions with large anthropogenic emissions in PD. This indicates that BVOCs will be more important for aerosol formation in the future, if the anthropogenic emissions decrease. The relative CDNC difference is also greater in the experiment with low anthropogenic emissions in both the tropics and the NH. There are areas (such as southeast Asia) where the relative differences in CDNC are close to zero in the $2\times CO_2+\Delta SST$ experiment and up to 30 % in the $2\times CO_2+\Delta SST$ LA experiment. That the effects on the clouds are largest in the $2\times CO_2+\Delta SST$ LA experiment is not surprising, since clouds formed in clean condition are most susceptible to aerosol perturbations (Spracklen and Rap, 2013).

Table 2. Difference in the global annual average NCF_{Ghan}, NDF_{Ghan} and total aerosol forcing (TAF_{Ghan}) between the FB-ON and FB-OFF simulations.

Experiments	ΔNCF_{Ghan} ($W\,m^{-2}$)	ΔNDF_{Ghan} ($W\,m^{-2}$)	ΔTAF_{Ghan} ($W\,m^{-2}$)
$2\times CO_2$	−0.11	−0.014	−0.12
$+\Delta SST$	−0.19	−0.025	−0.22
$2\times CO_2+\Delta SST$	−0.43	−0.058	−0.49
$2\times CO_2+\Delta SST$ LA	−0.66	−0.074	−0.73

The stronger BVOC impact on the clouds in the experiment with lower aerosol loading result in a larger impact from the feedback on the radiation budget. The difference in the yearly global average NCF_{Ghan} for the $2\times CO_2+\Delta SST$ LA is 53 % higher than for the $2\times CO_2+\Delta SST$ experiment; see Table 2. In addition, the direct effect associated with the feedback is larger when the anthropogenic aerosol load is reduced. The difference in NDF_{Ghan} is 29 % higher for the experiment with lower aerosol loading. These results show that the importance of the BVOC feedback will become substantially greater if, as expected, the anthropogenic aerosol emissions are reduced in the future. These results are interesting, especially since some large emitters have already started reducing their SO_2 emissions (Li et al., 2017). The total aerosol forcing associated with the feedback in the $2\times CO_2+\Delta SST$ (LA) experiment is -0.49 (-0.73) $W\,m^{-2}$, which is 13 (20) % of the positive radiative forcing (calculated according to Myhre et al., 1998) associated with a similar doubling of CO_2.

3.6 Limitations and uncertainties

The investigation of the effects of BVOCs is challenging since it involves complex interactions not only in the atmosphere but also in the biosphere. In this investigation, the focus has been on the potential atmospheric consequences of increased BVOC emissions. However, the future BVOC emissions are highly sensitive to what will happen to the vegetation. This was clearly seen in our simulations where we increased only the SST and found that GPP is reduced in several regions due to heat stress. This cancels or even reverses the BVOC feedback in these regions. How future vegetation will respond to climate change is still highly uncertain (Friend et al., 2014).

Our simulations do not allow changes in the distribution of the vegetation and therefore do not include any effects of geographical shifts in vegetation. A poleward shift in the vegetation could increase the BVOC emissions in these regions (Peñuelas and Staudt, 2010). Nevertheless, changes in surface albedo, as well as latent and sensible heat fluxes associated with such shifts (Bonan, 2008), could counteract/dominate parts of the effects seen from the increased BVOC emissions. Changes in land use also have the potential to affect the BVOC emissions but have not been taken into account in this study. A recent study by Hantson et al. (2017) including land use found no increase in BVOC emissions at the end of the century. However, they also note that the land use scenarios are highly uncertain.

There are also uncertainties associated with the emissions from the plants themselves. In MEGAN2.1, used in this study, CO_2 inhibition is included for isoprene. There are indications that the inhibition also affects monoterpenes and some studies include it also for monoterpenes (Arneth et al., 2016). Including CO_2 inhibition for monoterpenes could have reduced the difference in monoterpene emissions between the FB-ON and FB-OFF simulations and reduced the effect of the feedback. Plant stress due to heat or insect infestations can affect the magnitude and type of BVOC emissions (Zhao et al., 2017). These effects are very complex and have not been included in this study.

During the setup of the experiments of this study, we found that the model was sensitive to the diurnal variation in the BVOC emissions (also described in Sect. 2.2). The column burden of isoprene (monoterpene) was, on a global average, 57 (13) % higher when monthly averaged emission files without diurnal variation were used in the model instead of the interactive emissions. Adding a diurnal variation (the one included in CAM5.3) to the monthly emissions field improves the column burden values for isoprene, but for monoterpenes, the column burdens stay high. The resulting difference in the column burden of SOA (+5 % on a global average) is dampened by complex processes associated with nucleation and condensation. However, the lack of autocorrelation between the emissions and oxidants (when using monthly emissions) can result in longer lifetimes for the BVOC and a shift in region and level where the SOA formation occurs. This has been shown to affect the indirect aerosol effect (Karset et al., 2018). Monthly BVOC emission files should therefore be used with caution. In this study, prescribed oxidant fields at PD conditions with applied diurnal variation for OH and HO_2 were used. Running the model with more advanced gas-phase chemistry would have simulated the interactions between the BVOCs and the oxidants more realistically.

New particle formation, BVOC and SOA parameterisations are now implemented in many ESMs but are still under development and associated with uncertainties (e.g. Tsigaridis and Kanakidou, 2018; Makkonen et al., 2014; Gordon et al., 2016). The BVOC feedback mechanism is highly sensitive to the parameterisations associated with new particle and SOA formation. The yields associated with the formation of LVSOA and SVSOA from monoterpenes and isoprene are largely uncertain, which may significantly affect the feedback. The parameterisations of nucleation rates and early growth of the particles can also have a strong impact on the simulations of the feedback. Moreover, the SOA scheme in NorESM does not account for effects of temperature on partitioning of SOA precursors. Warmer temperatures might lead to less SOA formation with same amount of precursors, which would reduce the feedback. In addition, the SOA formation from biogenic precursors could be highly susceptible to modification by anthropogenic emissions of VOCs (Spracklen et al., 2011), which are not currently included in NorESM. We hope that the importance of the feedback found in this study will inspire further development of these parameterisations in ESMs.

Running the model with fixed SSTs and nudging provides a nice setup to study each step in the feedback loops at low computational cost, but it also comes with some limitations. The nudging enabled us to run the FB-ON and FB-OFF simulations with the same meteorological conditions. We can therefore conclude that the difference between the simulations was only associated with the BVOC emissions and the feedback and not caused by natural variability. The nudging does however mean that any impacts of the feedback on horizontal winds and pressure are not captured in this investigation. Moreover, the fixed SSTs and sea ice limit the temperature response to the feedback. There is some temperature response to forcing induced by the feedback over land but not over the oceans. The second-order feedbacks, such as decreasing BVOC emissions associated with the temperature decrease due to the enhanced negative cloud and direct forcing, will not be properly simulated with this setup. Investigating the feedback with free-running simulations using a coupled version of NorESM would be a very nice complement to this study.

In this paper, we have focused on the BVOC feedback mechanisms shown in Fig. 1, but there are other indirect effects of BVOCs that could influence the feedback that are not included in this study. Two such effects involve impacts on ozone production and methane lifetime. When BVOCs are

oxidised in the atmosphere, they affect the chemical composition as well as the oxidising capacity of the atmosphere. Firstly, BVOCs can contribute to enhanced ozone production if sufficient NO_x is available, while they can give a net consumption in low NO_x conditions (Monks et al., 2015). Secondly, the oxidation of BVOCs can decrease the oxidation capacity of the atmosphere, thus increasing the atmospheric lifetime of methane. Both of these effects could result in a positive radiative forcing with increased BVOC emissions. Previous studies have found BVOC-induced changes in the direct aerosol forcing to be roughly balanced by the changes in the forcing from ozone and methane (Unger, 2014; Scott et al., 2018b). This indicates that part of the forcing (the NDF in this study is 12 % of the total forcing) associated with BVOC feedback investigated in this paper could be offset by changes in ozone and methane lifetime.

Moreover, some of the processes in the BVOC feedback investigated here may affect the carbon budget; however, such effects are out of the scope of this paper.

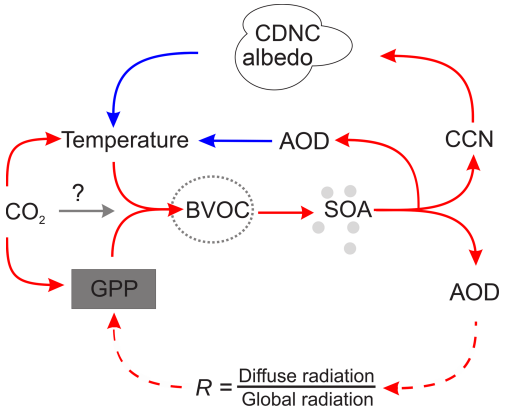

Figure 12. Our modified version of the BVOC feedback according to the results from this study. The red arrows in the figure indicate that if the variable at the start of the arrow increases, then the variable at the end of the arrow is also expected to increase. A blue arrow on the other hand means that an increase in the variable at the start of the arrow is expected to result in a decrease in the variable at the end of the arrow. The GPP branch of the feedback now has dashed lines and the changed AOD has been found to impact temperature.

4 Conclusions

An ESM has been used to investigate two feedbacks induced by increased emissions of BVOCs in response to higher CO_2 concentrations and/or temperature (Fig. 1). We find that higher BVOC emissions indeed lead to the formation of more SOA mass, as well as both higher aerosol number concentrations and larger particle sizes. This leads to clouds with more and smaller droplets and higher cloud water path. The changes in the clouds are found to contribute with an enhanced negative cloud forcing, confirming the possibility for BVOCs to contribute with a negative climate feedback. The feedback is strongest over and downwind of the boreal and tropical forests. Solely increasing the CO_2 levels produces a somewhat weaker feedback response than solely increasing the temperatures, but the strongest response comes from increasing both CO_2 and temperature.

In this investigation, we do not find that the enhanced aerosol scattering leads to a boost of GPP globally (see Fig. 1). The response of the GPP is instead dominated by the BVOC-induced changes of the clouds. The enhanced aerosol scattering associated with the feedback is however found to lead to a stronger negative forcing (direct effect). We would therefore suggest modifying the BVOC feedback in Fig. 1 as can be seen in Fig. 12. Because the GPP seems to be more affected by the cloud changes than the AOD changes, the arrows between AOD and GPP have been dashed. However, AOD can now be seen having a negative feedback on temperature. The combined effects from both altered cloud properties and AOD are found to contribute with a negative radiative effect of $-0.49\,\mathrm{W\,m^{-2}}$. To put this number in context, the radiative forcing from a doubling of CO_2 is about $3.7\,\mathrm{W\,m^{-2}}$. Thus, the forcing associated with the BVOC feedback could offset this by about 13 %, or even up to 20 %, given a strong reduction in anthropogenic aerosols. This leads us to conclude that the BVOC feedback is very relevant for estimating climate sensitivity with ESMs and providing model-based projections of the future climate.

There are still large uncertainties associated with the processes associated with the BVOC feedback, both in models and measurements. The aim of this study was not to provide a final answer regarding the importance of the feedback. Instead, we wanted to use the current knowledge implemented in NorESM to test the potential importance of including these processes in an ESM when predicting the future climate. The results from this study should encourage and inspire further research to improve the representation of these processes in ESMs.

Data availability. The CAM5.3-Oslo code is available for registered users by signing a respective license. In order to initiate this process, please contact noresm-ncc@met.no. Users should briefly state themselves as CESM users on the CESM website (http://www.cesm.ucar.edu/models/register/register.html, last access: 4 April 2019). The temporally averaged model output from the nine simulations in Table 1 is available here: https://doi.org/10.11582/2019.00008 (Sporre, 2019). The monthly data and the data from the spin-up and meteorological simulations will be shared upon request. The reason for not supplying and storing all the data online is the large size of the entire dataset.

Supplement. The supplement related to this article is available online at: https://doi.org/10.5194/acp-19-4763-2019-supplement.

Author contributions. MKS performed the model simulations, conducted the data analysis and wrote the manuscript. IHHK provided support during the setup of the model. SMB, IHKK, RM and TKB contributed with discussions regarding the experimental design, data analysis and manuscript.

Competing interests. The authors declare that they have no conflict of interest.

Special issue statement. This article is part of the special issue "BACCHUS – Impact of Biogenic versus Anthropogenic emissions on Clouds and Climate: towards a Holistic UnderStanding (ACP/AMT/GMD inter-journal SI)". It is not associated with a conference.

Acknowledgements. The research leading to these results has received funding from the European Union's Seventh Framework Programme (FP7/2007-2013) project BACCHUS under grant agreement no. 603445. This work was supported by LATICE, a strategic research area funded by the Faculty of Mathematics and Natural Sciences at the University of Oslo. This work has been financed by the research council of Norway (RCN) through the NOTUR/Norstore project NN9485K "Biogenic aerosols and climate feedbacks". Inger H. H. Karset has been financed by the research council of Norway through the project EVA and the NOTUR/Norstore projects (Sigma2 account: nn2345k, Norstore account: NS2345K). We would like to thank Alf Kirkevåg and Øivind Sealand for support in the work with NorESM.

Review statement. This paper was edited by Holger Tost and reviewed by two anonymous referees.

References

Abdul-Razzak, H. and Ghan, S. J.: A parameterization of aerosol activation: 2. Multiple aerosol types, J. Geophys. Res.-Atmos., 105, 6837–6844, https://doi.org/10.1029/1999JD901161, 2000.

Albrecht, B. A.: Aerosols, Cloud Microphysics, and Fractional Cloudiness, Science, 245, 1227–1230, https://doi.org/10.1126/science.245.4923.1227, 1989.

Arneth, A., Makkonen, R., Olin, S., Paasonen, P., Holst, T., Kajos, M. K., Kulmala, M., Maximov, T., Miller, P. A., and Schurgers, G.: Future vegetation–climate interactions in Eastern Siberia: an assessment of the competing effects of CO_2 and secondary organic aerosols, Atmos. Chem. Phys., 16, 5243–5262, https://doi.org/10.5194/acp-16-5243-2016, 2016.

Bentsen, M., Bethke, I., Debernard, J. B., Iversen, T., Kirkevåg, A., Seland, Ø., Drange, H., Roelandt, C., Seierstad, I. A., Hoose, C., and Kristjánsson, J. E.: The Norwegian Earth System Model, NorESM1-M – Part 1: Description and basic evaluation of the physical climate, Geosci. Model Dev., 6, 687–720, https://doi.org/10.5194/gmd-6-687-2013, 2013.

Bonan, G. B.: Forests and Climate Change: Forcings, Feedbacks, and the Climate Benefits of Forests, Science, 320, 1444–1449, https://doi.org/10.1126/science.1155121, 2008.

Carslaw, K. S., Boucher, O., Spracklen, D. V., Mann, G. W., Rae, J. G. L., Woodward, S., and Kulmala, M.: A review of natural aerosol interactions and feedbacks within the Earth system, Atmos. Chem. Phys., 10, 1701–1737, https://doi.org/10.5194/acp-10-1701-2010, 2010.

Friend, A. D., Lucht, W., Rademacher, T. T., Keribin, R., Betts, R., Cadule, P., Ciais, P., Clark, D. B., Dankers, R., Falloon, P. D., Ito, A., Kahana, R., Kleidon, A., Lomas, M. R., Nishina, K., Ostberg, S., Pavlick, R., Peylin, P., Schaphoff, S., Vuichard, N., Warszawski, L., Wiltshire, A., and Woodward, F. I.: Carbon residence time dominates uncertainty in terrestrial vegetation responses to future climate and atmospheric CO_2, P. Natl. Acad. Sci. USA, 111, 3280–3285, https://doi.org/10.1073/pnas.1222477110, 2014.

Gettelman, A. and Morrison, H.: Advanced Two-Moment Bulk Microphysics for Global Models. Part I: Off-Line Tests and Comparison with Other Schemes, J. Climate, 28, 1268–1287, https://doi.org/10.1175/JCLI-D-14-00102.1, 2015.

Ghan, S. J.: Technical Note: Estimating aerosol effects on cloud radiative forcing, Atmos. Chem. Phys., 13, 9971–9974, https://doi.org/10.5194/acp-13-9971-2013, 2013.

Glasius, M. and Goldstein, A. H.: Recent Discoveries and Future Challenges in Atmospheric Organic Chemistry, Environ. Sci. Tech., 50, 2754–2764, https://doi.org/10.1021/acs.est.5b05105, 2016.

Gordon, H., Sengupta, K., Rap, A., Duplissy, J., Frege, C., Williamson, C., Heinritzi, M., Simon, M., Yan, C., Almeida, J., Tröstl, J., Nieminen, T., Ortega, I. K., Wagner, R., Dunne, E. M., Adamov, A., Amorim, A., Bernhammer, A.-K., Bianchi, F., Breitenlechner, M., Brilke, S., Chen, X., Craven, J. S., Dias, A., Ehrhart, S., Fischer, L., Flagan, R. C., Franchin, A., Fuchs, C., Guida, R., Hakala, J., Hoyle, C. R., Jokinen, T., Junninen, H., Kangasluoma, J., Kim, J., Kirkby, J., Krapf, M., Kürten, A., Laaksonen, A., Lehtipalo, K., Makhmutov, V., Mathot, S., Molteni, U., Monks, S. A., Onnela, A., Peräkylä, O., Piel, F., Petäjä, T., Praplan, A. P., Pringle, K. J., Richards, N. A. D., Rissanen, M. P., Rondo, L., Sarnela, N., Schobesberger, S., Scott, C. E., Seinfeld, J. H., Sharma, S., Sipilä, M., Steiner, G., Stozhkov, Y., Stratmann, F., Tomé, A., Virtanen, A., Vogel, A. L., Wagner, A. C., Wagner, P. E., Weingartner, E., Wimmer, D., Winkler, P. M., Ye, P., Zhang, X., Hansel, A., Dommen, J., Donahue, N. M., Worsnop, D. R., Baltensperger, U., Kulmala, M., Curtius, J., and Carslaw, K. S.: Reduced anthropogenic aerosol radiative forcing caused by biogenic new particle formation, P. Natl. Acad. Sci. USA, 113, 12053–12058, https://doi.org/10.1073/pnas.1602360113, 2016.

Gordon, H., Kirkby, J., Baltensperger, U., Bianchi, F., Breitenlechner, M., Curtius, J., Dias, A., Dommen, J., Donahue, N. M., Dunne, E. M., Duplissy, J., Ehrhart, S., Flagan, R. C., Frege, C., Fuchs, C., Hansel, A., Hoyle, C. R., Kulmala, M., Kürten, A., Lehtipalo, K., Makhmutov, V., Molteni, U., Rissanen, M. P., Stozkhov, Y., Tröstl, J., Tsagkogeorgas, G., Wagner, R., Williamson, C., Wimmer, D., Winkler, P. M., Yan, C., and Carslaw, K. S.: Causes and importance of new particle formation in the present-day and pre-

industrial atmospheres, J. Geophys. Res.-Atmos., 122, 8739–8760, https://doi.org/10.1002/2017JD026844, 2017.

Guenther, A., Hewitt, C. N., Erickson, D., Fall, R., Geron, C., Graedel, T., Harley, P., Klinger, L., Lerdau, M., Mckay, W. A., Pierce, T., Scholes, B., Steinbrecher, R., Tallamraju, R., Taylor, J., and Zimmerman, P.: A global model of natural volatile organic compound emissions, J. Geophys. Res.-Atmos., 100, 8873–8892, https://doi.org/10.1029/94JD02950, 1995.

Guenther, A. B., Jiang, X., Heald, C. L., Sakulyanontvittaya, T., Duhl, T., Emmons, L. K., and Wang, X.: The Model of Emissions of Gases and Aerosols from Nature version 2.1 (MEGAN2.1): an extended and updated framework for modeling biogenic emissions, Geosci. Model Dev., 5, 1471–1492, https://doi.org/10.5194/gmd-5-1471-2012, 2012.

Hantson, S., Knorr, W., Schurgers, G., Pugh, T. A., and Arneth, A.: Global isoprene and monoterpene emissions under changing climate, vegetation, CO_2 and land use, Atmos. Environ., 155, 35–45, https://doi.org/10.1016/j.atmosenv.2017.02.010, 2017.

IPCC: Summary for Policymakers, in: Climate Change 2013: The Physical Science Basis, Contribution of Working Group I to the Fifth Assessment Report of the Intergovernmental Panel on Climate Change, edited by: Stocker, T. F., Qin, D., Plattner, G.-K., Tignor, M., Allen, S. K., Boschung, J., Nauels, A., Xia, Y., Bex, V., and Midgley, P. M., Cambridge University Press, Cambridge, UK, New York, NY, USA, 2013.

Iversen, T., Bentsen, M., Bethke, I., Debernard, J. B., Kirkevåg, A., Seland, Ø., Drange, H., Kristjansson, J. E., Medhaug, I., Sand, M., and Seierstad, I. A.: The Norwegian Earth System Model, NorESM1-M – Part 2: Climate response and scenario projections, Geosci. Model Dev., 6, 389–415, https://doi.org/10.5194/gmd-6-389-2013, 2013.

Jokinen, T., Berndt, T., Makkonen, R., Kerminen, V.-M., Junninen, H., Paasonen, P., Stratmann, F., Herrmann, H., Guenther, A. B., Worsnop, D. R., Kulmala, M., Ehn, M., and Sipilä, M.: Production of extremely low volatile organic compounds from biogenic emissions: Measured yields and atmospheric implications, P. Natl. Acad. Sci. USA, 112, 7123–7128, https://doi.org/10.1073/pnas.1423977112, 2015.

Karset, I. H. H., Berntsen, T. K., Storelvmo, T., Alterskjær, K., Grini, A., Olivié, D., Kirkevåg, A., Seland, Ø., Iversen, T., and Schulz, M.: Strong impacts on aerosol indirect effects from historical oxidant changes, Atmos. Chem. Phys., 18, 7669–7690, https://doi.org/10.5194/acp-18-7669-2018, 2018.

Khairoutdinov, M. and Kogan, Y.: A New Cloud Physics Parameterization in a Large-Eddy Simulation Model of Marine Stratocumulus, Mon. Weather Rev., 128, 229–243, 2000.

Kirkevåg, A., Iversen, T., Seland, Ø., Hoose, C., Kristjánsson, J. E., Struthers, H., Ekman, A. M. L., Ghan, S., Griesfeller, J., Nilsson, E. D., and Schulz, M.: Aerosol–climate interactions in the Norwegian Earth System Model – NorESM1-M, Geosci. Model Dev., 6, 207–244, https://doi.org/10.5194/gmd-6-207-2013, 2013.

Kirkevåg, A., Grini, A., Olivié, D., Seland, Ø., Alterskjær, K., Hummel, M., Karset, I. H. H., Lewinschal, A., Liu, X., Makkonen, R., Bethke, I., Griesfeller, J., Schulz, M., and Iversen, T.: A production-tagged aerosol module for Earth system models, OsloAero5.3 – extensions and updates for CAM5.3-Oslo, Geosci. Model Dev., 11, 3945–3982, https://doi.org/10.5194/gmd-11-3945-2018, 2018

Knohl, A. and Baldocchi, D. D.: Effects of diffuse radiation on canopy gas exchange processes in a forest ecosystem, J. Geophys. Res.-Biogeo., 113, 1–17, https://doi.org/10.1029/2007JG000663, 2008.

Kooperman, G. J., Pritchard, M. S., Ghan, S. J., Wang, M., Somerville, R. C. J., and Russell, L. M.: Constraining the influence of natural variability to improve estimates of global aerosol indirect effects in a nudged version of the Community Atmosphere Model 5, J. Geophys. Res.-Atmos., 117, 1–16, https://doi.org/10.1029/2012JD018588, 2012.

Kulmala, M., Suni, T., Lehtinen, K. E. J., Dal Maso, M., Boy, M., Reissell, A., Rannik, Ü., Aalto, P., Keronen, P., Hakola, H., Bäck, J., Hoffmann, T., Vesala, T., and Hari, P.: A new feedback mechanism linking forests, aerosols, and climate, Atmos. Chem. Phys., 4, 557–562, https://doi.org/10.5194/acp-4-557-2004, 2004.

Kulmala, M., Nieminen, T., Chellapermal, R., Makkonen, R., Bäck, J., and Kerminen, V.-M.: Climate Feedbacks Linking the Increasing Atmospheric CO 2 Concentration, BVOC Emissions, Aerosols and Clouds in Forest Ecosystems, chap. 17, in: Biology, Controls and Models of Tree Volatile Organic Compound Emissions, 5 edn., edited by: Niinemets, Ü. and Monson, R., Springer, Dordrecht, 489–508, https://doi.org/10.1007/978-94-007-6606-8, 2013.

Kulmala, M., Nieminen, T., Nikandrova, A., Lehtipalo, K., Manninen, H. E., Kajos, M. K., Kolari, P., Lauri, A., Petäjä, T., Krejci, R., Vesala, T., Kerminen, V. M., Nieminen, T., Kolari, P., Hari, P., Bäck, J., Krejci, R., Hansson, H. C., Swietlicki, E., Lindroth, A., Christensen, T. R., and Arneth, A.: CO2-induced terrestrial climate feedback mechanism: From carbon sink to aerosol source and back, Boreal Environ. Res., 19, 122–131, 2014.

Laothawornkitkul, J., Taylor, J. E., Paul, N. D., and Hewitt, C. N.: Biogenic volatile organic compounds in the Earth system, New Phytol., 183, 27–51, https://doi.org/10.1111/j.1469-8137.2009.02859.x, 2009.

Lehtinen, K. E., Dal Maso, M., Kulmala, M., and Kerminen, V. M.: Estimating nucleation rates from apparent particle formation rates and vice versa: Revised formulation of the Kerminen-Kulmala equation, J. Aerosol Sci., 38, 988–994, https://doi.org/10.1016/j.jaerosci.2007.06.009, 2007.

Li, C., McLinden, C., Fioletov, V., Krotkov, N., Carn, S., Joiner, J., Streets, D., He, H., Ren, X., Li, Z., and Dickerson, R. R.: India Is Overtaking China as the World's Largest Emitter of Anthropogenic Sulfur Dioxide, Sci. Rep., 7, 14304, https://doi.org/10.1038/s41598-017-14639-8, 2017.

Makkonen, R., Asmi, A., Kerminen, V.-M., Boy, M., Arneth, A., Hari, P., and Kulmala, M.: Air pollution control and decreasing new particle formation lead to strong climate warming, Atmos. Chem. Phys., 12, 1515–1524, https://doi.org/10.5194/acp-12-1515-2012, 2012.

Makkonen, R., Seland, Ø., Kirkevåg, A., Iversen, T., and Kristjánsson, J. E.: Evaluation of aerosol number concentrations in NorESM with improved nucleation parameterization, Atmos. Chem. Phys., 14, 5127–5152, https://doi.org/10.5194/acp-14-5127-2014, 2014.

Monks, P. S., Archibald, A. T., Colette, A., Cooper, O., Coyle, M., Derwent, R., Fowler, D., Granier, C., Law, K. S., Mills, G. E., Stevenson, D. S., Tarasova, O., Thouret, V., von Schneidemesser, E., Sommariva, R., Wild, O., and Williams, M. L.: Tropospheric ozone and its precursors from the urban to the global scale from

air quality to short-lived climate forcer, Atmos. Chem. Phys., 15, 8889–8973, https://doi.org/10.5194/acp-15-8889-2015, 2015.

Morison, J. I. L. and Lawlor, D. W.: Interactions between increasing CO_2 concentration and temperature on plant growth, Plant Cell Environ., 22, 659–682, https://doi.org/10.1046/j.1365-3040.1999.00443.x, 1999.

Morrison, H. and Gettelman, A.: A new two-moment bulk stratiform cloud microphysics scheme in the community atmosphere model, version 3 (CAM3), Part I: Description and numerical tests, J. Climate, 21, 3642–3659, https://doi.org/10.1175/2008JCLI2105.1, 2008.

Myhre, G., Highwood, E. J., Shine, K. P., and Stordal, F.: New estimates of radiative forcing due to well mixed greenhouse gases, Geophys. Res. Lett., 25, 2715–2718, https://doi.org/10.1029/98GL01908, 1998.

Oleson, K. W., Lawrence, D. M., Bonan, G. B., Drewniak, B., Huang, M., Koven, C. D., Levis, S., Li, F., Riley, W. J., Subin, Z. M., Swenson, S. C., Thornton, P. E., Bozbiyik, A., Fisher, R., Heald, C. L., Kluzek, E., Lamarque, J.-f., Lawrence, P. J., Leung, L. R., Lipscomb, W., Muszala, S., Ricciuto, D. M., Sacks, W., Sun, Y., Tang, J., and Yang, Z.-L.: Technical description of version 4.0 of the Community Land Model (CLM), NCAR/TN-503+STR NCAR Technical Note, p. 266, https://doi.org/10.5065/D6RR1W7M, 2013.

Paasonen, P., Nieminen, T., Asmi, E., Manninen, H. E., Petäjä, T., Plass-Dülmer, C., Flentje, H., Birmili, W., Wiedensohler, A., Hõrrak, U., Metzger, A., Hamed, A., Laaksonen, A., Facchini, M. C., Kerminen, V.-M., and Kulmala, M.: On the roles of sulphuric acid and low-volatility organic vapours in the initial steps of atmospheric new particle formation, Atmos. Chem. Phys., 10, 11223–11242, https://doi.org/10.5194/acp-10-11223-2010, 2010.

Paasonen, P., Asmi, A., Petäjä, T., Kajos, M. K., Äijälä, M., Junninen, H., Holst, T., Abbatt, J. P. D., Arneth, A., Birmili, W., van der Gon, H. D., Hamed, A., Hoffer, A., Laakso, L., Laaksonen, A., Richard Leaitch, W., Plass-Dülmer, C., Pryor, S. C., Räisänen, P., Swietlicki, E., Wiedensohler, A., Worsnop, D. R., Kerminen, V.-M., and Kulmala, M.: Warming-induced increase in aerosol number concentration likely to moderate climate change, Nat. Geosci., 6, 438–442, https://doi.org/10.1038/ngeo1800, 2013.

Park, S. and Bretherton, C. S.: The University of Washington Shallow Convection and Moist Turbulence Schemes and Their Impact on Climate Simulations with the Community Atmosphere Model, J. Climate, 22, 3449–3469, https://doi.org/10.1175/2008JCLI2557.1, 2009.

Peñuelas, J. and Staudt, M.: BVOCs and global change, Trends Plant Sci., 15, 133–144, https://doi.org/10.1016/j.tplants.2009.12.005, 2010.

Rap, A., Scott, C. E., Reddington, C. L., Mercado, L., Ellis, R. J., Garraway, S., Evans, M. J., Beerling, D. J., MacKenzie, A. R., Hewitt, C. N., and Spracklen, D. V.: Enhanced global primary production by biogenic aerosol via diffuse radiation fertilization, Nat. Geosci., 11, 640–644, https://doi.org/10.1038/s41561-018-0208-3, 2018.

Roderick, M. L., Farquhar, G. D., Berry, S. L., and Noble, I. R.: On the direct effect of clouds and atmospheric particles on the productivity and structure of vegetation, Oecologia, 129, 21–30, https://doi.org/10.1007/s004420100760, 2001.

Scott, C. E., Arnold, S. R., Monks, S. A., Asmi, A., Paasonen, P., and Spracklen, D. V.: Substantial large-scale feedbacks between natural aerosols and climate, Nat. Geosci., 11, 44–48, https://doi.org/10.1038/s41561-017-0020-5, 2018a.

Scott, C. E., Monks, S. A., Spracklen, D. V., Arnold, S. R., Forster, P. M., Rap, A., Äijälä, M., Artaxo, P., Carslaw, K. S., Chipperfield, M. P., Ehn, M., Gilardoni, S., Heikkinen, L., Kulmala, M., Petäjä, T., Reddington, C. L. S., Rizzo, L. V., Swietlicki, E., Vignati, E., and Wilson, C.: Impact on short-lived climate forcers increases projected warming due to deforestation, Nat. Commun., 9, 157, https://doi.org/10.1038/s41467-017-02412-4, 2018b.

Shrivastava, M., Cappa, C. D., Fan, J., Goldstein, A. H., Guenther, A. B., Jimenez, J. L., Kuang, C., Laskin, A., Martin, S. T., Ng, N. L., Petaja, T., Pierce, J. R., Rasch, P. J., Roldin, P., Seinfeld, J. H., Shilling, J., Smith, J. N., Thornton, J. A., Volkamer, R., Wang, J., Worsnop, D. R., Zaveri, R. A., Zelenyuk, A., and Zhang, Q.: Recent advances in understanding secondary organic aerosol: Implications for global climate forcing, Rev. Geophys., 55, 509–559, https://doi.org/10.1002/2016RG000540, 2017.

Smith, S. J., Rao, S., Riahi, K., van Vuuren, D. P., Calvin, K. V., and Kyle, P.: Future aerosol emissions: a multi-model comparison, Clim. Change, 138, 13–24, https://doi.org/10.1007/s10584-016-1733-y, 2016.

Sporre, M. K.: BVOC-aerosol-climate feedbacks – simulation data from NorESM, Data set, Norstore, https://doi.org/10.11582/2019.00008, last access: 29 March 2019.

Spracklen, D. V. and Rap, A.: Natural aerosol–climate feedbacks suppressed by anthropogenic aerosol, Geophys. Res. Lett., 40, 5316–5319, https://doi.org/10.1002/2013GL057966, 2013.

Spracklen, D. V., Jimenez, J. L., Carslaw, K. S., Worsnop, D. R., Evans, M. J., Mann, G. W., Zhang, Q., Canagaratna, M. R., Allan, J., Coe, H., McFiggans, G., Rap, A., and Forster, P.: Aerosol mass spectrometer constraint on the global secondary organic aerosol budget, Atmos. Chem. Phys., 11, 12109–12136, https://doi.org/10.5194/acp-11-12109-2011, 2011.

Tsigaridis, K. and Kanakidou, M.: The Present and Future of Secondary Organic Aerosol Direct Forcing on Climate, Curr. Clim. Change Rep., 4, 1–15, https://doi.org/10.1007/s40641-018-0092-3, 2018.

Tsigaridis, K., Daskalakis, N., Kanakidou, M., Adams, P. J., Artaxo, P., Bahadur, R., Balkanski, Y., Bauer, S. E., Bellouin, N., Benedetti, A., Bergman, T., Berntsen, T. K., Beukes, J. P., Bian, H., Carslaw, K. S., Chin, M., Curci, G., Diehl, T., Easter, R. C., Ghan, S. J., Gong, S. L., Hodzic, A., Hoyle, C. R., Iversen, T., Jathar, S., Jimenez, J. L., Kaiser, J. W., Kirkevåg, A., Koch, D., Kokkola, H., Lee, Y. H., Lin, G., Liu, X., Luo, G., Ma, X., Mann, G. W., Mihalopoulos, N., Morcrette, J.-J., Müller, J.-F., Myhre, G., Myriokefalitakis, S., Ng, N. L., O'Donnell, D., Penner, J. E., Pozzoli, L., Pringle, K. J., Russell, L. M., Schulz, M., Sciare, J., Seland, Ø., Shindell, D. T., Sillman, S., Skeie, R. B., Spracklen, D., Stavrakou, T., Steenrod, S. D., Takemura, T., Tiitta, P., Tilmes, S., Tost, H., van Noije, T., van Zyl, P. G., von Salzen, K., Yu, F., Wang, Z., Wang, Z., Zaveri, R. A., Zhang, H., Zhang, K., Zhang, Q., and Zhang, X.: The AeroCom evaluation and intercomparison of organic aerosol in global models, Atmos. Chem. Phys., 14, 10845–10895, https://doi.org/10.5194/acp-14-10845-2014, 2014.

Tunved, P., Hansson, H.-C., Kerminen, V.-M., Ström, J., Maso, M. D., Lihavainen, H., Viisanen, Y., Aalto, P. P., Komppula, M., and Kulmala, M.: High Natural Aerosol Loading over Boreal Forests, Science, 312, 261–263, https://doi.org/10.1126/science.1123052, 2006.

Twomey, S.: Pollution and the Planetary Albedo, Atmos. Environ., 8, 1251–1256, 1974.

Unger, N.: On the role of plant volatiles in anthropogenic global climate change, 41, 8563–8569, https://doi.org/10.1002/2014GL061616, 2014.

Vehkamäki, H., Kulmala, M., Napari, I., Lehtinen, K. E. J., Timmreck, C., Noppel, M., and Laaksonen, A.: An improved parameterization for sulfuric acid–water nucleation rates for tropospheric and stratospheric conditions, J. Geophys. Res., 107, 4622, https://doi.org/10.1029/2002JD002184, 2002.

Wilkinson, M. J., Monson, R. K., Trahan, N., Lee, S., Brown, E., Jackson, R. B., Polley, H. W., Fay, P. A., and Fall, R.: Leaf isoprene emission rate as a function of atmospheric CO2 concentration, Glob. Change Biol., 15, 1189–1200, https://doi.org/10.1111/j.1365-2486.2008.01803.x, 2009.

Zhang, G. J. and McFarlane, N. A.: Sensitivity of climate simulations to the parameterization of cumulus convection in the Canadian climate centre general circulation model, Atmos. Ocean, 33, 407–446, https://doi.org/10.1080/07055900.1995.9649539, 1995.

Zhang, K., Wan, H., Liu, X., Ghan, S. J., Kooperman, G. J., Ma, P.-L., Rasch, P. J., Neubauer, D., and Lohmann, U.: Technical Note: On the use of nudging for aerosol–climate model intercomparison studies, Atmos. Chem. Phys., 14, 8631–8645, https://doi.org/10.5194/acp-14-8631-2014, 2014.

Zhao, D. F., Buchholz, A., Tillmann, R., Kleist, E., Wu, C., Rubach, F., Kiendler-Scharr, A., Rudich, Y., Wildt, J., and Mentel, T. F.: Environmental conditions regulate the impact of plants on cloud formation, Nat. Commun., 8, 14067, https://doi.org/10.1038/ncomms14067, 2017.

Paper II

II

Large difference in aerosol radiative effects from BVOC-SOA treatment in three Earth system models

Moa K. Sporre, **Sara M. Blichner**, Roland Schrödner, Inger H. H. Karset, Terje K. Berntsen, Twan van Noije, Tommi Bergman, Declan O'Donnell, and Risto Makkonen

Atmospheric Chemistry and Physics, 2020

doi:10.5194/acp-20-8953-2020

Atmos. Chem. Phys., 20, 8953–8973, 2020
https://doi.org/10.5194/acp-20-8953-2020

Atmospheric Chemistry and Physics
Open Access
EGU

Large difference in aerosol radiative effects from BVOC-SOA treatment in three Earth system models

Moa K. Sporre[1,a], Sara M. Blichner[1], Roland Schrödner[2], Inger H. H. Karset[1], Terje K. Berntsen[1,3], Twan van Noije[4], Tommi Bergman[4,5], Declan O'Donnell[5], and Risto Makkonen[5,6]

[1]Department of Geosciences, University of Oslo, Postboks 1022 Blindern, 0315 Oslo, Norway
[2]Institute for Tropospheric Research, Permoserstr. 15, 04318 Leipzig, Germany
[3]CICERO Center for International Climate Research, Postboks 1129 Blindern, 0318 Oslo, Norway
[4]Royal Netherlands Meteorological Institute (KNMI), P.O. Box 201, 3730 AE De Bilt, the Netherlands
[5]Climate System Research, Finnish Meteorological Institute, P.O. Box 503, F00101, Helsinki, Finland
[6]Institute for Atmospheric and Earth System Research/Physics, Faculty of Science, University of Helsinki, P.O. Box 64, F00014, Finland
[a]now at: Department of Physics, Lund University, Box 118, 22100 Lund, Sweden

Correspondence: Moa K. Sporre (moa.sporre@nuclear.lu.se)

Received: 18 December 2019 – Discussion started: 4 February 2020
Revised: 12 May 2020 – Accepted: 12 June 2020 – Published: 29 July 2020

Abstract. Biogenic volatile organic compounds (BVOCs) emitted from vegetation are oxidised in the atmosphere and can form aerosol particles either by contributing to new particle formation or by condensing onto existing aerosol particles. As the understanding of the importance of BVOCs for aerosol formation has increased over the years, these processes have made their way into Earth system models (ESMs). In this study, sensitivity experiments are run with three different ESMs (the Norwegian Earth System Model (NorESM), EC-Earth and ECHAM) to investigate how the direct and indirect aerosol radiative effects are affected by changes in the formation of secondary organic aerosol (SOA) from BVOCs. In the first two sensitivity model experiments, the yields of SOA precursors from oxidation of BVOCs are changed by $\pm 50\,\%$. For the third sensitivity test, the formed oxidation products do not participate in the formation of new particles but are only allowed to condense onto existing aerosols. In the last two sensitivity experiments, the emissions of BVOC compounds (isoprene and monoterpenes) are turned off, one at a time. The goal of the study is to investigate whether it is of importance to treat SOA formation processes correctly in the models rather than to evaluate the correctness of the current treatment in the models.

The results show that the impact on the direct radiative effect (DRE) is linked to the changes in the SOA production in the models, where more SOA leads to a stronger DRE and vice versa. However, the magnitude by which the DRE changes (maximally $0.15\,\mathrm{W\,m^{-2}}$ globally averaged) in response to the SOA changes varies between the models, with EC-Earth displaying the largest changes. The results for the cloud radiative effects (CREs) are more complicated than for the DRE. The changes in CRE differ more among the ESMs, and for some sensitivity experiments they even have different signs. The most sensitive models are NorESM and EC-Earth, which have CRE changes of up to $0.82\,\mathrm{W\,m^{-2}}$. The varying responses in the different models are connected to where in the aerosol size distributions the changes in mass and number due to SOA formation occur, in combination with the aerosol number concentration levels in the models. We also find that interactive gas-phase chemistry as well as the new particle formation parameterisation has important implications for the DRE and CRE in some of the sensitivity experiments. The results from this study indicate that BVOC-SOA treatment in ESMs can have a substantial impact on the modelled climate but that the sensitivity varies greatly between the models. Since BVOC emissions have changed historically and will continue to change in the future, the spread in model results found in this study implies uncertainty into ESM estimates of aerosol forcing from land-use change and BVOC feedback strengths.

Published by Copernicus Publications on behalf of the European Geosciences Union.

1 Introduction

The climatic relevance of biogenic volatile organic compounds (BVOCs) emitted from vegetation has received increasing attention over the past years. Emitted BVOCs are oxidised in the atmosphere producing a number of different products with lower volatility. These can then form secondary organic aerosols (SOAs), increasing both aerosol number concentration (through new particle formation (NPF) and participation in early growth) and aerosol sizes (through condensation onto pre-existing particles) (Shrivastava et al., 2017). The formation of SOA from BVOCs can thus influence climate both through changes in cloud properties (indirect aerosol effects) (Twomey, 1974; Albrecht, 1989) and through changes in scattering and absorption of solar radiation by aerosols (direct aerosol effect) (Charlson et al., 1990).

BVOC emissions depend on various environmental factors, in particular temperature, radiation, CO_2 concentrations and land use, and are thus expected to have changed in the past and to continue to change in the future (e.g. Bonan, 2016; Hantson et al., 2017). Studies have found that future BVOC emissions are likely to increase due to warming and higher CO_2 concentrations and that BVOCs could dampen temperature increase and provide a negative climate feedback (Sporre et al., 2019; Paasonen et al., 2013; Kulmala et al., 2014; Scott et al., 2018; Carslaw et al., 2010). There are, however, a range of uncertainties associated with these feedbacks, including the strength of CO_2 inhibition on BVOC emissions (Arneth et al., 2007). Nevertheless, it is important to include these processes in Earth system models (ESMs) to estimate aerosol effects in the future but also in the past. SOA formation has been added to many models over recent years in response to the increased understanding of the importance of BVOCs to aerosol formation. However, uncertainties regarding these processes in models are large; e.g. Tsigaridis et al. (2014) show an order of magnitude variation between the 31 models in the vertical profile of organic aerosol mass in their intercomparison.

Organics constitute a large fraction of the atmospheric aerosol mass (Shrivastava et al., 2017; Zhang et al., 2007), and as much as 50 %–85 % of this can be SOA (Zhang et al., 2007; Glasius and Goldstein, 2016). In model estimates, biogenic SOA usually dominates the SOA budget (Glasius and Goldstein, 2016; Hallquist et al., 2009; Kelly et al., 2018). As an exception, Shrivastava et al. (2015) find biomass burning to be the largest source and biogenics to be the second largest. However, there are large seasonal and regional differences in sources, with biogenic SOA dominating in summer, while sources like wood burning can be more dominant in winter, particularly in populated regions (Glasius et al., 2018). Moreover, some studies have found that the biogenic SOA formation is anthropogenically controlled (Spracklen et al., 2011; Kanakidou et al., 2000; Carlton et al., 2010).

The SOA formation and processing pathways in the atmosphere are remarkably complex. To represent these in ESMs, a trade-off must be made between detail and computational cost (Tsigaridis et al., 2014). In reality, BVOCs consist of a myriad of compounds with different properties. However, in ESMs these are often reduced to be represented by 2–3 tracers, usually isoprene, monoterpenes (MTs) and sesquiterpenes, which constitute the main contributors to aerosol formation and are estimated to constitute around 50 %, 15 % and 3 %, respectively, of the total BVOC emissions (Guenther et al., 2012). The oxidation products of BVOCs, while in reality there is a large variety of compounds produced through a series of reactions (Glasius and Goldstein, 2016; Shrivastava et al., 2017), are lumped into a few tracers which can condense onto existing aerosols or contribute to NPF and early growth (Tsigaridis et al., 2014). Not all oxidation products have low enough volatility to be relevant for aerosol formation. Therefore, the percentage of low volatility products formed during the oxidation is described by yields for each oxidation reaction (e.g. Tsigaridis et al., 2014; Jokinen et al., 2015; Makkonen et al., 2014). Some models also use volatility basis sets or similar approaches to account for changes in volatility during the oxidation (Donahue et al., 2006, 2011; Yu, 2011).

All three models included in this study use two tracers representing the oxidation products from the BVOCs. One tracer represents the highly oxidised BVOCs which can take part in NPF and the early growth of the newly formed particles. This tracer will be denoted ELVOCs (extremely low volatility organic compounds) here. The other tracer represents the oxidation products with somewhat higher volatility that can condense onto larger aerosols, and this will be denoted by L/SVOCs (low volatility and semi-volatile organic compounds). However, the VOCs are not actually volatile in these models since the parameterisations only allow irreversible condensation of the organics.

As already mentioned, evidence suggests that low-volatility organics contribute at the earliest stages of NPF (Tröstl et al., 2016; Riccobono et al., 2014; Ehn et al., 2014; Kirkby et al., 2016; Riipinen et al., 2011, 2012; R. Zhang et al., 2012), and this is increasingly considered in global models. The formation or nucleation rate of new particles is typically parameterised with one parameterisation of binary nucleation of sulfuric acid (H_2SO_4) and water (H_2O) vapours for the entire atmosphere. However, since these nucleation parameterisations underestimate NPF in the boundary layer (BL) (Spracklen et al., 2006), an additional parameterisation involving sulfuric acid and organics that better captures the NPF in the BL is often added to the ESMs. These parameterisations are not always limited to the BL, but in this article we will refer to them as BL nucleation since they were introduced into the models to address the underestimation of NPF there.

There are large uncertainties in several of the processes representing SOA formation in ESMs. BVOC emissions are poorly constrained both locally and globally (Heald and Spracklen, 2015) and future changes in emissions are highly

uncertain, both because of scenario uncertainty and because vegetation response is uncertain (Hantson et al., 2017). In addition, the formation of low-volatility oxidation products depends on a number of variables, including oxidation capacity, NO_x concentrations (Shrivastava et al., 2017), specific BVOC species, etc., which results in large uncertainties in the yields (Jokinen et al., 2015). The representation of SOA in global models is currently under rapid development (Tsigaridis et al., 2014; Makkonen et al., 2014, 2012; Gordon et al., 2016, 2017; Dunne et al., 2016). It is important to understand the dynamics introduced by these parameterisations and how they interact with the other parts of the models – in particular those related to the direct and indirect aerosol effects, which have strong impacts on climate.

In this study we investigate the impact of choices in emissions of SOA precursors and yields of BVOC oxidation products on the climatic effects of SOA through a series of sensitivity experiments with three ESMs. The models have comparable treatments of SOA formation but have different aerosol schemes and different treatment of gas-phase chemistry. The comparison of the simulations for the different models and experiments thus gives us the possibility to investigate the sensitivities to common parameters. We investigate how the direct and indirect aerosol effects are impacted by the changes in yields and emissions, and from this we gain insight into how significant these parameters are for the radiative effects in the models. The goal is to better understand the processes controlling sensitivities in common setups of SOA parameterisations in ESMs currently. We do not conclude on whether these processes are treated correctly but rather if it is important that they are.

2 Method

2.1 Experimental setup

A set of sensitivity experiments was designed to investigate how changes to BVOC and SOA representations in the models affect clouds and radiation balance. Care was taken to design experiments that could be run with all three models. The five sensitivity experiments are listed.

- *Yield higher*. The EL/L/SVOC yields for the BVOC oxidation reactions (Table 2) are increased by 50 %.
- *Yield lower*. The EL/L/SVOC yields for the BVOC oxidation reactions are decreased by 50 %.
- *No ELVOCs*. The formation of ELVOCs is removed from the models. The total BVOC oxidation yields are kept constant, but all BVOC oxidation reactions produce L/SVOCs.
- *No isoprene*. The isoprene emissions in the models are turned off.
- *No MTs*. The MT emissions in the model are turned off.

For comparison purposes, a control simulation (*CTRL*) was run with the models. The *Yield higher* and *Yield lower* simulations directly increase or decrease the produced SOA mass, while the changes are more complex for the other three experiments. The *No ELVOCs* scenario strongly decreases the NPF in the BL and increases the mass of L/SVOCs, which can only condense onto existing particles. With the *No isoprene* and *No MTs* cases, the importance of the two classes of BVOCs for modelled SOA mass and particle size distributions is investigated. Whereas isoprene is, on a global scale, emitted in larger amounts compared to MTs, its oxidation reactions have smaller yields for SOA precursors than MTs. In addition, the modelled isoprene oxidation produces a very small quantity of ELVOCs (EC-Earth, ECHAM) or no (NorESM) ELVOCs. Therefore, with these two experiments both the amount of modelled SOA and the fraction of oxidation products participating in NPF are changed.

In order to have similar meteorological conditions in the three models, all simulations were nudged (Kooperman et al., 2012) to ERA-Interim (Dee et al., 2011) data for the years 2000–2005. Although this method may not capture all changes in the cloud radiative effect (CRE) since dynamical feedbacks are limited by the constrained meteorology (Lohmann and Hoose, 2009; Lin et al., 2016), previous studies with CAM5.3-Oslo found the effective radiative forcing from aerosol–cloud interactions (ERFaci) and ERFaci changes carried out with nudged configurations to be in the uncertainty range of that carried out with a free-running version of the model (Kirkevåg et al., 2018; Karset et al., 2018). The first year of the simulations has been discarded as spin-up and the last 5 years have been used for the analysis.

The radiative effects from aerosols and clouds in this study are calculated using the methods described by Ghan (2013). The direct radiative effect (DRE) is calculated by taking the difference between the top-of-atmosphere radiative flux and the radiative flux excluding scattering and absorption by aerosols (F_{clean}). The CRE is similarly calculated as the difference between F_{clean} and the radiation flux without the scattering and absorption by the clouds or aerosols ($F_{\text{clean, clear}}$).

2.2 Model similarities and dissimilarities

A more detailed description of each of the models will follow after this section. However, here we would like to highlight some of the key similarities and dissimilarities between the models (summarised in Table 1). The ESM model components are different between the three ESMs. The Norwegian Earth System Model (NorESM) and ECHAM have an atmospheric model which contains an aerosol module, while EC-Earth consists of a chemistry transport model coupled to an atmospheric general circulation model. Therefore, EC-Earth has a more advanced treatment of gas-phase chemistry, including interactive oxidant fields, while the other two mod-

Table 1. This table lists similarities and dissimilarities between the three ESMs of particular relevance for this study.

Properties	NorESM	EC-Earth	ECHAM
Aerosol model	OsloAero	M7	M7
BVOC emissions	MEGAN v2.1 interactive	MEGAN-MACC prescribed	MEGAN-MACC prescribed
Oxidant fields	Prescribed	Interactive	Prescribed
Oxidised BVOC tracers	ELVOC/L/SVOC	ELVOC/L/SVOC	ELVOC/L/SVOC
ELVOC formed from	MTs	Isoprene and MTs	Isoprene and MTs
Binary nucl. param.	Vehkamäki et al. (2002)	Vehkamäki et al. (2002)	Vehkamäki et al. (2002)
BL nucleation rate $J =$	$A_1[H_2SO_4] + A_2$[ELVOC]	$A_3[H_2SO_4]^2 \times$ [ELVOC]	$A_1[H_2SO_4] + A_2$[ELVOC]
Cloud activation scheme	Abdul-Razzak and Ghan (2000)	Abdul-Razzak and Ghan (2000)	Abdul-Razzak and Ghan (2000)

$A_1 = 6.1 \times 10^{-7}\,s^{-1}$, $A_2 = 3.9 \times 10^{-8}\,s^{-1}$, $A_3 = 3.27 \times 10^{-21}\,cm^{-6}\,s^{-1}$.

els have prescribed oxidant fields. The aerosol modules also differ between the models. NorESM has OsloAero (Kirkevåg et al., 2018), while EC-Earth and ECHAM both use M7 (Vignati et al., 2004) but different versions. As described in the Introduction section, the treatment of the oxidation products is similar between the models where all three models have one ELVOCs and one L/SVOC tracer. However, the BVOC oxidation differs between the models in terms of yield, number of oxidation reactions from BVOC to ELVOCs/L/SVOCs and which reactions produce which oxidation products, as can be seen in Table 2. Moreover, all three ESMs use the Model of Emissions of Gases and Aerosols from Nature (MEGAN) version 2.1 (Guenther et al., 2012). However, in NorESM, MEGAN is run interactively, while the other two models use emissions produced in offline simulations with MEGAN.

2.3 NorESM

NorESM (Bentsen et al., 2013; Kirkevåg et al., 2013; Iversen et al., 2013) is an ESM based on the Community Earth System Model (CESM) (Neale et al., 2012). The aerosol scheme in the Atmospheric Community Model (CAM) version 5.3 has been replaced by the aerosol scheme OsloAero (Kirkevåg et al., 2018). In this investigation, CAM5.3-Oslo (CAM with OsloAero) is coupled to the Community Land Model (CLM) version 4.5 (Oleson et al., 2013) run with satellite phenology (SP) vegetation. NorESM is run with prescribed sea surface temperature (SST) and sea ice concentrations at $1.9^\circ \times 2.5^\circ$ resolution. The horizontal winds and surface pressure are nudged to ERA-Interim data with a relaxation time of 6 h.

OsloAero is described as a production-tagged aerosol model, which consists of 12 log-normal-shaped background modes. The shape and size of these modes can be modified by coagulation and condensation. The modes are made up of background tracers which determine the number concentration and process tracers which change the shape of aerosol size distributions. The mass of the tracers is tracked, and the size distributions and optical properties are calculated using a look-up table approach (Kirkevåg et al., 2018).

NPF was recently added to OsloAero (Makkonen et al., 2014) and is now included as two background tracers: one for sulfate (SO_4) and one for SOA, forming one mode (Kirkevåg et al., 2018). Two types of NPF are included in OsloAero: (1) binary homogeneous sulfuric-acid–water nucleation according to Vehkamäki et al. (2002) and (2) an activation-type nucleation, in the BL, with a nucleation rate calculated from Eq. (18) in Paasonen et al. (2010). This nucleation rate is calculated from the concentrations of H_2SO_4 and ELVOCs available for nucleation. The nucleation rates are calculated for particles with a diameter of 2 nm, but the diameter of the nucleation tracers in OsloAero is 23.6 nm. The survival of these newly formed particles from nucleation to 23.6 nm diameter is parameterised dependent on coagulation sink and condensation growth rate in accordance with Lehtinen et al. (2007). In this study, contrary to Kirkevåg et al. (2018), we include all pre-existing particles in the calculation of coagulation sink. This modification was introduced into the model in order to have a more realistic survival rate of the particles between 2 and 23.5 nm.

The BVOC emissions used in the simulations are calculated interactively by MEGAN version 2.1 (Guenther et al., 2012), which is included in CLM. MEGAN thus uses the vegetation from CLM. The BVOC emissions depend on factors such as temperature, radiation, leaf area index and soil moisture. The model is run with a 30 min time step, and the coupling between CLM and CAM-Oslo is done at every time step, providing an interactive diurnal variation in the emissions. The BVOC emissions include isoprene and seven compounds which are lumped together as MTs in CAM-Oslo.

In CAM-Oslo, the emitted BVOCs are transformed into SOA through chemical reactions with ozone, hydroxyl (OH) and nitrate radical (NO_3). When MTs reacts with O_3, ELVOCs are formed, while the other five reactions yield only L/SVOCs. The reactions and their yields are given in Table 2. Fifty percent of the formed ELVOCs are available for nucleation, and the rest of the ELVOCs and the L/SVOCs condense onto pre-existing aerosol particles (Makkonen et al., 2014). The molar mass of both the ELVOCs and L/SVOCs is $168\,g\,mol^{-1}$. The oxidants are prescribed monthly fields

Table 2. Yields and resulting products from the reactions of BVOCs with oxidants to form ELVOC and L/SVOC for the three ESMs. In ECHAM, there are different yields for endocyclic MTs and the other MTs. The equations for the endocyclic MTs are written separately, and the other MTs are shown on the same rows as the MTs in the other models.

Model	NorESM	EC-Earth	ECHAM
Isop. + OH	0.05 L/SVOC	0.0097 L/SVOC + 0.0003 ELVOC	0.0482 L/SVOC + 0.0018 ELVOC
Isop. + O_3	0.05 L/SVOC	0.0099 L/SVOC + 0.0001 ELVOC	0.0498 L/SVOC + 0.00016 ELVOC
Isop. + NO_3	0.05 L/SVOC	–	–
MTs + OH	0.15 L/SVOC	0.14 L/SVOC + 0.01 ELVOC	0.14 L/SVOC + 0.01 ELVOC
MTs + O_3	0.15 ELVOC	0.1 L/SVOC + 0.05 ELVOC	0.147 L/SVOC + 0.003 ELVOC
MTs + NO_3	0.15 L/SVOC	–	–
Endocyclic MTs + OH	–	–	0.145 L/SVOC + 0.005 ELVOC
Endocyclic MTs + O_3	–	–	0.1 L/SVOC + 0.05 ELVOC

originating from a run with the full chemistry model CAM-chem (Lamarque et al., 2012).

CAM5.3-Oslo uses the cloud bulk microphysics scheme MG1.5 (Morrison and Gettelman, 2008; Gettelman and Morrison, 2015) with aerosol activation by Abdul-Razzak and Ghan (2000) for the stratiform clouds. Mass and number of cloud water and ice are treated prognostically, while the precipitation is diagnostic. The model also includes a shallow convection scheme (Park and Bretherton, 2009) and a deep convection scheme (Zhang and McFarlane, 1995).

2.4 EC-Earth

The Earth system model EC-Earth (Hazeleger et al., 2012; van Noije et al., 2014) includes an atmospheric general circulation model (GCM) based on cycle 36r4 of the Integrated Forecasting System (IFS) of the European Centre for Medium-Range Weather Forecasts (ECMWF). This is coupled to the atmospheric chemistry and transport model TM5 (Tracer Model 5; van Noije et al., 2014; Williams et al., 2017). For the present study, the EC-Earth release v3.2.3 in atmosphere-only mode (i.e. IFS + TM5) was used. TM5 treats the emission, transport, microphysical and chemical conversions, as well as deposition of atmospheric gases and aerosols. The latter are described with the size-resolved modal microphysics scheme M7 (Vignati et al., 2004). It uses seven log-normal size distributions (modes) of which four are soluble (nucleation, Aitken, accumulation, coarse) and three insoluble (Aitken, accumulation, coarse). The nucleation, Aitken, accumulation and coarse modes represent particles with dry diameters smaller than 10 nm, 10–100 nm and 100 nm–1 µm and larger than 1 µm, respectively. The considered aerosol species are sulfate, black carbon, organic matter (primary and secondary), mineral dust and sea salt. M7 tracks the number concentration in each mode and the mass of each species in each mode. The mode shape is constant, whereas median diameter, number of particles of each mode and their chemical composition can evolve freely. After growth by condensation and coagulation, the largest particles of each mode are shifted to the next larger mode. Particles in the insoluble modes that reach sufficient soluble coating are shifted to the respective soluble modes.

In addition, TM5 simulates the total particulate mass of nitrate, ammonium and methane sulfonic acid. When calculating optical properties, these components as well as the associated water uptake are assumed to be in the soluble accumulation mode. The gas-phase chemistry is described by a modified version of the Carbon Bond 05 (CB05) mechanism (Williams et al., 2017) using the photolysis scheme from Williams et al. (2012). SOA is produced from MTs and isoprene with the yields as presented in Table 2. Assumed molar masses for the two SOA species, ELVOCs and L/SVOCs, are 248 and 232 g mol^{-1}, respectively. Produced ELVOCs condense to soluble nucleation, Aitken, accumulation and coarse modes as well as to insoluble Aitken mode according to the respective condensation sink (depending on surface area). L/SVOCs condense to soluble Aitken, accumulation and coarse modes as well as insoluble Aitken mode according to the actual mode mass.

NPF is treated following Vehkamäki et al. (2002). In addition, NPF from H_2SO_4 and ELVOCs is calculated using the semi-empirical method by Riccobono et al. (2014) (see Table 1). The size of freshly nucleated sulfuric-acid–ELVOC clusters is assumed to be 1.7 nm. The early growth to 5 nm diameter is calculated following Kerminen and Kulmala (2002). The resulting number of these 5 nm particles is finally added to the nucleation mode.

The emissions of the SOA precursors isoprene and MTs are calculated using MEGAN-MACC (Sindelarova et al., 2014) for the year 2000 and depend on the underlying vegetation information. The BVOC emissions are prescribed monthly fields and with an applied diurnal variation. There is also a small fraction of MTs and isoprene emitted from biomass burning, which will participate in production of SOA.

For the present study, IFS is applied at a spectral truncation of T255 (corresponding to 0.7°) grid with 91 vertical levels. Emissions for TM5 are applied on a $0.5° \times 0.5°$ grid, whereas following processes and transport are calculated on $3° \times 2°$. The horizontal winds (via divergence and vorticity) and sur-

face pressure were nudged against ERA-Interim with a relaxation time of 8.25 h. The cloud droplet number concentration of stratiform clouds is calculated using Abdul-Razzak and Ghan (2000); it determines the effective radius of the cloud droplets and influences the lifetime of the clouds via its effect on the autoconversion of cloud liquid water to rain.

2.5 ECHAM

ECHAM5-HAM (Stier et al., 2005) is an aerosol–climate model originally developed at the Max Planck Institute for Meteorology, Hamburg. The Hamburg Aerosol Module (HAM) also employs the M7 aerosol microphysics module. The ECHAM-HAM simulations were performed in T63 spectral resolution with 31 hybrid-sigma vertical levels. The spectral atmospheric variables are nudged with standard ECHAM relaxation timescales: 6 h for vorticity, 24 h for pressure and temperature, and 48 h for divergence (Lohmann and Hoose, 2009).

We apply a modified version of ECHAM5.5-HAM2 (K. Zhang et al., 2012), which uses an improved numerical scheme (Kokkola et al., 2009) to compute the formation of sulfuric acid by oxidation of SO_2 and its removal by nucleation and condensation on pre-existing particles. We consider SOA formation from the biogenic precursors isoprene and MTs. The SOA formation mechanism (Jokinen et al., 2015) includes both kinetic condensation to Fuchs-corrected surface area (condensation sink). Moreover, the relative partitioning to the Aitken, accumulation or coarse mode is done according to pre-existing organic mass in the respective modes. The model considers three BVOC tracers: isoprene, endocyclic and other MTs. The BVOC emissions in ECHAM simulations were pre-computed monthly averages (Jokinen et al., 2015). The MEGAN2.1 (Guenther et al., 2012) was driven with input drivers described in Sindelarova et al. (2014), combining MERRA meteorological fields and MACC land cover data. However, the BVOC emission inventories did not separate endocyclic and other MTs; hence, their respective emissions were considered equal fractions. The reaction rates of SOA precursors with O_3, OH and NO_3 are described in Jokinen et al. (2015).

The ELVOC yields are based on extensive laboratory experiments (Jokinen et al., 2015), while the total (ELVOC+L/SVOC) yield is set to 15 % for MTs and 5 % for isoprene. ELVOCs provide early growth for nucleation mode particles, as they are distributed to the particle phase according to condensation sink. The low volatility and semivolatile products are distributed to particle phase according to particle-phase organic mass, as in Jokinen et al. (2015). Hence, after oxidation, no SOA products remain in the gas phase, but immediate condensation to aerosol phase is assumed. Simulations include organic vapours in the nucleation process according to Eq. (18) in Paasonen et al. (2010). The growth from nucleation to 3 nm is calculated according to Kerminen and Kulmala (2002), assuming growth by ELVOCs and sulfuric acid.

3 Results and discussions

We will start the results section by investigating the inter-model differences in the *CTRL* simulation among the three models. It is necessary to be aware of the differences between models before investigating the changes that the sensitivity simulations induce.

3.1 CTRL

3.1.1 BVOC emissions and concentrations

The three ESMs all use the same emission model (MEGAN), but the emissions of MTs and isoprene still vary between the models because of choices in land cover data and meteorology. For isoprene, NorESM has the lowest emissions rates of about 435 Tg yr^{-1}, while EC-Earth and ECHAM are somewhat higher with 572 and 526 Tg yr^{-1}, respectively; see Fig. 1g. The spatial distribution in the emissions also varies between the models. In NorESM, the isoprene emissions are highest in the Amazon region with somewhat smaller sources in Africa and the tropical islands of Indonesia (Fig. 1a). EC-Earth has the highest emission rates out of all the models but with the Amazonian maximum located further south than in NorESM (Fig. 1c). ECHAM has similar emission patterns to EC-Earth but with somewhat weaker emissions; see Fig. 1e.

For MTs, NorESM has the highest global emissions (118 Tg yr^{-1}) followed by EC-Earth (96 Tg yr^{-1}) and then ECHAM (77 Tg yr^{-1}) as can be seen in Fig. 1h. The largest differences in the emissions are in the tropics, in particular in the Amazonian region, where NorESM has up to twice as high annual emissions. The cause of the difference in emissions is related to the implementation of MEGAN used in the models. In NorESM, MEGAN is interactive and uses the vegetation from CLM as well as atmospheric conditions and radiation in the calculation of the BVOC emissions. EC-Earth and ECHAM, on the other hand, use prescribed BVOC emissions from MEGAN-MACC with a yearly as well as diurnal variation included (Sindelarova et al., 2014). The emissions from these two models are not the same because different meteorology was used in the generation of the emissions fields.

The column burdens of the BVOCs also differ between the models (not shown). The global mean column burden of isoprene is approximately 3 times higher in EC-Earth (1.0 kg m^{-2}) than in the other two models. This is in part because of significantly higher column burdens over the strong emission regions in South America and Africa, which are due to the interactive oxidant fields in EC-Earth. When interactive oxidant fields are used, the oxidants can be depleted and as a result the lifetime of BVOCs is increased. This does not occur in the other two models that have prescribed oxidation

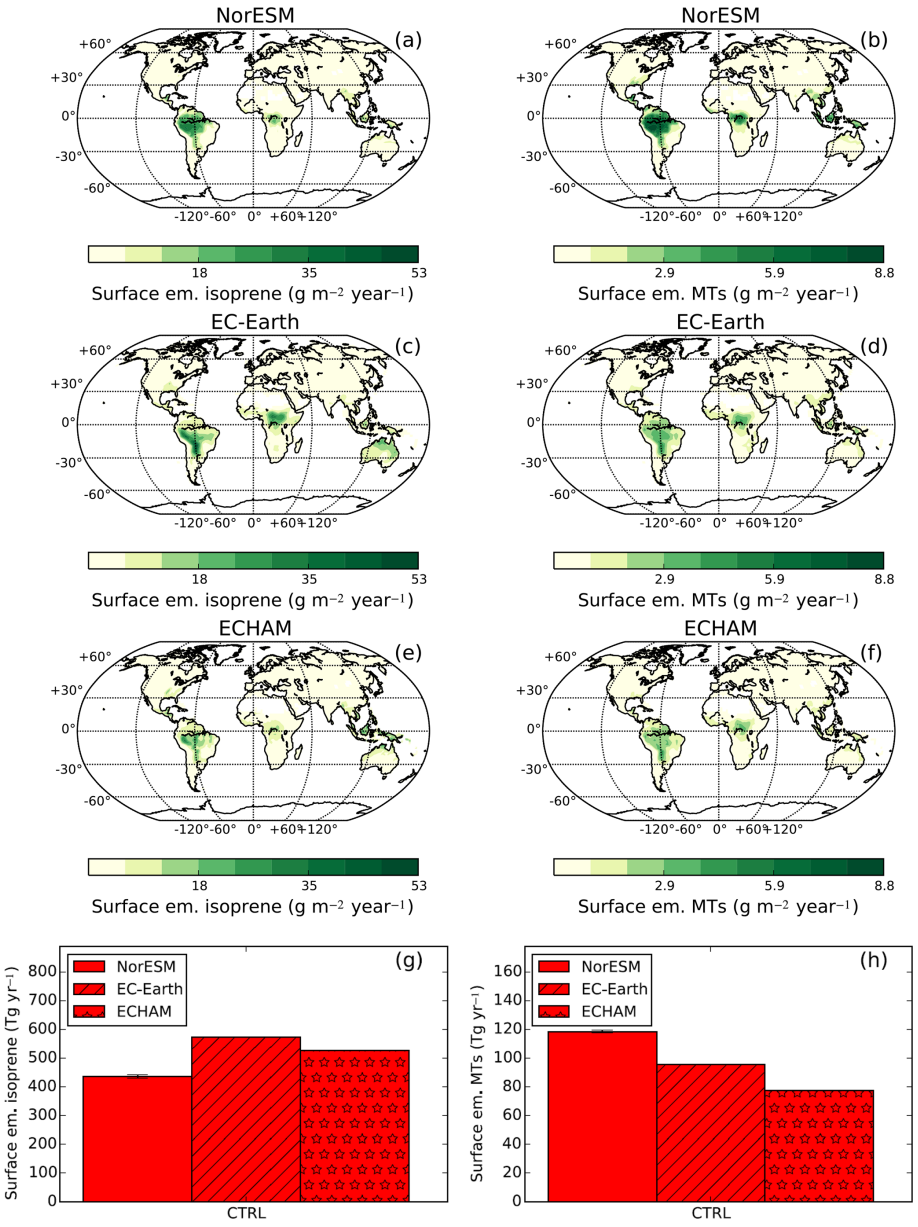

Figure 1. Maps of annually averaged surface emissions of isoprene **(a, c, e)** and monoterpenes (MTs) **(b, d, f)** for NorESM, EC-Earth and ECHAM. ECHAM and EC-Earth use prescribed emissions and there are therefore no error bars presented for these models. Also shown are the global yearly surface emissions of isoprene **(g)** and MTs **(h)**. The error bars denote the standard error of mean of the yearly averages.

fields. The MT column burdens are more similar between the models.

3.1.2 SOA formation and aerosol size distributions

There is a large range in the amount of SOA formed in the different models. In spite of having the lowest BVOC emissions (due to lower isoprene emissions), NorESM has the largest average annual production (85 Tg yr^{-1}), while ECHAM and EC-Earth have very similar and somewhat lower SOA production (52 Tg yr^{-1}); see Fig. 2a. The higher emissions in NorESM are likely a result of the higher MT emissions (which have the highest yields), in combination with higher yields for isoprene than EC-Earth. Also the assumed molar mass of the BVOC oxidation products will affect how much SOA mass is formed. The produced SOA mass in the models is in the range of the values found in Tsigaridis et al. (2014) but are higher than the median of the models included in that study.

In this paper we have averaged the size distribution and number concentration data globally over the model levels with pressures higher than 850 hPa, i.e. the bottom part of

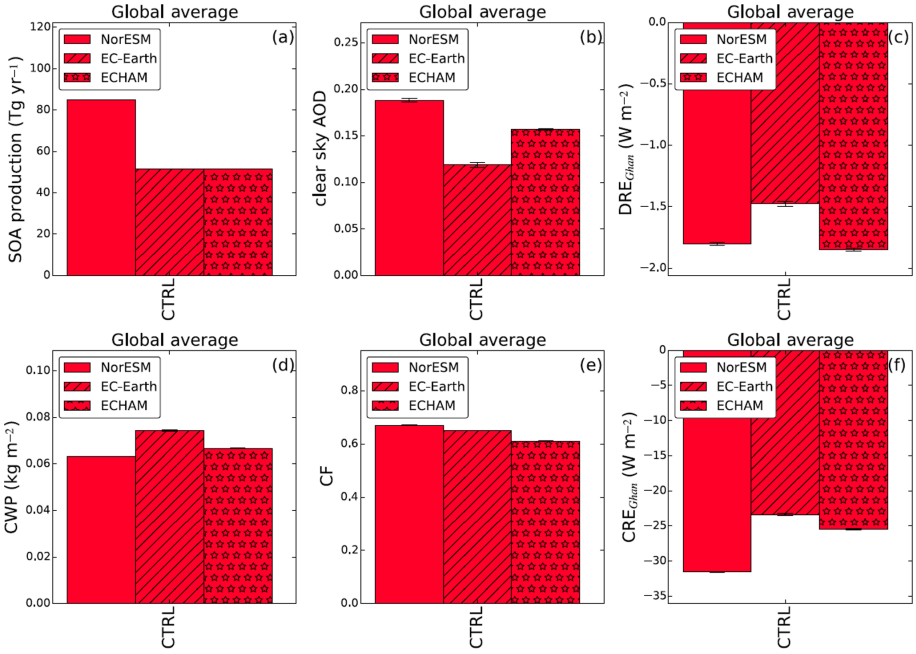

Figure 2. Bar plots of the total yearly global SOA production and the yearly averaged aerosol optical depth (AOD), direct radiative effect (DRE_{Ghan}), cloud water path (CWP), cloud fraction (CF) and cloud radiative effect (CRE_{Ghan}) for all three models for the *CTRL* experiment. The error bars denote the standard error of mean of the yearly averages.

the atmosphere. This choice was made since this part of the atmosphere contains most of the aerosol mass which is relevant for both the direct and indirect aerosol effects. Moreover, clouds in the ESMs use aerosol activation at the bottom of the clouds, and thus the aerosols at these levels are most important also for the indirect aerosol effects. The aerosol size distributions (for all particles) show large differences between the models even though ECHAM and EC-Earth both use the modal aerosol model M7; see Fig. 3. The most noticeable difference between the number size distribution of the models is that NorESM, which uses the aerosol model OsloAero, has no explicit nucleation mode. In NorESM, particles from NPF are added directly into SO_4/SOA nucleation mode which is in the Aitken-accumulation size range after growth through condensation. ECHAM's size distribution is dominated by a large nucleation mode which contains almost 2 orders of magnitude more particles than the nucleation mode in EC-Earth. Moreover, EC-Earth also has fewer particles than the other models in the largest particle sizes (diameters > 250 nm). Of the three models, ECHAM has the most particles at large sizes (diameters > 300 nm) as well as highest surface and volume of particles (Fig. 3b and c). Total aerosol number concentrations (Fig. 4) reveal that EC-Earth has the lowest aerosol number concentrations out of all models and ECHAM has the highest. This is still the case when comparing the number concentrations without the nucleation mode. Moreover, ECHAM has substantially higher aerosol number concentrations over the remote oceans (Fig. S1 in the Supplement) compared to the other two models. There are likely many different explanations as to why the size distributions and aerosol number concentrations are different in the models. Some plausible explanations include differences in wet deposition, nucleation rates and how the emissions in general are partitioned into the aerosol modes.

3.1.3 AOD and direct aerosol effects

The global average aerosol optical depth (AOD) is highest in NorESM (0.19, Fig. 2b) due to significantly higher AOD values over desert regions, in particular the Sahara (Fig. S1). This is associated with high dust emissions from the desert. ECHAM has the second highest global AOD values (0.16) and has somewhat higher AOD values over the ocean than the other two models. The direct aerosol effects (Fig. 2c) in the models resemble the results from the AOD. EC-Earth has lower globally averaged direct radiative effect (DRE_{Ghan}) than the other two models. This is a result of the low aerosol number concentrations, in particular at larger, radiation relevant sizes. This can also be seen in the AOD from EC-Earth. ECHAM has slightly stronger global average DRE_{Ghan} than NorESM even though NorESM has a higher average AOD. The reason for this is that many of the regions with large AOD in NorESM have very bright surfaces (e.g. deserts) and therefore result in a lower DRE_{Ghan} (Fig. S1).

3.1.4 Cloud properties and indirect aerosol effect

The cloud properties in the *CTRL* simulation are quite different in the models. EC-Earth has the lowest cloud droplet

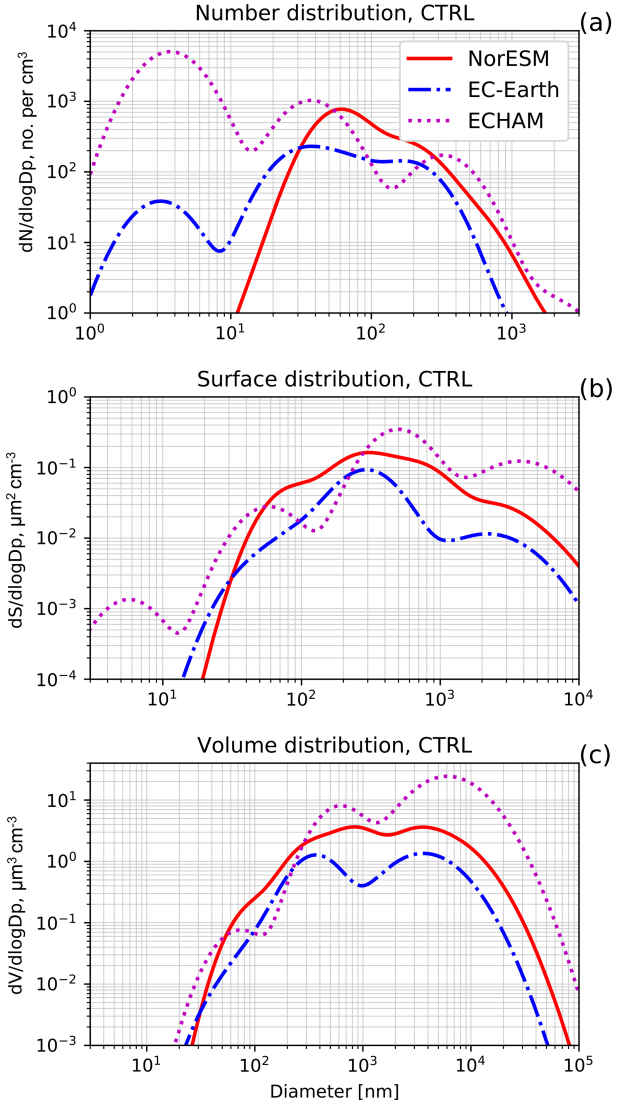

Figure 3. Globally averaged aerosol number size distributions **(a)**, surface size distributions **(b)** and volume size distributions from the three models from the *CTRL* simulation. The diameters are the dry diameters. Note the different scales on the x axis in the subplots.

number concentrations (Fig. S2), which is related to the low number concentrations of aerosol particles in this model. ECHAM, on the other hand, has the highest number of cloud condensation nuclei (CCN) and also the highest cloud droplet number concentration (CDNC). NorESM has larger droplet sizes than the other two models and the droplet size patterns are very different in the different models. Nevertheless, the total grid box cloud water path (CWP) is fairly similar between the three models but slightly higher in EC-Earth (Fig. 2d). The total cloud fractions (CF) in the models are also fairly similar with global average values between 0.61 and 0.67; see Fig. 2e. The cloud radiative effect (CRE_{Ghan}) is stronger in NorESM ($-31\,W\,m^{-2}$) compared to EC-Earth ($-23\,W\,m^{-2}$) and ECHAM ($-26\,W\,m^{-2}$); see Fig. 2f. Note that these are development versions of NorESM and EC-Earth which has not been tuned. The patterns of the CF and CRE_{Ghan} can be seen in Fig. S3.

3.2 *Yield higher* and *Yield lower*

The results from the sensitivity simulations will now be presented and discussed in three different sections. The sensitivity experiments are grouped according to the similarity in the results. In the first section, the *Yield higher* and *Yield lower* experiments are discussed.

3.2.1 Direct aerosol effects

First, the results regarding the changes in aerosol scattering and how these affect climate forcing are presented. In the *Yield higher* simulation the DRE_{Ghan} becomes stronger, i.e. more negative, and the opposite is true for the *Yield lower* simulation, for all three models (Fig. 5). These changes reflect the changes in SOA formation (Fig. 6) as more SOA leads to a stronger DRE_{Ghan}. Since NorESM has the largest SOA production, it also experiences the largest SOA production change in these simulations, approximately $\pm 38\,Tg\,yr^{-1}$. The changes in the other two models are of the order of $25\,Tg\,yr^{-1}$. Interestingly, an increase or decrease in the SOA precursor yields by 50 % results in an increase or decrease in SOA production by 50 % only in EC-Earth. In NorESM, the SOA production change is somewhat less than 50 % in both simulations. The explanation for this is that SOA is also produced from dimethyl sulfide (DMS) emissions from the ocean in NorESM (Kirkevåg et al., 2018), and these yields are not changed in the sensitivity simulations. For ECHAM, the effect is somewhat larger in the *Yield higher* simulation (+52 %) and smaller in the *Yield lower* simulation (−45 %).

The degree to which a SOA increase leads to a strengthening in the DRE_{Ghan} varies between the models. NorESM has the largest absolute increase and decrease in SOA formation in these two simulations, but it is EC-Earth that experiences the largest change in the DRE_{Ghan} with changes of $\pm 0.15\,W\,m^{-2}$. For reference, this number is roughly half of the radiative forcing due to aerosol–radiation interactions (RFari) best estimate in the Fifth Assessment Report by the IPCC (2013). ECHAM has the smallest changes in DRE_{Ghan} with values of approximately $\pm 0.03\,W\,m^{-2}$ even though this model has similar changes in SOA production to EC-Earth. The cause of the different responses in the different models is, at least partly, related to where in the aerosol size distribution the additional or removed SOA is located. For all three models in the *Yield higher* simulation, the globally averaged particle number concentrations increase at sizes relevant for scattering of solar radiation ($N_{d>100}$, number concentration of particles above 100 nm) (see Fig. 4). However, in ECHAM this increase is quite small; see Fig. 4f. The changes in particle number concentration in NorESM are quite large but

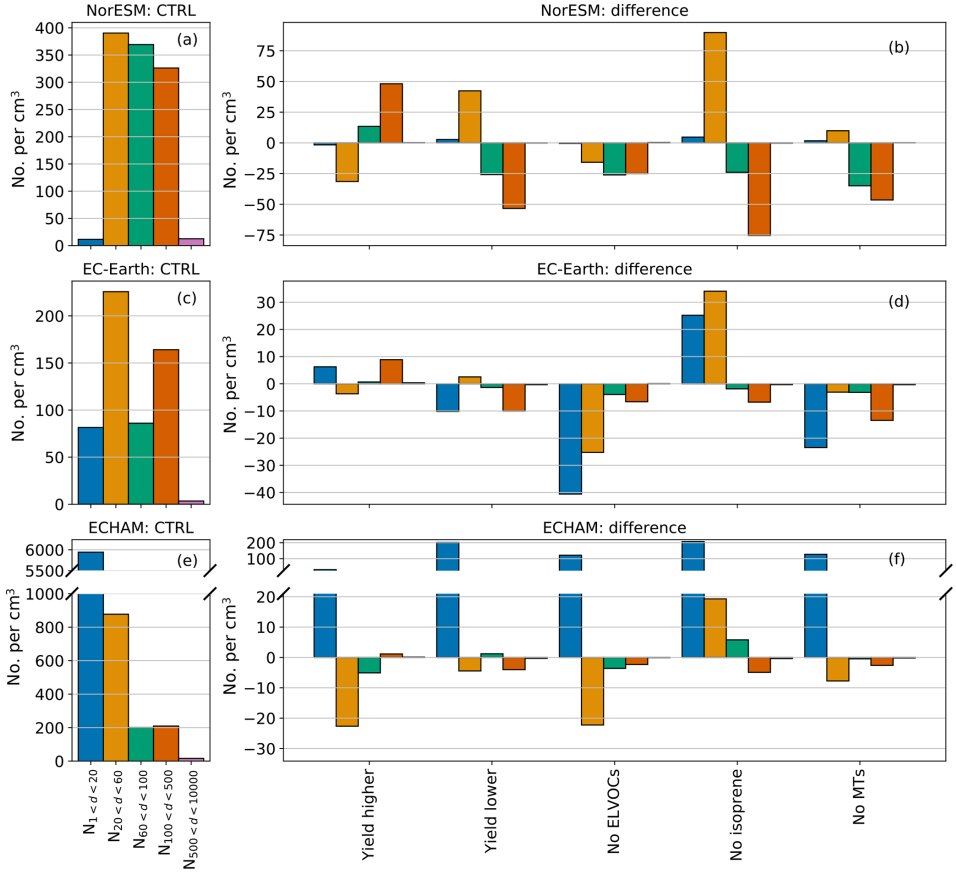

Figure 4. Bar plots of the number concentration of particles of selected sizes. In **(a)**, **(c)** and **(e)** the number concentrations from the *CTRL* simulations are shown. In **(b)**, **(d)** and **(f)** the absolute differences between the sensitivity simulations and the control simulations are shown for each size bin. Note that there are different scales used for the different models.

are mainly located close to the BVOC sources (not show). EC-Earth instead experiences these changes in the particle number concentration further downwind of the sources. This results in a more widespread change in DRE_{Ghan} in EC-Earth compared to the other two models (see Fig. S4) and thus a significantly higher global average DRE_{Ghan}. Similar but opposite changes are seen in the *Yield lower* simulation.

3.2.2 Indirect aerosol effects

The response of the indirect aerosol effects in the *Yield higher* and *Yield lower* sensitivity tests differs more than the direct effects. The CRE_{Ghan} in NorESM is strengthened (i.e. more negative) with increasing SOA production and vice versa; see Fig. 7. The changes in CRE_{Ghan} are $-0.27\,W\,m^{-2}$ (*Yield higher*) and $0.35\,W\,m^{-2}$ (*Yield lower*), indicating that these sensitivity simulations induce changes in the forcing of relevant magnitude. The globally averaged changes in EC-Earth have the same sign as those for NorESM but are lower (-0.11 and $+0.076\,W\,m^{-2}$); for ECHAM the changes are very small and not statistically significant. Also for the indirect effects, changes in the size distributions can be used to explain the changes in CRE_{Ghan}. While hygroscopicity might play a role, the effect is small in the activation scheme shared by the models (Abdul-Razzak and Ghan, 2000).

For NorESM, the higher (lower) SOA production in the *Yield higher* (*Yield lower*) simulation results in a shift in the size distribution to larger (smaller) sizes; see Fig. 4. For the *Yield higher* simulation, this results in higher CCN concentrations, higher CDNC, smaller cloud droplet effective radius (r_e) and larger CWP (Figs. S4–S7). The opposite change in these variables is seen in the *Yield lower* simulation. The main relative changes in cloud variables in NorESM are located over and downwind of the large BVOC emission sources in the tropics. Increased number of CCN generally means higher CDNC, lower r_e and higher CWP in all three models. For some regions, the CF decreases as CCN increases. The results regarding the changes in cloud parameters are shown in Figs. S5–S8 for the *Yield higher* and *Yield lower* simulations. Since the cloud response to the CCN changes are similar in all the models and simulations, we will mainly discuss CCN and CRE_{Ghan} changes for the other simulations.

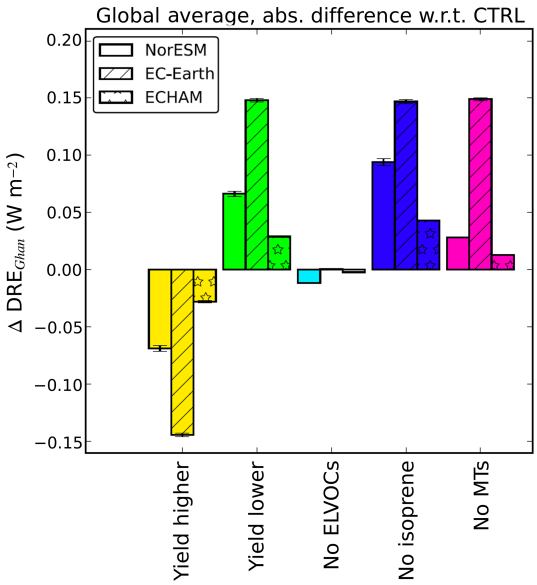

Figure 5. Bar plots of the average direct radiative effect (DRE_{Ghan}) difference between each sensitivity simulation and the *CTRL* simulations. Coloured bars indicate a significant difference in the simulation averages with a 95 % confidence interval. The error bars denote the standard error of mean of the yearly differences.

The essentially non-existing effects on the CRE_{Ghan} in ECHAM can also be explained using the size distribution. ECHAM experiences the smallest changes in particle number concentrations for particles with diameters greater than 100 nm; see Fig. 4f. However, for the smallest size ranges ($N_{1–60}$) ECHAM has the largest changes in the concentration of particles. Not surprisingly, the changes in number of these small particles do not affect the cloud formation in ECHAM, probably because they are too small to act as CCN when there is an abundance of particles at larger sizes (accumulation mode). Another interesting feature of ECHAM is that the changes in the size distribution are not mirrored in *Yield higher* and *Yield lower* simulations, which suggest non-linear dynamics caused by competition between NPF and condensation sink.

The rather small global changes in CRE_{Ghan} for EC-Earth are somewhat surprising since this model had the strongest response for the DRE_{Ghan}. However, investigating the maps of the changes in the CRE_{Ghan} for EC-Earth in Fig. 8c–d, one can see that the low global responses are caused by a pattern of opposite changes with magnitudes up to 4 W m^{-2}. In the *Yield higher* simulation, there is a strengthening of the CRE_{Ghan} close to large BVOC emission regions in the tropics, while over the remote oceans there is a weakening instead. The mirrored response is seen in the *Yield lower* simulation. Since the SOA production increases (decreases) globally in the *Yield higher* (*Yield lower*) simulation, the opposing patterns of CRE_{Ghan} are not directly related to changes of SOA production. Instead, the changes are related to different effects on the size distribution close to and far away from the BVOC sources as can be seen in Fig. 9 (the areas are shown in Fig. S21). For the *Yield higher* simulation, close to the sources, the increase in SOA production results in more accumulation mode particles ($N_{100–500}$), which leads to higher CCN concentrations and a stronger CRE_{Ghan}. Over the remote regions there is also an increase in accumulation mode particles, but this is accompanied by a larger decrease in particle concentrations in the Aitken mode (N_{20}–N_{60}). Since the aerosol concentrations are low in EC-Earth, in particular in these remote regions, the particles in the Aitken mode can also be activated as CCN because reduced competition effects give higher maximum supersaturation during cloud droplet activation. As a result, the CCN concentrations in these remote regions decrease when the SOA formation increases. This leads to a weakening of the CRE_{Ghan} (positive values). The changes in the *Yield lower* mirror those in the *Yield higher* simulation.

3.3 *No ELVOCs*

In this second section of results from the sensitivity simulations the results from the *No ELVOCs* simulation are presented. This simulation is different from the other simulations since only the type of SOA precursor is changed and not the quantity of precursors.

3.3.1 Direct aerosol effects

In terms of the direct effects, the global changes are small in all three models. For NorESM, there is a small but statistically significant strengthening of the DRE_{Ghan}, but the other two models do not display significant changes (see Fig. 5). The change in NorESM can be explained by changes in aerosol number concentrations over and downwind of the Amazon. Since there are no ELVOCs contributing to nucleation in this simulation, the NPF is reduced and with this the number concentration of smaller particles. This decrease is particularly strong over the Amazon since the MT emissions are very high here (see Fig. 1b) and ELVOCs can only be produced from MTs in NorESM. The strong decrease in small particles and increased vapours available for condensation (L/SVOCs) in this region means that more particles can grow to sizes where they act as efficient scatterers of solar radiation. This effect over the Amazon in NorESM is big enough to affect the global DRE_{Ghan}.

NorESM produces a large number of particles close to the BVOC emissions sources and, since the model does not contain a nucleation mode, these particles are introduced into the Aitken mode. The nucleated particles thus reach larger sizes closer to the sources than in the other two models, where the particles are introduced into a nucleation mode and shifted to the Aitken mode at a later time step while they are transported. This could be part of the explanation of why the BVOC effects in NorESM, in general, are located closer to

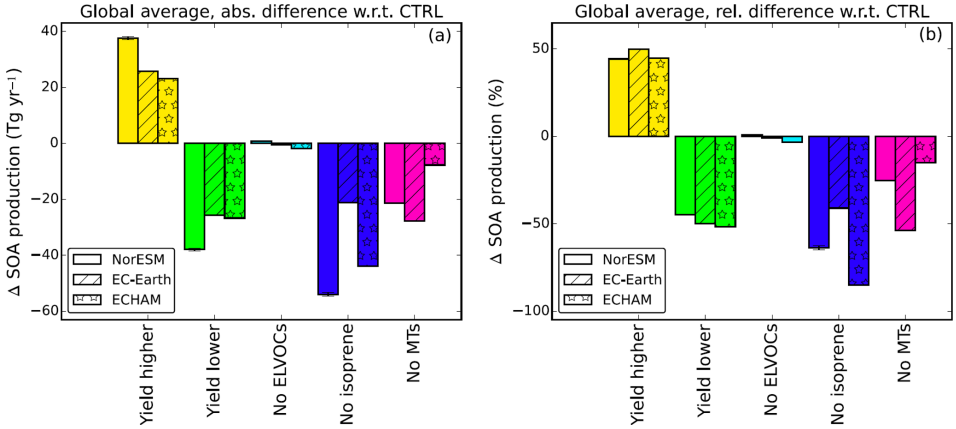

Figure 6. Bar plots of the average yearly SOA production changes in the three models. In **(a)**, the absolute difference between each sensitivity simulation and the *CTRL* simulations is shown and in **(b)** the relative differences between the sensitivity simulations and the control simulations are shown for all three models. Coloured bars indicate a significant difference in the simulation averages with a 95 % confidence interval. The error bars denote the standard error of mean of the yearly differences.

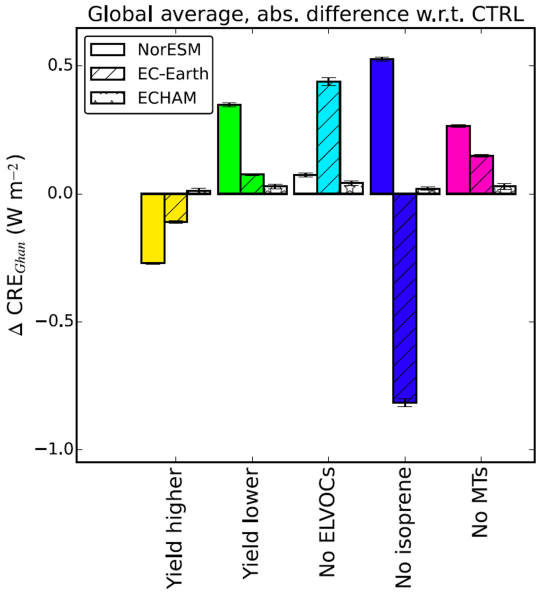

Figure 7. Bar plots of the global average cloud radiative effect (CRE_{Ghan}) between each sensitivity simulation and the *CTRL* simulations. Coloured bars indicate a significant difference in the simulation averages with a 95 % confidence interval. The error bars denote the standard error of mean of the yearly differences.

the sources than in EC-Earth. Moreover, in comparison to NorESM, EC-Earth has lower oxidant concentrations close to the large BVOC sources (not shown), which limits the SOA production in these regions and increases the amount of BVOC transported away from the sources. Hence, the overall effect is more widespread than in NorESM.

3.3.2 Indirect aerosol effects

For the indirect aerosol effects, EC-Earth is the only model that has significant changes for this simulation. The CRE_{Ghan} is weakened (less negative) by 0.44 W m^{-2} as can be seen in Fig. 7. This strong change in the CRE_{Ghan} is caused by a more or less strong worldwide decrease in the aerosol number concentration at almost all sizes (except particles above 500 nm). This results in a reduction of CCN which leads to a weakened CRE_{Ghan}. This strong decrease in CCN in EC-Earth occurs since the nucleation rates involving ELVOCs are calculated from a product of the H_2SO_4 and ELVOC concentrations (see Table 1). Thus, the removal of ELVOCs in this simulation removes all the BL NPF in EC-Earth. The other two models instead calculate the nucleation rates as the sum of H_2SO_4 and ELVOC concentrations and thus retain BL NPF from H_2SO_4. This results in quite different spatial patterns of the reduction in total aerosol number concentrations in the different models. For NorESM and ECHAM, the reductions occur close to the BVOC sources. For EC-Earth, on the other hand, the reductions are largest over regions that have large anthropogenic SO_2 emissions such as Europe, North America and Australia (not shown). This widespread reduction in CCN in combination with EC-Earth having low aerosol concentrations (which makes the clouds more sensitive to aerosol perturbations, Spracklen and Rap, 2013) results in a significant weakening of the CRE_{Ghan} in this simulation.

ECHAM has no significant change in the CRE_{Ghan} when the ELVOCs are removed. As for the first two experiments, the changes in the particle concentrations in the accumulation mode are small (Fig. 4). ECHAM, unlike the other models, experiences an increase in nucleation mode particles in this simulation. This is somewhat unexpected since removal of ELVOCs is expected to result in a decrease in NPF. However,

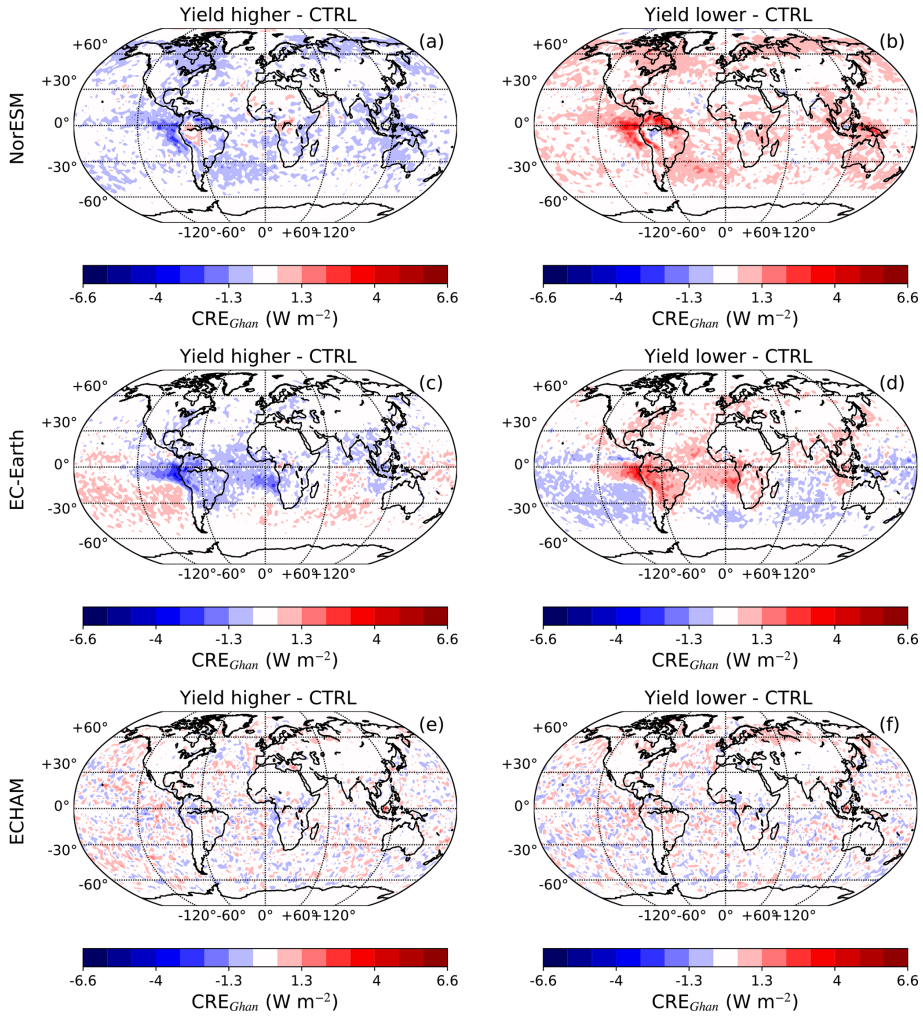

Figure 8. Maps of the difference in the average cloud radiative effect (CRE_{Ghan}) between the *Yield higher* **(a, c, d)** and *Yield lower* **(b, d, h)** with respect to the *CTRL* simulation. This is shown for NorESM **(a, b)**, EC-Earth **(c, d)** and ECHAM **(e, f)**.

this simulation shows that the nucleation rate parameterisation in ECHAM is not very sensitive to ELVOC concentrations. Nevertheless, the growth of the newly formed particles is highly dependent on the ELVOC concentrations and, since the particles do not grow to larger sizes, more particles remain in the nucleation mode. This results in increasing the concentration in the nucleation mode and decreasing number concentrations at larger sizes.

3.4 *No isoprene* and *No MTs*

In this last result section the *No isoprene* and *No MTs* simulations will be shown and discussed.

3.4.1 Direct aerosol effects

The DRE_{Ghan} is reduced (less negative) in all models in both these simulations since the SOA formation goes down when the BVOC emissions are reduced. The strongest effects on the DRE_{Ghan} are seen in EC-Earth with approximately 0.15 W m^{-2} changes for the *No isoprene* and *No MTs* simulations (Fig. 5). The reductions in DRE_{Ghan} for NorESM are about twice as large as those for ECHAM for the *No MTs* simulation. Moreover, both NorESM and ECHAM have almost an order of magnitude smaller decreases than in EC-Earth. In NorESM and ECHAM the changes in DRE_{Ghan} are located fairly close to the sources, while in EC-Earth they have a larger geographical spread (Fig. S15). This is the main cause for the large changes in the global DRE_{Ghan} in EC-Earth. The decrease in DRE_{Ghan} is explained by a reduction in the concentration of particles relevant for scattering (diameters above 100 nm).

The difference in SOA production between these cases reflects the proportion of SOA originating from isoprene and MTs, respectively. NorESM and ECHAM have the largest reductions in the *No isoprene* case, indicating that isoprene is the dominant SOA precursor, while EC-Earth has the largest

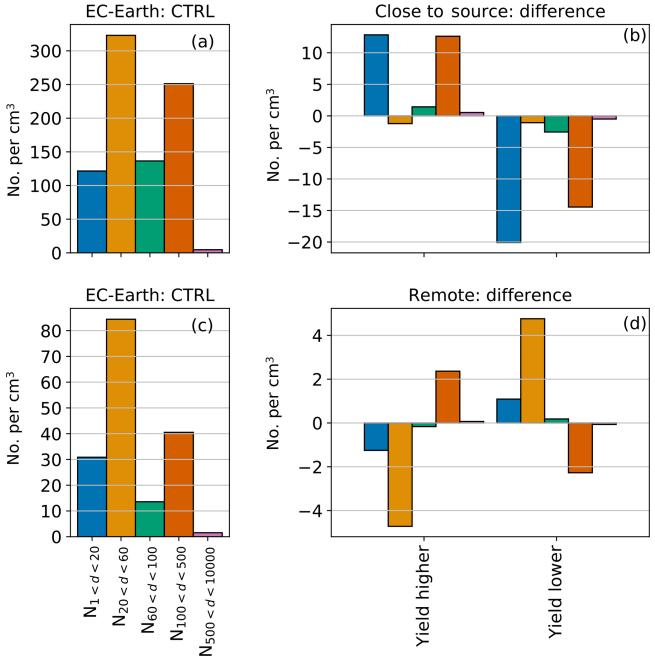

Figure 9. Bar plots of the number concentration of particles of selected sizes ranges for EC-Earth, close to and far away from the sources. In panels **(a)** and **(c)** the number concentrations from the *CTRL* simulations are shown. In panels **(b)** and **(d)** the differences between the sensitivity simulations and the *CTRL* simulations are shown for each size bin. Note that there are different scales used for the different regions. The areas defined as close and remote are based on changes in CCN concentrations (positive or negative) at 1 % supersaturation. These areas can be seen in Fig. S21.

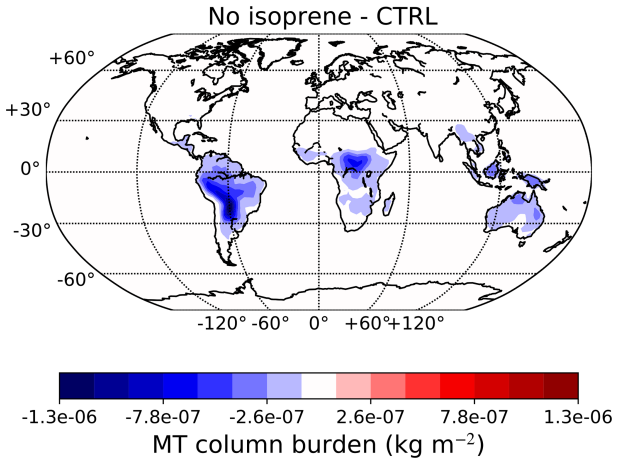

Figure 10. Map of the difference in the average MT column burden between the *No isoprene* and *CTRL* simulations for EC-Earth.

reduction in the *No MTs* simulation, indicating MTs are the dominant precursors. The difference in dominating precursors in the different models is mainly a result of different yields. The EC-Earth isoprene yields are 1 % (ELVOCs + L/SVOCs), 15 times lower than for MTs, while in NorESM and ECHAM the isoprene yield is 5 %, 3 times smaller than for MTs.

In the *No isoprene* simulation we also see an interesting feature connected to the interactive gas-phase chemistry in EC-Earth. Over large emission regions in the tropics, the column burden of MTs decreases when we remove the isoprene emissions; see Fig. 10. The decrease in the MT column burden is caused by a greater availability of OH when there is no isoprene present. The concentration of O_3 is reduced since the oxidation of isoprene results in the production of O_3. However, the loss rate of MT to O_3 oxidation is less important than OH, and thus the overall result is a reduction in column burden. This occurs only in EC-Earth due to the interactive chemistry in TM5. This does not increase the amount of SOA formed from MTs, but it affects where this SOA is formed, causing formation of SOA to occur closer to the sources. Additionally it favours the L/SVOCs over ELVOCs (see Table 2) because oxidation with OH will dominate more over reactions with O_3, and MT oxidation with O_3 has a higher ELVOC yield (5 %) than with OH (1 %).

3.4.2 Indirect aerosol effects

The *No isoprene* simulation displays the largest and also the most divergent results out of all simulations for the indirect aerosol effects. NorESM has a weakened CRE_{Ghan} by 0.53 W m^{-2}, while EC-Earth has a strengthened CRE_{Ghan} by -0.82 W m^{-2}. These numbers show that there is a substantial impact on the CRE_{Ghan} from the isoprene emissions in NorESM and EC-Earth. The magnitude of these numbers is in the range of and larger than the best estimate of the IPCC (2013) ERFaci relative to 1750 of -0.55 W m^{-2}. ECHAM, on the other hand, experiences a non-significant change in CRE_{Ghan}; see Fig. 7. Interestingly, all three models show a somewhat similar change in the size distribution as can be seen in Fig. 4. Isoprene mainly produces L/SVOCs in the models, and the removal of isoprene therefore leads to a shift in the particle size distribution towards smaller particles. For ECHAM, the aerosol concentration changes at CCN relevant sizes are very small and the clouds are virtually unaffected by this change. NorESM, on the other hand, experiences a quite large decrease in accumulation mode particles, which results in a decrease in CCN and weakening of the CRE_{Ghan}. EC-Earth also experiences a decrease in particles above 100 nm. Moreover, the Aitken mode in EC-Earth has a large absolute increase. This is due to more NPF when the condensation and coagulation sink decreases (more on this in the next section). Since the aerosol number concentrations in EC-Earth are so low, even aerosol particles in the Aitken mode can be activated as CCN and the increase in Aitken mode particles leads to increased CCN concentrations. This results in a strengthening of the CRE_{Ghan}, in particular over the oceans (Fig. S20). Thus, similar changes in the size distribution lead to vastly different responses in the three models depending

on aerosol number concentrations and different size distribution dynamics.

For the *No MTs* simulation, EC-Earth and NorESM have a weakened CRE_{Ghan}, while ECHAM experiences no significant change in the CRE_{Ghan}. The MT oxidation is the main source for ELVOCs in all three models (the only source in NorESM). It was therefore expected that turning off the emission of MTs would reduce the number of small particles in the models. However, this behaviour is only seen in EC-Earth where the global mean particle number concentration decreases at all sizes globally (see Fig. 4). For NorESM, the number of small particles instead increases while the number of larger particles decreases (due to less condensational growth of the particles), indicating that the loss of L/SVOCs (condensation) from MTs is more important than the loss of ELVOCs (NPF) for the size in this model. In ECHAM the number of nucleation mode particles increases and the number of larger particles decreases, which reduces the sink for small nuclei. Similarly to the *No ELVOCs* simulation, the reduction in ELVOCs leads to limited growth of the nucleation mode particles and therefore an increase in this mode. However, the changes in ECHAM are again very small and do not affect the clouds. Both NorESM and EC-Earth experience a decrease in CCN and therefore a weakened CRE_{Ghan}. The global CRE_{Ghan} response in EC-Earth in this simulation is, as for the simulations with changed yields, a result of compensating opposite patterns of CRE_{Ghan} close to (weakening) and far away (strengthening) from the sources.

3.5 Further discussion and implications

The introduction of particles from NPF should in theory and in the models be dependent on the interplay between available vapours for nucleation, condensation losses of these vapours and loss of newly formed particles due to coagulation. Adequately parameterising these processes is a challenge, and the balance between them varies between the models and also sometimes between regions in the same model. Regional variation is seen in EC-Earth where the NPF response varies depending on the distance from the sources, even if both regions experience the same sign in SOA production change. If we take the *Yields lower* experiment as an example, close to the sources, the decrease in VOCs leads to a reduction in both larger particles and NPF (Fig. 9). In remote regions, on the other hand, the coagulation sink for newly formed particles is reduced because of a reduction in larger particles. This increases the probability of NPF particles surviving to larger sizes. Thus, even though the total aerosol mass is decreased, the mass is partitioned to smaller sizes and the total number concentration is increased. Finally, since EC-Earth generally has low particle number concentrations in these regions, even these smaller particles are activated to form cloud droplets and produce a negative CRE. A similar effect can be seen in the *No isoprene* case for EC-Earth where we also see a strong negative CRE_{Ghan} associated with an increase in number concentrations (in spite of a decrease in total mass); see Figs. 7 and 6.

The above example for EC-Earth raises a more general point: the relationship between SOA production and CCN and aerosols relevant for radiation is highly non-linear. If ELVOCs are important for NPF and early growth, then an increase in ELVOCs could lead to more particles formed but also less condensate to grow the existing particles to climate relevant sizes (CCN, direct radiation effects). On the other hand, if H_2SO_4 is driving the NPF, SOA might be more important through changing the coagulation sink for NPF; more SOA could lead to less NPF and the effect on CCN will depend on the particles that are left. Thus, NPF does not necessarily lead to higher CCN concentrations.

Another factor of importance to NPF impact on the size distribution is the size at which new particles are added to the aerosol scheme. In EC-Earth and ECHAM, the particle growth and survival to 3 nm (ECHAM) and 5 nm (EC-Earth) are parameterised separately and then the particles are added to the nucleation mode. The size at which these particles are added makes a difference for the transferal of particles to the Aitken mode: in EC-Earth the added particles at 5 nm are already above the number median diameter of the mode, and thus some of these will always be transferred to the Aitken mode. In ECHAM, on the other hand, the addition of newly formed particles to the nucleation mode will decrease the number median diameter of the mode and can even decrease the number of particles that are transferred to Aitken mode. If NPF is continuously high, the particles can thus even be inhibited to grow to larger sizes. How much the radii of modes are allowed to change in combination with adding the particles at different sizes could be part of the explanation of why EC-Earth and ECHAM show such different changes in aerosol size distributions even though both models use the M7 aerosol module. NorESM also has a separate parameterisation for the growth and survival of the NPF particles up to a radius of 23 nm when the particles are added to the tracer for NPF. This growth occurs in one time step of the model (30 min). Hence, the particles grow very rapidly and reach Aitken mode sizes close to the sources.

This investigation shows that interactive oxidants can play an important role in determining, in particular, where the SOA formation occurs. The reduction in MT column burden over tropical forests when isoprene is removed illustrates that using interactive oxidants may limit the SOA formation in certain regions. This shifts the SOA formation further downstream from the sources, which results in more widespread climatic effects from BVOCs. Moreover, the results from the *No isoprene* experiment in the EC-Earth model show that there can be feedback mechanisms through interactive oxidants that affect SOA formation. In general, the removal of isoprene results in less formation of O_3 since its production is linked to the oxidation of isoprene. The reduction in O_3 means there is less O_3 available for SOA formation, which can lead to a further reduction in SOA production. Neverthe-

less, in the *No isoprene* experiment the removal of isoprene also leads to a higher availability of OH for the oxidation of monoterpenes, which then is oxidised closer to the sources. This results in an increase in SVOC formation from monoterpenes. In summary, changes in emissions can feed back to SOA formation both through effects on the oxidation capacity of the atmosphere and through changing the balance between the oxidants and thus the total SOA production due to different yields for different oxidants.

There are clearly large differences in the aerosol size distributions and how the changes in these sensitivity experiments affect the size distributions in the models. This is in spite of quite similar simplified treatments of SOA formation in the three models. Our findings show that the location of the SOA mass in the size distribution is critical for CCN concentrations, which agree with the results in Riipinen et al. (2011). The present study implies that further model development and evaluation is needed in terms of how new particle and SOA formation affect the size distribution. However, there are still large uncertainties in how these models should behave with regards to these processes (Glasius and Goldstein, 2016; Riipinen et al., 2011).

However, there are also other uncertainties and limitations with regards to the SOA processes in these models. One such limitation in the models in this study is the assumption that L/SVOCs are condensing irreversibly on pre-existing aerosol particles. More realistic parameterisations of this process, such as volatility basis set parameterisations, are starting to make their way into global climate models (Tsigaridis and Kanakidou, 2018). However, the gain from introducing a number of additional tracers required in such parameterisations need to be balanced against the increased computational expense to become readily used in ESMs. Another limitation is the lack of anthropogenic SOA in the models, as currently all anthropogenic emissions are treated as primary emissions. Anthropogenic impact on SOA formation through gas-phase chemistry, e.g. NO_x impact on yields, is also not included in these models at this point. Impacts from vegetation on the organic aerosol budget through primary biological organic aerosols are also missing in this study. The treatment of organic aerosol in ESMs is currently in rapid development. Model evaluation against observations is an important tool in this development work, though it is out of the scope of this article.

Over the past years, more and more studies have investigated the BVOC climate impact from pre-industrial to present day (Heald and Geddes, 2016; Scott et al., 2017; Unger, 2014) and also into the future, including possible BVOC climate feedbacks (Sporre et al., 2019; Makkonen et al., 2012; Scott et al., 2018; Paasonen et al., 2013). The results regarding the BVOC impact on climate have a large spread among the different studies. This study indicates that at least parts of these differences could be related to varying sensitivity to BVOC and SOA changes in the models used in the different studies. The decrease in isoprene emissions since 1850 has been estimated to be approximately 15 % (Scott et al., 2017; Unger, 2014), and in this study the removal of all isoprene emissions leads to a change in the total aerosol radiative effect by $0.62\,\mathrm{W\,m^{-2}}$ in NorESM and $-0.67\,\mathrm{W\,m^{-2}}$ in EC-Earth, which is a $1.29\,\mathrm{W\,m^{-2}}$ difference. Hence, assuming the changes in radiative effects are not too far from linear, the decrease in isoprene emissions since pre-industrial would introduce an uncertainty in the aerosol forcing of an order of magnitude of $0.19\,\mathrm{W\,m^{-2}}$ using these models. This sensitivity study reveals that NorESM, EC-Earth and ECHAM would produce very different results if used to investigate the climatic impacts of BVOCs.

4 Conclusions

The impact of BVOC emission and SOA formation on particle size distribution, cloud properties and radiative effects has been compared among three ESMs: NorESM, EC-Earth and ECHAM. In five different sensitivity studies, the effect of changed yields of BVOC oxidation, volatility of the oxidised BVOCs and contribution of precursor gases has been investigated.

We found that both the direct and indirect aerosol effects in the models are substantially affected by changes in SOA precursor yields and BVOC emissions. The $\mathrm{DRE_{Ghan}}$ is strengthened (by up to $0.15\,\mathrm{W\,m^{-2}}$) by more SOA and vice versa. Even though the changes in $\mathrm{DRE_{Ghan}}$ have the expected sign of the response to changes in SOA production in all three models and simulations, the sensitivity of the $\mathrm{DRE_{Ghan}}$ to SOA production changes varies between the models. This is connected to how much of the SOA production changes affect the parts of the modelled size distributions where the particles act most efficiently as scatterers of solar radiation. The results from this study show that EC-Earth is the model with most widespread changes of the accumulation- and coarse-mode particles, and hence largest sensitivity of $\mathrm{DRE_{Ghan}}$. ECHAM is least sensitive here since the SOA changes mostly affect the small particles and are relatively small.

The changes in the $\mathrm{CRE_{Ghan}}$ are stronger (up to $-0.82\,\mathrm{W\,m^{-2}}$) than for the $\mathrm{DRE_{Ghan}}$ and more complex. The $\mathrm{CRE_{Ghan}}$ changes do not necessarily follow the SOA changes and can be of different sign for different models and even different regions in the same model. Again, size distribution dynamics are crucial for understanding the sensitivity of the cloud properties and $\mathrm{CRE_{Ghan}}$ in the models. Also for the $\mathrm{CRE_{Ghan}}$, ECHAM is the least sensitive model. Overall, the small effects on the size distributions at CCN-relevant sizes in this model means that the clouds in ECHAM are virtually unaffected by the sensitivity simulations. The clouds in NorESM are quite strongly affected by the sensitivity simulations, mainly because of shifts in the size distribution. These shifts are mainly a result of changes in condensational growth, and thus the condensation of L/SVOCs is very im-

portant for the climate impact of BVOCs in NorESM. EC-Earth is the most sensitive model out of the three models also for the cloud effects. This results from a combination of a size distribution quite sensitive to NPF in combination with low aerosol number concentrations in EC-Earth, which makes the clouds sensitive to aerosol perturbations. Moreover, the NPF in EC-Earth is more sensitive to the ELVOC concentrations than the other models since the BL nucleation rate is calculated from the product of the H_2SO_4 and ELVOC concentrations, while the other two models used the sum of the concentrations (see Table 1).

We can conclude that the BVOC treatment in the ESMs is of importance and can introduce substantial uncertainties in aerosol climate effects and forcing. There is need for more development and testing of these parameterisations in ESMs with respect to how the NPF parameterisations affect the size distributions.

Data availability. The temporally averaged model output from the six simulations used in the paper from all three models is available here: https://doi.org/10.11582/2020.00032 (Sporre, 2020). The monthly data will be shared upon request. The reason for not supplying and storing all the data online is the large size of the entire dataset.

Supplement. The supplement related to this article is available online at: https://doi.org/10.5194/acp-20-8953-2020-supplement.

Author contributions. MKS performed the model simulations with NorESM. MKS and SMB did the data analysis and wrote the article. RS performed the model simulations with EC-Earth and wrote parts of the paper. RM performed the model simulations with ECHAM and wrote parts of the paper. IHHK provided support during the setup NorESM. TvN, TB and DO co-developed the EC-Earth version used during the study and provided support for the EC-Earth simulations. MKS, SMB, RS, RM, IHKK and TKB contributed with discussions regarding the experimental design and data analysis. All contributors have contributed to the discussions regarding the article.

Competing interests. The authors declare that they have no conflict of interest.

Financial support. The research leading to these results has received funding from the European Union's Seventh Framework Programme (FP7/2007-2013) project BACCHUS under grant agreement no. 603445. This work was supported by LATICE, a strategic research area funded by the Faculty of Mathematics and Natural Sciences at the University of Oslo. This work has been financed by the Research Council of Norway (RCN) through the NOTUR/Norstore project NN9485K (biogenic aerosols and climate feedbacks). Inger H. H. Karset has been financed by the Research Council of Norway through the project EVA and the NOTUR/Norstore projects (Sigma2 account: nn2345k, Norstore account: NS2345K). Twan van Noije and Tommi Bergman received funding from the European Union's Horizon 2020 research and innovation programme project CRESCENDO under grant agreement no. 641816.

Review statement. This paper was edited by Kostas Tsigaridis and reviewed by three anonymous referees.

References

Abdul-Razzak, H. and Ghan, S. J.: A parameterization of aerosol activation: 2. Multiple aerosol types, J. Geophys. Res.-Atmos,, 105, 6837–6844, https://doi.org/10.1029/1999JD901161, 2000.

Albrecht, B. A.: Aerosols, Cloud Microphysics, and Fractional Cloudiness, Science, 245, 1227–1230, https://doi.org/10.1126/science.245.4923.1227, 1989.

Arneth, A., Niinemets, Ü., Pressley, S., Bäck, J., Hari, P., Karl, T., Noe, S., Prentice, I. C., Serça, D., Hickler, T., Wolf, A., and Smith, B.: Process-based estimates of terrestrial ecosystem isoprene emissions: incorporating the effects of a direct CO_2-isoprene interaction, Atmos. Chem. Phys., 7, 31–53, https://doi.org/10.5194/acp-7-31-2007, 2007.

Bentsen, M., Bethke, I., Debernard, J. B., Iversen, T., Kirkevåg, A., Seland, Ø., Drange, H., Roelandt, C., Seierstad, I. A., Hoose, C., and Kristjánsson, J. E.: The Norwegian Earth System Model, NorESM1-M – Part 1: Description and basic evaluation of the physical climate, Geosci. Model Dev., 6, 687–720, https://doi.org/10.5194/gmd-6-687-2013, 2013.

Bonan, G.: Ecological Climatology, Cambridge University Press, 3rd Edn., 2016.

Carlton, A. G., Pinder, R. W., Bhave, P. V., and Pouliot, G. A.: To What Extent Can Biogenic SOA be Controlled?, Environ. Sci. Technol., 44, 3376–3380, https://doi.org/10.1021/es903506b, 2010.

Carslaw, K. S., Boucher, O., Spracklen, D. V., Mann, G. W., Rae, J. G. L., Woodward, S., and Kulmala, M.: A review of natural aerosol interactions and feedbacks within the Earth system, Atmos. Chem. Phys., 10, 1701–1737, https://doi.org/10.5194/acp-10-1701-2010, 2010.

Charlson, R. J., Langner, J., and Rodhe, H.: Sulphate aerosol and climate, Nature, 348, p. 22, https://doi.org/10.1038/348022a0, 1990.

Dee, D. P., Uppala, S. M., Simmons, A. J., Berrisford, P., Poli, P., Kobayashi, S., Andrae, U., Balmaseda, M. A., Balsamo, G., Bauer, P., Bechtold, P., Beljaars, A. C. M., van de Berg, L., Bidlot, J., Bormann, N., Delsol, C., Dragani, R., Fuentes, M., Geer, A. J., Haimberger, L., Healy, S. B., Hersbach, H., Hólm, E. V., Isaksen, L., Kållberg, P., Köhler, M., Matricardi, M., McNally, A. P., Monge-Sanz, B. M., Morcrette, J., Park, B., Peubey, C., de Rosnay, P., Tavolato, C., Thépaut, J., and Vitart, F.: The ERA-Interim reanalysis: configuration and performance of the data assimilation system, Q. J. Roy. Meteor. Soc., 137, 553–597, https://doi.org/10.1002/qj.828, 2011.

Donahue, N. M., Robinson, A. L., Stanier, C. O., and Pandis, S. N.: Coupled Partitioning, Dilution, and Chemical Aging of

Semivolatile Organics, Environ. Sci. Technol., 40, 2635–2643, https://doi.org/10.1021/es052297c, 2006.

Donahue, N. M., Epstein, S. A., Pandis, S. N., and Robinson, A. L.: A two-dimensional volatility basis set: 1. organic-aerosol mixing thermodynamics, Atmos. Chem. Phys., 11, 3303–3318, https://doi.org/10.5194/acp-11-3303-2011, 2011.

Dunne, E. M., Gordon, H., Kürten, A., Almeida, J., Duplissy, J., Williamson, C., Ortega, I. K., Pringle, K. J., Adamov, A., Baltensperger, U., Barmet, P., Benduhn, F., Bianchi, F., Breitenlechner, M., Clarke, A., Curtius, J., Dommen, J., Donahue, N. M., Ehrhart, S., Flagan, R. C., Franchin, A., Guida, R., Hakala, J., Hansel, A., Heinritzi, M., Jokinen, T., Kangasluoma, J., Kirkby, J., Kulmala, M., Kupc, A., Lawler, M. J., Lehtipalo, K., Makhmutov, V., Mann, G., Mathot, S., Merikanto, J., Miettinen, P., Nenes, A., Onnela, A., Rap, A., Reddington, C. L. S., Riccobono, F., Richards, N. A. D., Rissanen, M. P., Rondo, L., Sarnela, N., Schobesberger, S., Sengupta, K., Simon, M., Sipilä, M., Smith, J. N., Stozkhov, Y., Tomé, A., Tröstl, J., Wagner, P. E., Wimmer, D., Winkler, P. M., Worsnop, D. R., and Carslaw, K. S.: Global atmospheric particle formation from CERN CLOUD measurements, Science, 354, 1119–1124, https://doi.org/10.1126/science.aaf2649, 2016.

Ehn, M., Thornton, J. A., Kleist, E., Sipilä, M., Junninen, H., Pullinen, I., Springer, M., Rubach, F., Tillmann, R., Lee, B., Lopez-Hilfiker, F., Andres, S., Acir, I.-H., Rissanen, M., Jokinen, T., Schobesberger, S., Kangasluoma, J., Kontkanen, J., Nieminen, T., Kurtén, T., Nielsen, L. B., Jørgensen, S., Kjaergaard, H. G., Canagaratna, M., Maso, M. D., Berndt, T., Petäjä, T., Wahner, A., Kerminen, V.-M., Kulmala, M., Worsnop, D. R., Wildt, J., and Mentel, T. F.: A large source of low-volatility secondary organic aerosol, Nature, 506, 476–479, https://doi.org/10.1038/nature13032, 2014.

Gettelman, A. and Morrison, H.: Advanced Two-Moment Bulk Microphysics for Global Models. Part I: Off-Line Tests and Comparison with Other Schemes, J. Climate, 28, 1268–1287, https://doi.org/10.1175/JCLI-D-14-00102.1, 2015.

Ghan, S. J.: Technical Note: Estimating aerosol effects on cloud radiative forcing, Atmos. Chem. Phys., 13, 9971–9974, https://doi.org/10.5194/acp-13-9971-2013, 2013.

Glasius, M. and Goldstein, A. H.: Recent Discoveries and Future Challenges in Atmospheric Organic Chemistry, Environ. Sci. Technol., 50, 2754–2764, https://doi.org/10.1021/acs.est.5b05105, 2016.

Glasius, M., Hansen, A. M. K., Claeys, M., Henzing, J. S., Jedynska, A. D., Kasper-Giebl, A., Kistler, M., Kristensen, K., Martinsson, J., Maenhaut, W., Nøjgaard, J. K., Spindler, G., Stenström, K. E., Swietlicki, E., Szidat, S., Simpson, D., and Yttri, K. E.: Composition and sources of carbonaceous aerosols in Northern Europe during winter, Atmos. Environ., 173, 127–141, https://doi.org/10.1016/j.atmosenv.2017.11.005, 2018.

Gordon, H., Sengupta, K., Rap, A., Duplissy, J., Frege, C., Williamson, C., Heinritzi, M., Simon, M., Yan, C., Almeida, J., Tröstl, J., Nieminen, T., Ortega, I. K., Wagner, R., Dunne, E. M., Adamov, A., Amorim, A., Bernhammer, A.-K., Bianchi, F., Breitenlechner, M., Brilke, S., Chen, X., Craven, J. S., Dias, A., Ehrhart, S., Fischer, L., Flagan, R. C., Franchin, A., Fuchs, C., Guida, R., Hakala, J., Hoyle, C. R., Jokinen, T., Junninen, H., Kangasluoma, J., Kim, J., Kirkby, J., Krapf, M., Kürten, A., Laaksonen, A., Lehtipalo, K., Makhmutov, V., Mathot, S., Molteni, U., Monks, S. A., Onnela, A., Peräkylä, O., Piel, F., Petäjä, T., Praplan, A. P., Pringle, K. J., Richards, N. A. D., Rissanen, M. P., Rondo, L., Sarnela, N., Schobesberger, S., Scott, C. E., Seinfeld, J. H., Sharma, S., Sipilä, M., Steiner, G., Stozhkov, Y., Stratmann, F., Tomé, A., Virtanen, A., Vogel, A. L., Wagner, A. C., Wagner, P. E., Weingartner, E., Wimmer, D., Winkler, P. M., Ye, P., Zhang, X., Hansel, A., Dommen, J., Donahue, N. M., Worsnop, D. R., Baltensperger, U., Kulmala, M., Curtius, J., and Carslaw, K. S.: Reduced anthropogenic aerosol radiative forcing caused by biogenic new particle formation, P. Natl. Acad. Sci. USA, 113, 12053–12058, https://doi.org/10.1073/pnas.1602360113, 2016.

Gordon, H., Kirkby, J., Baltensperger, U., Bianchi, F., Breitenlechner, M., Curtius, J., Dias, A., Dommen, J., Donahue, N. M., Dunne, E. M., Duplissy, J., Ehrhart, S., Flagan, R. C., Frege, C., Fuchs, C., Hansel, A., Hoyle, C. R., Kulmala, M., Kürten, A., Lehtipalo, K., Makhmutov, V., Molteni, U., Rissanen, M. P., Stozkhov, Y., Tröstl, J., Tsagkogeorgas, G., Wagner, R., Williamson, C., Wimmer, D., Winkler, P. M., Yan, C., and Carslaw, K. S.: Causes and importance of new particle formation in the present-day and preindustrial atmospheres, J. Geophys. Res.-Atmos., 122, 8739–8760, https://doi.org/10.1002/2017JD026844, 2017.

Guenther, A. B., Jiang, X., Heald, C. L., Sakulyanontvittaya, T., Duhl, T., Emmons, L. K., and Wang, X.: The Model of Emissions of Gases and Aerosols from Nature version 2.1 (MEGAN2.1): an extended and updated framework for modeling biogenic emissions, Geosci. Model Dev., 5, 1471–1492, https://doi.org/10.5194/gmd-5-1471-2012, 2012.

Hallquist, M., Wenger, J. C., Baltensperger, U., Rudich, Y., Simpson, D., Claeys, M., Dommen, J., Donahue, N. M., George, C., Goldstein, A. H., Hamilton, J. F., Herrmann, H., Hoffmann, T., Iinuma, Y., Jang, M., Jenkin, M. E., Jimenez, J. L., Kiendler-Scharr, A., Maenhaut, W., McFiggans, G., Mentel, Th. F., Monod, A., Prévôt, A. S. H., Seinfeld, J. H., Surratt, J. D., Szmigielski, R., and Wildt, J.: The formation, properties and impact of secondary organic aerosol: current and emerging issues, Atmos. Chem. Phys., 9, 5155–5236, https://doi.org/10.5194/acp-9-5155-2009, 2009.

Hantson, S., Knorr, W., Schurgers, G., Pugh, T. A., and Arneth, A.: Global isoprene and monoterpene emissions under changing climate, vegetation, CO_2 and land use, Atmos. Environ., 155, 35–45, https://doi.org/10.1016/j.atmosenv.2017.02.010, 2017.

Hazeleger, W., Wang, X., Severijns, C., Ştefănescu, S., Bintanja, R., Sterl, A., Wyser, K., Semmler, T., Yang, S., van den Hurk, B., van Noije, T., van der Linden, E., and van der Wiel, K.: EC-Earth V2.2: description and validation of a new seamless earth system prediction model, Clim. Dynam., 39, 2611–2629, https://doi.org/10.1007/s00382-011-1228-5, 2012.

Heald, C. L. and Geddes, J. A.: The impact of historical land use change from 1850 to 2000 on secondary particulate matter and ozone, Atmos. Chem. Phys., 16, 14997–15010, https://doi.org/10.5194/acp-16-14997-2016, 2016.

Heald, C. L. and Spracklen, D. V.: Land Use Change Impacts on Air Quality and Climate, Chem. Rev., 115, 4476–4496, https://doi.org/10.1021/cr500446g, 2015.

IPCC: Summary for Policymakers, in: Climate Change 2013: The Physical Science Basis. Contribution of Working Group I to the Fifth Assessment Report of the Intergovernmental Panel on Cli-

mate Change, edited by: Stocker, T. F., Qin, D., Plattner, G.-K., Tignor, M., Allen, S. K., Boschung, J., Nauels, A., Xia, Y., Bex, V., and Midgley, P. M., Cambridge University Press, Cambridge, United Kingdom and New York, NY, USA, 2013.

Iversen, T., Bentsen, M., Bethke, I., Debernard, J. B., Kirkevåg, A., Seland, Ø., Drange, H., Kristjansson, J. E., Medhaug, I., Sand, M., and Seierstad, I. A.: The Norwegian Earth System Model, NorESM1-M – Part 2: Climate response and scenario projections, Geosci. Model Dev., 6, 389–415, https://doi.org/10.5194/gmd-6-389-2013, 2013.

Jokinen, T., Berndt, T., Makkonen, R., Kerminen, V.-M., Junninen, H., Paasonen, P., Stratmann, F., Herrmann, H., Guenther, A. B., Worsnop, D. R., Kulmala, M., Ehn, M., and Sipilä, M.: Production of extremely low volatile organic compounds from biogenic emissions: Measured yields and atmospheric implications, P. Natl. Acad. Sci. USA, 112, 7123–7128, https://doi.org/10.1073/pnas.1423977112, 2015.

Kanakidou, M., Tsigaridis, K., Dentener, F. J., and Crutzen, P. J.: Human-activity-enhanced formation of organic aerosols by biogenic hydrocarbon oxidation, J. Geophys. Res.-Atmos., 105, 9243–9354, https://doi.org/10.1029/1999JD901148, 2000.

Karset, I. H. H., Berntsen, T. K., Storelvmo, T., Alterskjær, K., Grini, A., Olivié, D., Kirkevåg, A., Seland, Ø., Iversen, T., and Schulz, M.: Strong impacts on aerosol indirect effects from historical oxidant changes, Atmos. Chem. Phys., 18, 7669–7690, https://doi.org/10.5194/acp-18-7669-2018, 2018.

Kelly, J. M., Doherty, R. M., O'Connor, F. M., and Mann, G. W.: The impact of biogenic, anthropogenic, and biomass burning volatile organic compound emissions on regional and seasonal variations in secondary organic aerosol, Atmos. Chem. Phys., 18, 7393–7422, https://doi.org/10.5194/acp-18-7393-2018, 2018.

Kerminen, V. M. and Kulmala, M.: Analytical formulae connecting the "real" and the "apparent" nucleation rate and the nuclei number concentration for atmospheric nucleation events, J. Aerosol Sci., 33, 609–622, https://doi.org/10.1016/S0021-8502(01)00194-X, 2002.

Kirkby, J., Duplissy, J., Sengupta, K., Frege, C., Gordon, H. Williamson, C., Heinritzi, M., Simon, M., Yan, C., Almeida, J., Tröstl, J., Nieminen, Ortega, T., Wagner, R., Adamov, A., Amorim, A., Bernhammer, A., Bianchi, F., Breitenlechner, M., Brilke, S., Chen, X., Craven, J., Dias, A., Ehrhart, S., Flagan, R. C., Franchin, A., Fuchs, C., Guida, R., Hakala, J., Hoyle, C. R., Jokinen, T., Junninen, H. Kangasluoma, J., Kim, J., Krapf, M. Kürten, A., Laaksonen, A., Lehtipalo, K., Makhmutov, V., Mathot, S., Molteni, U., Onnela, A., Peräkylä, O., Piel, F., Petäjä, T., Praplan, A. P., Pringle, K., Rap, A., Richards, N., Riipinen, I., Rissanen, M. P., Rondo, L., Sarnela, N., Schobesberger, S., Scott, C., Seinfeld, J. H., Sipilä, M., Steiner, G., Stozhkov, Y., Stratmann, F., Tomé, A., Virtanen, A., Vogel, A., Wagner, A., Wagner, P., Weingartner, E., Wimmer, D., Winkler, P., Ye, P., Zhang, X., Hansel, A., Dommen, J., Donahue, N. M., Worsnop, D., Baltensperger, U., Kulmala, M., Carslaw, K. S., and Curtius, J.: Ion-induced nucleation of pure biogenic particles, Nature, 533, 521–526, https://doi.org/10.1038/nature17953, 2016.

Kirkevåg, A., Iversen, T., Seland, Ø., Hoose, C., Kristjánsson, J. E., Struthers, H., Ekman, A. M. L., Ghan, S., Griesfeller, J., Nilsson, E. D., and Schulz, M.: Aerosol–climate interactions in the Norwegian Earth System Model – NorESM1-M, Geosci. Model Dev., 6, 207–244, https://doi.org/10.5194/gmd-6-207-2013, 2013.

Kirkevåg, A., Grini, A., Olivié, D., Seland, Ø., Alterskjær, K., Hummel, M., Karset, I. H. H., Lewinschal, A., Liu, X., Makkonen, R., Bethke, I., Griesfeller, J., Schulz, M., and Iversen, T.: A production-tagged aerosol module for Earth system models, OsloAero5.3 – extensions and updates for CAM5.3-Oslo, Geosci. Model Dev., 11, 3945–3982, https://doi.org/10.5194/gmd-11-3945-2018, 2018.

Kokkola, H., Hommel, R., Kazil, J., Niemeier, U., Partanen, A.-I., Feichter, J., and Timmreck, C.: Aerosol microphysics modules in the framework of the ECHAM5 climate model – intercomparison under stratospheric conditions, Geosci. Model Dev., 2, 97–112, https://doi.org/10.5194/gmd-2-97-2009, 2009.

Kooperman, G. J., Pritchard, M. S., Ghan, S. J., Wang, M., Somerville, R. C. J., and Russell, L. M.: Constraining the influence of natural variability to improve estimates of global aerosol indirect effects in a nudged version of the Community Atmosphere Model 5, J. Geophys. Res.-Atmos., 117, 1–16, https://doi.org/10.1029/2012JD018588, 2012.

Kulmala, M., Nieminen, T., Nikandrova, A., Lehtipalo, K., Manninen, H. E., Kajos, M. K., Kolari, P., Lauri, A., Petäjä, T., Krejci, R., Vesala, T., Kerminen, V. M., Nieminen, T., Kolari, P., Hari, P., Bäck, J., Krejci, R., Hansson, H. C., Swietlicki, E., Lindroth, A., Christensen, T. R., and Arneth, A.: CO_2-induced terrestrial climate feedback mechanism: From carbon sink to aerosol source and back, Boreal Environ. Res., 19, 122–131, 2014.

Lamarque, J.-F., Emmons, L. K., Hess, P. G., Kinnison, D. E., Tilmes, S., Vitt, F., Heald, C. L., Holland, E. A., Lauritzen, P. H., Neu, J., Orlando, J. J., Rasch, P. J., and Tyndall, G. K.: CAM-chem: description and evaluation of interactive atmospheric chemistry in the Community Earth System Model, Geosci. Model Dev., 5, 369–411, https://doi.org/10.5194/gmd-5-369-2012, 2012.

Lehtinen, K. E., Dal Maso, M., Kulmala, M., and Kerminen, V. M.: Estimating nucleation rates from apparent particle formation rates and vice versa: Revised formulation of the Kerminen-Kulmala equation, J. Aerosol Sci., 38, 988–994, https://doi.org/10.1016/j.jaerosci.2007.06.009, 2007.

Lin, G., Wan, H., Zhang, K., Qian, Y., and Ghan, S. J.: Can nudging be used to quantify model sensitivities in precipitation and cloud forcing?, J. Adv. Model. Earth Sy., 8, 1073–1091, https://doi.org/10.1002/2016MS000659, 2016.

Lohmann, U. and Hoose, C.: Sensitivity studies of different aerosol indirect effects in mixed-phase clouds, Atmos. Chem. Phys., 9, 8917–8934, https://doi.org/10.5194/acp-9-8917-2009, 2009.

Makkonen, R., Asmi, A., Kerminen, V.-M., Boy, M., Arneth, A., Guenther, A., and Kulmala, M.: BVOC-aerosol-climate interactions in the global aerosol-climate model ECHAM5.5-HAM2, Atmos. Chem. Phys., 12, 10077–10096, https://doi.org/10.5194/acp-12-10077-2012, 2012.

Makkonen, R., Seland, Ø., Kirkevåg, A., Iversen, T., and Kristjánsson, J. E.: Evaluation of aerosol number concentrations in NorESM with improved nucleation parameterization, Atmos. Chem. Phys., 14, 5127–5152, https://doi.org/10.5194/acp-14-5127-2014, 2014.

Morrison, H. and Gettelman, A.: A new two-moment bulk stratiform cloud microphysics scheme in the community atmosphere model, version 3 (CAM3). Part I: De-

scription and numerical tests, J. Climate, 21, 3642–3659, https://doi.org/10.1175/2008JCLI2105.1, 2008.

Neale, R. B., Gettelman, A., Park, S., Chen, C.-c., Lauritzen, P. H., Williamson, D. L., Conley, A. J., Kinnison, D., Marsh, D., Smith, A. K., Vitt, F., Garcia, R., Lamarque, J.-f., Mills, M., Tilmes, S., Morrison, H., Cameron-smith, P., Collins, W. D., Iacono, M. J., Easter, R. C., Liu, X., Ghan, S. J., Rasch, P. J., and Taylor, M. A.: Description of the NCAR Community Atmosphere Model (CAM 5.0), NCAR Technical Notes, Ncar/Tn-464+Str, p. 214, https://doi.org/10.5065/D6N877R0., 2012.

Oleson, K. W., Lawrence, D. M., Bonan, G. B., Drewniak, B., Huang, M., Koven, C. D., Levis, S., Li, F., Riley, W. J., Subin, Z. M., Swenson, S. C., Thornton, P. E., Bozbiyik, A., Fisher, R., Heald, C. L., Kluzek, E., Lamarque, J.-f., Lawrence, P. J., Leung, L. R., Lipscomb, W., Muszala, S., Ricciuto, D. M., Sacks, W., Sun, Y., Tang, J., and Yang, Z.-L.: Technical description of version 4.0 of the Community Land Model (CLM), NCAR/TN-503+STR NCAR Technical Note, p. 266, available at: http://www.cesm.ucar.edu/models/cesm1.2/clm/CLM45_Tech_Note.pdf (last access: 15 July 2020), 2013.

Paasonen, P., Nieminen, T., Asmi, E., Manninen, H. E., Petäjä, T., Plass-Dülmer, C., Flentje, H., Birmili, W., Wiedensohler, A., Hõrrak, U., Metzger, A., Hamed, A., Laaksonen, A., Facchini, M. C., Kerminen, V.-M., and Kulmala, M.: On the roles of sulphuric acid and low-volatility organic vapours in the initial steps of atmospheric new particle formation, Atmos. Chem. Phys., 10, 11223–11242, https://doi.org/10.5194/acp-10-11223-2010, 2010.

Paasonen, P., Asmi, A., Petäjä, T., Kajos, M. K., Äijälä, M., Junninen, H., Holst, T., Abbatt, J. P. D., Arneth, A., Birmili, W., van der Gon, H. D., Hamed, A., Hoffer, A., Laakso, L., Laaksonen, A., Richard Leaitch, W., Plass-Dülmer, C., Pryor, S. C., Räisänen, P., Swietlicki, E., Wiedensohler, A., Worsnop, D. R., Kerminen, V.-M., and Kulmala, M.: Warming-induced increase in aerosol number concentration likely to moderate climate change, Nat. Geosci., 6, 438–442, https://doi.org/10.1038/ngeo1800, 2013.

Park, S. and Bretherton, C. S.: The University of Washington Shallow Convection and Moist Turbulence Schemes and Their Impact on Climate Simulations with the Community Atmosphere Model, J. Climate, 22, 3449–3469, https://doi.org/10.1175/2008JCLI2557.1, 2009.

Riccobono, F., Schobesberger, S., Scott, C. E., Dommen, J., Ortega, I. K., Rondo, L., Almeida, J., Amorim, A., Bianchi, F., Breitenlechner, M., David, A., Downard, A., Dunne, E. M., Duplissy, J., Ehrhart, S., Flagan, R. C., Franchin, A., Hansel, A., Junninen, H., Kajos, M., Keskinen, H., Kupc, A., Kürten, A., Kvashin, A. N., Laaksonen, A., Lehtipalo, K., Makhmutov, V., Mathot, S., Nieminen, T., Onnela, A., Petäjä, T., Praplan, A. P., Santos, F. D., Schallhart, S., Seinfeld, J. H., Sipilä, M., Spracklen, D. V., Stozhkov, Y., Stratmann, F., Tomé, A., Tsagkogeorgas, G., Vaattovaara, P., Viisanen, Y., Vrtala, A., Wagner, P. E., Weingartner, E., Wex, H., Wimmer, D., Carslaw, K. S., Curtius, J., Donahue, N. M., Kirkby, J., Kulmala, M., Worsnop, D. R., and Baltensperger, U.: Oxidation Products of Biogenic Emissions Contribute to Nucleation of Atmospheric Particles, Science, 344, 717–721, https://doi.org/10.1126/science.1243527, 2014.

Riipinen, I., Pierce, J. R., Yli-Juuti, T., Nieminen, T., Häkkinen, S., Ehn, M., Junninen, H., Lehtipalo, K., Petäjä, T., Slowik, J., Chang, R., Shantz, N. C., Abbatt, J., Leaitch, W. R., Kerminen, V.-M., Worsnop, D. R., Pandis, S. N., Donahue, N. M., and Kulmala, M.: Organic condensation: a vital link connecting aerosol formation to cloud condensation nuclei (CCN) concentrations, Atmos. Chem. Phys., 11, 3865–3878, https://doi.org/10.5194/acp-11-3865-2011, 2011.

Riipinen, I., Yli-Juuti, T., Pierce, J. R., Petaja, T., Worsnop, D. R., Kulmala, M., and Donahue, N. M.: The contribution of organics to atmospheric nanoparticle growth, Nat. Geosci., 5, 553–458, https://doi.org/10.1038/ngeo1499, 2012.

Scott, C. E., Monks, S. A., Spracklen, D. V., Arnold, S. R., Forster, P. M., Rap, A., Carslaw, K. S., Chipperfield, M. P., Reddington, C. L. S., and Wilson, C.: Impact on short-lived climate forcers (SLCFs) from a realistic land-use change scenario via changes in biogenic emissions, Faraday Discuss., 200, 101–120, https://doi.org/10.1039/c7fd00028f, 2017.

Scott, C. E., Monks, S. A., Spracklen, D. V., Arnold, S. R., Forster, P. M., Rap, A., Äijälä, M., Artaxo, P., Carslaw, K. S., Chipperfield, M. P., Ehn, M., Gilardoni, S., Heikkinen, L., Kulmala, M., Petäjä, T., Reddington, C. L. S., Rizzo, L. V., Swietlicki, E., Vignati, E., and Wilson, C.: Impact on short-lived climate forcers increases projected warming due to deforestation, Nat. Commun., 9, 157, https://doi.org/10.1038/s41467-017-02412-4, 2018.

Shrivastava, M., Easter, R. C., Liu, X., Zelenyuk, A., Singh, B., Zhang, K., Ma, P. L., Chand, D., Ghan, S., Jimenez, J. L., Zhang, Q., Fast, J., Rasch, P. J., and Tiitta, P.: Global transformation and fate of SOA: Implications of low-volatility SOA and gas-phase fragmentation reactions, J. Geophys. Res.-Atmos., 120, 4169–4195, https://doi.org/10.1002/2014JD022563, 2015.

Shrivastava, M., Cappa, C. D., Fan, J., Goldstein, A. H., Guenther, A. B., Jimenez, J. L., Kuang, C., Laskin, A., Martin, S. T., Ng, N. L., Petaja, T., Pierce, J. R., Rasch, P. J., Roldin, P., Seinfeld, J. H., Shilling, J., Smith, J. N., Thornton, J. A., Volkamer, R., Wang, J., Worsnop, D. R., Zaveri, R. A., Zelenyuk, A., and Zhang, Q.: Recent advances in understanding secondary organic aerosol: Implications for global climate forcing, Rev. Geophys., 55, 509–559, https://doi.org/10.1002/2016RG000540, 2017.

Sindelarova, K., Granier, C., Bouarar, I., Guenther, A., Tilmes, S., Stavrakou, T., Müller, J.-F., Kuhn, U., Stefani, P., and Knorr, W.: Global data set of biogenic VOC emissions calculated by the MEGAN model over the last 30 years, Atmos. Chem. Phys., 14, 9317–9341, https://doi.org/10.5194/acp-14-9317-2014, 2014.

Sporre, M. K.: Data for: Large difference in aerosol radiative effects from BVOC-SOA treatment in three ESMs, Data set, Norstore, https://doi.org/10.11582/2020.00032, last access: 22 July 2020.

Sporre, M. K., Blichner, S. M., Karset, I. H. H., Makkonen, R., and Berntsen, T. K.: BVOC–aerosol–climate feedbacks investigated using NorESM, Atmos. Chem. Phys., 19, 4763–4782, https://doi.org/10.5194/acp-19-4763-2019, 2019.

Spracklen, D. V. and Rap, A.: Natural aerosol–climate feedbacks suppressed by anthropogenic aerosol, Geophys. Res. Lett., 40, 5316–5319, https://doi.org/10.1002/2013GL057966, 2013.

Spracklen, D. V., Carslaw, K. S., Kulmala, M., Kerminen, V.-M., Mann, G. W., and Sihto, S.-L.: The contribution of boundary layer nucleation events to total particle concentrations on regional and global scales, Atmos. Chem. Phys., 6, 5631–5648, https://doi.org/10.5194/acp-6-5631-2006, 2006.

Spracklen, D. V., Jimenez, J. L., Carslaw, K. S., Worsnop, D. R., Evans, M. J., Mann, G. W., Zhang, Q., Canagaratna, M. R.,

Allan, J., Coe, H., McFiggans, G., Rap, A., and Forster, P.: Aerosol mass spectrometer constraint on the global secondary organic aerosol budget, Atmos. Chem. Phys., 11, 12109–12136, https://doi.org/10.5194/acp-11-12109-2011, 2011.

Stier, P., Feichter, J., Kinne, S., Kloster, S., Vignati, E., Wilson, J., Ganzeveld, L., Tegen, I., Werner, M., Balkanski, Y., Schulz, M., Boucher, O., Minikin, A., and Petzold, A.: The aerosol-climate model ECHAM5-HAM, Atmos. Chem. Phys., 5, 1125–1156, https://doi.org/10.5194/acp-5-1125-2005, 2005.

Tröstl, J., Chuang, W. K., Gordon, H., Heinritzi, M., Yan, C., Molteni, U., Ahlm, L., Frege, C., Bianchi, F., Wagner, R., Simon, M., Lehtipalo, K., Williamson, C., Craven, J. S., Duplissy, J., Adamov, A., Almeida, J., Bernhammer, A.-K., Breitenlechner, M., Brilke, S., Dias, A., Ehrhart, S., Flagan, R. C., Franchin, A., Fuchs, C., Guida, R., Gysel, M., Hansel, A., Hoyle, C. R., Jokinen, T., Junninen, H., Kangasluoma, J., Keskinen, H., Kim, J., Krapf, M., Kürten, A., Laaksonen, A., Lawler, M., Leiminger, M., Mathot, S., Möhler, O., Nieminen, T., Onnela, A., Petäjä, T., Piel, F. M., Miettinen, P., Rissanen, M. P., Rondo, L., Sarnela, N., Schobesberger, S., Sengupta, K., Sipilä, M., Smith, J. N., Steiner, G., Tomè, A., Virtanen, A., Wagner, A. C., Weingartner, E., Wimmer, D., Winkler, P. M., Ye, P., Carslaw, K. S., Curtius, J., Dommen, J., Kirkby, J., Kulmala, M., Riipinen, I., Worsnop, D. R., Donahue, N. M., and Baltensperger, U.: The role of low-volatility organic compounds in initial particle growth in the atmosphere, Nature, 533, 527–531, https://doi.org/10.1038/nature18271, 2016.

Tsigaridis, K. and Kanakidou, M.: The Present and Future of Secondary Organic Aerosol Direct Forcing on Climate, Current Climate Change Reports, 4, 1–15, https://doi.org/10.1007/s40641-018-0092-3, 2018.

Tsigaridis, K., Daskalakis, N., Kanakidou, M., Adams, P. J., Artaxo, P., Bahadur, R., Balkanski, Y., Bauer, S. E., Bellouin, N., Benedetti, A., Bergman, T., Berntsen, T. K., Beukes, J. P., Bian, H., Carslaw, K. S., Chin, M., Curci, G., Diehl, T., Easter, R. C., Ghan, S. J., Gong, S. L., Hodzic, A., Hoyle, C. R., Iversen, T., Jathar, S., Jimenez, J. L., Kaiser, J. W., Kirkevåg, A., Koch, D., Kokkola, H., Lee, Y. H., Lin, G., Liu, X., Luo, G., Ma, X., Mann, G. W., Mihalopoulos, N., Morcrette, J.-J., Müller, J.-F., Myhre, G., Myriokefalitakis, S., Ng, N. L., O'Donnell, D., Penner, J. E., Pozzoli, L., Pringle, K. J., Russell, L. M., Schulz, M., Sciare, J., Seland, Ø., Shindell, D. T., Sillman, S., Skeie, R. B., Spracklen, D., Stavrakou, T., Steenrod, S. D., Takemura, T., Tiitta, P., Tilmes, S., Tost, H., van Noije, T., van Zyl, P. G., von Salzen, K., Yu, F., Wang, Z., Wang, Z., Zaveri, R. A., Zhang, H., Zhang, K., Zhang, Q., and Zhang, X.: The AeroCom evaluation and intercomparison of organic aerosol in global models, Atmos. Chem. Phys., 14, 10845–10895, https://doi.org/10.5194/acp-14-10845-2014, 2014.

Twomey, S.: Pollution and the Planetary Albedo, Atmos. Environ., 8, 1251–1256, 1974.

Unger, N.: On the role of plant volatiles in anthropogenic global climate change, Geophys. Res. Lett., 41, 8563–8569, https://doi.org/10.1002/2014GL061616, 2014.

van Noije, T. P. C., Le Sager, P., Segers, A. J., van Velthoven, P. F. J., Krol, M. C., Hazeleger, W., Williams, A. G., and Chambers, S. D.: Simulation of tropospheric chemistry and aerosols with the climate model EC-Earth, Geosci. Model Dev., 7, 2435–2475, https://doi.org/10.5194/gmd-7-2435-2014, 2014.

Vehkamäki, H., Kulmala, M., Napari, I., Lehtinen, K. E. J., Timmreck, C., Noppel, M., and Laaksonen, A.: An improved parameterization for sulfuric acid–water nucleation rates for tropospheric and stratospheric conditions, J. Geophys. Res., 107, 4622, https://doi.org/10.1029/2002JD002184, 2002.

Vignati, E., Wilson, J., and Stier, P.: M7: An efficient size-resolved aerosol microphysics module for large-scale aerosol transport models, J. Geophys. Res-Atmos., 109, D22202, https://doi.org/10.1029/2003JD004485, 2004.

Williams, J. E., Strunk, A., Huijnen, V., and van Weele, M.: The application of the Modified Band Approach for the calculation of on-line photodissociation rate constants in TM5: implications for oxidative capacity, Geosci. Model Dev., 5, 15–35, https://doi.org/10.5194/gmd-5-15-2012, 2012.

Williams, J. E., Boersma, K. F., Le Sager, P., and Verstraeten, W. W.: The high-resolution version of TM5-MP for optimized satellite retrievals: description and validation, Geosci. Model Dev., 10, 721–750, https://doi.org/10.5194/gmd-10-721-2017, 2017.

Yu, F.: A secondary organic aerosol formation model considering successive oxidation aging and kinetic condensation of organic compounds: global scale implications, Atmos. Chem. Phys., 11, 1083–1099, https://doi.org/10.5194/acp-11-1083-2011, 2011.

Zhang, G. J. and McFarlane, N. A.: Sensitivity of climate simulations to the parameterization of cumulus convection in the Canadian climate centre general circulation model, Atmos.-Ocean, 33, 407–446, https://doi.org/10.1080/07055900.1995.9649539, 1995.

Zhang, K., O'Donnell, D., Kazil, J., Stier, P., Kinne, S., Lohmann, U., Ferrachat, S., Croft, B., Quaas, J., Wan, H., Rast, S., and Feichter, J.: The global aerosol-climate model ECHAM-HAM, version 2: sensitivity to improvements in process representations, Atmos. Chem. Phys., 12, 8911–8949, https://doi.org/10.5194/acp-12-8911-2012, 2012.

Zhang, Q., Jimenez, J. L., Canagaratna, M. R., Allan, J. D., Coe, H., Ulbrich, I., Alfarra, M. R., Takami, A., Middlebrook, A. M., Sun, Y. L., Dzepina, K., Dunlea, E., Docherty, K., DeCarlo, P. F., Salcedo, D., Onasch, T., Jayne, J. T., Miyoshi, T., Shimono, A., Hatakeyama, S., Takegawa, N., Kondo, Y., Schneider, J., Drewnick, F., Borrmann, S., Weimer, S., Demerjian, K., Williams, P., Bower, K., Bahreini, R., Cottrell, L., Griffin, R. J., Rautiainen, J., Sun, J. Y., Zhang, Y. M., and Worsnop, D. R.: Ubiquity and dominance of oxygenated species in organic aerosols in anthropogenically-influenced Northern Hemisphere midlatitudes, Geophys. Res. Lett., 34, L13801, https://doi.org/10.1029/2007GL029979, 2007.

Zhang, R., Khalizov, A., Wang, L., Hu, M., and Xu, W.: Nucleation and Growth of Nanoparticles in the Atmosphere, Chem. Rev., 112, 1957–2011, https://doi.org/10.1021/cr2001756, 2012.

Paper III

Implementing a sectional scheme for early aerosol growth from new particle formation in the Norwegian Earth System Model v2: comparison to observations and climate impacts

Sara M. Blichner, Moa K. Sporre, Risto Makkonen, and Terje K. Berntsen

Geoscientific Model Development Discussions, 2020

doi:10.5194/gmd-2020-357

III

https://doi.org/10.5194/gmd-2020-357
Preprint. Discussion started: 12 November 2020

Geoscientific Model Development Discussions
Open Access
EGU

Implementing a sectional scheme for early aerosol growth from new particle formation in the Norwegian Earth System Model v2: comparison to observations and climate impacts

Sara M. Blichner[1], Moa K. Sporre[2], Risto Makkonen[3,4], and Terje K. Berntsen[1]

[1]Department of Geosciences, University of Oslo, Oslo, Norway
[2]Department of Physics, Lund University, Lund, Sweden
[3]Institute for Atmospheric and Earth System Research / Physics, Faculty of Science, University of Helsinki, Finland
[4]Climate System Research, Finnish Meteorological Institute, Helsinki, Finland

Correspondence: Sara Marie Blichner (s.m.blichner@geo.uio.no)

Abstract. Aerosol-cloud interactions contribute with a large portion of the spread in estimates of climate forcing, climate sensitivity and future projections. An important part of this uncertainty is how much new particle formation (NPF) contributes to cloud condensation nuclei (CCN), and furthermore, how this changes with changes in anthropogenic emissions. Incorporating NPF and early growth in Earth System Models (ESMs) is, however, challenging both due to uncertain parameters (e.g. participating vapours), structural challenges (numerical description of growth from $\sim$1 to $\sim$100 nm), and due to large scale of ESM grid compared to NPF scale.A common approach in ESMs is to represent the particle size distribution by a certain number of log-normal modes. Sectional schemes on the other hand, where the size distribution is represented by bins, are considered closer to first principles because they do not make an a priori assumption about the size distribution.

In order to improve the representation of early growth, we have implemented a sectional scheme for the smallest particles (5–39.6 nm diameter) in the Norwegian Earth System Model (NorESM), feeding particles into the original aerosol scheme. This is, to our knowledge, the first time such an approach has been tried. We find that including the sectional scheme for early growth improves the aerosol number concentration in the model when comparing against observations, particularly in the 50–100 nm diameter range. Furthermore, we find that the model with the sectional scheme produces much less particles than the original scheme in polluted regions, while it produces more in remote regions and the free troposphere, indicating a potential impact on the estimated aerosol forcing. Finally, we analyse the effect on cloud-aerosol interactions and find that the effect of changes in NPF efficiency on clouds is highly heterogeneous in space. While in remote regions, more efficient NPF leads to higher cloud droplet number concentration (CDNC), in polluted regions the opposite is in fact the case.

1 Introduction

The formation of new particles in the atmosphere, known as new particle formation (NPF) occurs through the clustering and nucleation of low volatile vapours. These particles can then influence the climate by growing via condensation to sizes where they act as cloud condensation nuclei (CCN) (Twomey, 1974; Albrecht, 1989) – or even by interacting directly with radiation if they grow large enough (Boucher et al., 2013). NPF has received increasing attention in recent years due to the aforementioned

https://doi.org/10.5194/gmd-2020-357
Preprint. Discussion started: 12 November 2020


Geoscientific Model Development Discussions
Open Access
EGU

climate impacts as well as its implications on human health. This has lead to new insights into the mechanisms involved in NPF and subsequently, new parameterization schemes have been developed and included in Earth System Models (ESMs). For example, Gordon et al. (2016) showed that including a NPF pathways from pure organic nucleation nucleation (Kirkby et al., 2016; Riccobono et al., 2014; Gordon et al., 2017, 2016; Dunne et al., 2016; Tröstl et al., 2016) in a global aerosol model, resulted in a considerable diminishing of the estimated negative forcing due to aerosol–cloud interactions since pre-industrial times (+0.22 $\mathrm{W/m^2}$, 27 %). This result illustrates the importance of adequately representing the effects of NPF in ESMs for our understanding of historical forcing and thus climate sensitivity, especially considering that cloud–aerosol interactions are estimated to be responsible for a large fraction of the observed negative radiative forcing since pre-industrial times (Boucher et al., 2013).

In spite of NPF being subject to a lot of research over the recent years, there is still uncertainty about the species involved in both nucleation, and the subsequent particle growth (Kerminen et al., 2018; Lee et al., 2019). In order for successful NPF, particles must form and grow up to a decent size, often defined to be out of the nucleation mode, i.e., 10 nm. Due to the Kelvin effect, only atmospheric gases with very low volatility are able to contribute to the inital steps on NPF, and in many atmospheric conditions the growth rates provided are too slow for for particles to survive losses to coagulation and evaporation (Semeniuk and Dastoor, 2018). Sulphuric acid is known to be the most important species for nucleation due to its low vapor pressure, while bases such as amines and ammonia may enhance the nucleation rate (Lee et al., 2019; Kerminen et al., 2018). There is evidence that extremely low volatile organic vapors also contribute significantly, especially in remote areas (Semeniuk and Dastoor, 2018; Dunne et al., 2016; Riccobono et al., 2014). For the subsequent growth of the particles, the Kelvin effect decreases and condensing organics of higher volatility, predominantly originating from the oxidation of biogenic volatile organic compounds (BVOCs), become more and more dominant and are essential in most environments (Riipinen et al., 2011; Tröstl et al., 2016).

During all the stages of particle growth, the particles are subject to coagulation, reducing the number of particles that form and that grow to sizes where they can act as CCN (~ 50 nm in diameter (Kerminen et al., 2012)). The majority of this coagulation will occur with particles that are already in the CCN size range, and thus results in a net loss of particles that could eventually act as CCN. However, when two small particles (below the CCN size range) coagulate, this contributes to growth of the combined particle which could then become a CCN (e.g. Kerminen et al. (2018); Lee et al. (2013); Schutgens and Stier (2014)). This effect though, is only significant in highly polluted regions. The survival rate of NPF-particles to CCN sizes is therefore in general depend on a competition between the particle growth rate by condensation and the coagulation sink.

The formation of new particles is tightly constrained by negative feedbacks. If NPF is high, the result will be an increase in particle number and with it, an increase the available surface area for condensation. This will lead to an increase in both condensation– and coagulation sink, which further decreases the growth rate and increases the coagulation sink of new particles forming. The result is then a supression of further NPF (Westervelt et al., 2014, 2013; Semeniuk and Dastoor, 2018; Carslaw et al., 2013; Kerminen et al., 2018; Schutgens and Stier, 2014, etc). These loss processes which constrain the survival of new particles to larger sizes may in fact often be more important than nucleation rate in itself. For example, Carslaw et al. (2013), show that Global Model of Aerosol Processes (GLOMAP) has low sensitivity of number of particle larger than 50 nm to nucleation rate parameterizations, but a high sensitivity to processes affecting the coagulation loss of newly formed particles.

https://doi.org/10.5194/gmd-2020-357
Preprint. Discussion started: 12 November 2020


Geoscientific Model Development Discussions
Open Access
EGU

This underlines the importance of adequately representing the processes that constrain the formation of new particles. If not we could end up with models where both aerosol number concentration and CCN are over-sensitive to changes in emissions.

While there is a large body of work on describing when NPF happens in many individual environments, the transferal of this to a generalized context (which is what is needed for a climate model), is very uncertain. In other words, based on knowledge of what drives NPF in a specific environment it is not easy to derive a general parameterization (Kerminen et al., 2018; Lee et al., 2019).

In the perspective of an ESM, aerosols only become relevant when they approach ~ 50 nm in diameter and start to become relevant as CCN (Kerminen et al., 2012). However, because the formation of particles in this size range is highly dependent on aerosol dynamics at smaller sizes, climate models need to treat these dynamics with a sufficient degree of accuracy. Since climate models are required to run hundreds of years of simulations within a reasonable time span, this involves a trade-off between representing the physical process to the best of our scientific understanding on one hand, and computational cost on the other hand.

In ESMs, it is common to use modal schemes to represent the particle size distribution – i.e. describing the distribution as the sum of some number of log-normal modes (Stier et al., 2005; Liu et al., 2005; Mann et al., 2010; Vignati et al., 2004, etc.). On the other hand, sectional schemes – where the size distribution is represented by bins (Spracklen et al., 2005; Kokkola et al., 2008, etc.) – are in general considered closer to first principles because they do not make an a priori assumption about the size distribution. Nevertheless, modal schemes are generally favored in ESMs because they require fewer tracers and are much cheaper computationally.

Any size resolving aerosol scheme must have a cut-off diameter where explicit modelling of aerosol number, growth and losses begin. One natural choice is the size of the critical cluster, around 1 nm (Lee et al., 2013). While this means that the entire size distribution of particles is treated, it adds disproportionate computational cost to the simulation for aerosols with a very short atmospheric lifetime (both due to growth out of the size range and high sensitivity to coagulation) (see e.g. Lee et al. (2013)). An alternative is to parameterize the growth and coagulation loss of particles up to a larger diameter, which is the approach used in most ESMs (Kerminen and Kulmala, 2002; Kerminen et al., 2004; Lehtinen et al., 2007; Anttila et al., 2010). These methods involve estimating the flux or the formation of particles at the cut-off diameter, be it modal or sectional, based on estimated growth rate and coagulation sink (see details in methods).

There are several drawbacks of this approach, especially if the chosen cut-off diameter is high. The most important one is that it assumes steady state, i.e. the same constant growth rates from the particle is formed up to the cut-off value, which in reality could take several time steps and long enough for conditions to change substantially (hours). A particle may form under conditions with a high growth rate, but in the time it would take for the particle to grow to the cut-off diameter, the growth rate might decrease due to an increased condensation sink by the many new particles being formed. In a model with a relatively high cut-off, this would lead to an overestimation of the growth rate of the nucleated particle, which would in turn lead to an overestimation of the formation rate at the cut-off (Olenius and Riipinen, 2017; Lee et al., 2013). Olenius and Riipinen (2017) test the effect of the cut-off diameter by explicitly modelling the formation of particles from vapour molecule to 10 nm diameter and find an over-prediction of a factor of two to orders of magnitude. Similarly, Lee et al. (2013) suggest that during

https://doi.org/10.5194/gmd-2020-357
Preprint. Discussion started: 12 November 2020


Geoscientific Model Development Discussions
Open Access
EGU

nucleation events, the smallest particles (<10 nm) can be a significant condensation sink, thus regulating the nucleation via reduced concentrations of precursors. They investigate the effects of cut-off diameter with a sectional aerosol scheme in the GISS-TOMAS model, and compare 1 nm cut-off with 3 nm and 10 nm cut-offs using Kerminen et al. (2004) to parameterize the survival of nucleated particles to the cut-off. They find that the using a 10 nm cut-off leads to an overestimation of CCN at 0.2 % supersaturation, with 10–20 % overestimation in the surface layer in most of the northern hemisphere, while the globally averaged change to CCN(0.2%) is minor. Furthermore, a 10 nm cut-off produces a high bias in the concentration of particles larger than 10 nm (N_{10}) of up to a factor of 3–5 in regions with high nucleation. In addition, they find that the 10 nm cut-off is sensitive to the time step.

Another drawback of a high cut-off diameter is that most of these parameterizations neglect self coagulation within the sub-cut-off size range, which can be an important growth mechanism during intense new particle formation events. This concern is, however, taken into account in the Anttila et al. (2010) parameterization.

Finally, if the cut-off diameter is high, the time and location where the new particles are inserted into the aerosol model may be effected since the parameterized growth would add the particles, at the cut-off size, in the same time step as they would be formed, i.e. within ~ 0.5 hour. In reality, this growth could take several hours to days, depending on location, at which point the airmass may have moved considerably. This is in particular the case of a high cut-off value, like in NorESM (23.6 nm) (Kirkevåg et al., 2018).

In order to improve the representation of early particle growth, we have implemented a sectional scheme for the smallest particles (5–39.6 nm diameter) in the aerosol scheme in the Norwegian Earth System Model (NorESM). The sectional scheme acts as an intermediate step during NPF and feeds the grown particles into the original modal scheme. This is, to our knowledge, the first time such a hybrid approach has been attempted. The sectional scheme currently involves two condensing species (sulphuric acid and low volatility organics) and 5 bins. The aerosol scheme with these changes will be referred to as OsloAeroSec. A schematic of the changes from the OsloAero (the original model) to OsloAeroSec is shown in Fig. 1. The motivation is

1. In the original modal scheme in NorESM, the smallest mode has an initial mean radius of 23.6 nm. Particles from new particle formation are inserted into this mode using the parameterization from Lehtinen et al. (2007). It thus does not take into account dynamics within the sub-23.6 nm range (e.g. competition for condensing vapours and growth of particles over more than one time step).

2. Including a sectional scheme for this size range brings the modelling of early growth closer to first principals while keeping an acceptable computational cost because the number of species involved is low. A sectional scheme within this range represents a good alternative to a nucleation mode which is known to have problems with transferring particles to the larger mode, due to the addition of new particles reducing the median radius of the mode.

In the following we start by describing the aerosol scheme in NorESM (section 2.1) and then the newly implemented sectional scheme for early growth (section 2.2). Next, in section 4.1, we show that the new scheme gives improvements in the

https://doi.org/10.5194/gmd-2020-357
Preprint. Discussion started: 12 November 2020


Geoscientific Model Development Discussions
Open Access
EGU

CCN relevant particle number concentration and sizedistribution when compared to observational data from Asmi et al. (2011) consisting of 24 stations in Europe and compiled as part of the EUSAAR project. Finally, we present the global changes in the state of aerosols and following cloud properties in the model with the new scheme (OsloAeroSec) compared to the original model (section 4.2).

2 Model description

We start by briefly describing the Norwegian Earth System Model (NorESM) in general before giving a detailed description of its aerosol model, OsloAero, in section 2.1. After this in section 2.2, we will describe what changes to said aerosol scheme that have been introduced in OsloAeroSec. In general, the aerosol scheme after NPF and early growth is left as it is. The only exception to this is that we have also included some changes to the diurnal variability of OH, described in section 2.3.

The Norwegian Earth System Model version 2 (NorESM2) (Seland et al., 2020b; Bentsen et al., 2013; Kirkevåg et al., 2013; Iversen et al., 2013) is largely based on the Community Earth System Model (CESM) version 2 (Danabasoglu et al., 2020; Neale et al., 2012). The aerosol scheme in CESM2 is replaced by OsloAero6 (described below) (Kirkevåg et al., 2018) and the atmospheric component is thus named CAM-Nor6. Furthermore, the ocean model in CESM2 is replaced by Bergen Layered Ocean Model (BLOM) (Seland et al., 2020b), though this is not used in this study as all simulations are run with prescribed sea surface temperature (SST) and sea ice concentrations. The land model is, as in CESM2, is the Community Land Model (CLM) version 5 (Lawrence et al., 2019).

2.1 OsloAero: Aerosol scheme in NorESM

The aerosol scheme in NorESM, OsloAero, is a production tagged aerosol model. The most notable difference to other aerosol models is that the aerosol mass is divided into "background" tracers and "process" tracers. The background tracers form log-normal modes which decide the number concentration, while the process tracers alter this initial log normal distribution and their chemical composition. Examples of background tracers are dust, sea salt or particles from NPF, while examples of process tracers are sulphate condensate, sulphate coagulate and organic condensate. After the process tracers are applied, the resulting distribution of the "mixtures" are not (necessarily) log normal anymore. The mass of the tracers is tracked, and the size distributions for cloud activation and optical properties are calculated using a look-up table approach (Kirkevåg et al., 2018).

2.1.1 Chemistry:

CAM-Nor6 has a simplified chemistry scheme for sulfur and organic species, using the chemical pre-processor MOZART (Emmons et al., 2010). Pre-calculated monthly mean oxidant fields consisting of OH, O_3, NO_3 and HO_2 are read from file (for discussion see Karset et al. (2018)).

Condensing tracers in the model are H_2SO_4 and two tracers of organics produced by the oxidation of BVOCs, low volatility organics ($SOAG_{LV}$) and semi-volatile organics ($SOAG_{SV}$). The model treats both organic tracers as non-volatile during con-

https://doi.org/10.5194/gmd-2020-357
Preprint. Discussion started: 12 November 2020


Geoscientific Model Development Discussions
Open Access
EGU

densation, but represents the volatility by separating which processes each tracer can contribute to: $SOAG_{LV}$ can contribute in new particle formation (NPF) and early growth, while $SOAG_{SV}$ only contributes to condensational growth.

H_2SO_4 is emitted directly or produced from oxidation of SO_2 by OH or aqueous-phase oxidation by H_2O_2 and O_3 (Tie et al., 2001). SO_2 is either emitted directly or produced by oxidation of DMS. The condensing organic tracers, $SOAG_{LV}$ and $SOAG_{SV}$, are formed from oxidation isoprene and monoterpenes. The emissions of isoprene and monoterpene are calculated online in each time step using the Model of Emissions of Gases and Aerosols from Nature version 2.1 (MEGAN2.1) (Guenther et al., 2012) which is incorporated into CLM5. The atmospheric tracer includes only one tracer for monoterpenes, and thus the emissions of 21 monoterpene species from MEGAN2.1 are lumped together (Kirkevåg et al., 2018). In addition, production of methansulfonic acid (MSA) by oxidation of DMS is taken into account, but since the model lacks a tracer for MSA, 20% of the MSA is put in the $SOAG_{LV}$ tracer and 80% in the $SOAG_{SV}$.

For complete overview of reactions and reaction rates, see Table 2 in Karset et al. (2018).

2.1.2 Condensation:

Following is a description of the condensation routine in chronological order within one time step. The production rate, P_{gas}, of a condensing gas is calculated in the gas phase chemistry (section 2.1.1 and the condensation sink, L_{cond} $[1/\text{s}]$, is calculated based on the surface area of the background aerosols. Finally, using the initial concentration of the gas, C_{old}, from the previous time step, an intermediate concentration, C_{int}, is derived by solving the discrete Euler backwards equation,

$$\frac{C_{\text{int}} - C_{\text{old}}}{\Delta t} = P_{\text{gas}} - L_{\text{cond}} C_{\text{int}} \tag{1}$$

$$C_{\text{int}} = \frac{C_{\text{old}} + P_{\text{gas}} \Delta t}{1 + L_{\text{cond}} \Delta t}. \tag{2}$$

This intermediate concentration is then used in the formation of new particles (described in the next section). The NPF subroutine returns an intermediate nucleated mass loss rate, $J_{m,\text{nuc}}$. This nucleated mass is then used to calculate a nucleation loss rate, L_{nuc} $[1/\text{s}]$:

$$L_{\text{nuc}} = \frac{J_{m,\text{nuc}}}{C_{\text{int}}} \tag{3}$$

The new gas concentration, C_{new}, is calculated by solving the discrete Euler backwards equation again, including the loss rate to nucleation:

$$C_{\text{new}} = \frac{C_{\text{old}} + P_{\text{gas}} \Delta t}{1 + L_{\text{cond}} \Delta t + L_{\text{nuc}} \Delta t} \tag{4}$$

Finally, the total gas lost to condensation and nucleation, ΔC, is calculated by

$$C_{\text{new}} - C_{\text{old}} = P_{\text{gas}} \Delta t - \Delta C \tag{5}$$

$$\Delta C = P_{\text{gas}} \Delta t + C_{\text{old}} - C_{\text{new}} \tag{6}$$

This condensate/nucleate, ΔC, is then transferred to the corresponding process tracer for condensate of the species (e.g. sulphur condensate) and the background tracer for new particle formation particles. The mass transfer is done based on their

https://doi.org/10.5194/gmd-2020-357
Preprint. Discussion started: 12 November 2020


Geoscientific Model Development Discussions
Open Access
EGU

relative contribution to the total loss rate – i.e. the fraction that is moved to the NPF tracer is $f_{\text{nuc}} = L_{\text{nuc}}/(L_{\text{nuc}} + L_{\text{cond}})$ and the fraction to condensation is $f_{\text{cond}} = 1 - f_{\text{nuc}}$.

2.1.3 New particle formation:

The tracers contributing to NPF are H_2SO_4 and organics (see Makkonen et al. (2014)). As mentioned above, $SOAG_{SV}$ does not contribute to new particles formation. In addition, only half of the $SOAG_{LV}$ concentration in each time step is assumed to be low volatility enough to contribute, and this fraction will be denoted as ELVOC in the following. The nucleation rate is parameterized with Vehkamäki et al. (2002) for binary sulfuric acid-water nucleation in the entire atmosphere and in addition, equation 18 from Paasonen et al. (2010) is added to represent boundary layer nucleation. The Paasonen et al. (2010, eq.18) parameterization is as follows:

$$J_{\text{nuc}} = A_1[\text{H}_2\text{SO}_4] + A_2[\text{ELVOC }] \tag{7}$$

where J_{nuc} [1/s] is the nucleation rate and $A_1 = 6.1 \times 10^{-7}$ s^{-1} and $A_2 = 3.9 \times 10^{-8}$ s^{-1}.

The survival of particles from nucleation at $d_{\text{nuc}} \approx 2$ nm, to the background mode holding the NPF particles, number median diameter 23.6 nm, is parameterized by Lehtinen et al. (2007). The formation rate, $J_{d_{\text{mode}}}$ of particles at the smallest mode is calculated by

$$J_{d_{\text{mode}}} = J_{\text{nuc}} \exp\Big(-\gamma d_{\text{nuc}} \frac{CoagS(d_{\text{nuc}})}{GR}\Big) \tag{8}$$

where, d_{nuc} is the diameter of the nucleated particle, $CoagS(d_{\text{nuc}})$ is the coagulation sink of the particles [h^{-1}], GR is the growth rate [nm/h] of the particle (from H_2SO_4 and ELVOC, calculated using eq. 21 from Kerminen and Kulmala (2002)) and γ is a function of d_{mode} and d_{nuc}:

$$\gamma = \frac{1}{m+1}\Big[\Big(\frac{d_{\text{mode}}}{d_{\text{nuc}}}\Big)^{(m+1)} - 1\Big],\ m = -1.6. \tag{9}$$

Furthermore, $CoagS(d_{\text{nuc}})$ is calculated from $CoagS(d_{\text{mode}})$ assuming a power-law dependency on diameter, $CoagS(d_{\text{nuc}}) = CoagS(d_{\text{mode}}) \cdot \left(\frac{d_{\text{nuc}}}{d_{\text{mode}}}\right)^m$ (Lehtinen et al., 2007, eq. 5).

Since Kirkevåg et al. (2018), we have developed an improvement to the new particle formation rate (also used in Sporre et al. (2019, 2020)). The $CoagS(d_{\text{nuc}})$ previously included only coagulation onto accumulation and coarse mode particles, but we amended this to include coagulation onto all pre-existing particles. This modification gives a lower and more realistic survival rate of particles from formation at 2 to 23.6 nm.

2.1.4 Coagulation:

OsloAero takes into account coagulation between Aitken mode particles and accumulation- and coarse mode particles, with coagulation coefficients from the Fuchs form for Brownian diffusion (section 12.3 in Seinfeld and Pandis (1998)). Technically, a normalized coagulation sink is calculated for each relevant combination of background modes, assuming some fixed prior

https://doi.org/10.5194/gmd-2020-357
Preprint. Discussion started: 12 November 2020


Geoscientific Model Development Discussions
Open Access
EGU

condensation/coagulation growth. To compute the normalized coagulation sink, the size distribution is split into 44 bins for the coagulation receiver mode (the larger particle) and a coagulation sink with each bin is calculated and normalized by the number concentration. This way, the normalized coagulation sink only has to be computed once. In addition, coagulation of aerosols with cloud droplets is estimated. See Seland et al. (2008) for more detail.

2.2 OsloAeroSec: New sectional scheme

The purpose of introducing the sectional scheme is to get a more realistic growth and loss dynamic within the smallest aerosol sizes, with the aim of better modelling aerosol–climate effects. These smallest particles have insignificant effects on climate directly, but rather play a role through how they affect the size distribution of the larger particles. For this reason, we do not let the aerosols in the sectional scheme directly affect the radiation and cloud parameterizations, but rather consider only how new particle formation through nucleation, condensation and coagulation affect the larger aerosols in the modal scheme.

The sectional scheme currently consists of five bins (though this is flexible) and the bin sizes are set according to a discrete geometric distribution – the volume-ratio distribution (Jacobson, 2005, sec.13.3) – as follows: Let $d_1, d_2, \ldots, d_5$ be the diameter for each bin and $v_1, v_2, \ldots, v_5$ be the volume per particle for each bin. Each particle in the bin is assumed to have this same volume (Jacobson, 2005). The volume-ratio distribution ensures that the volume per particle ratio between adjacent bins is fixed, i.e.,

$$r_v = \frac{v_{i+1}}{v_i} \tag{10}$$

is fixed. This gives that the ratio between the diameter in adjacent bins, r_d will be:

$$r_d = \frac{d_{i+1}}{d_i} = (r_v)^{1/3}. \tag{11}$$

Particles are moved into the original aerosol scheme in the NPF background mode when they reach $d_{\text{max}} = 39.6$ nm which is the volume median diameter of this mode. The volume median diameter is chosen to preserve both number and mass of the particles. Note that d_{max} is the diameter where the particles are moved to the modal scheme. The choice of d_{min}, the smallest diameter bin, is flexible, and we have chosen 5 nm here. So for number of bins, N,

$$r_d = \left(\frac{d_{\text{max}}}{d_{\text{min}}}\right)^{\frac{1}{N}}, \tag{12}$$

where $d_{\text{max}} = 39.6$ nm, $d_{\text{min}} = 5$ nm and $N = 5$.

The sectional scheme includes condensation from two precursors, H_2SO_4 and $SOAG_{LV}$, while $SOAG_{SV}$ is considered not low volatile enough. This gives a total of N (number of bins) $\times 2$ tracers for the model to keep track of, keeping computational costs reasonable.

2.2.1 Nucleation:

Nucleation is still parameterized with Vehkamäki et al. (2002) for binary sulfuric acid-water nucleation in the entire atmosphere, the boundary layer nucleation has been updated from (Paasonen et al., 2010, eq.18)(see eq. 7) to Riccobono et al.

https://doi.org/10.5194/gmd-2020-357
Preprint. Discussion started: 12 November 2020


Geoscientific Model Development Discussions
Open Access
EGU

(2014):

$$J_{\text{nuc}} = A_3[\text{H}_2\text{SO}_4]^2[\text{ELVOC }] \tag{13}$$

where $A_3 = 3.27 \times 10^{-21}$ cm^6 s^{-1}

The update was done both due to the Riccobono et al. (2014) parameterization being based on later and thus more recent research and due to the fact that NPF was too high and lasting too long with the Paasonen et al. (2010) parameterization in CAM6-Oslo. The rate at which particles are introduced into the smallest bin, $J_{d_{\text{min}}}$, is still parameterized with eq. 8 defined above (Lehtinen et al., 2007), but with $d_{\text{form}} = d_{\text{min}}$ so that the cut-off size smaller than before.

2.2.2 Condensation

The condensation is done in the same way as for OsloAero6, except that the calculated loss rate to condensation L_{cond} now is the sum of loss to condensation onto the background modes from OsloAero and the condensation onto the sectional bins, $L_{\text{cond}} = L_{\text{cond,modes}} + L_{\text{cond,sec}}$, in equations 2 and 4. Furthermore, the total gas lost, ΔC, calculated by eq. 6, is then distributed as

$$f_{\text{nuc}} = \frac{L_{\text{nuc}}}{L_{\text{nuc}} + L_{\text{cond,modes}} + L_{\text{cond,sec}}} \tag{14}$$

$$f_{\text{cond,sec}} = \frac{L_{\text{cond,sec}}}{L_{\text{nuc}} + L_{\text{cond,modes}} + L_{\text{cond,sec}}} \tag{15}$$

$$f_{\text{cond,modes}} = \frac{L_{\text{cond,modes}}}{L_{\text{nuc}} + L_{\text{cond,modes}} + L_{\text{cond,sec}}} \tag{16}$$

where $f_{\text{nuc}} + f_{\text{cond,sec}} + f_{\text{cond,modes}} = 1$. In other words, the condensate added to the modes is $C_{\text{lost,tot}} \cdot f_{\text{cond,modes}}$. In the same fashion, condensing mass to the sectional scheme is distributed to the different bins by the strength of their respective condensational sinks:

$$f_{bin(d_i)} = f_{\text{cond,sec}} \cdot \frac{L_{\text{cond,bin}(d_i)}}{L_{\text{cond,sec}}} \tag{17}$$

so that the condensate added to any bin, d_i, is equal to $\Delta C \cdot f_{\text{cond,bin}(d_i)}$.

Finally, the condensational growth of particles within the sectional scheme is done in quasi-stationary structure (Jacobson, 1997), meaning the particles grow in volume but are fitted back onto the full stationary grid between each time-step (Jacobson, 2005, sec 13.3). This is done by assuming that (1) the total volume is constant before and after the transfer between the bins, and (2) the total number is the same. Let v_i and v_{i+1} be the volume of a particle in bin i and the next bin, $i+1$, priory to any growth. Let v_i' be the volume of a particle in bin i after growth. Furthermore, let N_i be the number of particles in bin i priory to growth and ΔN_{i+1} be the number of particles moved to the next bin $i+1$. Since we do not have any evaporating species, we can easily solve the equation conserving both number and volume of aerosol for each species:

$$v_i' N_i = v_i(N_i - \Delta N_{i+1}) + v_{i+1}\Delta N_{i+1} \tag{18}$$

https://doi.org/10.5194/gmd-2020-357
Preprint. Discussion started: 12 November 2020


Geoscientific Model Development Discussions

and solving for ΔN_{i+1} gives

$$\Delta N_{i+1} = N_i \cdot \frac{v_i' - v_i}{v_{i+1} - v_i}. \tag{19}$$

After the particle mass is moved in this way, the freshly nucleated particles from the same time step are added to the smallest bin. The rationale behind this is that the nucleated particles in the same time step do not take part in the condensation sink calculation, and thus including them before the redistribution of mass on the sectional grid, would only imply adding particles with no added condensate.

2.2.3 Coagulation:

In addition to the unchanged coagulation in the original OsloAero scheme (see section 2.1.4), we calculate the coagulation sink of the sectional particles onto all larger particles. This is done in the same way between particles in the original OsloAero scheme, in that a normalized coagulation sink is calculated for each background mode, by dividing the size distribution into 44 bins. When sectional particles coagulate with particles in the "modal" scheme, their mass is transferred to the corresponding process tracer for condensate. This is done for simplicity and because the alternative would be to place them in the coagulation tracers – one of the process tracers – in the original scheme, which will only contribute to changes in the larger particles.

In addition to this, coagulation between the particles in the sectional scheme is taken into account. When two particles in the sectional scheme collide, this results in the loss of the particle in the smaller bin, and the addition of mass to the particle in the larger bin. After this is done in each time step, the mass in the sectional scheme is redistributed in the same way as after condensation (see previous section).

2.3 Chemistry: changes to oxidant diurnal variation:

The oxidant concentrations of hydroxyl radical (OH), nitrate radical (NO_3), hydroperoxy radical (HO_2) and ozone (O_3) in the model are prescribed by 3D monthly mean fields (see Seland et al. (2020b)). On top of this, a diurnal cycle is applied to OH, HO_2 and NO_3. In the default version of the model, the diurnal cycle for OH basically a step function based on whether it is before or after sunrise. Since OH in particular is very important for the diurnal cycle of H_2SO_4, this leads to more or less a step function in H_2SO_4 concentrations as well, which is not very realistic in terms of NPF. We therefore implemented a simple sine shape to the daily variation in place of the step function.

3 Model simulations and output post processing

3.1 Simulation description

In the following analysis we include simulations with three versions of the CAM6-Nor.

- A simulation with OsloAeroSec, referred to simply as "OsloAeroSec" (see sec. 2.2)
- A simulation with the default version of OsloAero (see sec.2.1), referred to as "OsloAero$_{def}$"

https://doi.org/10.5194/gmd-2020-357
Preprint. Discussion started: 12 November 2020


Geoscientific Model Development Discussions
Open Access
EGU

– A simulation with the default version of OsloAero, but with the same changes to the nucleation rate (eq. 13) and oxidants (see sec. 2.3) as OsloAeroSec. Referred to as "OsloAero$_{imp}$".

The last simulation, OsloAero$_{imp}$, is added in order to separate the changes done in OsloAeroSec to the nucleation rate and the diurnal concentration in the oxidants (described above) to the effect of adding a sectional scheme. The simulation characteristics are also summarized in Table 1.

NorESM2 is run with CAM6-Nor (release-noresm2.0.1, https://github.com/NorESMhub/NorESM) Kirkevåg et al. (2018) coupled to the Community Land Model version 5 (CLM5) (Lawrence et al., 2019) in BGC (biogeochemistry) mode and prognostic crops. We use prescribed sea surface temperature (SST) and sea ice concentrations at 1.9 $\times$ 2.5 $^\circ$ resolution (Hurrell et al., 2008). Simulations are run from 2007 and throughout 2014 with CMIP6 historical emissions and greenhouse gas concentrations (Seland et al., 2020b) and nudged meteorology (horizontal wind and surface pressure) to ERA-Interim (Berrisford et al., 2011) using a relaxation time of 6 hours (Kooperman et al., 2012) (as described in Karset (2020, sec 4.1)). The year 2007 is discarded as spin-up. The initial conditions for all simulations are taken from a simulation with CAM6-Nor run from 2000 and throughout 2006.

3.2 Post-processing of model output

All figures, except comparisons to observations (described below), are produced from monthly mean output files from the model. When we present figures showing averaged values over maps, these are either column burdens or "near-surface" averages of the variable in question. The "near-surface" averages are calculated as the average of all grid cells below 850 hPa, weighted by the grid cell pressure thickness to account for the mass in the grid cell. Cloud radiative effects and direct radiative effects are calculated as described in (Ghan, 2013).

For the model to model comparisons, we include an analysis of whether the change is significant. Dots are included in the plots to indicate where the difference between the two models is significant with a two-tailed paired Student's t–test with 95 % confidence interval.

When we compare the model runs, we compare model version with and without an explicit treatment of the smallest particles. We therefore introduce the following subgroups of particle number concentration. We refer to particle number concentrations excluding particles in the sectional scheme, as N_a. This includes all the particles for the OsloAero simulations (OsloAero$_{def}$ and OsloAero$_{imp}$), but excludes the particles still in the sectional scheme for OsloAeroSec. Furthermore, the total number of aerosols, we refer to as N_{tot}, and the concentration of aerosols in the sectional scheme will be referred to as N_{sec}. Finally, the aerosol scheme also tracks the number of particles in the modal scheme originating from NPF, and this we denote by $\mathrm{N}_{\mathrm{NPF}}$. This is summed up in Table 3. Note that changes in $\mathrm{N}_{\mathrm{NPF}}$ and N_a in general follow the same patterns, because we do not introduce changes to other particles than those from NPF.

https://doi.org/10.5194/gmd-2020-357
Preprint. Discussion started: 12 November 2020

Geoscientific Model Development Discussions
Open Access
EGU

3.3 Processing of model output data prior to comparison with observations

We compare the nudged model simulations for years 2008 and 2009 to observed size distributions from the EUSAAR dataset from Asmi et al. (2011). The dataset contains time series of hourly data for number concentrations of particles with diameter between 30 and 50 nm (N_{30-50}), 50 and 500 nm (N_{50-500}), 100 and 500 nm ($N_{100-500}$) and finally 250 and 500 nm ($N_{250-500}$). In this study, we focus on the concentration of particles with diameter between 50 and 100 nm, i.e. $N_{50-100} = N_{50-500} - N_{100-500}$. Throughout the simulation period, we output hourly mean values describing the modelled size distribution.

The model outputs a log-normal fitting to the size distribution in terms of parameters for 12 log-normal modes. In other words, the total size distribution is

$$\frac{dN}{d(d_p)} = \sum_{i}^{12} \frac{dN_i}{d(d_p)}. \tag{20}$$

Each term $\frac{dN_i}{d(d_p)}$ is furthermore defined in terms of output parameters from the modal number median diameter, $d_{m,i}$, geometric standard deviation, S_i, and the number concentration in the mode, N_i:

$$\frac{dN_i}{d(d_p)} = \frac{N_i}{d_p log(S_i)\sqrt{2\pi}} exp\Big(-\frac{(log(d_p) - log(d_{m,i}))^2}{2log(S_i)}\Big). \tag{21}$$

For each mode, we can then calculate the number of particles in a size from diameter d_1 to d_2 by

$$N_{i,d_1-d_2} = N_i(d < d_2) - N_i(d < d_1) \tag{22}$$

where N_i is the cumulative distribution function of the distribution in eq. 21, thus

$$N_i(d < x) = \frac{1}{2} + \frac{1}{2}\text{erf}\Big[\frac{log(x) - log(d_{m,i})}{\sqrt{2}log(S_i)}\Big]. \tag{23}$$

The total number concentration in a size range is thus $N_{d_1-d_2} = \sum_{i=1}^{12} N_{i,d_1-d_2}$. We calculate these variables for each hour and do further statistics on the result. By using such a fine time resolution, we avoid a common imprecision arising when averaging the parameters of the size distribution, $r_{m,i}$ and S_i, over a longer time period (i.e. monthly output).

Furthermore, for the comparison of size distributions, we calculate $\frac{dN}{dlog(d_p)} = d_p \frac{dN}{d(d_p)}$ for an array of diameters and do further statistics on the hourly values.

4 Results and discussion

4.1 Comparison to EUSAAR dataset

In this comparison we focus on N_{50-100} because particles smaller than 50 nm are unlikely to be relevant for CCN and particles above 100 nm are less effected by the changes to the NPF scheme (see e.g. the size distributions in Fig. 6).

https://doi.org/10.5194/gmd-2020-357
Preprint. Discussion started: 12 November 2020


Geoscientific Model Development Discussions
Open Access
EGU

Figures 2 and 3 show the distribution of the modelled minus the observed values for N_{50-100} in hourly resolution and with all valid station data included.

From Fig. 2 we can see a clear improvement with OsloAeroSec, compared to both OsloAero$_{def}$ and OsloAero$_{imp}$. The improvement is most pronounced in summer, where OsloAero$_{def}$ and OsloAero$_{imp}$ overestimate N_{50-100}, while it is also clear in autumn and spring. It is also encouraging that OsloAeroSec has a clear decrease in the times when the number concentration is highly over-estimated, while there is not a similar increase in times when it is under-estimated. Furthermore, we see that changes to nucleation parameterization and diurnal variation in oxidants in OsloAero$_{imp}$ reduce the bias compared to OsloAero$_{def}$. In winter, NPF is low, so we see little difference between the different schemes. Figure 3 shows the same as Fig. 2 but for each individual station. OsloAeroSec (OsloAeroSec) shows improvement against OsloAero (OsloAero$_{def}$ and OsloAero$_{imp}$) in most stations during JJA, while sometimes underestimating N_{50-100} in MAM (e.g. VHL, MPZ, HWL).

The annual variability of both models and observations are shown in Fig. 4, where the monthly median (solid line) and percentiles (16th to 84th) are plotted for each station. Again it is clear that OsloAeroSec in general reduces the high bias of OsloAero$_{def}$ and OsloAero$_{imp}$, and especially when the bias is very high (e.g. OBK, HPB, FKL, ZSF, CMN, BEO). The exceptions that stand out are e.g. CBW, JRC, ZEP and KPO, where all versions of the model do rather poorly, both in absolute numbers and in terms of representing the annual variability. This might indicate that aerosol or precursor emission in the model are not accurate, e.g. due to local sources that are unaccounted for in the model. For CBW, NPF should not be an important source of aerosols during winter and autumn (Mamali et al., 2018), so it is likely that other aerosols are responsible for the underestimation during these seasons. Dall'Osto et al. (2018) note a strong influence of local anthropogenic emissions at this station, which is likely not captured in the CMIP6 emissions. However, during summer, the model may well show an underestimation of production of particles from NPF which becomes slightly worse with OsloAeroSec. According to Dall'Osto et al. (2018), NPF should be most frequent in JRC and KPO during spring, which the N_{50-100} does not really reflect, probably due to other particles dominating the annual variability. Furthermore, at ZEP station, the concentrations are underestimated in all months except late autumn and winter. At this station the concentrations in the sectional scheme (see Fig. 6,S7-S10), reveal that there is relatively many particles forming at this location, but they do not survive to 50 nm. All models perform badly here, with OsloAeroSec and OsloAero$_{imp}$ performing slightly worse than OsloAero$_{def}$. In PLA and WAL, the OsloAeroSec results in too low values, while OsloAero$_{def}$ and OsloAero$_{imp}$ perform better. In station MHD, FKL, ZSF, CMN and BEO, the models overestimation of N_{50-100} is reduced OsloAeroSec, but is still significantly too high.

The normalized root mean square error (NRMSE) is improved with OsloAeroSec for both N_{50-100} and N_{50-500}, while it stays more or less the same for $N_{100-500}$. The NRMSE is shown in Fig. 5 and is calculated for each season and each model version, using hourly resolution and all available data. The greatest improvement is seen in N_{50-100} and in summer, followed by SON and MAM, while DJF is mostly unchanged. N_{50-500} shows improvement in the same seasons, while there is little change in prediction skill for $N_{100-500}$.

This is likely due to the fact that the particles in CAM6-Nor, are not transferred to larger modes by condensational growth, so in these simulations, changes in $N_{100-500}$ are decided by the tail one NPF-particle mode. Changes are thus determined by

https://doi.org/10.5194/gmd-2020-357
Preprint. Discussion started: 12 November 2020


Geoscientific Model Development Discussions
Open Access
EGU

number of particles and how much condensate is added to the mode, i.e. the change in the number median diameter of the mode.

Even though the N_{50-100} improves, Fig. 6 reveals that at the concentrations at smaller sizes are overestimated in most locations. The figure shows the size distribution of particles at each station from both observations and the three versions of CAM6-Nor. For the sectional scheme, the distribution is the sum of particles in the sectional scheme and the modal scheme. This is why it has "spikes", and why there is often a large reduction in $dN/dlog_{10}D$ at the intersection between the sectional scheme and the modal scheme which might be misunderstood to mean that disproportionately many particles are lost in the transition between sectional and modal scheme. The distribution in the sectional scheme, without adding the modal particles, is shown with the dashed line. One important reason why the sectional scheme overestimated the number of particles for this may be that the number of particles above $\sim$100 nm is underestimated in all the models versions in most of the stations (see e.g. the surface distribution in Fig. S6).

This is particularly pronounced in summer, where the number of particles in the sectional scheme is particularly high (see Fig. S8). Since NPF mostly influences nucleation and Aitken mode particles, this is likely due to other aerosol sources not being adequately represented in the model. This leads to an underestimation of coagulation sink and hence an overestimation of the formation rate. To the same effect, the condensation sink may be too low, again leading to too many new particles forming. This is particularly clear in the arctic station Zeppelin (ZEP), where the measurements show a peak in particles between 100 nm and 200 nm, which are completely missing in the models. The combination of a too high formation rate, and a slow condensation growth rate, leads to too many particles in the smaller sizes.

Overall, adding the explicit treatment of the smaller particles in OsloAeroSec does improve the representation of CCN relevant particles in the model. We especially reduce number concentrations where they are very highly overestimated.

4.2 Comparison to original model:

The following section will present general differences in OsloAeroSec compared to the two versions of the original model, OsloAero$_{def}$ and OsloAero$_{imp}$. For this analysis, we make use of the full global model output in monthly mean resolution. We will start with comparing the particle number concentrations and properties of the aerosols. The original version of the CAM6-Nor aerosol scheme does not explicitly model the smallest particles, so in order to get an apples-to-apples comparison, we focus on properties relevant for climate, as represented by the modal aerosol scheme when comparing OsloAeroSec to OsloAero$_{def}$ and OsloAero$_{imp}$. See table 3 for a summary of the definitions of the variables defining number concentration. We then proceed to changes in cloud properties and finally the radiative effect.

4.2.1 Aerosols:

The total number of particles, N$_{tot}$, increases in OsloAeroSec compared to OsloAero$_{def}$ and OsloAero$_{imp}$ due to the addition of particles not explicitly treated before. In Fig. 7 the absolute number of sectional particles, N$_{sec}$, in OsloAeroSec is shown (a and c) together with the total number of particles, N$_{tot}$, (right, b and d). The maps in Fig. 7a and b show near surface averages,

https://doi.org/10.5194/gmd-2020-357
Preprint. Discussion started: 12 November 2020


Geoscientific Model Development Discussions
Open Access
EGU

as defined above in section 3.2. As can be seen from Fig.7d, the change is particularly strong in the upper troposphere, where N_{tot} is very low in OsloAero$_{imp}$ and OsloAero$_{def}$.

Figure 8a shows averaged profiles of N_a for each model version, while b and c show maps of the near-surface relative difference in OsloAeroSec compared to OsloAero$_{def}$ and OsloAero$_{imp}$, respectively. On average, the global near-surface N_a decreases in OsloAeroSec by 15 % compared to OsloAero$_{imp}$ and 36.2 % compared to OsloAero$_{def}$. However, at high latitudes the change relative to OsloAero$_{imp}$ is small, or positive, especially over the southern ocean. When considering the vertical change shown in Fig. 8 a), OsloAeroSec has less particles close to the surface, while the difference is reduced further up in the atmosphere. In the free troposphere the difference becomes positive, meaning further away from the surface, OsloAeroSec lets more particles survive through early growth. For the global average this happens roughly at 700 hPa, while over ocean, it happens already at 800 hPa. Over the continents, OsloAero$_{imp}$ is always higher, though the difference decreases with height. From these results, we can conclude that on average the sectional scheme produces more particles in more remote regions, both horizontally and vertically.

In all model versions, the growth of the particles from nucleation to the smallest mode happens by condensation of the two tracers H_2SO_4 and SOAG$_{LV}$.The relative contribution of H_2SO_4 and SOAG$_{LV}$ to this growth changes with OsloAeroSec, but interestingly, also between OsloAero$_{def}$ and OsloAero$_{imp}$. Figure 9a shows the SOA fraction of the particles that have survived to the modal scheme averaged over regions. Firstly, the SOA fraction goes down in OsloAero$_{imp}$ compared to OsloAero$_{def}$ and secondly, globally it goes up with OsloAeroSec. We start with exploring the difference between OsloAero$_{def}$ and OsloAero$_{imp}$. These two simulations have the same parameterization for survival of particles from nucleation up to the model scheme (see section 2.2), but OsloAero$_{imp}$ has an improved diurnal variation in the oxidants resulting in a higher, diurnal peak in H_2SO_4 (not shown). Additionally, the nucleation parameterization in OsloAero$_{imp}$ is on the form H_2SO_4 $^2\times$ELVOC, meaning that as H_2SO_4 increases, the nucleation rate increases to the power of two, while in OsloAero$_{def}$ the increase is linear with both H_2SO_4 and ELVOC. Furthermore, because the growth from nucleation to modal scheme happens within one time step in these simulations, the fraction of the growth from SOA is entirely based on H_2SO_4 and ELVOC at the moment of nucleation. This means that if most of the particles form when H_2SO_4 is at it's highest, H_2SO_4 will also dominate the post-nucleation growth. This explains the reduced contribution of SOA in OsloAero$_{imp}$ relative to OsloAero$_{def}$.

The change seen in OsloAeroSec compared to OsloAero$_{def}$ and OsloAero$_{imp}$, on the other hand, can be explained by two factors: (1) though OsloAeroSec has the same changes to oxidants and nucleation parameterization as OsloAero$_{imp}$, the particles grow in the sectional scheme over more than one time step, and thus be exposed to different concentrations of H_2SO_4 and SOAG$_{LV}$. Thus, the concentrations at the time of nucleation will be less dominant for the growth. (2) In OsloAero$_{def}$ and OsloAero$_{imp}$ only ELVOC, which is 50% of the SOAG$_{LV}$, will contribute to growing the particles up to the modal scheme, while in OsloAeroSec 100% of the SOAG$_{LV}$ can contribute after the particles have reached the sectional scheme (5 nm), thus increasing the SOA fraction. The result is a combination of these effects, in some regions, like over the Amazon, the effect seems to be dominated by the change in nucleation timing such that the SOA fraction goes down compared to OsloAero$_{def}$. In most regions the effect is that the SOA fraction increases.

https://doi.org/10.5194/gmd-2020-357
Preprint. Discussion started: 12 November 2020


Geoscientific Model Development Discussions
Open Access
EGU

Note that the changes in hygroscopicity from this are minor and are mitigated by the fact that additional condensate is added to the particles after they reach the modal scheme.

The strength and sign of the change in number concentration between OsloAeroSec and the original model varies with location.

To investigate what conditions lead to the changes in NPF particles, we focus on the difference in N_{NPF} between OsloAeroSec and OsloAero$_{imp}$ and analyse its relationship to relevant variables in OsloAero$_{imp}$. Thus, we can analyse under which conditions in the model (polluted, clean, high NPF etc.) N_{NPF} increases or decreases with the sectional scheme. Figure 10 shows the relationship for nucleation rate (J_{nuc}, a), growth rate (GR, b), H_2SO_4 (c), SOAG$_{LV}$ (d), N_{NPF} (e) and coagulation sink for newly formed particles (CoagS, f). This 2D histogram includes each grid cell below 100 hPa and monthly mean values are used for each grid-cell.

Firstly, most of the variables show a branch with a strong negative relationship with the change in N_{NPF} (ΔN_{NPF}). Further investigation shows that the grid-cells that constitute this branch are mainly close to the surface and, as can be seen from Fig. 10e, where N_{NPF} and CoagS are high. In other words, what we are seeing is that in regions with high CoagS and N_{NPF}, the sectional scheme reduces the number of particles that survives drastically and more the higher they were initially in OsloAero$_{imp}$. This resembles what we saw when comparing to station data, where in particular the very high over-estimations were reduced.

For the other grid-cells, where N_{NPF} and CoagS are lower, there is another branch showing a positive relationship with GR, H_2SO_4 and SOAG$_{LV}$. From panel e and f, it is clear that these grid-cells have N_{NPF} concentrations under roughly 100 cm^{-3} and CoagS under roughly 10^{-3} h^{-1}. In this regime the sectional scheme allows more particles to survive, and condensational growth is more important.

In sum this means that in regions with very high number concentrations initially, the sectional scheme reduces the number of particles that survive proportional to the coagulation sink/initial number of particles, while when the number of particles is initially small, the sectional scheme lets more particles survive and the change is more proportional to the concentration of condensing vapors.

As mentioned before, the Lehtinen et al. (2007) parameterization assumes steady-state GR and CoagS throughout the growth up to the aerosol model cut-off diameter, while in reality the aerosol often forms e.g. when the GR is high and the CoagS is relatively low. The steady-state assumption is likely to give especially biased results in areas with high variability in aerosol and precursor concentration. Since this is especially the case in areas with high aerosol concentration, like the boundary layer, this may be why it is especially here that the sectional scheme reduces N_{NPF}. In the sectional scheme, the particles may grow over some time and space before reaching the modal scheme, and thus experience other concentrations.

4.2.2 Cloud–aerosol interactions

The sectional scheme affects the CCN concentrations by influencing the number of particles that survive to the modal scheme, and thus also influences the cloud droplet activation scheme. The changes to cloud properties are shown in Fig. 11 e–h and Fig. 12. We include variables that indicate changes to cloud properties from cloud aerosol interaction. Unfortunately, CCN calculations are not currently available for CAM6-Nor.

https://doi.org/10.5194/gmd-2020-357
Preprint. Discussion started: 12 November 2020


Geoscientific Model Development Discussions
Open Access
EGU

We start by discussing the changes in OsloAeroSec compared to OsloAero$_{imp}$ shown in the right column of Fig. 11 and 12. Figure 11f and h show the change between OsloAeroSec and OsloAero$_{imp}$ in cloud droplet number concentration (CDNC) and r_e averaged over longitude and time. These plots reveal that the CDNC increases and r_e decreases at most latitudes and heights, except above $\sim 40\,^{\circ}$N.

Considering the change in N_{NPF} shown in Fig 11b, the change in cloud properties reveals a highly non-linear response in Fig. 11f, where the CDNC increases (and similarly r_e decreases) both where there are more N_{NPF} (high in the southern hemisphere atmosphere) and where there are fewer (near surface in the tropics). To investigate this, we show in Fig. 13a and b the Pearson correlation coefficient between ΔN_{NPF} and ΔCDNC calculated for each latitude and pressure level, along time (monthly mean) and longitude. The pattern shows that in remote regions, i.e. polar and high troposphere, higher N_{NPF} is positively correlated with higher CDNC, while in less remote regions, the opposite is the case. The correlations are very similar when comparing to OsloAero$_{def}$ (Fig. 13a) and OsloAero$_{imp}$ (Fig. 13b). These regions correspond roughly to regions of low particle concentrations (upper atmosphere) and high particle concentrations (surface). The reason for these correlations is likely that when the number of particles decrease, the amount of condensate available for each particle increases, thus increasing the number median diameter of each mode. This is seen in Fig. 11b and d, where we have inverse patterns in the difference in N_{NPF} and number median radius for NPF particles (NMR_{NPF}). Since decreasing the number of particles in general causes the remaining particles to be bigger, there may be fewer particles in total, but a larger fraction of the ones that are left is likely to activate. This is true in general, but in polluted regions, where there are many particles to compete for the same water vapour, the maximum supersaturation will be lower and the minimum activation diameter will be higher than in remote regions. Therefore, the change in size of the mode may be more important than the change in number. In more remote regions, the maximum supersaturation will be higher and the activation diameter smaller and thus the number of particles to activate will be more dependent on absolute number in the mode than the number median radius of the mode. Additionally, in highly polluted areas, an increased number of particles may inhibit activation because more particles compete for the same water vapor.

Keeping this in mind, the cloud property changes are easier to explain. When the number concentration decreases in remote regions, the CDNC (r_e) increases (decreases) and the opposite for non-remote regions.

In general these results are reflected in Fig. 12 showing the changes in cloud properties on maps. There are significant differences over large parts of the high latitude regions and the Amazon: an increase in column integrated cloud droplet number (col$_{droplets}$, b), a decrease in cloud top effective droplet radius (r_e(CT), d) and an increase in total cloud water path (CWP, f). Note that, there is a reverse pattern over the northern hemisphere continent, where col$_{droplets}$ decreases, r_e(CT) increases and CWP decreases.

The difference in N_{NPF} between OsloAeroSec and OsloAero$_{def}$ in Fig. 11a, shows a stronger and more prevalent decrease than the difference between OsloAeroSec and OsloAero$_{imp}$ in b, due to the fact that OsloAero$_{def}$ has, in general, more particles than OsloAero$_{imp}$.

https://doi.org/10.5194/gmd-2020-357
Preprint. Discussion started: 12 November 2020


Geoscientific Model Development Discussions
Open Access
EGU

The cloud effects follow closely the same rationale as for OsloAeroSec versus OsloAero$_{imp}$, explained above: the decrease in polluted regions (tropics, close to the surface) give an increase in CDNC, while a decrease in remote regions (northern hemisphere, free troposphere) gives a decrease in CDNC.

The right column in Fig. 12 shows maps for the relative difference between OsloAeroSec and OsloAero$_{def}$. In this case the hemispheric asymmetry is clearer than for OsloAeroSec versus OsloAero$_{imp}$: in the northern hemisphere above $\sim 30°$, we have a decrease in col$_{droplets}$ (a), r_e clearly increases (c), CWP decreases (e) and the net cloud effect is a slight warming (g). Over the south pole and large parts of the tropics, the opposite is the case.

The result is that the cloud effects of particles from NPF may depend highly on where these are formed.

4.2.3 Radiative effects

The changes in cloud properties discussed in the section above entail changes to the net cloud radiative effect (NCRE), shown in Fig. 12g and d. The globally averaged NCRE becomes more negative with OsloAeroSec compared to both OsloAero$_{def}$ (-0.05 Wm^{-2}) and OsloAero$_{imp}$ (-0.11 Wm^{-2}). The globally averaged ΔNCRE is less negative for OsloAeroSec–OsloAero$_{def}$, because there are quite strong compensating positive values in the northern mid– to high latitudes.

Aerosols can scatter or absorb radiation directly and this effect is referred to as the direct aerosol effect. The changes in aerosol size distribution induced by using OsloAeroSec can not only affect the climate through changes in the cloud radiative effect, but also to a lesser extent through changes in the direct aerosol effect. We calculate the direct aerosol effect by the method of Ghan (2013). The change in direct aerosol radiative effect (DRE) is shown in Fig. 14. In general the change is small with up to $\pm \sim 0.4$ Wm^{-2} regionally and 0.03 Wm^{-2} and 0.02 Wm^{-2} globally compared to OsloAero$_{def}$ and OsloAero$_{imp}$, respectively. This is because the influence of the sectional scheme on the particles large enough to interact directly with radiation is rather small. What we do see is likely due to the fact that when number concentrations decrease (increase), we get an increase (decrease) in condensate available for each particle. Thus more (less) particles grow into the range where they can interact directly with radiation. This is illustrated by the top two rows in Fig. 11 showing N_{NPF} and number median radius of the NPF particles which have inverse patterns and was also seen in (Sporre et al., 2020).

5 Implications and further discussion

From the results above, it is clear that including explicit treatment of the early growth in OsloAeroSec does increase prediction skill compared to the original parameterization for particles above 50 nm in diameter. The difference is largest in summer, where the sectional scheme reduces the number of particles in N_{50-100} substantially, bringing it closer to the observed values. While the overestimation of particles above 50 nm is vastly reduced with OsloAeroSec, there is still a considerable overestimation of the smallest particles (below $\sim 20\mathrm{nm}$). This indicates that NPF is either too high or too frequent in the model and this is probably linked to the models having too few larger particles (above $\sim 100\mathrm{nm}$) and thus too low coagulation sink. Furthermore, the underestimation of the larger particles also leads to less available surface area and and too low condensation sink, which may lead to too high H_2SO_4 and/or SOAG$_{LV}$ concentrations and thus too high nucleation rates.

https://doi.org/10.5194/gmd-2020-357
Preprint. Discussion started: 12 November 2020


Geoscientific Model Development Discussions
Open Access
EGU

Our results also go in line with Lee et al. (2013) and Olenius and Riipinen (2017), who show that a higher cut-off diameter leads to over prediction of the aerosol number concentration. They remark that the most likely explanation is the steady-state assumption used in the parameterizations (in our case Lehtinen et al. (2007)). We consider this as the most likely explanation for the reduction in particles in the modal scheme with OsloAeroSec in our runs as well. In addition, we find that the reduction in number of particles in the modal scheme is largest where the concentration was largest initially, and that in clean, remote regions, there is actually an increase in particle number.

In OsloAeroSec we let more organics ($SOAG_{LV}$ and ELVOC) contribute to growth after 5 nm than is considered in $OsloAero_{def}$ and $OsloAero_{imp}$ (only ELVOC), which is likely why, in the higher atmosphere, OsloAeroSec often produces more particles than $OsloAero_{imp}$. However, this also illustrate the advantage of a sectional scheme, namely that it is possible to differentiate condensation by particle size.

Related to this, we show that the choice of nucleation parameterization together with the representation of the chemical diurnal variation, has a large influence on the SOA and H_2SO_4 contribution to the growth of NPF fraction in particles. This is especially true when the cutoff diameter is high, as in $OsloAero_{def}$ and $OsloAero_{imp}$. The reason is that the Riccobono et al. (2014) formulation is non-linear, as apposed to the Paasonen et al. (2010) parameterization and thus forms proportionately more particles when H_2SO_4 concentrations are high. Including the sectional scheme (OsloAeroSec) counteracts this, both because of particles growing for more than one time step, and that more $SOAG_{LV}$ is allowed to contribute to growth.

In sum these effects illustrate that including NPF in global climate models, often with a very simplified chemistry, should be done with care. A parameterization may very well be physically sound, but might still give biased results if it is subjected to unrealistic (diurnal) variability concentrations. If the cutoff diameter is high, and the nucleation parameterization has a super-linear relationship with H_2SO_4, the influence of organics on survival to larger sizes might be diminished, resulting in a weaker response to changes in BVOC-emissions either in terms of climate feedbacks or forcing for e.g. deforestation/afforestation (Sporre et al., 2019, 2020).

As mentioned, the changes introduced by inserting a sectional scheme are heterogeneous in space and time. The number concentration of modal scheme particles in general decrease where concentrations initially were high and increase where they were low. A topic for further research is therefore how this would influence the modelled effective radiative forcing from cloud-aerosol interaction (ERFaci). If the OsloAeroSec produces more particles in the cleaner pre-industrial atmosphere, and less in the present day atmosphere, it could reduce the ERFaci. Furthermore, the response to both historical and future changes in BVOC emissions may also be different (Sporre et al., 2020), due to a larger role in the early growth.

Furthermore, considering only the station observation comparison and the general decline in CCN-size number concentration, one might be inclined to think that the same improvement could be achieved by simply reducing the nucleation rate or the survival rate from the (Lehtinen et al., 2007) parameterization. However, the fact that the sectional scheme produces more particles in the remote atmosphere shows that such a quick fix would in fact not produce the same climatic effects and quite possibly give other sensitivities to emission changes.

https://doi.org/10.5194/gmd-2020-357
Preprint. Discussion started: 12 November 2020


Geoscientific Model Development Discussions
Open Access
EGU

Interestingly, the cloud–aerosol effects show clear non-linearities and contradict the simplest assumption that more NPF leads to more CCN which lead to brighter clouds. The correlation between CDNC and NPF particles (N_{NPF}, Fig.13) rather show that in polluted regions more NPF results in less CDNC and the reverse in remote regions. This is due to the fact that when NPF increases, the condensate is spread over more particles, reducing the individual particle size so that fewer are activated as CCNs at a given supersaturation (an effect shown in e.g. Sullivan et al. (2018)).

A weakness of the approach of merging a sectional scheme and a modal scheme is that the sectional scheme will grow the particles to size of the volume median diameter of the particles, but when they are inserted into the modal scheme, these particles are represented with a mode distribution, meaning some of them will "shrink" again i.e. be on the lower tail of the distribution. However, this is not uniquely a problem for the sectional scheme – any modal representation of aerosol particles include this effect, the original parameterization in CAM6-Nor makes the same "error". However, improving the early growth parameterization shines a light on this inconsistency – especially because when we plot the size distribution, the number of small particles becomes the sum of the sectional scheme and the modal approximation.

Furthermore, we include a limited number of processes for the sectional scheme (nucleation, coagulation and condensation, while wet/dry deposition are assumed negligible). This is done for simplicity, and is also consistent with the processes considered when using Lehtinen et al. (2007) to parameterize the early growth. Including dry and wet deposition might decrease the number concentrations in the model.

The oxidant concentrations in these simulations are read from monthly mean files and used with a superimposed diurnal variation. Any factor that could impact the oxidant concentration – be it changes in chemical sinks or changes to radiation – will not be accounted for. Since new particle formation is very dependent on this chemistry (see e.g. Lee et al. (2019)), this inhibits how well the model can come to reality.

In terms of computational cost, we tested running one month with standard output fields and the setup described in section 3.1, i.e. active land model and atmosphere, and the computational cost is increased by $\sim$15 % with OsloAeroSec compared to OsloAero$_{def}$.

6 Conclusions

A sectional scheme has been included in the aerosol scheme in CAM6-Nor to explicitly treat the early growth of particles and subsequently feed particles into the pre-existing aerosol scheme. The scheme includes two condensing species, SOAG$_{LV}$ and H_2SO_4, and 5 bins. In addition, the diurnal variation in the oxidant concentrations has been improved, and the nucleation parameterization has been updated.

We compare a simulation with the implemented sectional scheme, OsloAeroSec, to two simulations with different versions of the original scheme – one with the default nucleation scheme and oxidant concentrations, OsloAero$_{def}$, and one where these are updated to match the sectional scheme, OsloAero$_{imp}$.

We compare the model output to observations of aerosol concentrations from 2008 and 2009 from 24 stations in Europe (EUSAAR, (Asmi et al., 2011)). We find that all versions of the model overestimates the particles smaller than 100 nm, while

https://doi.org/10.5194/gmd-2020-357
Preprint. Discussion started: 12 November 2020


Geoscientific Model Development Discussions
Open Access
EGU

the sectional scheme shows clear improvement compared to the other two. The largest improvements are in the N_{50-100} in the summer, while changes are insignificant over a 100 nm in diameter.

In general, the sectional scheme reduces the number of particles in the modal scheme near the surface while increasing it further up in the atmosphere and in remote regions.

The decrease in polluted regions is likely due to overestimation in the original scheme due to the high cut-off diameter of the aerosol scheme (Olenius and Riipinen, 2017; Lee et al., 2013).

The relative contributions of H_2SO_4 and $SOAG_{LV}$ to the early growth of the particles changes between all the model versions. This is due to the complex interplay between in the introduction of diurnal variation of the oxidants, changes to the nucleation equation and the introduction of a sectional scheme. This illustrates that care must be taken when implementing NPF in global models because a highly simplified chemistry may have unintended effects on the sensitivities of NPF to e.g. changing emissions emissions.

We also analyse the cloud changes and show how the effect of the changes in NPF are heterogeneous in space. An assumption that more particles from NPF leads to more activated CCN and increased CDNC fails in most regions close to the surface, where the inverse is true. Higher up in the atmosphere and in remote regions however, the relationship holds.

In general, this study shows that combining a sectional scheme for early growth with a modal scheme for the larger particles is both possible and that this treatment of early growth improves the representation in the smaller parts of CCN size range.

Code and data availability. The output data from the simulations used are available for download at https://doi.org/10.11582/2020.00056 (Blichner, 2020a). The model code of NorESM2, release 2.0.1, is available at https://doi.org/10.5281/zenodo.3760870 (Seland et al., 2020a). The code modifications in OsloAeroSec, simulation configurations and setup instructions are released at https://doi.org/10.5281/zenodo.4265057 (Blichner, 2020b). The postprocessing code used to produce the figures are available at https://doi.org/10.5281/zenodo.4265033 (Blichner, 2020c).

Author contributions. SMB did the model code development and performed the simulations with NorESM. SMB did the data analysis and wrote the manuscript. RM and SMB contributed with the idea. SMB, MKS and TKB contributed with discussions regarding the experimental design and data analysis. All contributors have contributed to the discussions regarding the manuscript.

Competing interests. No competing interests.

Acknowledgements. This work was funded under the LATICE strategic research initiative funded by the Faculty of Mathematics and Natural Sciences at the University of Oslo. This work has been financed by the Research Council of Norway (RCN) through the NOTUR/Norstore

https://doi.org/10.5194/gmd-2020-357
Preprint. Discussion started: 12 November 2020

Geoscientific Model Development Discussions
Open Access
EGU

project NN2806K and NS9066K. We would like to thank the EUSAAR project for use of the measurements. Thanks to Diego Aliaga for help and discussions on the data analysis and visualization. Inger Helene Karset for scientific discussions.

https://doi.org/10.5194/gmd-2020-357
Preprint. Discussion started: 12 November 2020

Geoscientific Model Development Discussions
Open Access
EGU

References

Albrecht, B. A.: Aerosols, Cloud Microphysics, and Fractional Cloudiness, Science, 245, 1227–1230, https://doi.org/10.1126/science.245.4923.1227, 1989.

Anttila, T., Kerminen, V.-M., and Lehtinen, K. E. J.: Parameterizing the Formation Rate of New Particles: The Effect of Nuclei Self-Coagulation, Journal of Aerosol Science, 41, 621–636, https://doi.org/10.1016/j.jaerosci.2010.04.008, 2010.

Asmi, A., Wiedensohler, A., Laj, P., Fjaeraa, A.-M., Sellegri, K., Birmili, W., Weingartner, E., Baltensperger, U., Zdimal, V., Zikova, N., Putaud, J.-P., Marinoni, A., Tunved, P., Hansson, H.-C., Fiebig, M., Kivekäs, N., Lihavainen, H., Asmi, E., Ulevicius, V., Aalto, P. P., Swietlicki, E., Kristensson, A., Mihalopoulos, N., Kalivitis, N., Kalapov, I., Kiss, G., de Leeuw, G., Henzing, B., Harrison, R. M., Beddows, D., O'Dowd, C., Jennings, S. G., Flentje, H., Weinhold, K., Meinhardt, F., Ries, L., and Kulmala, M.: Number Size Distributions and Seasonality of Submicron Particles in Europe 2008–2009, Atmospheric Chemistry and Physics, 11, 5505–5538, https://doi.org/10.5194/acp-11-5505-2011, 2011.

Bentsen, M., Bethke, I., Debernard, J. B., Iversen, T., Kirkevåg, A., Seland, Ø., Drange, H., Roelandt, C., Seierstad, I. A., Hoose, C., and Kristjánsson, J. E.: The Norwegian Earth System Model, NorESM1-M – Part 1: Description and Basic Evaluation of the Physical Climate, Geoscientific Model Development, 6, 687–720, https://doi.org/10.5194/gmd-6-687-2013, 2013.

Berrisford, P., Dee, D., Poli, P., Brugge, R., Fielding, M., Fuentes, M., Kållberg, P., Kobayashi, S., Uppala, S., and Simmons, A.: The ERA-Interim Archive Version 2.0, p. 23, 2011.

Blichner, S. M.: Data for: Implementing a Sectional Scheme for Early Aerosol Growth from New Particle Formation in the Norwegian Earth System Model v2: Comparison to Observations and Climate Impacts, https://doi.org/10.11582/2020.00056, 2020a.

Blichner, S. M.: Sarambl/OAS-Code-Setup: Pre-Publication Release, Zenodo, https://doi.org/10.5281/zenodo.4265057, 2020b.

Blichner, S. M.: Sarambl/OAS-DEV: Pre-Publication Release, Zenodo, https://doi.org/10.5281/zenodo.4265033, 2020c.

Boucher, O., Randall, D., Artaxo, P., Bretherton, C., Feingold, G., Forster, P., Kerminen, V.-M., Kondo, Y., Liao, H., Lohmann, U., Rasch, P., Satheesh, S., Sherwood, S., Stevens, B., and Zhang, X.: Clouds and Aerosols, in: Climate Change 2013: The Physical Science Basis. Contribution of Working Group I to the Fifth Assessment Report of the Intergovernmental Panel on Climate Change, edited by Stocker, T., Qin, D., Plattner, G.-K., Tignor, M., Allen, S., Boschung, J., Nauels, A., Xia, Y., Bex, V., and Midgley, P., pp. 571–658, Cambridge University Press, Cambridge, United Kingdom and New York, NY, USA, 2013.

Carslaw, K. S., Lee, L. A., Reddington, C. L., Mann, G. W., and Pringle, K. J.: The Magnitude and Sources of Uncertainty in Global Aerosol, Faraday Discussions, 165, 495–512, https://doi.org/10.1039/C3FD00043E, 2013.

Dall'Osto, M., Beddows, D. C. S., Asmi, A., Poulain, L., Hao, L., Freney, E., Allan, J. D., Canagaratna, M., Crippa, M., Bianchi, F., de Leeuw, G., Eriksson, A., Swietlicki, E., Hansson, H. C., Henzing, J. S., Granier, C., Zemankova, K., Laj, P., Onasch, T., Prevot, A., Putaud, J. P., Sellegri, K., Vidal, M., Virtanen, A., Simo, R., Worsnop, D., O'Dowd, C., Kulmala, M., and Harrison, R. M.: Novel Insights on New Particle Formation Derived from a Pan-European Observing System, Scientific Reports, 8, 1482, https://doi.org/10.1038/s41598-017-17343-9, 2018.

Danabasoglu, G., Lamarque, J.-F., Bacmeister, J., Bailey, D. A., DuVivier, A. K., Edwards, J., Emmons, L. K., Fasullo, J., Garcia, R., Gettelman, A., Hannay, C., Holland, M. M., Large, W. G., Lauritzen, P. H., Lawrence, D. M., Lenaerts, J. T. M., Lindsay, K., Lipscomb, W. H., Mills, M. J., Neale, R., Oleson, K. W., Otto-Bliesner, B., Phillips, A. S., Sacks, W., Tilmes, S., van Kampenhout, L., Vertenstein, M., Bertini, A., Dennis, J., Deser, C., Fischer, C., Fox-Kemper, B., Kay, J. E., Kinnison, D., Kushner, P. J., Larson, V. E., Long, M. C.,

https://doi.org/10.5194/gmd-2020-357
Preprint. Discussion started: 12 November 2020

Mickelson, S., Moore, J. K., Nienhouse, E., Polvani, L., Rasch, P. J., and Strand, W. G.: The Community Earth System Model Version 2 (CESM2), Journal of Advances in Modeling Earth Systems, 12, e2019MS001 916, https://doi.org/10.1029/2019MS001916, 2020.

Dunne, E. M., Gordon, H., Kürten, A., Almeida, J., Duplissy, J., Williamson, C., Ortega, I. K., Pringle, K. J., Adamov, A., Baltensperger, U., Barmet, P., Benduhn, F., Bianchi, F., Breitenlechner, M., Clarke, A., Curtius, J., Dommen, J., Donahue, N. M., Ehrhart, S., Flagan, R. C., Franchin, A., Guida, R., Hakala, J., Hansel, A., Heinritzi, M., Jokinen, T., Kangasluoma, J., Kirkby, J., Kulmala, M., Kupc, A., Lawler, M. J., Lehtipalo, K., Makhmutov, V., Mann, G., Mathot, S., Merikanto, J., Miettinen, P., Nenes, A., Onnela, A., Rap, A., Reddington, C. L. S., Riccobono, F., Richards, N. A. D., Rissanen, M. P., Rondo, L., Sarnela, N., Schobesberger, S., Sengupta, K., Simon, M., Sipilä, M., Smith, J. N., Stozkhov, Y., Tomé, A., Tröstl, J., Wagner, P. E., Wimmer, D., Winkler, P. M., Worsnop, D. R., and Carslaw, K. S.: Global Atmospheric Particle Formation from CERN CLOUD Measurements, Science, 354, 1119–1124, https://doi.org/10.1126/science.aaf2649, 2016.

Emmons, L. K., Walters, S., Hess, P. G., Lamarque, J.-F., Pfister, G. G., Fillmore, D., Granier, C., Guenther, A., Kinnison, D., Laepple, T., Orlando, J., Tie, X., Tyndall, G., Wiedinmyer, C., Baughcum, S. L., and Kloster, S.: Description and Evaluation of the Model for Ozone and Related Chemical Tracers, Version 4 (MOZART-4), Geoscientific Model Development, 3, 43–67, https://doi.org/10.5194/gmd-3-43-2010, 2010.

Ghan, S. J.: Technical Note: Estimating Aerosol Effects on Cloud Radiative Forcing, Atmos. Chem. Phys., 13, 9971–9974, https://doi.org/10.5194/acp-13-9971-2013, 2013.

Gordon, H., Sengupta, K., Rap, A., Duplissy, J., Frege, C., Williamson, C., Heinritzi, M., Simon, M., Yan, C., Almeida, J., Tröstl, J., Nieminen, T., Ortega, I. K., Wagner, R., Dunne, E. M., Adamov, A., Amorim, A., Bernhammer, A.-K., Bianchi, F., Breitenlechner, M., Brilke, S., Chen, X., Craven, J. S., Dias, A., Ehrhart, S., Fischer, L., Flagan, R. C., Franchin, A., Fuchs, C., Guida, R., Hakala, J., Hoyle, C. R., Jokinen, T., Junninen, H., Kangasluoma, J., Kim, J., Kirkby, J., Krapf, M., Kürten, A., Laaksonen, A., Lehtipalo, K., Makhmutov, V., Mathot, S., Molteni, U., Monks, S. A., Onnela, A., Peräkylä, O., Piel, F., Petäjä, T., Praplan, A. P., Pringle, K. J., Richards, N. A. D., Rissanen, M. P., Rondo, L., Sarnela, N., Schobesberger, S., Scott, C. E., Seinfeld, J. H., Sharma, S., Sipilä, M., Steiner, G., Stozhkov, Y., Stratmann, F., Tomé, A., Virtanen, A., Vogel, A. L., Wagner, A. C., Wagner, P. E., Weingartner, E., Wimmer, D., Winkler, P. M., Ye, P., Zhang, X., Hansel, A., Dommen, J., Donahue, N. M., Worsnop, D. R., Baltensperger, U., Kulmala, M., Curtius, J., and Carslaw, K. S.: Reduced Anthropogenic Aerosol Radiative Forcing Caused by Biogenic New Particle Formation, Proceedings of the National Academy of Sciences, 113, 12 053–12 058, https://doi.org/10.1073/pnas.1602360113, 2016.

Gordon, H., Kirkby, J., Baltensperger, U., Bianchi, F., Breitenlechner, M., Curtius, J., Dias, A., Dommen, J., Donahue, N. M., Dunne, E. M., Duplissy, J., Ehrhart, S., Flagan, R. C., Frege, C., Fuchs, C., Hansel, A., Hoyle, C. R., Kulmala, M., Kürten, A., Lehtipalo, K., Makhmutov, V., Molteni, U., Rissanen, M. P., Stozkhov, Y., Tröstl, J., Tsagkogeorgas, G., Wagner, R., Williamson, C., Wimmer, D., Winkler, P. M., Yan, C., and Carslaw, K. S.: Causes and Importance of New Particle Formation in the Present-Day and Preindustrial Atmospheres: CAUSES AND ROLE OF NEW PARTICLE FORMATION, Journal of Geophysical Research: Atmospheres, 122, 8739–8760, https://doi.org/10.1002/2017JD026844, 2017.

Guenther, A. B., Jiang, X., Heald, C. L., Sakulyanontvittaya, T., Duhl, T., Emmons, L. K., and Wang, X.: The Model of Emissions of Gases and Aerosols from Nature Version 2.1 (MEGAN2.1): An Extended and Updated Framework for Modeling Biogenic Emissions, Geoscientific Model Development, 5, 1471–1492, https://doi.org/10.5194/gmd-5-1471-2012, 2012.

Hurrell, J. W., Hack, J. J., Shea, D., Caron, J. M., and Rosinski, J.: A New Sea Surface Temperature and Sea Ice Boundary Dataset for the Community Atmosphere Model, Journal of Climate, 21, 5145–5153, https://doi.org/10.1175/2008JCLI2292.1, 2008.

https://doi.org/10.5194/gmd-2020-357
Preprint. Discussion started: 12 November 2020

Iversen, T., Bentsen, M., Bethke, I., Debernard, J. B., Kirkevåg, A., Seland, Ø., Drange, H., Kristjansson, J. E., Medhaug, I., Sand, M., and Seierstad, I. A.: The Norwegian Earth System Model, NorESM1-M – Part 2: Climate Response and Scenario Projections, Geoscientific Model Development, 6, 389–415, https://doi.org/10.5194/gmd-6-389-2013, 2013.

Jacobson, M. Z.: Development and Application of a New Air Pollution Modeling System — Part III. Aerosol-Phase Simulations, Atmospheric Environment, 31, 587–608, https://doi.org/10.1016/S1352-2310(96)00201-4, 1997.

Jacobson, M. Z.: Fundamentals of Atmospheric Modeling: Second Edition, Cambridge University Press, Cambridge, second edn., https://doi.org/10.1017/CBO9781139165389, 2005.

Karset, I. H. H.: Enhancing the Confidence in Estimates of Effective Radiative Forcing by Aerosol through Improved Global Modelling, 2020.

Karset, I. H. H., Berntsen, T. K., Storelvmo, T., Alterskjær, K., Grini, A., Olivié, D., Kirkevåg, A., Seland, Ø., Iversen, T., and Schulz, M.: Strong Impacts on Aerosol Indirect Effects from Historical Oxidant Changes, Atmospheric Chemistry and Physics, 18, 7669–7690, https://doi.org/10.5194/acp-18-7669-2018, 2018.

Kerminen, V.-M. and Kulmala, M.: Analytical Formulae Connecting the "Real" and the "Apparent" Nucleation Rate and the Nuclei Number Concentration for Atmospheric Nucleation Events, Journal of Aerosol Science, 33, 609–622, https://doi.org/10.1016/S0021-8502(01)00194-X, 2002.

Kerminen, V.-M., Anttila, T., Lehtinen, K., and Kulmala, M.: Parameterization for Atmospheric New-Particle Formation: Application to a System Involving Sulfuric Acid and Condensable Water-Soluble Organic Vapors, Aerosol Science and Technology, 38, 1001–1008, https://doi.org/10.1080/027868290519085, 2004.

Kerminen, V.-M., Paramonov, M., Anttila, T., Riipinen, I., Fountoukis, C., Korhonen, H., Asmi, E., Laakso, L., Lihavainen, H., Swietlicki, E., Svenningsson, B., Asmi, A., Pandis, S. N., Kulmala, M., and Petäjä, T.: Cloud Condensation Nuclei Production Associated with Atmospheric Nucleation: A Synthesis Based on Existing Literature and New Results, Atmospheric Chemistry and Physics, 12, 12 037–12 059, https://doi.org/10.5194/acp-12-12037-2012, 2012.

Kerminen, V.-M., Chen, X., Vakkari, V., Petäjä, T., Kulmala, M., and Bianchi, F.: Atmospheric New Particle Formation and Growth: Review of Field Observations, Environ. Res. Lett., 13, 103 003, https://doi.org/10.1088/1748-9326/aadf3c, 2018.

Kirkby, J., Duplissy, J., Sengupta, K., Frege, C., Gordon, H. Williamson, C., Heinritzi, M., Simon, M., Yan, C., Almeida, J., Tröstl, J., Nieminen, Ortega, T., Wagner, R., Adamov, A., Amorim, A., Bernhammer, A., Bianchi, F., Breitenlechner, M., Brilke, S., Chen, X., Craven, J., Dias, A., Ehrhart, S., Flagan, R. C., Franchin, A., Fuchs, C., Guida, R., Hakala, J., Hoyle, C. R., Jokinen, T., Junninen, H. Kangasluoma, J., Kim, J., Krapf, M. Kürten, A., Laaksonen, A., Lehtipalo, K., Makhmutov, V., Mathot, S., Molteni, U., Onnela, A., Peräkylä, O., Piel, F., Petäjä, T., Praplan, A. P., Pringle, K., Rap, A., Richards, N., Riipinen, I., Rissanen, M. P., Rondo, L., Sarnela, N., Schobesberger, S., Scott, C., Seinfeld, J. H., Sipilä, M., Steiner, G., Stozhkov, Y., Stratmann, F., Tomé, A., Virtanen, A., Vogel, A., Wagner, A., Wagner, P., Weingartner, E., Wimmer, D., Winkler, P., Ye, P., Zhang, X., Hansel, A., Dommen, J., Donahue, N. M., Worsnop, D., Baltensperger, U., Kulmala, M., Carslaw, K. S., and Curtius, J.: Ion-Induced Nucleation of Pure Biogenic Particles, Nature, https://doi.org/10.1038/nature17953, 2016.

Kirkevåg, A., Iversen, T., Seland, Ø., Hoose, C., Kristjánsson, J. E., Struthers, H., Ekman, A. M. L., Ghan, S., Griesfeller, J., Nilsson, E. D., and Schulz, M.: Aerosol–Climate Interactions in the Norwegian Earth System Model – NorESM1-M, Geosci. Model Dev., 6, 207–244, https://doi.org/10.5194/gmd-6-207-2013, 2013.

Kirkevåg, A., Grini, A., Olivié, D., Seland, Ø., Alterskjær, K., Hummel, M., Karset, I. H. H., Lewinschal, A., Liu, X., Makkonen, R., Bethke, I., Griesfeller, J., Schulz, M., and Iversen, T.: A Production-Tagged Aerosol Module for Earth System Models, OsloAero5.3 –

https://doi.org/10.5194/gmd-2020-357
Preprint. Discussion started: 12 November 2020

Extensions and Updates for CAM5.3-Oslo, Geoscientific Model Development Discussions, pp. 1–72, https://doi.org/10.5194/gmd-2018-46, 2018.

Kokkola, H., Korhonen, H., Lehtinen, K. E. J., Makkonen, R., Asmi, A., Järvenoja, S., Anttila, T., Partanen, A.-I., Kulmala, M., Järvinen, H., Laaksonen, A., and Kerminen, V.-M.: SALSA – a Sectional Aerosol Module for Large Scale Applications, Atmospheric Chemistry and Physics, 8, 2469–2483, https://doi.org/10.5194/acp-8-2469-2008, 2008.

Kooperman, G. J., Pritchard, M. S., Ghan, S. J., Wang, M., Somerville, R. C. J., and Russell, L. M.: Constraining the Influence of Natural Variability to Improve Estimates of Global Aerosol Indirect Effects in a Nudged Version of the Community Atmosphere Model 5, Journal of Geophysical Research: Atmospheres, 117, https://doi.org/10.1029/2012JD018588, 2012.

Lawrence, D. M., Fisher, R. A., Koven, C. D., Oleson, K. W., Swenson, S. C., Bonan, G., Collier, N., Ghimire, B., van Kampenhout, L., Kennedy, D., Kluzek, E., Lawrence, P. J., Li, F., Li, H., Lombardozzi, D., Riley, W. J., Sacks, W. J., Shi, M., Vertenstein, M., Wieder, W. R., Xu, C., Ali, A. A., Badger, A. M., Bisht, G., van den Broeke, M., Brunke, M. A., Burns, S. P., Buzan, J., Clark, M., Craig, A., Dahlin, K., Drewniak, B., Fisher, J. B., Flanner, M., Fox, A. M., Gentine, P., Hoffman, F., Keppel-Aleks, G., Knox, R., Kumar, S., Lenaerts, J., Leung, L. R., Lipscomb, W. H., Lu, Y., Pandey, A., Pelletier, J. D., Perket, J., Randerson, J. T., Ricciuto, D. M., Sanderson, B. M., Slater, A., Subin, Z. M., Tang, J., Thomas, R. Q., Martin, M. V., and Zeng, X.: The Community Land Model Version 5: Description of New Features, Benchmarking, and Impact of Forcing Uncertainty, Journal of Advances in Modeling Earth Systems, 11, 4245–4287, https://doi.org/10.1029/2018MS001583, 2019.

Lee, S.-H., Gordon, H., Yu, H., Lehtipalo, K., Haley, R., Li, Y., and Zhang, R.: New Particle Formation in the Atmosphere: From Molecular Clusters to Global Climate, Journal of Geophysical Research: Atmospheres, 124, 7098–7146, https://doi.org/10.1029/2018JD029356, 2019.

Lee, Y. H., Pierce, J. R., and Adams, P. J.: Representation of Nucleation Mode Microphysics in a Global Aerosol Model with Sectional Microphysics, Geoscientific Model Development, 6, 1221–1232, https://doi.org/10.5194/gmd-6-1221-2013, 2013.

Lehtinen, K. E. J., Dal Maso, M., Kulmala, M., and Kerminen, V.-M.: Estimating Nucleation Rates from Apparent Particle Formation Rates and Vice Versa: Revised Formulation of the Kerminen–Kulmala Equation, Journal of Aerosol Science, 38, 988–994, https://doi.org/10.1016/j.jaerosci.2007.06.009, 2007.

Liu, X., Penner, J. E., and Herzog, M.: Global Modeling of Aerosol Dynamics: Model Description, Evaluation, and Interactions between Sulfate and Nonsulfate Aerosols, Journal of Geophysical Research: Atmospheres, 110, https://doi.org/10.1029/2004JD005674, 2005.

Makkonen, R., Seland, Ø., Kirkevåg, A., Iversen, T., and Kristjánsson, J. E.: Evaluation of Aerosol Number Concentrations in NorESM with Improved Nucleation Parameterization, Atmos. Chem. Phys., 14, 5127–5152, https://doi.org/10.5194/acp-14-5127-2014, 2014.

Mamali, D., Mikkilä, J., Henzing, B., Spoor, R., Ehn, M., Petäjä, T., Russchenberg, H., and Biskos, G.: Long-Term Observations of the Background Aerosol at Cabauw, The Netherlands, Science of The Total Environment, 625, 752–761, https://doi.org/10.1016/j.scitotenv.2017.12.136, 2018.

Mann, G. W., Carslaw, K. S., Spracklen, D. V., Ridley, D. A., Manktelow, P. T., Chipperfield, M. P., Pickering, S. J., and Johnson, C. E.: Description and Evaluation of GLOMAP-Mode: A Modal Global Aerosol Microphysics Model for the UKCA Composition-Climate Model, Geoscientific Model Development, 3, 519–551, https://doi.org/10.5194/gmd-3-519-2010, 2010.

Neale, R. B., Gettelman, A., Park, S., Chen, C.-c., Lauritzen, P. H., Williamson, D. L., Conley, A. J., Kinnison, D., Marsh, D., Smith, A. K., Vitt, F., Garcia, R., Lamarque, J.-f., Mills, M., Tilmes, S., Morrison, H., Cameron-smith, P., Collins, W. D., Iacono, M. J., Easter, R. C., Liu, X., Ghan, S. J., Rasch, P. J., and a Taylor, M.: Description of the NCAR Community Atmosphere Model (CAM 5.0). NCAR Technical Notes., Ncar/Tn-464+Str, p. 214, https://doi.org/10.5065/D6N877R0., 2012.

https://doi.org/10.5194/gmd-2020-357
Preprint. Discussion started: 12 November 2020

Olenius, T. and Riipinen, I.: Molecular-Resolution Simulations of New Particle Formation: Evaluation of Common Assumptions Made in Describing Nucleation in Aerosol Dynamics Models, Aerosol Science and Technology, 51, 397–408, https://doi.org/10.1080/02786826.2016.1262530, 2017.

Paasonen, P., Nieminen, T., Asmi, E., Manninen, H. E., Petäjä, T., Plass-Dülmer, C., Flentje, H., Birmili, W., Wiedensohler, A., Hõrrak, U., Metzger, A., Hamed, A., Laaksonen, A., Facchini, M. C., Kerminen, V.-M., and Kulmala, M.: On the Roles of Sulphuric Acid and Low-Volatility Organic Vapours in the Initial Steps of Atmospheric New Particle Formation, Atmos. Chem. Phys., 10, 11 223–11 242, https://doi.org/10.5194/acp-10-11223-2010, 2010.

Riccobono, F., Schobesberger, S., Scott, C. E., Dommen, J., Ortega, I. K., Rondo, L., Almeida, J., Amorim, A., Bianchi, F., Breitenlechner, M., David, A., Downard, A., Dunne, E. M., Duplissy, J., Ehrhart, S., Flagan, R. C., Franchin, A., Hansel, A., Junninen, H., Kajos, M., Keskinen, H., Kupc, A., Kürten, A., Kvashin, A. N., Laaksonen, A., Lehtipalo, K., Makhmutov, V., Mathot, S., Nieminen, T., Onnela, A., Petäjä, T., Praplan, A. P., Santos, F. D., Schallhart, S., Seinfeld, J. H., Sipilä, M., Spracklen, D. V., Stozhkov, Y., Stratmann, F., Tomé, A., Tsagkogeorgas, G., Vaattovaara, P., Viisanen, Y., Vrtala, A., Wagner, P. E., Weingartner, E., Wex, H., Wimmer, D., Carslaw, K. S., Curtius, J., Donahue, N. M., Kirkby, J., Kulmala, M., Worsnop, D. R., and Baltensperger, U.: Oxidation Products of Biogenic Emissions Contribute to Nucleation of Atmospheric Particles, Science, 344, 717–721, https://doi.org/10.1126/science.1243527, 2014.

Riipinen, I., Pierce, J. R., Yli-Juuti, T., Nieminen, T., Häkkinen, S., Ehn, M., Junninen, H., Lehtipalo, K., Petäjä, T., Slowik, J., Chang, R., Shantz, N. C., Abbatt, J., Leaitch, W. R., Kerminen, V.-M., Worsnop, D. R., Pandis, S. N., Donahue, N. M., and Kulmala, M.: Organic Condensation: A Vital Link Connecting Aerosol Formation to Cloud Condensation Nuclei (CCN) Concentrations, Atmospheric Chemistry and Physics, 11, 3865–3878, https://doi.org/10.5194/acp-11-3865-2011, 2011.

Schutgens, N. a. J. and Stier, P.: A Pathway Analysis of Global Aerosol Processes, Atmospheric Chemistry and Physics, 14, 11 657–11 686, https://doi.org/10.5194/acp-14-11657-2014, 2014.

Seinfeld, J. H. and Pandis, S. N.: Atmospheric Chemistry and Physics from Air Pollution to Climate Change, John Wiley, New York, 1998.

Seland, ø., Iversen, T., KirkevåG, A., and Storelvmo, T.: Aerosol-Climate Interactions in the CAM-Oslo Atmospheric GCM and Investigation of Associated Basic Shortcomings, Tellus A, 60, 459–491, https://doi.org/10.1111/j.1600-0870.2008.00318.x, 2008.

Seland, Ø., Bentsen, M., Olivié, D., Toniazzo, T., Gjermundsen, A., Graff, L. S., Debernard, J. B., Gupta, A. K., He, Y., Kirkevåg, A., Schwinger, J., Tjiputra, J., Aas, K. S., Bethke, I., Fan, Y., Gao, S., Griesfeller, J., Grini, A., Guo, C., Ilicak, M., Karset, I. H. H., Landgren, O., Liakka, J., Moree, A., Moseid, K. O., Nummelin, A., Spensberger, C., Tang, H., Zhang, Z., Heinze, C., Iversen, T., and Schulz, M.: NorESM2 Source Code as Used for CMIP6 Simulations, Zenodo, https://doi.org/10.5281/zenodo.3760870, 2020a.

Seland, Ø., Bentsen, M., Seland Graff, L., Olivié, D., Toniazzo, T., Gjermundsen, A., Debernard, J. B., Gupta, A. K., He, Y., Kirkevåg, A., Schwinger, J., Tjiputra, J., Schancke Aas, K., Bethke, I., Fan, Y., Griesfeller, J., Grini, A., Guo, C., Ilicak, M., Hafsahl Karset, I. H., Landgren, O., Liakka, J., Onsum Moseid, K., Nummelin, A., Spensberger, C., Tang, H., Zhang, Z., Heinze, C., Iverson, T., and Schulz, M.: The Norwegian Earth System Model, NorESM2 – Evaluation of theCMIP6 DECK and Historical Simulations, Geoscientific Model Development Discussions, pp. 1–68, https://doi.org/10.5194/gmd-2019-378, 2020b.

Semeniuk, K. and Dastoor, A.: Current State of Aerosol Nucleation Parameterizations for Air-Quality and Climate Modeling, Atmospheric Environment, 179, 77–106, https://doi.org/10.1016/j.atmosenv.2018.01.039, 2018.

Sporre, M. K., Blichner, S. M., Karset, I. H. H., Makkonen, R., and Berntsen, T. K.: BVOC–Aerosol–Climate Feedbacks Investigated Using NorESM, Atmospheric Chemistry and Physics, 19, 4763–4782, https://doi.org/10.5194/acp-19-4763-2019, 2019.

https://doi.org/10.5194/gmd-2020-357
Preprint. Discussion started: 12 November 2020

Sporre, M. K., Blichner, S. M., Schrödner, R., Karset, I. H. H., Berntsen, T. K., van Noije, T., Bergman, T., O'Donnell, D., and Makkonen, R.: Large Difference in Aerosol Radiative Effects from BVOC-SOA Treatment in Three ESMs, Atmospheric Chemistry and Physics Discussions, pp. 1–38, https://doi.org/10.5194/acp-2019-1166, 2020.

Spracklen, D. V., Pringle, K. J., Carslaw, K. S., Chipperfield, M. P., and Mann, G. W.: A Global Off-Line Model of Size-Resolved Aerosol Microphysics: I. Model Development and Prediction of Aerosol Properties, Atmospheric Chemistry and Physics, 5, 2227–2252, https://doi.org/10.5194/acp-5-2227-2005, 2005.

Stier, P., Feichter, J., Kinne, S., Kloster, S., Vignati, E., Wilson, J., Ganzeveld, L., Tegen, I., Werner, M., Balkanski, Y., Schulz, M., Boucher, O., Minikin, A., and Petzold, A.: The Aerosol-Climate Model ECHAM5-HAM, Atmospheric Chemistry and Physics, 5, 1125–1156, https://doi.org/10.5194/acp-5-1125-2005, 2005.

Sullivan, R. C., Crippa, P., Matsui, H., Leung, L. R., Zhao, C., Thota, A., and Pryor, S. C.: New Particle Formation Leads to Cloud Dimming, npj Climate and Atmospheric Science, 1, 1–9, https://doi.org/10.1038/s41612-018-0019-7, 2018.

Tie, X., Brasseur, G., Emmons, L., Horowitz, L., and Kinnison, D.: Effects of Aerosols on Tropospheric Oxidants: A Global Model Study, Journal of Geophysical Research: Atmospheres, 106, 22 931–22 964, https://doi.org/10.1029/2001JD900206, 2001.

Tröstl, J., Chuang, W. K., Gordon, H., Heinritzi, M., Yan, C., Molteni, U., Ahlm, L., Frege, C., Bianchi, F., Wagner, R., Simon, M., Lehtipalo, K., Williamson, C., Craven, J. S., Duplissy, J., Adamov, A., Almeida, J., Bernhammer, A.-K., Breitenlechner, M., Brilke, S., Dias, A., Ehrhart, S., Flagan, R. C., Franchin, A., Fuchs, C., Guida, R., Gysel, M., Hansel, A., Hoyle, C. R., Jokinen, T., Junninen, H., Kangasluoma, J., Keskinen, H., Kim, J., Krapf, M., Kürten, A., Laaksonen, A., Lawler, M., Leiminger, M., Mathot, S., Möhler, O., Nieminen, T., Onnela, A., Petäjä, T., Piel, F. M., Miettinen, P., Rissanen, M. P., Rondo, L., Sarnela, N., Schobesberger, S., Sengupta, K., Sipilä, M., Smith, J. N., Steiner, G., Tomè, A., Virtanen, A., Wagner, A. C., Weingartner, E., Wimmer, D., Winkler, P. M., Ye, P., Carslaw, K. S., Curtius, J., Dommen, J., Kirkby, J., Kulmala, M., Riipinen, I., Worsnop, D. R., Donahue, N. M., and Baltensperger, U.: The Role of Low-Volatility Organic Compounds in Initial Particle Growth in the Atmosphere, Nature, 533, 527–531, https://doi.org/10.1038/nature18271, 2016.

Twomey, S.: Pollution and the Planetary Albedo, Atmospheric Environment (1967), 8, 1251–1256, https://doi.org/10.1016/0004-6981(74)90004-3, 1974.

Vehkamäki, H., Kulmala, M., Napari, I., Lehtinen, K. E. J., Timmreck, C., Noppel, M., and Laaksonen, A.: An Improved Parameterization for Sulfuric Acid–Water Nucleation Rates for Tropospheric and Stratospheric Conditions, Journal of Geophysical Research: Atmospheres, 107, 4622, https://doi.org/10.1029/2002JD002184, 2002.

Vignati, E., Wilson, J., and Stier, P.: M7: An Efficient Size-Resolved Aerosol Microphysics Module for Large-Scale Aerosol Transport Models: AEROSOL MICROPHYSICS MODULE, Journal of Geophysical Research: Atmospheres, 109, n/a–n/a, https://doi.org/10.1029/2003JD004485, 2004.

Westervelt, D. M., Pierce, J. R., Riipinen, I., Trivitayanurak, W., Hamed, A., Kulmala, M., Laaksonen, A., Decesari, S., and Adams, P. J.: Formation and Growth of Nucleated Particles into Cloud Condensation Nuclei: Model–Measurement Comparison, Atmospheric Chemistry and Physics, 13, 7645–7663, https://doi.org/10.5194/acp-13-7645-2013, 2013.

Westervelt, D. M., Pierce, J. R., and Adams, P. J.: Analysis of Feedbacks between Nucleation Rate, Survival Probability and Cloud Condensation Nuclei Formation, Atmospheric Chemistry and Physics, 14, 5577–5597, https://doi.org/10.5194/acp-14-5577-2014, 2014.

https://doi.org/10.5194/gmd-2020-357
Preprint. Discussion started: 12 November 2020

Geoscientific Model Development Discussions
Open Access
EGU

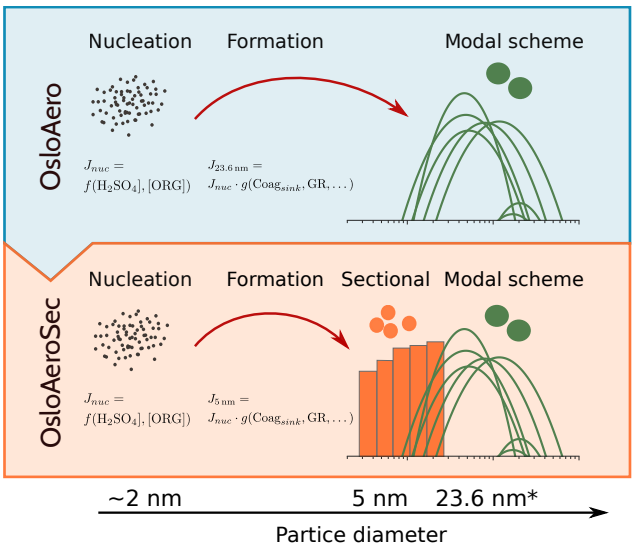

Figure 1. Illustration of changes from OsloAero to OsloAeroSec. In both versions, the nucleation rate is calculated at around 2 nm followed by a calculation of the formation rate (the particles surviving) at 5 nm and 23.6 nm in OsloAeroSec and OsloAero respectively, with Lehtinen et al. (2007). In OsloAero, these particles are inserted directly into the modal scheme, while in OsloAeroSec, the particles are inserted into the sectional scheme where they can be affected by growth and coagulation over time and space. Finally, the particles in the sectional scheme are moved from the last bin of the sectional scheme to the modal scheme. *23.6 nm is the number median diameter of the mode the particles from the sectional scheme are moved to, but particles are actually grown to the volume median diameter before they are moved to the modal scheme in order to conserve mass.

https://doi.org/10.5194/gmd-2020-357
Preprint. Discussion started: 12 November 2020

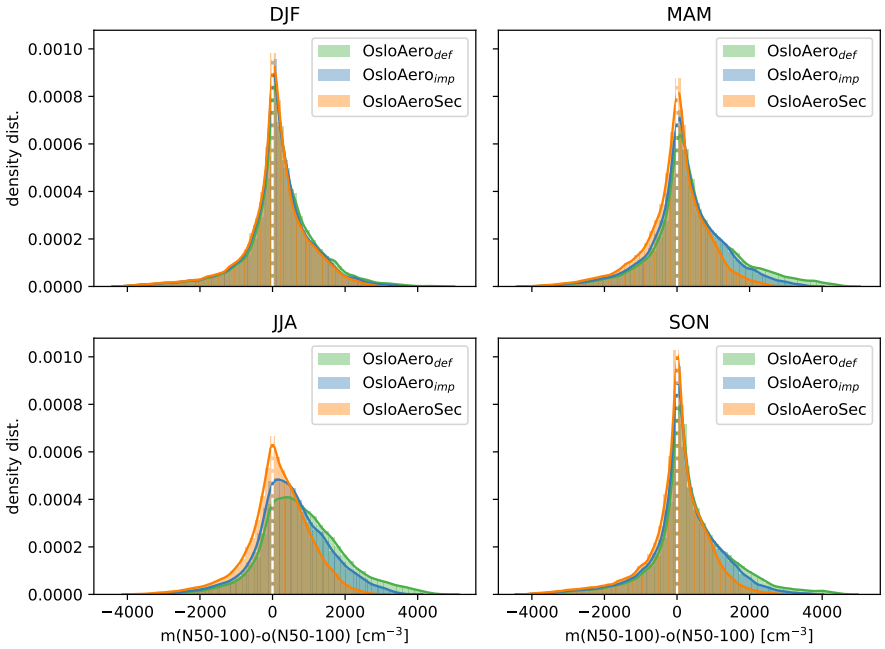

Figure 2. Seasonal distribution of modelled N_{50-100} minus observed N_{50-100} for all EUSAAR stations (Asmi et al., 2011). We use hourly resolution and all available station data is is included.

https://doi.org/10.5194/gmd-2020-357
Preprint. Discussion started: 12 November 2020

Geoscientific Model Development Discussions
Open Access
EGU

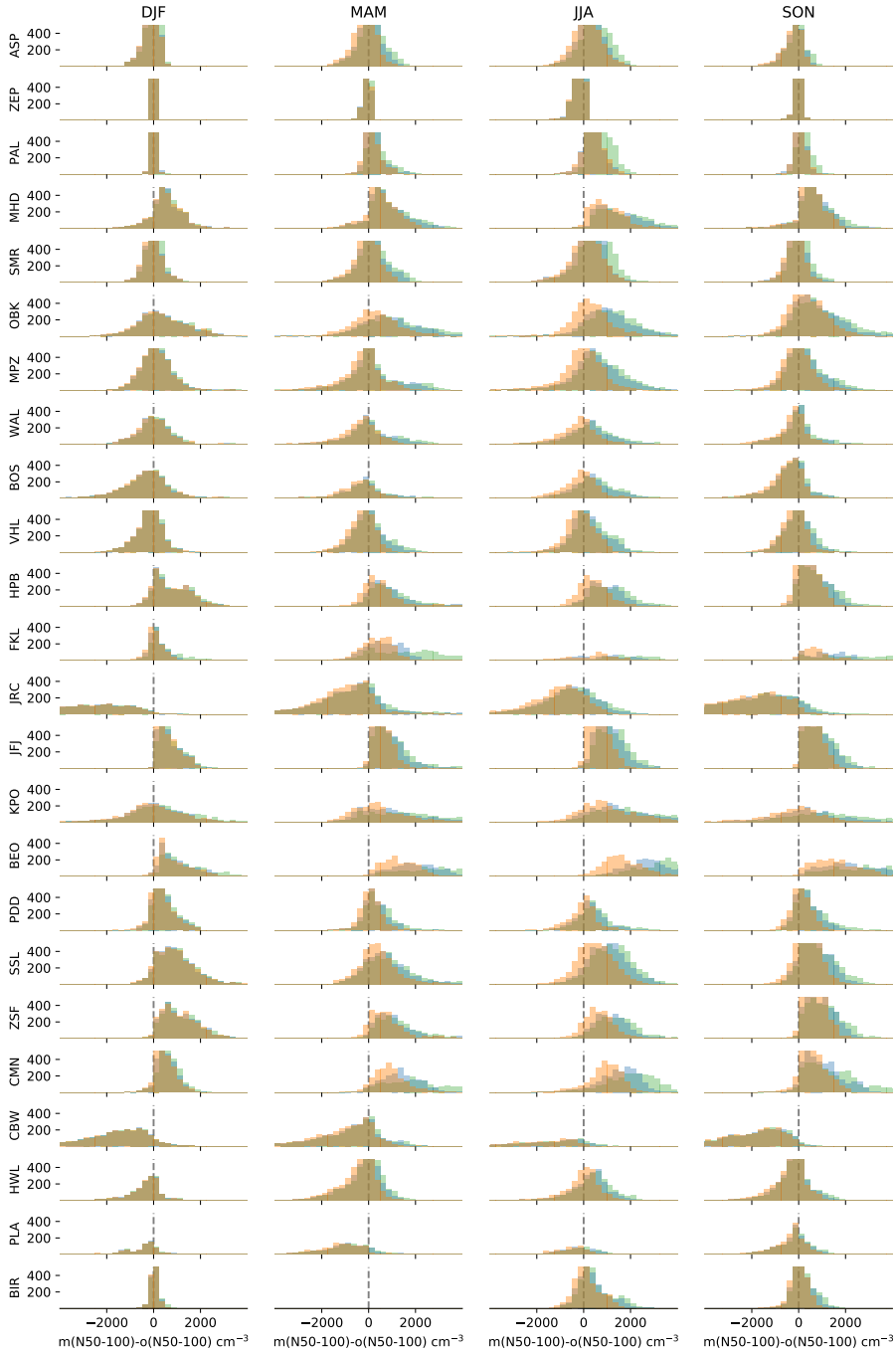

Figure 3. Histogram of modelled N_{50-100} minus observed N_{50-100} for each season and EUSAAR station (Asmi et al., 2011). We use hourly resolution and all available station data is is included. Zeppelin (ZEP), Mace Head (MHD), Aspvreten (ASP), SMEAR II (SMR), Pallas (PAL), Kosetice (OBK), Vavihill (VHL), Melpitz (MPZ), Waldhof (WAL), Bösel (BOS), Hohenpeissenberg (HPB), K-Puszta (KPO), JRC-Ispra (JRC), Finokalia (FKL), Jungfraujoch (JFJ), Schauinsland (SSL), Zugspitze (ZSF), Monte Cimone (CMN), BEO Moussala (BEO), Puy de Dôme (PDD) Preila (PLA), Birkenes b (BIR), Harwell (HWL), Cabauw (CBW).

https://doi.org/10.5194/gmd-2020-357
Preprint. Discussion started: 12 November 2020

Geoscientific Model Development Discussions
Open Access
EGU

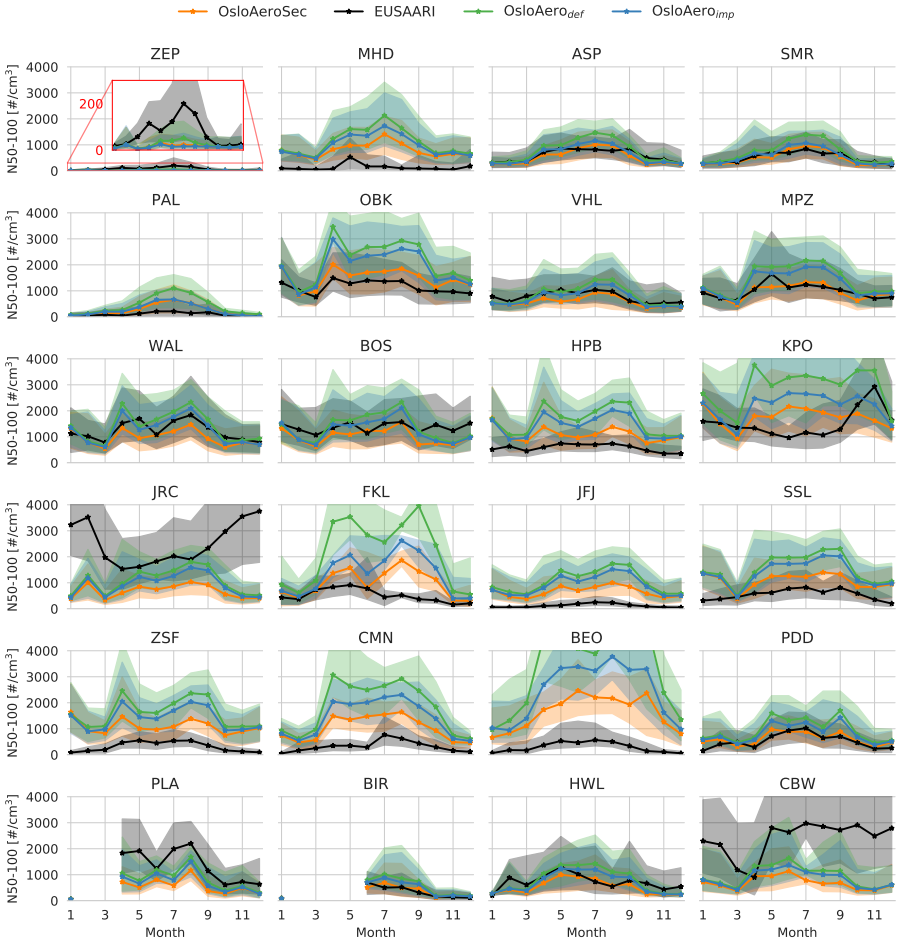

Figure 4. N_{50-100} monthly median (solid line) and percentiles (shaded, 16th to 84th) for each station for each model version and the observed values (Asmi et al., 2011). Stations where the full graph is not shown due to the axis limits are shown in full in Fig. S1.

https://doi.org/10.5194/gmd-2020-357
Preprint. Discussion started: 12 November 2020

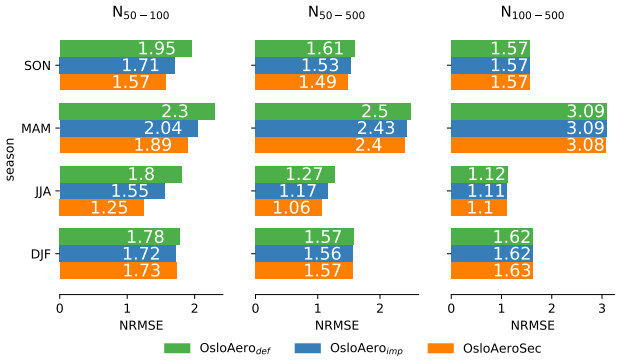

Figure 5. Normalized root mean square error (NRMSE) for each season and each model version compared to the EUSAAR dataset (Asmi et al., 2011). The root mean square error is normalized by the mean of the observed values.

https://doi.org/10.5194/gmd-2020-357
Preprint. Discussion started: 12 November 2020

Geoscientific Model Development Discussions
Open Access
EGU

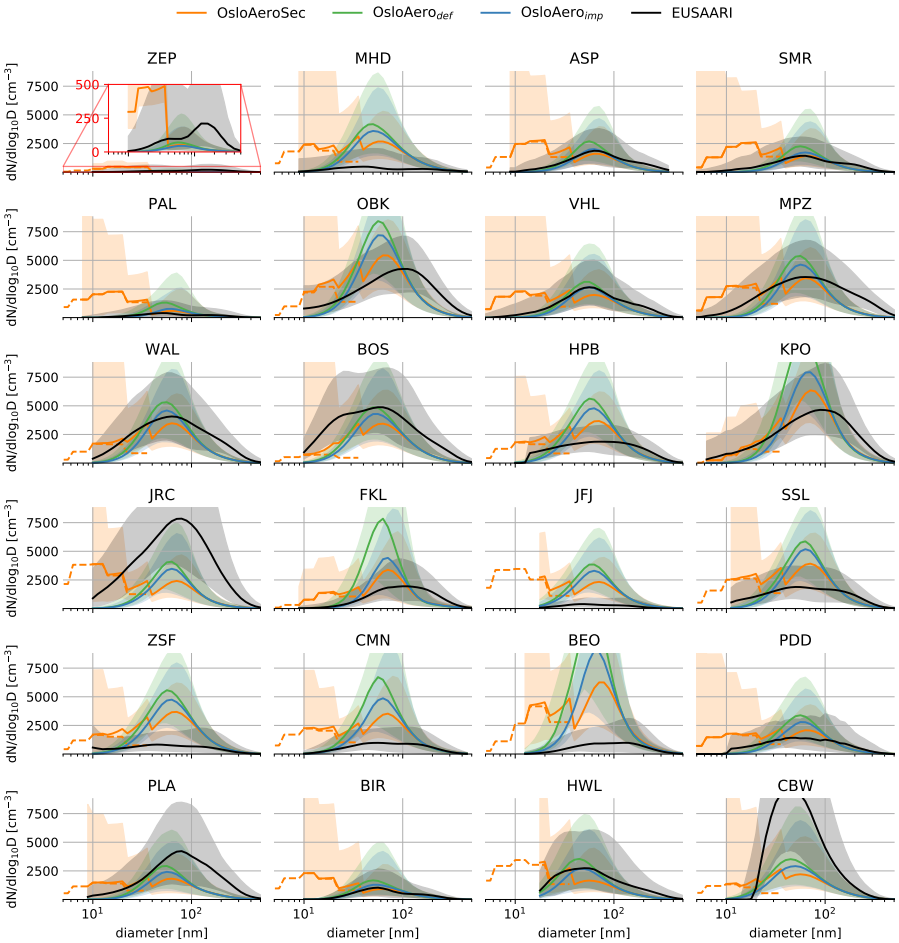

Figure 6. Median (solid line) particle number size distribution and shading from 16th to 84th percentiles for observations (Asmi et al., 2011) and models. All data when and where observations are available is included.

https://doi.org/10.5194/gmd-2020-357
Preprint. Discussion started: 12 November 2020

Geoscientific Model Development Discussions
Open Access
EGU

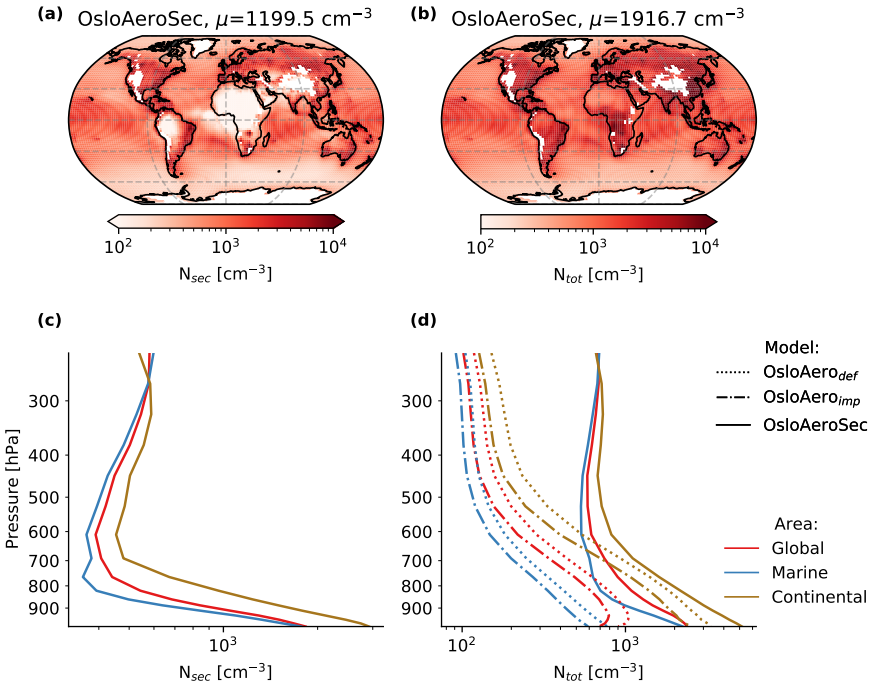

Figure 7. Modelled particle number concentrations. The top panels shows maps near-surface average concentrations for N_{sec} (a) and N_{tot} (b) in OsloAeroSec. The bottom panels show average profiles globally, over continents (continental) and over ocean (marine) for N_{sec} (c) and N_{tot} (d). In d, $OsloAero_{def}$ and $OsloAero_{imp}$ are also included.

https://doi.org/10.5194/gmd-2020-357
Preprint. Discussion started: 12 November 2020

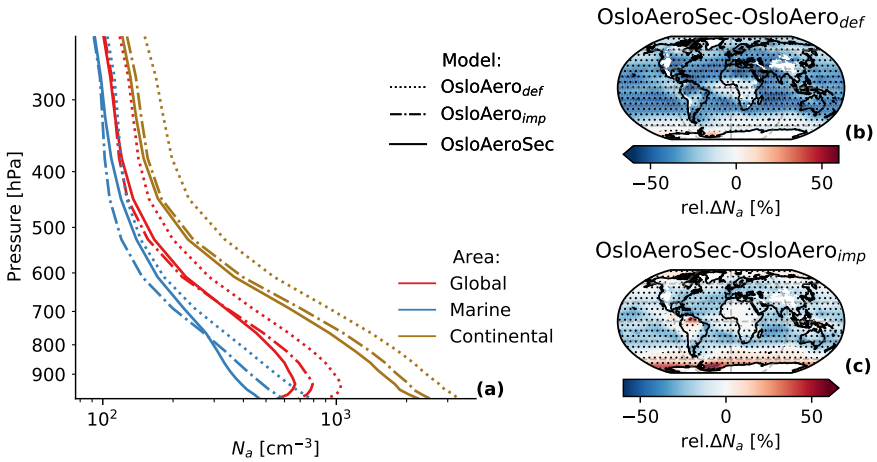

Figure 8. Comparison of N_a from OsloAero$_{def}$ and OsloAero$_{imp}$ to OsloAeroSec. Panel a shows profiles for mean of regions (global, marine and continental) for the model versions. Panel b and c show the relative difference in near-surface mean of OsloAeroSec to OsloAero$_{def}$ and OsloAero$_{imp}$, respectively. Areas where the difference is significant (95%) are marked with dots.

https://doi.org/10.5194/gmd-2020-357
Preprint. Discussion started: 12 November 2020

Geoscientific Model Development Discussions
Open Access
EGU

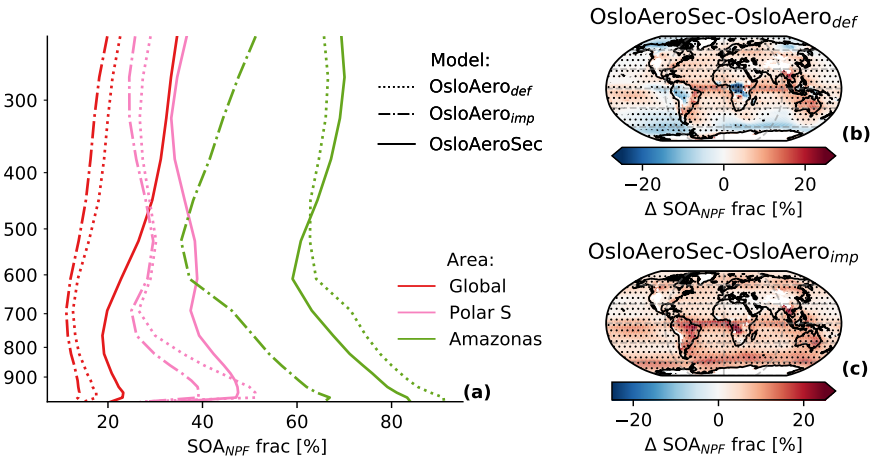

Figure 9. The SOA fraction of N_{NPF} mass (SOA_{NPF}), i.e. the fraction of the growth of the particles before they reach the modal scheme which is due to organics. Panel a shows profiles for regions (Global, Polar S(outh), Amazonas) with each model. Panels b and c show the difference in near-surface mean values for OsloAeroSec minus $OsloAero_{def}$ and $OsloAero_{imp}$ (c), respectively. Areas where the difference is significant (95%) are marked with dots.

https://doi.org/10.5194/gmd-2020-357
Preprint. Discussion started: 12 November 2020

Geoscientific Model Development Discussions
Open Access
EGU

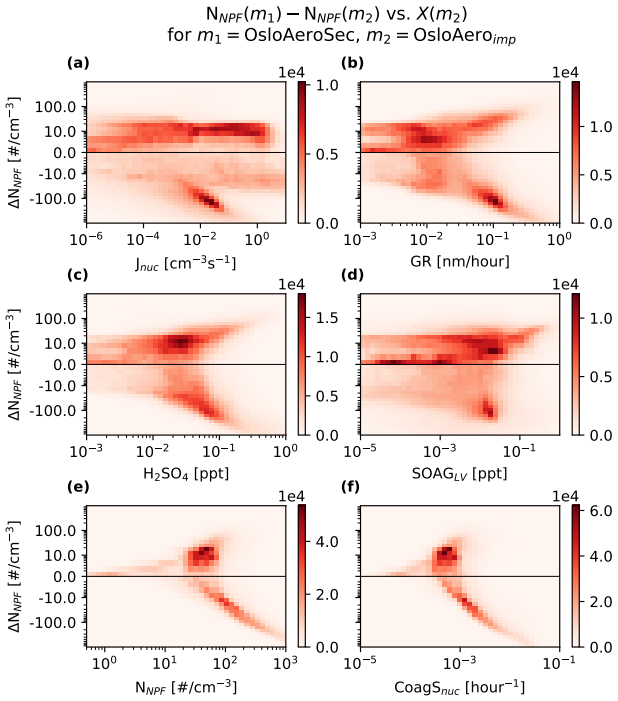

Figure 10. Two-dimensional histogram of the relation between various factors in the original model run OsloAero$_{imp}$, and the change in number of particles from NPF, N_{NPF} between OsloAeroSec and OsloAero$_{imp}$. The color shows the number of model grid cells which fall within the x,y-range using monthly mean files. Only grid cells below 100 hPa are included. The values on the x-scale are the nucleation rate (a), the growth rate of newly formed particles (b), the mixing ratio of H_2SO_4 (c), the mixing ratio of $SOAG_{LV}$ (d), the concentration of particles from NPF (e) and the coagulation sink for newly formed particles (f). See Fig. S12 for the same plot, but with N_{NPF} from OsloAero$_{imp}$, i.e. not the change.

https://doi.org/10.5194/gmd-2020-357
Preprint. Discussion started: 12 November 2020

Geoscientific Model Development Discussions
Open Access
EGU

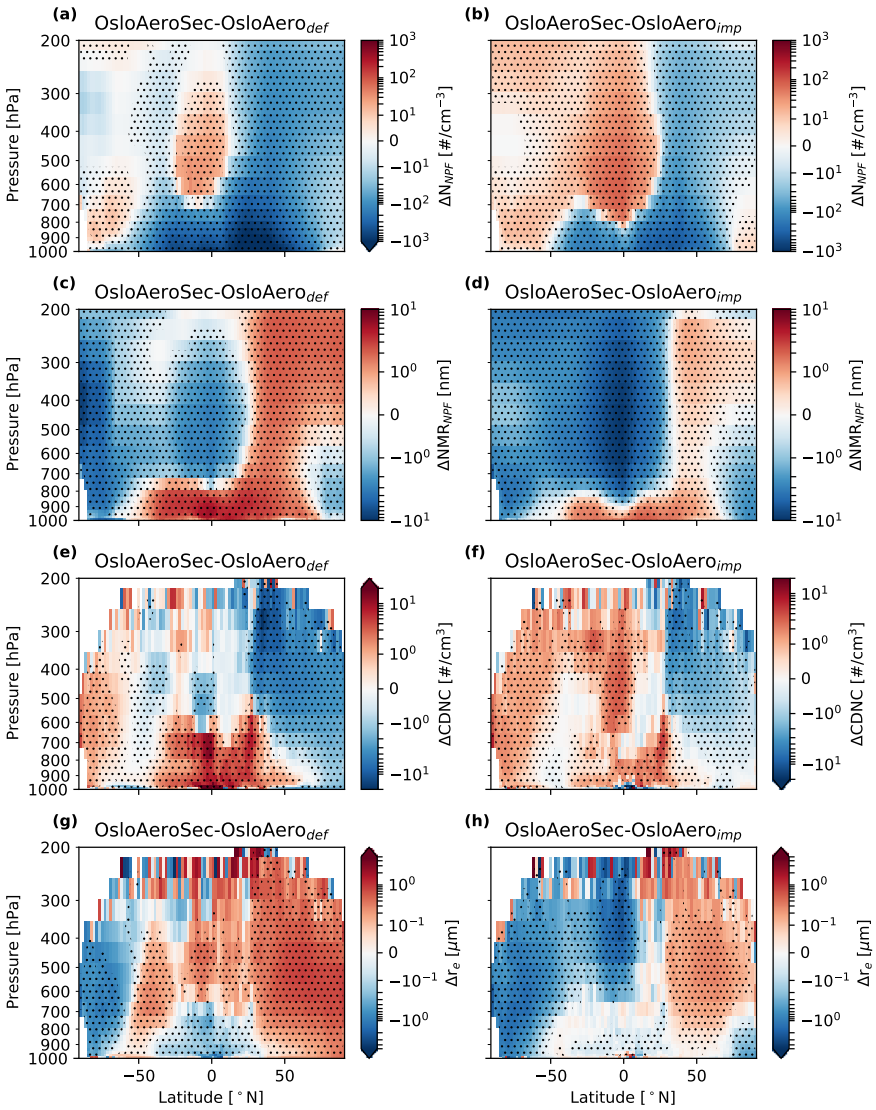

Figure 11. Zonally averaged change between OsloAeroSec and OsloAero$_{def}$ (left column) and OsloAeroSec and OsloAero$_{imp}$ (right column) in in N_{NPF} (a and b), number median radius for NPF-particles (NMR_{NPF}, c and d), cloud droplet number concentration (CDNC, e and f) and cloud drop number concentration (r_e, g and h). Areas where the difference is significant (95%) are marked with dots.

https://doi.org/10.5194/gmd-2020-357
Preprint. Discussion started: 12 November 2020

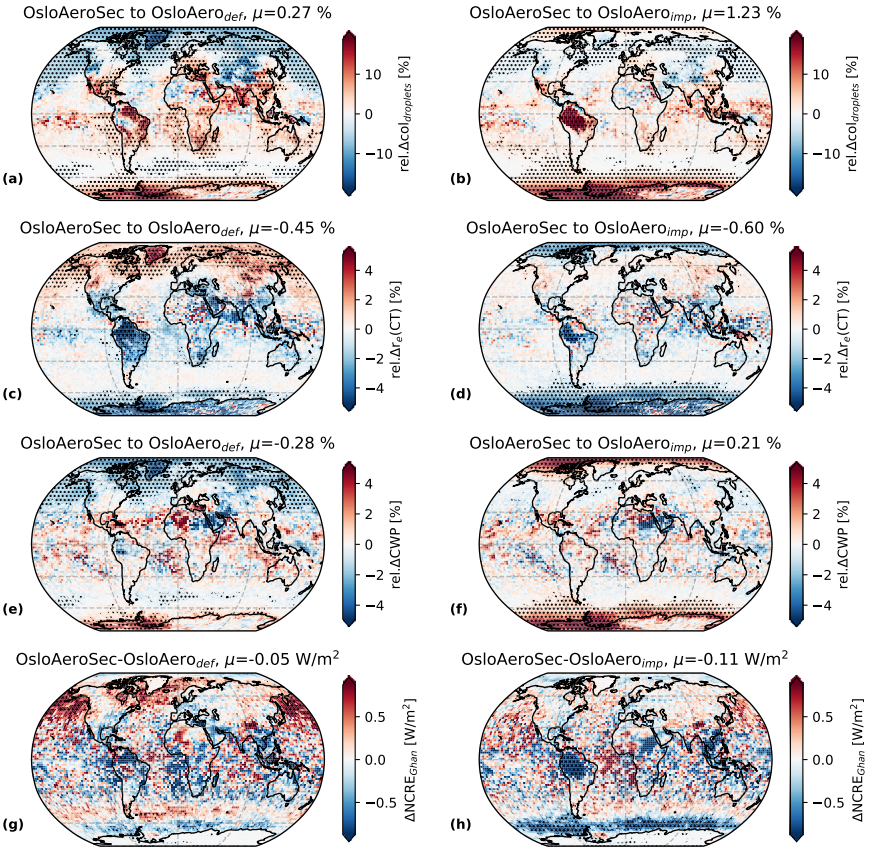

Figure 12. Changes to cloud properties. The left column shows the difference between OsloAeroSec and OsloAero$_{def}$ and the right column shows the difference between OsloAeroSec and OsloAero$_{imp}$. Panels a and b show the relative difference in cloud top droplet number concentration (CDNC(CT)), panels c and d show the relative difference in effective droplet radius at cloud top (r_r(CT)), panels e and f show the relative difference in cloud water path (CWP) and finally panel g and h show the difference in net cloud radiative effect (NCRE) calculated as recommended in Ghan (2013). Areas where the difference is significant (95%) are marked with dots.

https://doi.org/10.5194/gmd-2020-357
Preprint. Discussion started: 12 November 2020

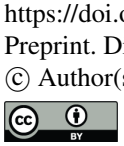

Geoscientific Model Development Discussions
Open Access
EGU

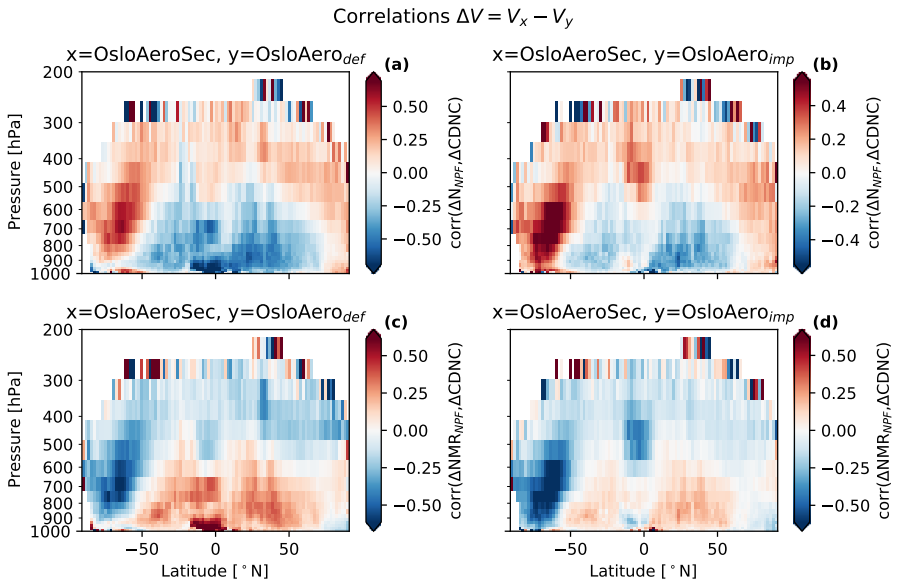

Figure 13. Correlations between the change in CDNC and N_{NPF} (top) and number median radius of the NPF particles (NMR_{NPF})(bottom). Plots on the left side are for the difference OsloAeroSec $-$ OsloAero$_{def}$ ($\Delta V = V_{\text{OsloAeroSec}} - V_{\text{OsloAero}_{def}}$ for variable V) and plots on the right are for OsloAeroSec $-$ OsloAero$_{imp}$.

https://doi.org/10.5194/gmd-2020-357
Preprint. Discussion started: 12 November 2020

Geoscientific Model Development Discussions
Open Access
EGU

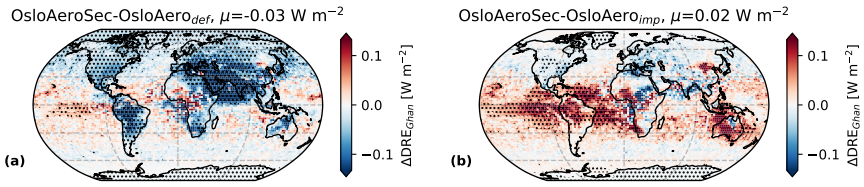

Figure 14. Change in direct aerosol effect for OsloAeroSec minus OsloAero$_{def}$ (a) and OsloAeroSec minus OsloAero$_{imp}$ (b). The direct radiative effect is calculated as recommended by Ghan (2013). Areas where the difference is significant (95 %) are marked with dots.

https://doi.org/10.5194/gmd-2020-357
Preprint. Discussion started: 12 November 2020

Geoscientific Model Development Discussions
Open Access
EGU

Table 1. Simulation overview. See detailed description in section 3.

Simulation	Nucleation parameterization	Oxidant treatment	Early growth treatment
OsloAeroSec	$A_3[H_2SO_4]^2 \times$ [ELVOC] *	Improved diurnal variation	Lehtinen et al. (2007) + sectional scheme
OsloAero$_{imp}$	$A_3[H_2SO_4]^2 \times$ [ELVOC] *	Improved diurnal variation	Lehtinen et al. (2007)
OsloAero$_{def}$	$A_1[H_2SO_4]$ + A_2[ELVOC] †	Default diurnal variation	Lehtinen et al. (2007)

$A_1 = 6.1 \times 10^{-7}\ s^{-1}$
$A_2 = 3.9 \times 10^{-8}\ s^{-1}$
$A_3 = 3.27 \times 10^{-21}\ cm^6 s^{-1}$
* Riccobono et al. (2014)
† Paasonen et al. (2010)

https://doi.org/10.5194/gmd-2020-357
Preprint. Discussion started: 12 November 2020

Geoscientific Model Development Discussions
Open Access
EGU

Table 2. Region overview. These regions are used to create vertical average profiles.

Region name	Description	Latitudes	Longitudes
Continental	Grid boxes with >50% land		
Marine	Grid boxes with <50% land		
Global			
Polar N		66.5 – 90 °N	180 °W – 180 °E
Polar S		66.5 – 90 °S	180 °W – 180 °E
Amazonas		16 °S – 2 °N	74 – 50 °W

https://doi.org/10.5194/gmd-2020-357
Preprint. Discussion started: 12 November 2020

Geoscientific Model Development Discussions
Open Access
EGU

Table 3. Model variable definitions.

Variable name	Definition
N_a	Number of particles excluding those in the sectional scheme
N_{tot}	Number of particles including those in the sectional scheme
N_{sec}	Number of particles in the sectional scheme
N_{NPF}	Number of particles from NPF excluding those in the sectional scheme
$N_{d_1-d_2}$	Number of particles with diameter d such that $d_1 \leq d \leq d_2$
N_{d_1}	Number of particles with diameter d such that $d_1 \leq d$

Paper IV

Reduced effective radiative forcing from cloud-aerosol interactions (ERF_{aci}) with improved treatment of early aerosol growth in an Earth System Model

Sara M. Blichner, Moa Sporre, and Terje K. Berntsen

Submitted to Atmospheric Chemistry and Physics , 2021

IV

Reduced effective radiative forcing from cloud-aerosol interactions (ERF_{aci}) with improved treatment of early aerosol growth in an Earth System Model

Sara M. Blichner[1], Moa K. Sporre[2], and Terje K. Berntsen[1]

[1]Departmenet of Geosciences and Centre for Biogeochemistry in the Anthroposcene, University of Oslo, Oslo, Norway
[2]Department of Physics, Lund University, Lund, Sweden

Correspondence: Sara Marie Blichner (s.m.blichner@geo.uio.no)

Abstract. Historically, aerosols of anthropogenic origin have offset some of the warming from increased atmospheric greenhouse gas concentrations. The strength of this negative aerosol forcing is, however, highly uncertain – especially the part originating from cloud-aerosol interactions. An important part of this uncertainty originates from our lack of knowledge about the pre-industrial aerosols and how many of these would have acted as cloud condensation nuclei (CCN). In order to simulate CCN concentrations in models, we must adequately model secondary aerosols, including new particle formation (NPF) and early growth, which contributes with a large part of atmospheric CCN. In this study, we investigate the effective radiative forcing (ERF) from cloud–aerosol interactions (ERF_{aci}) with an improved treatment of early particle growth, presented in (Blichner et al., 2020). We compare the improved scheme to the default scheme, OsloAero, both part of the atmospheric component of the Norwegian Earth System Model v2 (NorESM2). The improved scheme, OsloAeroSec, includes a sectional scheme that treats the growth of the particles from 5–39.6 nm which thereafter inputs the particles to the smallest mode in the pre-existing, modal aerosol scheme. The default scheme parameterizes the growth of particles from nucleation and up to the smallest mode, a process that can take several hours. The explicit treatment of the early growth in OsloAeroSec on the other hand, captures the changes in atmospheric condition during this growth time both in terms of air mass mixing, transport and condensation and coagulation.

We find that the ERF_{aci} with the sectional scheme is $-1.16\,\mathrm{Wm}^{-2}$, which is $0.13\,\mathrm{Wm}^{-2}$ weaker compared to the default scheme. This reduction originates from OsloAeroSec producing more particles than the default scheme in pristine, low-aerosol-concentration areas and less NPF particles in high-aerosol areas. We find, perhaps surprisingly, that NPF inhibits cloud droplet activation in polluted/high-aerosol-concentration regions because the NPF particles increase the condensation sink and reduces the growth of the larger particles which may otherwise activate. This means that in these high-aerosol regions, the model with lowest NPF – OsloAeroSec – will have highest cloud droplet activation and thus more reflective clouds. In pristine/low aerosol regions however, NPF enhances cloud droplet activation, because the NPF particles themselves tend to activate.

Lastly, we find that sulphate emissions in the present day simulations increase the hygroscopicity of the secondary aerosols compared to the pre-industrial simulations. This makes NPF particles more relevant for cloud droplet activation in the present day than the pre-industrial atmosphere, because the increased hygroscopicity means they can activate at smaller sizes.

1 Introduction

Since pre-industrial times, humans have significantly shaped our climate through emitting greenhouse gases to the atmosphere. However, the warming induced from these emissions has been masked by the cooling effects of anthropogenic emissions of aerosols and their precursors (Myhre et al., 2013). This cooling is highly uncertain and dominates the spread in estimates of radiative forcing and observationally based estimates of climate sensitivity (Myhre et al., 2013).

The present-day atmospheric aerosols state is challenging to fully characterize due to its fast-changing nature, making point observations hard to generalize. The pre-industrial atmosphere, however, is even more challenging since we cannot rely on direct observations, and thus is only accessible through putting our best knowledge of aerosol processes and sources into models. The pre-industrial atmospheric state is furthermore, very important for estimating the cooling by aerosol cloud interactions (Carslaw et al., 2013) because the cloud albedo is more sensitive to perturbations in a "cleaner" atmosphere (Carslaw et al., 2013; Twomey, 1991). There are two main reasons for this. Firstly, cloud droplets form around cloud condensation nuclei (CCN) when the air mass is cooled, normally through adiabatic lifting. The number of particles that will act as CCN and form cloud droplets is dependent on the maximum achieved supersaturation during the cloud formation and how many particles can activate at this supersaturation – which dependent on size and hygroscopicity. If there are many large CCN, then these will activate "early" during the cloud formation and constitute a water vapor sink which limits the maximum supersaturation and therefore the number of CCN which can activate. We will refer to this effect as supersaturation adjustment. Secondly, cloud albedo A increases with change in cloud droplet number concentration (CDNC) roughly as $dA/d\text{CDNC} = A(1-A)/(3\text{CDNC})$, which entails a lower increase in albedo with a higher baseline CDNC (Twomey, 1991; Carslaw et al., 2013). Therefore, an initial state with higher CCN concentration will be less sensitive to CCN perturbations than an initial state with lower CCN concentrations (Twomey, 1959; Bellouin et al., 2020; Carslaw et al., 2013).

One important, but poorly understood, process for adequately simulating the pre-industrial atmosphere is new particle formation (NPF), i.e. the formation and growth of new particles in the atmosphere which can grow to act as CCN. Roughly speaking, the efficiency of NPF – i.e. how many particles are formed per available condensate – in the pre-industrial atmosphere will determine if the aerosol mass is distributed as very few, very large particles or many smaller particles. Especially in a clean atmosphere, this can play a large role for CCN and CDNC concentrations. Over recent years, the understanding of the drivers of NPF has increased significantly due to improved instrumentation and extensive research (Kerminen et al., 2018; Lee et al., 2019). However, adequately capturing NPF in climate models is difficult due to the requirement for computational efficiency combined with the fine scale of the governing processes, in addition to incomplete scientific understanding of the mechanisms involved (Kerminen et al., 2018; Lee et al., 2019).

NPF starts with the formation of a cluster of molecules which must then activate with respect to the condensing atmospheric vapors and grow into larger sizes ($\sim$10 nm) (Kerminen et al., 2018; Semeniuk and Dastoor, 2018). Due to the Kelvin effect, few gases have low enough volatility to participate in the very first stages of NPF, while as the particles grow, more gases contribute (Semeniuk and Dastoor, 2018). During this growth, the particles are subject to coagulation with larger particles which constitute a loss in number concentration (Kerminen et al., 2018). The coagulation sink is approximately proportionally

to $1/d_p^m$, where d_p is the particle diameter and m is a parameter describing the background aerosol concentrations (typically 1.6-1.8) (Lehtinen et al., 2007). It is therefore important for successful NPF that the growth rate (GR) is high enough for the particles to quickly grow to larger sizes where the coagulation sink is lower (Lehtinen et al., 2007). Both Lee et al. (2013) and Olenius and Riipinen (2017) show that omitting explicit modelling of this early aerosol growth and rather parameterizing the survival percentage of particles (e.g. Kerminen and Kulmala, 2002; Lehtinen et al., 2007), lead to significant overestimation of particles. This is mainly because parameterizing the growth means assuming steady state conditions during the growth, i.e. that growth rate and coagulation sink are constant, there is no mixing and so on. This assumption is usually not appropriate, especially since the growth can take many hours or even grow over days.

The importance of adequately capturing NPF in modelling the pre-industrial atmosphere is illustrated in a study by Gordon et al. (2016), which shows a major reduction (27 %) in estimated forcing from cloud albedo change when including a nucleation pathway from pure biogenic organics. NPF is subject to several constraints which would indicate more efficient NPF in the pre-industrial atmosphere compared to the present day. Firstly, since the pre-existing aerosol concentrations and thus condensation sink will be lower, the pre-cursor concentrations are higher *per emissions* than in the present day atmosphere. In other words, the if sulphuric acid emissions in the pre-industrial and present day atmosphere were the same, the pre-industrial atmosphere would have higher sulphuric acid concentrations because the condensation sink will be lower. Secondly, the coagulation sink of the clusters and newly formed particles is smaller in a cleaner atmosphere (Carslaw et al., 2013; Gordon et al., 2017).

To better capture the early growth of particles from formation to CCN sizes, we have previously implemented a sectional scheme in the aerosol scheme, OsloAero, of the Norwegian earth system model (Blichner et al., 2020). We refer to the aerosol scheme with the sectional scheme as OsloAeroSec. OsloAeroSec includes 5 bins and 2 condensing species (H_2SO_4 and low volatile organics) and treats only the growth/loss of particles from formation at 5 nm and up to the pre-existing modal aerosol scheme at 39.6 nm diameter, in which climate (cloud/radiation) interactions are considered. See Fig. 1 for illustration of the scheme. This work was motivated by 1) the smallest mode in the aerosol scheme OsloAero6 is quite large (number median diameter 23.6 nm), meaning that the growth up to 23.6 nm is parameterized. As mentioned above, this has been shown to lead to significant overestimates of the particle formation (Lee et al., 2013; Olenius and Riipinen, 2017). 2) A sectional scheme explicitly grows the particles and does not a priori assume a shape to the size distribution. In this way it is more physically realistic than including e.g. a nucleation mode. Additionally, the sectional scheme allows for differentiating which organic vapors can contribute to the growth from 5 nm and upwards compared to from nucleation and up to 5 nm.

Our results presented in Blichner et al. (2020), show considerable improvement in the representation of CCN size particles (> 50 nm) compared to observations, significantly reducing the frequent high bias in the original model. This goes in line with Olenius and Riipinen (2017) and Lee et al. (2013). On the other hand, the sectional scheme shows an increase in particle number concentrations in remote areas like the polar regions and the free troposphere.

Motivated by both the improvement to the aerosol scheme, and the spatial difference in aerosol formation from the original scheme (remote versus polluted), we here investigate the implications of the growth treatment in OsloAeroSec for the pre-industrial and present-day atmosphere respectively and especially for the estimated cooling from aerosol–cloud interactions since pre-industrial times.

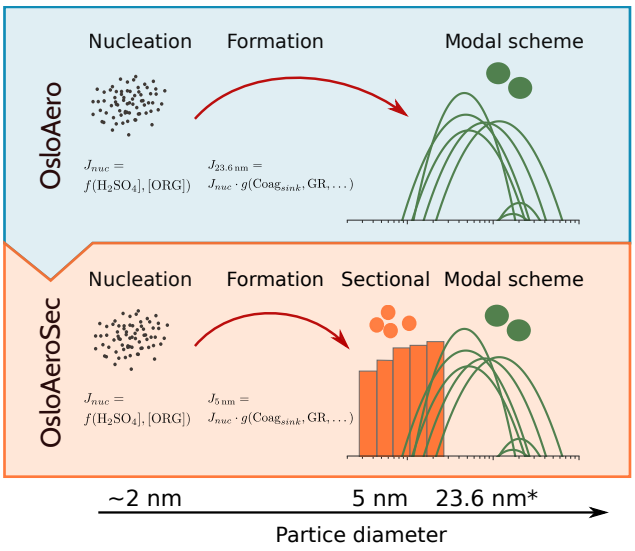

Figure 1. Illustration of changes from OsloAero to OsloAeroSec. In both versions, the nucleation rate is calculated at around 2 nm followed by a calculation of the formation rate (the particles surviving) at 5 nm and 23.6 nm in OsloAeroSec and OsloAero respectively, with Lehtinen et al. (2007). In OsloAero, these particles are inserted directly into the modal scheme, while in OsloAeroSec, the particles are inserted into the sectional scheme where they can be affected by growth and coagulation over time and space. Finally, the particles in the sectional scheme are moved from the last bin of the sectional scheme to the modal scheme. *23.6 nm is the number median diameter of the mode the particles from the sectional scheme are moved to, but particles are actually grown to the volume median diameter before they are moved to the modal scheme in order to conserve mass. From (Blichner et al., 2020).

The cooling effect is commonly quantified by the radiative forcing (RF) or effective radiative forcing (ERF), which are measures of the change in the net radiation into the atmosphere with adding a climate forcing agent. RF is, by the International Panel of Climate Change's Assessment Report 5 (IPCC AR5) (Boucher et al., 2013) definition, the change in net downwards radiative flux at the tropopause from perturbing the forcing agent, keeping the state variables in the troposphere fixed, but allowing the stratosphere to adjust. However, the ERF is in general considered a better indicator of induced surface temperature change, because of so called "rapid adjustments" in the atmospheric column which may offset or augment the temperature change from the RF, depending on the forcing agent (Bellouin et al., 2020). In this paper, we therefore use ERF definition as introduced in IPCC AR5, namely the change in top of the atmosphere downwards net flux while allowing adjustments in clouds, temperature, humidity etc. in the atmospheric column, but keeping the sea surface temperature fixed.

2 Model description

The Norwegian Earth System Model v2 (NorESM2) (Seland et al., 2020b; Bentsen et al., 2013; Kirkevåg et al., 2013; Iversen et al., 2013) is developed with a basis in the Community Earth System Model (CESM) (Danabasoglu et al., 2020; Neale et al., 2012). Firstly, the ocean component, which is not active in these runs since we use fixed sea surface temperature (fSST), is

replaced by Bergen Layered Ocean Model (BLOM) (Seland et al., 2020b). Secondly, the atmospheric component, CAM-Nor6, differs from the Community Atmosphere Model v6 (CAM6) in CESM in that has aerosol scheme is replaced by OsloAero6 (Kirkevåg et al., 2018) which we describe briefly below.

In this study we investigate the sensitivities of our sectional scheme for early growth which was newly implemented into OsloAero6 Blichner et al. (2020). Both the original aerosol scheme, referred to as OsloAero, and our version with the sectional scheme implemented, referred to as OsloAeroSec, are described in depth in (Blichner et al., 2020, submitted). We will therefore only give a brief description of the aerosol scheme here.

All runs are done with CAM-Nor6 coupled with the Community Land Model v5 (CLM5) in BGC(biogeochemistry) mode and prognostic crop (Lawrence et al., 2019), prescribed sea ice and sea surface temperatures.
In the following, we start by describing CAM6-Nor in general with the default aerosol scheme, OsloAero, before describing the changes introduced in OsloAeroSec.

2.1 CAM6-Nor

As mentioned earlier, CAM6-Nor shares many characteristics with CAM6 (Bogenschutz et al., 2018), while the aerosol scheme exchanged for OsloAero, described below in sec. 2.1.1. The cloud macrophysics are treated with The Cloud Layers Unified by Binormals (CLUBB Bogenschutz et al., 2013) model. The microphysics for stratiform and shallow convection clouds is the two-moment bulk from Gettelman and Morrison (2015) (MG2), while the deep convection microphysics are treated with a simplified single–moment representation based on Zhang and McFarlane (1995). The cloud activation of aerosols is done with Abdul-Razzak and Ghan (2000). See Bogenschutz et al. (2018) for more details about the clouds.

2.1.1 OsloAero

OsloAero is often referred to as a "production-tagged" aerosol module, meaning that the model to a large extent keeps track of the processes that each tracer has gone through (e.g. coagulation, condensation etc). A key difference to other aerosol modules is that it divides the tracers into "process" tracers and "background" tracers. The idea is that the background tracers decide the number concentration, while the process tracers modify the initial size distribution and chemical composition with a look-up table approach (Bentsen et al., 2013; Kirkevåg et al., 2018, 2013; Iversen et al., 2013; Seland et al., 2020b). The background tracers form initial log-normal modes, but after the process tracers are applied, the distribution of the resulting "mixtures" is not necessarily log normal anymore. This distribution is then used for the optical properties and cloud activation.

The chemistry scheme in NorESM uses the preprocessor MOZART Emmons et al. (2010) to produce a simplified scheme for sulfur and organic species. The oxidant concentrations, hydroxyl radicale (OH), ozone (O_3), nitrate radical (NO_3) and hydroperoxyl (HO_2), are read from file and interpolated from monthly mean. The chemistry scheme treats the oxidation of sulphur dioxide (SO_2), dimethyl sulfide (DMS), isoprene and monoterpenes. For a more detailed discussion of the chemistry see Karset et al. (2018), and for a complete overview of reactions and reaction rates, see in particular Table 2 therein.

The aerosol scheme contains three condensing tracers, H_2SO_4, and two organic species, namely $SOAG_{LV}$ and $SOAG_{SV}$. The H_2SO_4 is produced through oxidation, or emitted directly into the atmosphere. The two organic tracers are produced through oxidation of monoterpene and isoprene, where each reaction has a certain yield of $SOAG_{LV}$ and $SOAG_{SV}$. The reactions of isoprene with OH, O_3 and NO_3 all yield 5 percent $SOAG_{SV}$, while $\mathrm{monoterpene} + OH$ and $\mathrm{monoterpene} + NO_3$ yield 15 % $SOAG_{SV}$. Finally, monoterpene reacting with $\mathrm{monoterpene} + O_3$ yields 15 % $SOAG_{LV}$, thus being the only reaction yielding $SOAG_{LV}$.

During condensation these are all treated as non-volatile, but we separate between $SOAG_{LV}$ and $SOAG_{SV}$ because only $SOAG_{LV}$ is considered low-volatile enough to contribute to NPF. In fact only 50 % of the $SOAG_{LV}$ in each time step is assumed to be low enough volatility to contribute to nucleation, and we will refer to this fraction of the $SOAG_{LV}$ as ELVOC.

New particle formation is parameterized by using an intermediate concentration of H_2SO_4 and ELVOC in each time step to calculate a nucleation rate followed by a calculation of how many particles survive the growth up to the background mode keeping the particles from NPF (23.6 nm in number median diameter).

The nucleation rate is calculated using Vehkamäki et al. (2002) for binary sulfuric acid-water nucleation and equation 18 from Paasonen et al. (2010) to represent boundary layer nucleation.

This survival of particles from nucleation at $d_{\mathrm{nuc}} \approx 2\,\mathrm{nm}$, the NPF mode is parameterized (number median diameter $d_{\mathrm{mode}} = 23.6\,\mathrm{nm}$) by Lehtinen et al. (2007):

$$J_{d_{\mathrm{mode}}} = J_{\mathrm{nuc}} \exp\Big(-\gamma d_{\mathrm{nuc}} \frac{CoagS(d_{\mathrm{nuc}})}{GR} \Big) \tag{1}$$

where $J_{d_{\mathrm{mode}}}$ is the formation rate at d_{mode}, d_{nuc} is the diameter of the nucleated particle, $CoagS(d_{\mathrm{nuc}})$ is the coagulation sink of the particles $[\mathrm{h}^{-1}]$, GR is the growth rate $[\mathrm{nmh}^{-1}]$ of the particle (from H_2SO_4 and ELVOC, calculated using eq.$\tilde{2}$1 from Kerminen and Kulmala (2002)) and γ is a function of d_{form} and d_{nuc}:

$$\gamma = \frac{1}{m+1}\Big[\Big(\frac{d_{\mathrm{form}}}{d_{\mathrm{nuc}}}\Big)^{(m+1)} - 1\Big],\ m = -1.6. \tag{2}$$

2.2 OsloAeroSec

We have implemented a sectional scheme for modelling the growth of particles from nucleation up to the mode which keeps the NPF particles in NorESM (number median diameter 23.6 nm) (Blichner et al., 2020). The scheme is described in detail in Blichner et al. (2020). The scheme contains five bin sizes set according to a discrete geometric distribution (Jacobson, 2005, sec.13.3) and two condensing vapors: H_2SO_4 and $SOAG_{LV}$. The condensation of these species is treated as non-volatile and after condensation, the particles are "grown" (moved) to adjacent bins according to a quasi-stationary structure (Jacobson, 1997, 2005).

Coagulation is accounted for both between particles in the sectional scheme and with particles in the modal scheme. When two particles in the sectional scheme coagulate, this contributes to grow the particles, while if they coagulate with particles in the modal scheme, their mass is added to a process tracer in OsloAero (see Blichner et al. (2020) for more details).

When the particles have grown to the volume median diameter of the NPF mode in OsloAero, the particle mass is moved to the NPF mode, thus conserving both volume and number.

Finally, in this version of the model, we have also added improvements to the diurnal variation of the oxidant concentrations, described below.

2.3 Chemistry: changes to oxidant diurnal variation:

The oxidant concentration in CAM6-Nor are read from prescribed 3D monthly mean fields (Seland et al., 2020b) with a diurnal cycle superimposed on OH, HO_2 and NO_3. In the case of OH, this is basically a step function based on before vs after sunrise, which in turn lead to a step function in the H_2SO_4 concentration and an unrealistic NPF diurnal cycle. In OsloAeroSec, we therefore implemented a simple sine shape on the daily variation in OH, to improve the realism of NPF.

3 Simulation setup

All simulations are performed with NorESM2 release 2.0.1 with 1.9° (latitude) × 2.5° (longitude) resolution with 32 height levels from the surface to $\sim$2.2 hPa in hybrid sigma coordinates. The time step is 0.5 hour. We use a configuration with active atmosphere (CAM6-Nor6 Seland et al., 2020b) and land component (CLM5-BGC, Lawrence et al., 2019), while sea ice and sea surface temperatures are read from file. We use the fixed SST method combined with nudging to estimate effective radiative forcing (ERF) from aerosol–cloud interaction, ERF_{aci}, and ERF from aerosol-radiation interactions, ERF_{ari} (Hansen et al., 2005; Forster et al., 2016). This means that we use prescribed SST and sea ice and perturb the anthropogenic aerosol emissions.

We use nudging against model produced meteorology to constrain the natural variability (Kooperman et al., 2012; Zhang et al., 2014; Forster et al., 2016), nudging the horizontal wind components (U,V) and surface pressure with a relaxation time of 6 hours (as described in Karset (2020, sec 4.1)). Only nudging U, V and surface pressure is preferable over nudging more variables (temperature, humidity, energy fluxes, surface drag etc), because it allows for rapid adjustments which should be included in ERF_{aci}. See Karset (2020, ch. 4.1) for discussion.

In addition, we use the method proposed by Karset et al. (2018) to estimate the effective radiative forcing, i.e. we use not only to the anthropogenic aerosol emissions but also the oxidants from the present day atmosphere.

To produce the meteorology, we first ran a 7 years simulation (plus 2 years discarded as spin up), MMET_{1850} with the default model, $\mathrm{OsloAero}_{def}$. This was done with standard CMIP6 pre-industrial (here meaning 1850) forcing and emissions.

Two simulations were performed with each model version:

***PI** Pre-industrial (1850) simulation nudged to MMET_{1850}

***PD** Simulation with aerosol emissions and oxidant fields from "present day" (2014) nudged to pre-industrial meteorology (MMET_{1850})

These are the simulations used to calculate the ERF and which are analyzed in the result section. Emissions of aerosol and precursors for both the present and pre-industrial are from Hoesly et al. (2018); van Marle et al. (2017). Oxidant fields are as described in Seland et al. (2020b), from Danabasoglu et al. (2020).

Table 1. Abbreviations for model configurations and versions.

	Abbreviation	Description
Configurations:		
	*PI	pre-industrial (1850) run with 1850 aerosol emissions and oxidants
	*PD	pre-industrial (1850) run with anthropogenic emissions and oxidant fields from present day (2014)
Model versions:		
	OsloAero$_{def}$*	Run with OsloAero$_{def}$
	OsloAero$_{imp}$*	Run with OsloAero$_{imp}$
	OsloAeroSec*	Run with OsloAeroSec

The *PI simulations were all initialized from a two-year simulation with OsloAero$_{def}$ model version with pre-industrial conditions and free meteorology (SPINUP_PI). Similarly, the *PDsimulations, were all initialized from a two-year simulation with OsloAero$_{def}$ model version with free meteorology and pre-industrial conditions but present day aerosol emissions and oxidant fields (SPINUP_PD). MMET_PI, SPINUP_PI and SPINUP_PD were all initialized from a 30-year simulation with PI configuration.

Table 2 summarizes the model simulations and table 1 summarizes the abbreviations for the model versions and configurations.

4 Terminology

Because we are comparing model versions with and without the sectional scheme, we will only discuss particle number concentrations of particles in the modal OsloAero part of the scheme, that is excluding the ones still in the sectional scheme. This gives us an apples-to-apples comparison with the original model version. We will use N_a to refer to total aerosol concentration, excluding the particles in the sectional scheme, and N_{NPF} for the subset of these particles originating from NPF. Furthermore, we use N_{d_1,d_2} to refer to the particles with a diameter larger than d_1 but smaller than d_2. These definitions are summarized in Table 3.

We will use the term *NPF efficiency* or *the efficiency of NPF* to describe model to model differences in how many NPF particles are produced with the same emissions (PI or PD). If model version A and B are both run with the same setup (e.g. pre-industrial emissions), and model A produces more NPF particles than model B, we will say that A has higher NPF efficiency than B.

We use the Ghan (2013) method for calculating ERF$_{aci}$ and ERF$_{ari}$, meaning that we output the net radiation at the top of the atmosphere, F, and in addition output calls to the radiation scheme with clean (no aerosols), F_{clean} and clean and clear (no aerosol, no clouds), $F_{\text{clean,clear}}$. Thus, the direct aerosol radiative effect is $\text{DIR}_{Ghan} = F - F_{\text{clean}}$ and the cloud radiative effect

Table 2. Description of runs. See Table 1 for meaning of configuration abbreviations.
*30 year run with *PI configuration

Simulation name	Model version	Configuration	Initialized from	Meteorology	Years
MMET_PI	OsloAero$_{def}$	*PI	*	Free meteorology	1–8
SPINUP_PI	OsloAero$_{def}$	*PI	*	Free meteorology	1–2
SPINUP_PD	OsloAero$_{def}$	*PD	*	Free meteorology	1–2
PI runs:					
OsloAero$_{def}$_PI	OsloAero$_{def}$	*PI	SPINUP_PI	Nudged MMET_PI	(3)4-8
OsloAero$_{imp}$_PI	OsloAero$_{imp}$	*PI	SPINUP_PI	Nudged MMET_PI	(3)4-8
OsloAeroSec_PI	OsloAeroSec	*PI		Nudged MMET_PI	(3)4-8
PDruns:					
OsloAero$_{def}$_PD	OsloAero$_{def}$	*PD	SPINUP_PD	Nudged MMET_PI	(3)4-8
OsloAero$_{imp}$_PD	OsloAero$_{imp}$	*PD	SPINUP_PD	Nudged MMET_PI	(3)4-8
OsloAeroSec_PD	OsloAeroSec	*PD	SPINUP_PD	Nudged MMET_PI	(3)4-8

Table 3. Model variable definitions.

Variable name	Definition
N_a	Number of particles excluding those in the sectional scheme
N_{NPF}	Number of particles from NPF excluding those in the sectional scheme
$N_{d_1-d_2}$	Number of particles with diameter d such that $d_1 \leq d \leq d_2$
N_{d_1}	Number of particles with diameter d such that $d_1 \leq d$

is CRE $= F_{\text{clean}} - F_{\text{clean,clear}}$. It follows further that ERF$_{ari}$ $= \Delta$DIR$_{Ghan} = \Delta(F - F_{\text{clean}})$ and ERF$_{aci}$ $= \Delta$CRE $= \Delta(F_{\text{clean}} - F_{\text{clean,clear}})$, where Δ signifies the difference between PD and PI.

5 Results and discussion

We will start by presenting globally averaged ERF$_{ari}$ and ERF$_{aci}$ in the model versions, and how these relate to PI to PD changes in globally averaged aerosol and cloud properties (section 5.1). Next, in section 5.2, we present a series of hypothesis for the differences in ERF$_{ari}$ and ERF$_{aci}$ between the model versions, which we will use to analyze the results.

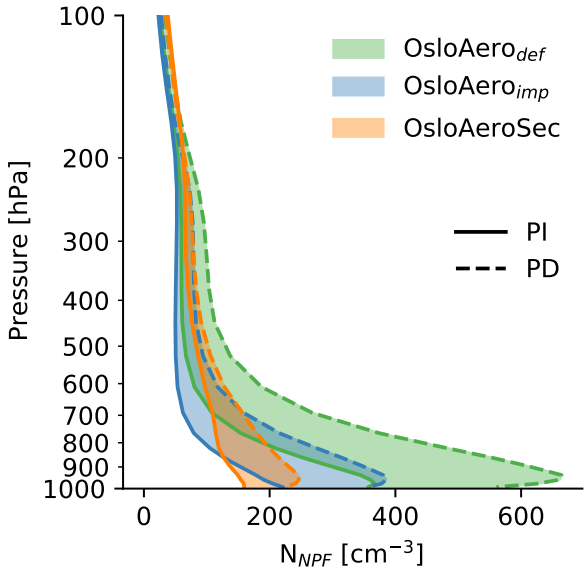

Figure 2. Globally averaged concentration of aerosols from NPF. The solid lines show the concentration in the PI simulation, while the dashed lines show the concentration in the PD. The shading signifies the change in each model.

In section 5.3, we discuss the PI to PD changes on a regional level, before discussing the PI and PD simulations separately in sections 5.4 and 5.5. We discuss all model versions where this is helpful for understand the results, but we otherwise focus on OsloAeroSec versus OsloAero$_{def}$, because OsloAero$_{def}$ is the version used in CMIP6.

5.1 Global averages: Aerosol number and ERF

5.1.1 Aerosol number

In general, the sectional scheme produces more particles than the original scheme in very pristine environments, while producing fewer in areas with high aerosol concentrations (Blichner et al., 2020). This is reflected in the globally averaged profiles of NPF particles, N_{NPF}, for each model version shown in Fig. 2. In the PD simulations, OsloAeroSec mostly has lower N_{NPF} concentrations than the other model versions, surpassing OsloAero$_{imp}$ only above $\sim 650\,\mathrm{hPa}$. However, in the cleaner PI atmosphere, OsloAeroSec has N_{NPF} concentrations closer to, or even higher, than the other two schemes. OsloAeroSec has higher N_{NPF} concentrations above $\sim 850\,\mathrm{hPa}$ and $\sim 700\,\mathrm{hPa}$ compared to OsloAero$_{imp}$ and OsloAero$_{def}$, respectively. Close to the surface, where aerosol concentrations in general are higher, OsloAeroSec has lower N_{NPF} that the other two models, even in the PI simulation.

As we shall explain more in depth later, these changes in NPF in clean remote versus higher aerosol concentration areas, are important for ERF_{aci} because the NPF particles are more likely to activate in pristine regions, while may even act to suppress activation in the more polluted regions.

Furthermore, note that even though $\mathrm{OsloAero}_{imp}$ is the same as OsloAeroSec, excluding the sectional scheme, the profile is qualitatively different: OsloAeroSec has fewer particles close to the ground and much more further up in the PI atmosphere, see section 5.6.

5.1.2 ERF

The globally averaged ERF_{aci} is significantly influenced by the introduction of the sectional scheme, as is seen in Fig. 3 showing total, shortwave and longwave components of ERF_{aci}, and ERF_{ari}. The ERF_{aci} is $0.13\,\mathrm{Wm}^{-2}$ weaker in OsloAeroSec compared to $\mathrm{OsloAero}_{def}$. The ERF_{aci} with $\mathrm{OsloAero}_{imp}$ and $\mathrm{OsloAero}_{def}$ is roughly the same (difference of $0.01\,\mathrm{Wm}^{-2}$). Also, the total radiative effect from aerosols, $\mathrm{ERF}_{aci+ari}$, is lower $\sim$0.1 Wm^{-2} in OsloAeroSec compared to both $\mathrm{OsloAero}_{def}$ and $\mathrm{OsloAero}_{imp}$. One can further see in Fig. 3, that the difference in the ERF_{aci} between the OsloAeroSec and $\mathrm{OsloAero}_{def}$ is completely caused by difference in the SW forcing. Moreover, even though $\mathrm{OsloAero}_{imp}$ has roughly the same ERF_{aci} as $\mathrm{OsloAero}_{def}$ it has a significant strengthening of the forcing in both the SW and LW component that ends up cancelling each other out in the total forcing. Lastly, the direct effective aerosol forcing, ERF_{ari}, is also shown in Fig. 3 and the direct effect is slightly closer to zero with OsloAeroSec than $\mathrm{OsloAero}_{def}$ and $\mathrm{OsloAero}_{imp}$ ($\sim$-0.03 Wm^{-2} smaller than $\mathrm{OsloAero}_{def}$ and $\mathrm{OsloAero}_{imp}$). It may seem surprising that both $\mathrm{OsloAero}_{def}$ and $\mathrm{OsloAero}_{imp}$ have positive ERF_{ari}. Note that we are using Ghan (2013) to calculate ERF_{ari} and that other methods may give a slightly different result. Smith et al. (2020) show comparisons of different estimates of the ERF_{ari} for CMIP6 models and find similar values to ours for NorESM with the Ghan (2013) method, while e.g. the approximate partial radiative perturbation (APRP) method while the APRP method gave a negative ERF_{ari} for the same simulations. The difference between OsloAeroSec and the default model likely originates from OsloAeroSec producing fewer particles than $\mathrm{OsloAero}_{def}$ in the PD simulation and thus allowing the remaining particles to grow larger and thus scatter radiation more efficiently (Blichner et al., 2020).

As discussed in the introduction, ERF_{aci} depends both on the increase in CCN between PI and PD and on the number of CCN in the PI base state. The less CCN there is in the base state, the larger the impact of a given increase in CCN will be, because the clouds are more susceptible. As OsloAeroSec has much lower particle number concentrations than $\mathrm{OsloAero}_{def}$ in the PI, we might expect OsloAeroSec to have a less CCN/CDNC and weaker (less negative) NCRE_{Ghan} in the PI. In this case OsloAeroSec would have clouds that are more susceptible to change from PI to PD, than $\mathrm{OsloAero}_{def}$. The opposite is in fact the case, as can be seen in Fig. 4 which relates the column burden of $\mathrm{N_{NPF}}$ particle mass (which, due to the technical setup of OsloAero, is proportional to the number) to the net cloud radiative effect (NCRE_{Ghan}). While the column burden of $\mathrm{N_{NPF}}$ is lower in OsloAeroSec compared to $\mathrm{OsloAero}_{def}$, the NCRE_{Ghan} is stronger (more negative). On the other hand, $\mathrm{OsloAero}_{imp}$ has the lowest column burden of $\mathrm{N_{NPF}}$ and the weakest NCRE_{Ghan}, and thus follows the logic that a "cleaner" atmosphere gives a less negative (weaker) NCRE_{Ghan}. In the PD simulations, OsloAeroSec has the lowest column burden of $\mathrm{N_{NPF}}$ of all the models and approximately the same NCRE_{Ghan} as $\mathrm{OsloAero}_{def}$, while $\mathrm{OsloAero}_{imp}$ has a less negative NCRE_{Ghan} than

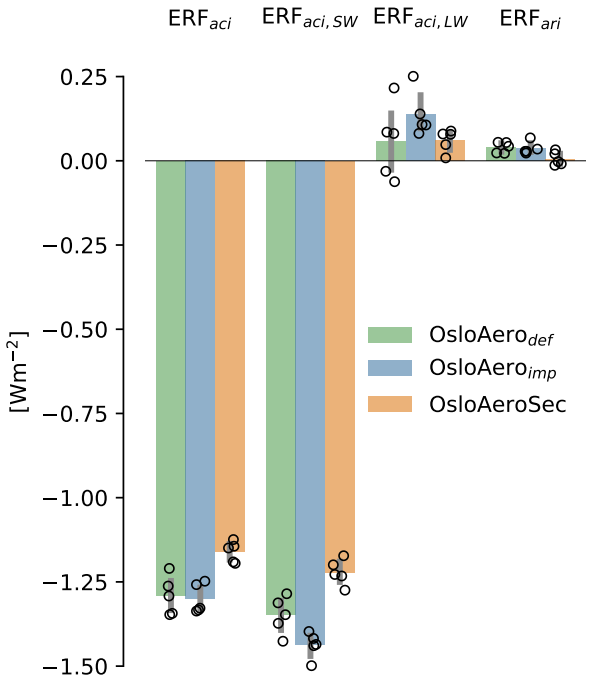

Figure 3. Globally averaged effective radiative forcings (ERF) from aerosols. ERF$_{aci}$ is the ERF from aerosol-cloud interaction, ERF$_{aci,SW}$ and ERF$_{aci,LW}$ are the short wave and long wave component of ERF$_{aci}$ and ERF$_{ari}$ is the ERF from aerosol radiation interaction alone. All are computed in accordance with Ghan (2013). The circles are the the averages for each individual year in the 5 year simulations and the gray bar indicates the 95% confidence interval of the mean.

the other two. Since ERF$_{aci}$ = NCRE$_{Ghan\ \mathrm{PD}}$ − NCRE$_{Ghan\ \mathrm{PI}}$, it is clear from Fig. 4, that most of the difference between the schemes originate in different NCRE$_{Ghan}$ in the PI simulations; -0.15 and $-0.24\,\mathrm{Wm}^{-2}$ compared to OsloAero$_{def}$ and OsloAero$_{imp}$, respectively. The difference in the PD simulations partially compensate this but is considerably smaller; -0.02 and $-0.1\,\mathrm{Wm}^{-2}$ compared to OsloAero$_{def}$ and OsloAero$_{imp}$, respectively. Furthermore and maybe surprisingly, this plot shows that the change in NCRE$_{Ghan}$ per change in column burden N$_{\mathrm{NPF}}$ (i.e., the slope of the line in Fig. 4), is much more negative for OsloAeroSec than for the other two model versions.

5.2 Reasons for differences in ERF$_{aci}$

From what we have seen so far, it is first of all clear that changes in the PI NCRE$_{Ghan}$ are dominating the difference in ERF$_{aci}$ between the models, i.e. the spread in modelled NCRE$_{Ghan}$ between the models is larger in PI than in PD. Secondly, we have seen that at least in globally averaged properties, more efficient NPF, meaning more particles with the same emissions, does not necessarily lead to a stronger negative NCRE$_{Ghan}$. To explain the somewhat unintuitive relationship between particle number

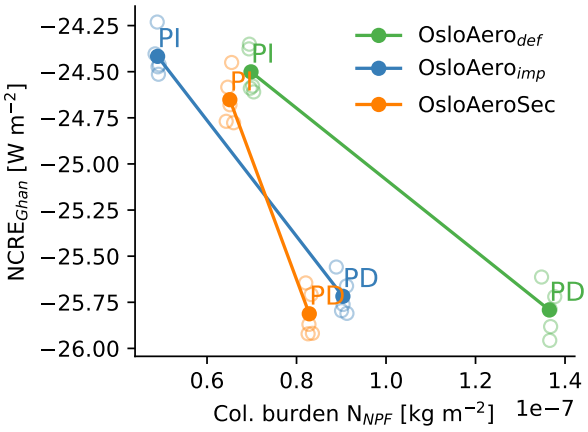

Figure 4. Globally averaged aerosol values of NCRE$_{Ghan}$ (y-axis) and column burden of NPF particles (x-axis) for the pre-industrial (PI) and present day (PD) atmosphere. The circles show each annual average and are included to indicate the variability.

and NCRE$_{Ghan}$, we must consider also their geographical distributions with respect to where the NPF particles are likely to activate in clouds and contribute to CDNC. In this section we first outline some important processes and then layout some hypothesis for the difference in NCRE$_{Ghan}$ with OsloAeroSec compared to the other versions. These will serve to ease the rest of the results and discussion.

The cloud droplet activation of particles and resulting CDNC depend on the following factors: 1) The maximum achieved supersaturation (S_{max}) together with the hygroscopicity of the particles decide the activation diameter of each mode, 2) S_{max} depends on the updraft velocity, but is also influenced by supersaturation adjustment due to the uptake of water vapor from large(r) particles which activate "early" during lifting, and finally, 3) the absolute number of particles in each mode which are larger than the activation diameter and thus activate.

Furthermore, note that the number of particles from NPF is strongly negatively correlated with the number median diameter of the modes in the size distribution, both the NPF mode and the larger modes. This is because the total available surface area is larger when there are more NPF particles, which means the available condensate is distributed to more numerous, but smaller particles. This leads, as we will show, to NPF inhibiting cloud droplet activation in many regions in the model.

Figure 5 illustrates the effect of changing the NPF efficiency on CDNC in two different environments. For simplicity, let us assume that we are comparing two models with different NPF efficiency; model A with high NPF efficiency and model B with low NPF efficiency. As noted above, model A will have more numerous, but smaller, particles (A1 and A2 in Fig. 5), while model B will have fewer, but larger particles (B1 and B2 in Fig. 5). Furthermore, we will consider two different environments. Environment 1 has a small activation diameter because, e.g. there are few large particles (no early activation) or the updraft is strong (A1 and B1 in Fig. 5). Environment 2 has a large activation diameter because, e.g. it has high emissions of large primary particles which activate early and limit the maximum supersaturation (A2 and B2 in Fig. 5). In this simplification we assume

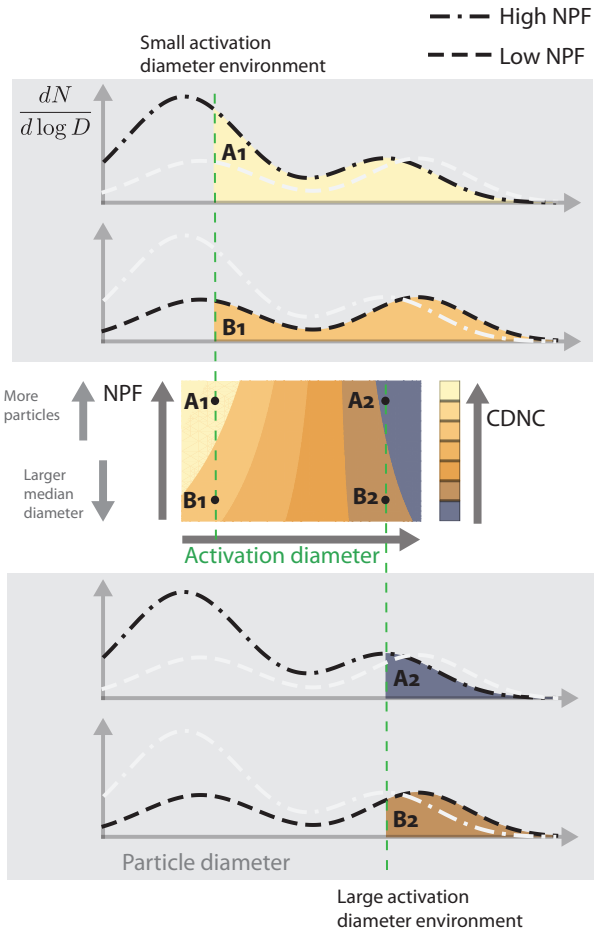

Figure 5. Schematic illustrating the influence of NPF on cloud droplet activation and CDNC. The top and bottom panel shows what happens to activation in two different environments (1 and 2) and for two models; one model with high NPF efficiency (A) and one with low NPF efficiency (B). Let us first consider environment 1 (top panels): here the activation diameter is small (either due to strong updrafts, few large particles or high hygroscopicity) and particles all the way down to the mode holding the NPF particles ($\sim$ Aitken mode) activate. In this environment model A will activate more particles than model B and have higher CDNC. Next let us consider environment 2 (bottom panels): here the activation diameter is large (due to weak updrafts, supersaturation adjustment due to larger particles or hygroscopicity) and only the largest particles activate. Here model B will activate more particles than model A because the size of the larger particles is what dominates.

that the activation diameter does not change between model A and B. This is not strictly true, but a good assumption because the inter-model changes in S_{max} (Fig. S14) and hygroscopicity (Fig. S19) are small and do not dominate the response in terms of CDNC.

We start with environment 1 where the activation diameter is small (e.g. Antarctica). This is illustrated by the two size distributions, A1 and B1, on the top in Fig. 5. In this environment model A (high NPF efficiency, A1) will result in higher

cloud droplet activation and higher CDNC than model B (low NPF efficiency, B1). This is because a considerable fraction of the small NPF mode particles activate, and thus the decrease in the size of the larger particles does not matter.

Next we consider environment 2 where the activation diameter is large (e.g. a polluted area like China).This is illustrated by the two size distributions, A2 and B2, at the bottom of in Fig. 5. In this environment model A with high NPF efficiency (A2) will result in lower cloud droplet activation and lower CDNC than model B with a low NPF efficiency (B2). This is because the change in the diameter of the larger particles is the only thing which is matters for activation, since the smaller particles will not activate anyways.

In this simplified thought example, we can say that in environment 1 (small activation diameter), NPF enhances cloud droplet activation while in environment 2 (large activation diameter), NPF inhibits cloud droplet activation.

With all this in mind, we can lay out some plausible hypothesis that might contribute to a weaker ERF_{aci} in OsloAeroSec compared to the other model versions:

1. **Smaller $\Delta_{\text{PD-PI}}\mathbf{N}_a$:** The difference in ERF_{aci} is due to a smaller change in number concentration between PI and PD in OsloAeroSec than the other model versions

2. **Higher $\mathbf{N}_a$ in PI:** OsloAeroSec produces more particles under PI conditions and therefore the clouds are less susceptible to increased anthropogenic emissions

3. **Higher activation in PI:** The number of particles that actually act as CCN and activate is higher with OsloAeroSec than the other model versions in the PI simulations, leading to a higher baseline CDNC. This is due to

   (a) more efficient NPF in remote regions where NPF enhances activation

   (b) less efficient NPF in regions where NPF inhibits activation (only larger particles activate)

4. **Lower activation in PD:** The number of particles that actually act as CCN and activate is lower with OsloAeroSec than the other model versions with PD emissions, leading to a weaker ERF_{aci}. This is

   (a) due to lower NPF efficiency regions where NPF enhances activation

Hypothesis 2 has partly already been disproven because in terms of global averages, $\mathrm{OsloAero}_{def}$ has higher particle number concentrations than OsloAeroSec all the way up to approximately $700\,\mathrm{hPa}$ (with most of the liquid clouds being below this level).

5.3 Pre-industrial to present day changes

We start by considering hypothesis 1, and how the PI to PD change looks on a regional level in OsloAeroSec versus $\mathrm{OsloAero}_{def}$.

This is shown in Fig. 6 where the first row is the change between PD and PI ($\Delta_{\text{PD-PI}}$) for OsloAeroSec and the two subsequent rows are the difference to this first quantity, $\Delta_{\text{PD-PI}}$, between the model versions ($\Delta_{\text{PD-PI}}$(OsloAeroSec) minus

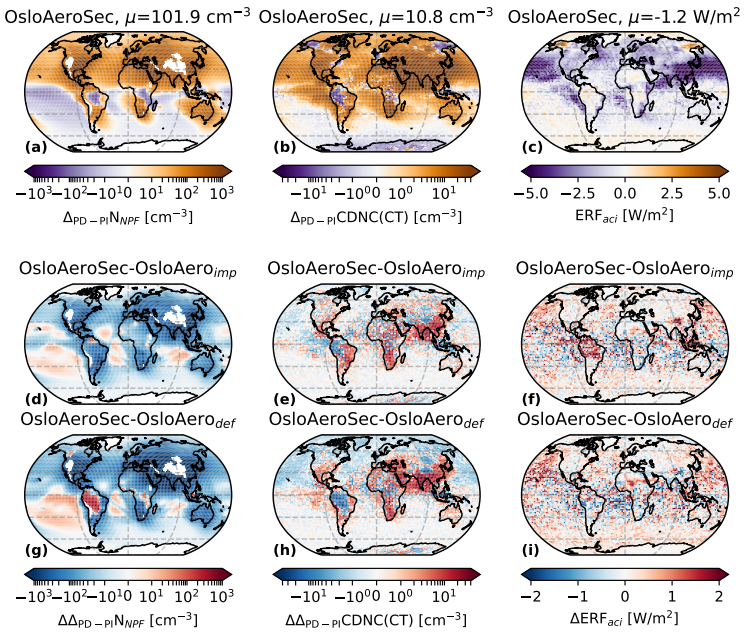

Figure 6. Annual average values of near surface N_{NPF} concentrations (left column), cloud top droplet number concentration (CDNC(CT), middle column) and NCRE$_{Ghan}$ (right column). The top panel shows the PD - PI for OsloAeroSec while the second and third rows show the change in this value (PD-PI) from OsloAero$_{imp}$ (second row) and OsloAero$_{def}$ (third row) to OsloAeroSec. The N_{NPF} values are are averaged up to 850 hPa and weighted by pressure thickness of each grid cell.

$\Delta_{\text{PD-PI}}$(OsloAero$_{imp}$) and $\Delta_{\text{PD-PI}}$(OsloAeroSec) minus $\Delta_{\text{PD-PI}}$(OsloAero$_{def}$), denoted $\Delta\Delta_{\text{PD-PI}}$). The first column, showing the near surface averaged N_{NPF}, shows that, as expected, most of the PI to PD change happens in the northern hemisphere. This is consistent with the major anthropogenic emission sources being located here. Over ocean regions in the Southern Hemisphere, there is even a small decrease in NPF particles many places. Comparing to OsloAero$_{def}$ (row 3) we see that OsloAeroSec has a smaller increase in N_{NPF} from PI to PD, except in the South Pacific and over the Amazon. Especially high pollution areas over land stand out as strongly negative. Note that the first column in Fig. S8 shows the same but for zonal averages, and underlines that $\Delta_{\text{PD-PI}}N_{NPF}$ is higher in OsloAero$_{def}$ than OsloAeroSec all through the atmospheric column.

The second column shows the change in cloud droplet number concentration at cloud top (CDNC(CT)). Again the first row shows $\Delta_{\text{PD-PI}}$CDNC(CT), which, as expected, shows an increase – in particular in the northern hemisphere. Comparing OsloAeroSec to OsloAero$_{def}$ (row 3) however, the first thing that stands out is that, somewhat surprisingly, $\Delta\Delta_{\text{PD-PI}}$CDNC(CT) is positive over polluted regions, meaning that the PI to PD increase in CDNC(CT) is stronger with OsloAeroSec than with OsloAero$_{def}$, in spite of N_{NPF} increasing less with OsloAeroSec. In other words, in these regions we are in the bottom panel of Fig. 5, where more particles are added with OsloAero$_{def}$ than OsloAeroSec, but fewer of these extra particles are activating

into cloud droplets. Meanwhile, in more remote regions, like the North Pacific and the Arctic, we are in the top panel of Fig. 5 and CDNC(CT) increases less with OsloAeroSec than OsloAero$_{def}$, following the more expected logic that a smaller increase in particle number lead to a smaller increase in cloud droplets from PI to PD.

Finally, the last column shows the ERF$_{aci}$. Here we see (first row, c), that the ERF$_{aci}$ is strongly negative over the North Pacific as well as over China and India. The difference in ERF$_{aci}$ between the models shows that the remote Pacific dominates in making ERF$_{aci}$ more strongly negative in OsloAero$_{def}$ than in OsloAeroSec. Even though the increase in CDNC(CT) from PI to PD is stronger in polluted regions with OsloAeroSec, these regions seem to have reached saturation with respect to changing albedo and the ERF$_{aci}$ changes little between the model versions.

To summarize with regard to hypothesis 1: the change in particle number between PI and PD is indeed smaller with OsloAeroSec than the other model versions, but this can only explain the change in CDNC in remote regions (North Pacific, Siberia etc). Furthermore, as mentioned earlier, we need to consider the influence of the baseline aerosol state in PI, and not just the change between PI and PD.

5.4 The pre-industrial atmosphere: model to model differences

To consider hypothesis 3, "Higher activation in PI", we now consider differences between OsloAeroSec and the default model versions in the PI separately from PD (covered in the next section).

Figure 7 shows the near surface concentration of N_{NPF} in the PI simulation (left column) for OsloAeroSec (a) and the relative difference in this value between the model versions (b and c). We see that compared to OsloAero$_{def}$, N_{NPF} is lower in OsloAeroSec almost everywhere in PI. However, as is seen in Fig. 8c, showing the zonally averaged difference, this decrease with OsloAeroSec is mostly confined to the near-surface areas. The decrease in N_{NPF} with OsloAeroSec near the surface switches to an increase higher up in the atmosphere.

5.4.1 Cloud properties

OsloAeroSec has a higher cloud droplet number concentration at cloud top (CDNC(CT)) than OsloAero$_{def}$ in most of the PI atmosphere, as can be seen in Fig. 9a. This is despite that OsloAeroSec has lower N_{NPF} concentrations in most near-surface areas compared to OsloAero$_{def}$. We must therefore investigate what happens to the size distribution, rather than just the absolute number. Figure 9c, e and g, shows the OsloAeroSec to OsloAero$_{def}$ difference in number concentrations of N_{100}, N_{150} and N_{200}. The N_{100} concentration (c), is lower in OsloAeroSec than OsloAero$_{def}$ most places in the PI atmosphere, while N_{150} (e) and N_{200} (g) are higher. This follows the mechanism explained in section 5.2, that lower NPF efficiency in OsloAeroSec leads to fewer, but larger particles. The higher concentrations in OsloAeroSec of e.g. N_{200}, comes from the modes shifting to higher median diameters when the number of NPF particles is lower. There is also a good correspondence between the difference in N_{150} and/or N_{200} and the difference in CDNC in most areas in the atmosphere. Note in for example the Amazon area, where much lower concentrations of N_{100} (and NPF efficiency) are associated with much higher concentrations of N_{200}, but not N_{150}. That the CDNC is higher here, tells us that the activation diameter here is probably usually between

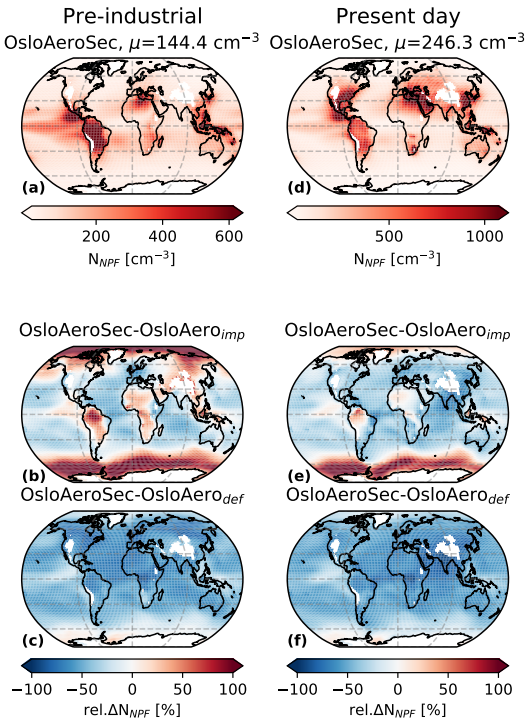

Figure 7. Top row: Annual average near surface N_{NPF} concentrations for OsloAeroSec for PI (left) and PD (right). Rows 2–3: the relative difference of OsloAeroSec to OsloAero$_{imp}$ (row 2) and OsloAero$_{def}$ (row 3) for PI (left) and PD (right), respectively. All values are averaged up to 850 hPa and weighted by pressure thickness of each grid cell.

150–200 nm. Additionally, the supersaturation is higher in OsloAeroSec due to fewer particles that compete for the water vapor (see figure S13), which has a small positive impact on the number of particles which activate.

To investigate further these relationships between changes in N_d and CDNC in the PI simulations, we compute the correlation between ΔCDNC and ΔN_d where Δ signifies the difference between OsloAeroSec and OsloAero$_{def}$. First we compute the correlation between ΔCDNC and ΔN_{NPF} over time and longitude, shown in Fig. 10c. This reveals that close to the surface, ΔCDNC and ΔN_{NPF} are mostly negatively correlated indicating that these areas, NPF inhibits activation. In remote regions, like e.g. the Southern Ocean or high in the free troposphere, there is a positive correlation between ΔN_{NPF} and ΔCDNC, indicating that here we are in a NPF enhanced activation regime and significant parts of the NPF mode particles activate.

Second, we compute the correlations between ΔCDNC and ΔN_{50}, ΔN_{100}, ΔN_{150}, ΔN_{200} and ΔN_{250} for different regions (see Table 4 for definitions) at different heights. These relationships for the PI simulations are shown in Fig. 11, column 1. If ΔCDNC correlates clearly with the change in concentration of particles above some diameter d, N_d, this indicates that these

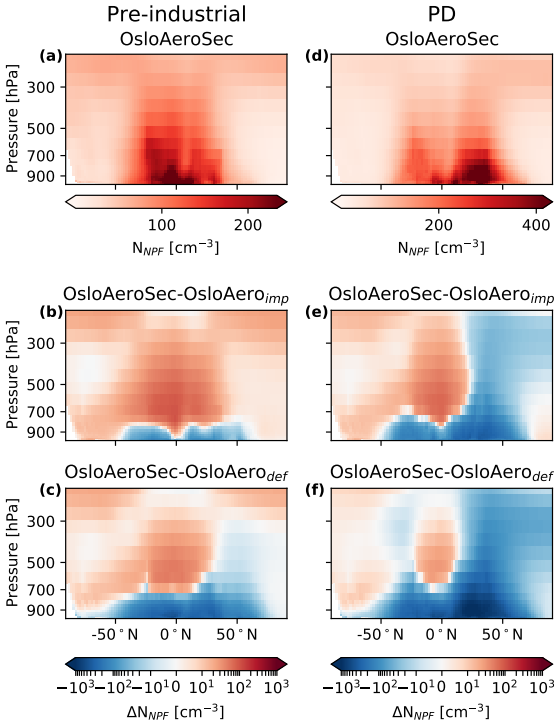

Figure 8. Top row: Zonally and annually averaged concentrations of N_{NPF} for OsloAeroSec for PI (left) and PD (right). Rows 2–3: the absolute difference of OsloAeroSec to OsloAero$_{imp}$ (row 2) and OsloAero$_{def}$ (row 3) for PI (left) and PD (right), respectively.

Table 4. Region overview. These regions are used to create vertical average profiles.

Region name	Latitudes	Longitudes
Global	All	All
Antarctic	60–90 °S	180 °W – 180 °E
Pacific S	30 °N – 60 °N	170°E – 120 ° W
Pacific N	60 °S – 30 °S	170°E – 140 ° W

particle sizes are relevant for cloud droplet activation in the region. On the other hand if there is a negative correlation, this indicates that the particles are too small to activate.

Globally, Fig. 11a, show that CDNC correlates strongest with N_{200} and N_{250} close to the surface, with an anti-correlation with N_{50} and N_{100}. The sign of the correlations switch at around 600 hPa. In the relatively clean Antarctic (here defined as

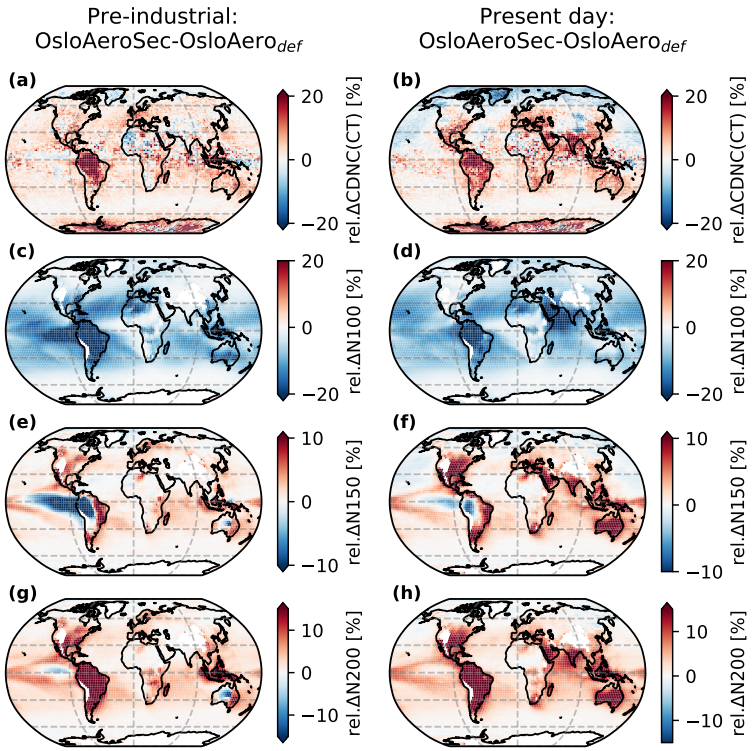

Figure 9. Top row: Relative difference in annual average cloud top cloud droplet number concentrations (CDNC(CT)) at cloud top between OsloAeroSec and OsloAero$_{def}$. Row 2–3: difference in average particle number concentration for particles larger than 100 nm (row 2), 150 nm (row 3) and 200 nm (row 4). The left column shows the difference for the pre-industrial atmosphere and the right column shows the difference for the present day atmosphere. The average particle concentrations are calculated by averaging up to 850 hPa and averaging by pressure difference.

below 60 °S), the correlation is positive with the smaller particles, i.e. N_{50}, throughout the atmosphere. This indicates that NPF enhances activation in Antarctica and that the number of particles dominates, rather than the size of the particles. Figures 11e and g show the South and North Pacific, and are included because they show opposite sign in CDNC for the PD simulations and we will discuss them further in the next section. In the PI simulations, however, the South Pacific shows a clear correlation with the larger particles (diameters larger than 150, 200 and 250), while in the North Pacific, the correlation is close to zero or insignificant.

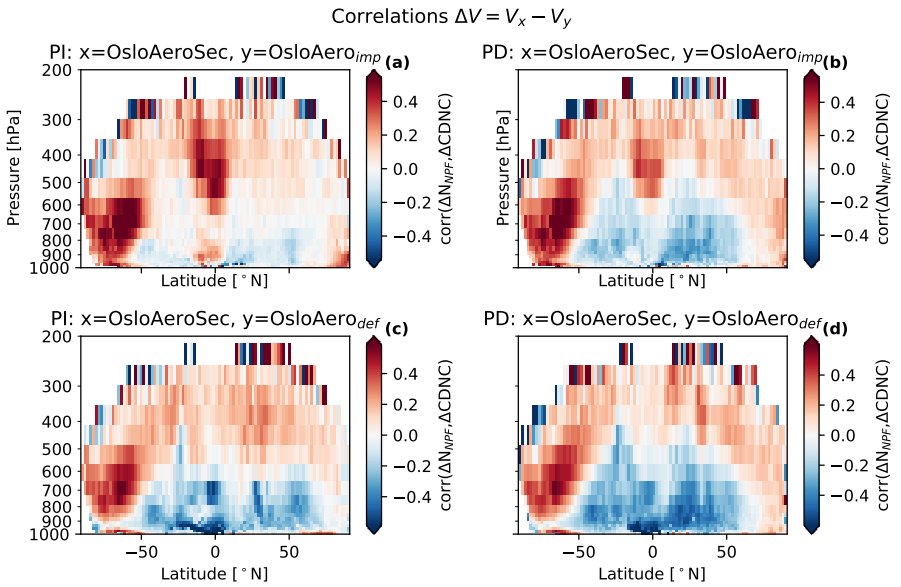

Figure 10. Correlations between the absolute difference in CDNC and the absolute difference in N_{NPF} between the model versions, calculated from monthly mean files over time and longitude. The correlations from the difference between OsloAeroSec and OsloAero$_{imp}$ is shown in the top row. The correlations from the difference between OsloAeroSec and OsloAero$_{def}$ is shown in the bottom row. The correlations in the PI simulations are shown to the left and the ones for the PD simulations to the right.

5.4.2 Summary hypothesis 3: Higher activation in the pre-industrial atmosphere

We do indeed see higher aerosol activation and higher CDNC with OsloAeroSec in the PI simulations. This is due to a combination of two things: 1) In pristine areas, NPF particles are likely to activate and lead to higher CDNC – i.e. NPF enhances activation. In these areas OsloAeroSec in general produces more NPF particles than OsloAero$_{def}$ and thus CDNC increases. 2) In areas with higher aerosol number concentrations, NPF particles are unlikely to activate and NPF inhibits cloud droplet activation due to reducing the size of the larger particles. In these regions, OsloAeroSec in general produces less NPF particles than OsloAero$_{def}$ and thus CDNC increases.

5.5 The present day atmosphere: model to model differences

We now move to consider differences in the PD simulations between OsloAeroSec and OsloAero$_{def}$ and will discuss the hypothesis 4, “Lower activation in PD”.

While with PI emissions, there are large regions, especially at higher altitudes where OsloAeroSec produced more NPF particles than the other model versions. With PD emissions, these areas shrink, as the atmosphere becomes less pristine overall. This is seen in Fig. 7d-f (near surface average), and Fig. 8d-f (zonal average). Furthermore, it is interesting to see the impact of emissions in the Northern Hemisphere versus the Southern Hemisphere in the PD simulations. In the Northern Hemisphere,

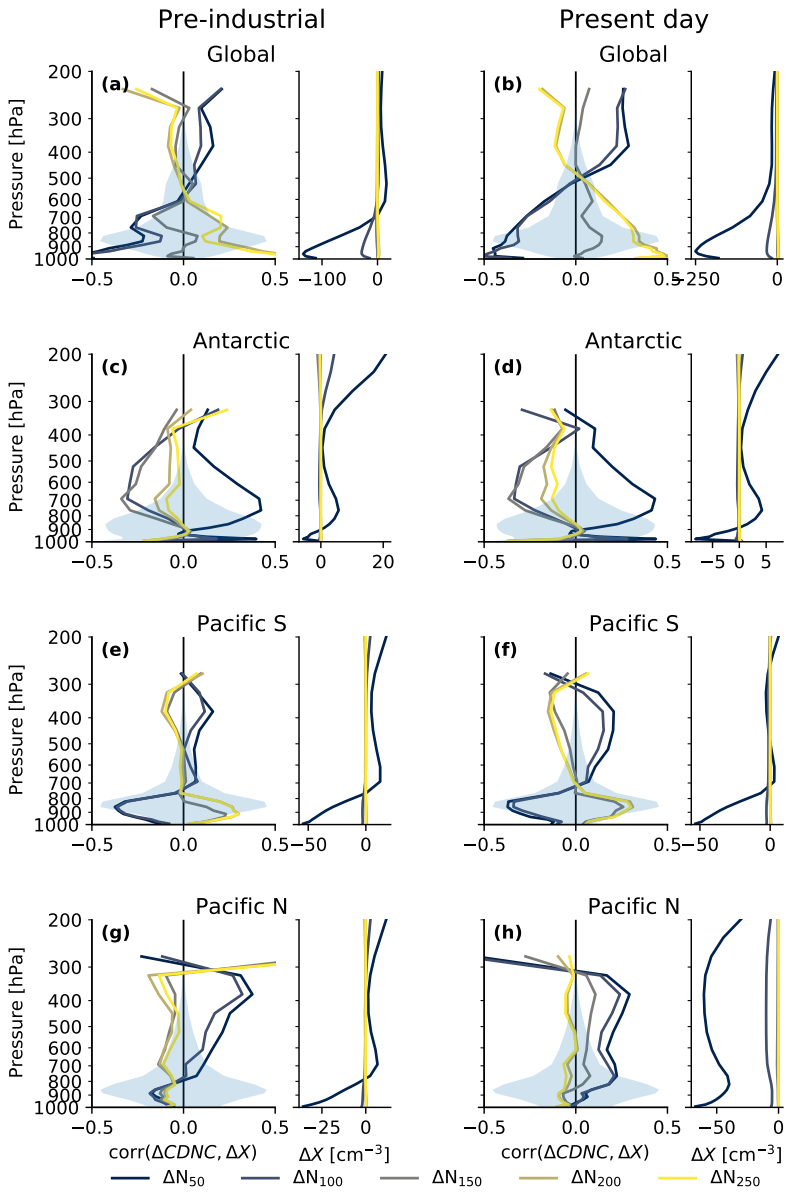

Figure 11. Left panel of each subplot: Correlations by pressure level between the absolute difference between OsloAero$_{def}$ and OsloAeroSec in cloud droplet number concentration (ΔCDNC) and the absolute difference in number of particles with diameters above 50, 100, 150,200 and 250 nm for different regions. The blue shaded signifies the fractional occurrence of liquid cloud and is included to give an idea of where the aerosols may actually have a noticeable impact on clouds. The right panel of each subplot shows the change in the aerosol concentration for the relevant region. See Table 4 for definitions of regions.

OsloAeroSec produces fewer particles than the other model versions at most heights and latitudes, while the opposite is the case for the Southern Hemisphere. This is likely due to a combination of much higher emissions and more vertical mixing in the Northern than Southern Hemisphere. In other words, larger parts of the Northern Hemisphere pass into a pollution level regime where the sectional scheme produces fewer particles than the others.

5.5.1 Cloud properties

Figure 9b shows that the difference in CDNC(CT) between OsloAeroSec and OsloAero$_{def}$ in the PD simulations. The Southern Hemisphere resembles the difference in PI (Fig. 9a) with widespread increase in CDNC. In the middle– to high northern latitudes, on the other hand, CDNC is lower in OsloAeroSec than in OsloAero$_{def}$, opposite of in the PI simulations. In these last pristine northern regions, more NPF particles in OsloAero$_{def}$ seem indeed to lead to higher CDNC than in OsloAeroSec.

Let us again consider the model to model difference in size distribution. Figure 9d, f and h, shows ΔN_{100}, ΔN_{150} and ΔN_{200}. Here we see that the pristine northern hemisphere ΔCDNC resembles most the change in N_{100}, while in the Southern hemisphere, ΔCDNC resembles more that of the larger particles (N_{150} andN_{200}). Note especially how the polluted regions in the PD simulations around India and China have higher concentrations of N_{200} and N_{150} in OsloAeroSec than OsloAero$_{def}$ and corresponding higher CDNC. In these polluted regions, NPF in general inhibits cloud droplet activation because the activation diameter is large (bottom panel in Fig. 5). This is because there are many large particles which activate early and act as a sink for water vapor, thus reducing S_{max} and increasing the activation diameter (see Fig. S13b). On the other hand, the decreases in CDNC in OsloAeroSec compared to OsloAero$_{def}$ in the PD northern high latitudes correspond better to the change in the smaller particles, N_{100} and partially N_{150}. This indicates that in these regions NPF enhances cloud droplet activation due to a smaller activation diameter (top panel in Fig. 5). Note that this is different in the PI and PD simulations: in the PD simulations, the CDNC goes down with OsloAeroSec in the northern high latitudes, in the PI it goes up. The reason for this is that the activation diameter depends both on the maximum supersaturation *and* the hygroscopicity. The hygroscopicity of the particles almost doubles from the PI to the PD, due to increased sulphate emissions (see Fig. S19). The more hygroscopic particles in the PD simulations can then activate at smaller diameters (given the same S$_{max}$). The regions where CDNC is enhanced by NPF thus spreads in the pristine northern latitudes, favoring cloud droplet activation in OsloAero$_{def}$ over OsloAeroSec. Mark that the difference in hygroscopicity is large between the PI and PD simulations (again, see S19), but small ($\sim 5\%$) between the different model versions.

It is thus clear that hygroscopicity plays a role, but only in terms of making the effect of NPF particles different in the PI and in the PD simulations, where with PD emissions the NPF particles are more likely to activate. In other words, because hygroscopicity increases in PD, the areas where NPF enhances cloud activation expand in the PD northern hemisphere compared to the pre-industrial atmosphere.

Let us again consider the correlations between ΔCDNC and N$_{\text{NPF}}$, ΔN_{50}, ΔN_{100}, ΔN_{150}, ΔN_{200} and ΔN_{250} for different regions, shown for the PD atmosphere in Fig. 10 and Fig. 11b, d, f and h.

Globally, the correlation of ΔCDNC with the change in larger particles is more pronounced in the PD than the PI simulations (Fig. 11b and Fig. 10d), possibly indicating a stronger super saturation adjustment (reduced S_{max}) with more polluted PD emission conditions, leading to a higher activation diameter.

Furthermore, we investigate the North and South Pacific separately in Figs. 11e–h, because these two show opposite sign in the PD simulations: in the North Pacific, OsloAeroSec has lower CDNC than OsloAero$_{def}$, while in the South Pacific OsloAeroSec has higher CDNC (see Fig. S2b). In the South Pacific (e and f), the CDNC correlates best with the larger particles (diameter above 150 nm) in both PI and PD. In the North Pacific on the other hand, the correlation is not clear for any particle number in the PI (g) and slightly positive for the smaller particles sizes in PD (h). The likely cause for the difference between the two cases is that 1) the South Pacific has higher concentrations of larger sea salt particles than the North Pacific (not shown), which can limit the maximum supersaturation and thus lead to a higher activation diameter, and 2) as mentioned above, the sulphate emissions are much higher in the PD Northern hemisphere, leading to more hygroscopic particles, and a lower activation diameter. In the South Pacific, we are therefore at the bottom panel of the sketch in Fig. 5, while in the North Pacific, we are more on the top panel. Note again that the hygroscopicity between the model versions with the same emissions (either with PI *or* PD emissions) changes very little (Fig. S19), which is why we only discuss changes between the PI and PD.

5.5.2 Summary hypothesis 4: Lower activation in the present day atmosphere

The discussion above shows that regionally, lower cloud droplet activation and CDNC with OsloAeroSec in the PD simulations, does indeed play a role in reducing the ERF$_{aci}$ in the pristine high northern latitudes and the North Pacific. Here the CDNC is lower with OsloAeroSec than OsloAero$_{def}$ and thus OsloAero$_{def}$ has a stronger negative cloud radiative effect in the PD simulations. On the other hand, cloud droplet activation and CDNC in more polluted regions is higher with OsloAeroSec than OsloAero$_{def}$ (see Fig. 9b) in the PD simulations. This does, however, not have as big an impact on radiation (see e.g. Fig. S9) firstly because these areas are mostly continental and the cloud radiative effect is larger over dark ocean surfaces (e.g. the North Pacific) and secondly because the CDNC is already high in these regions with OsloAero$_{def}$ and thus the clouds are less susceptible to the increase to OsloAeroSec (see introduction for description of this effect). Furthermore, we have found that hygroscopicity changes from PI to PD plays a role by reducing the activation diameter and making NPF particles more likely to activate in the PD simulations compared to the PI. This means that the areas where NPF enhances cloud droplet activation expands and thus there are larger areas where OsloAero$_{def}$ has higher CDNC than OsloAeroSec. Both these factors result in a lower CDNC in the high northern latitudes with OsloAeroSec, and a corresponding lower magnitude in NCRE$_{Ghan}$.

5.6 Comparison to OsloAero$_{imp}$

We have mostly focused on the comparison of OsloAeroSec to OsloAero$_{def}$ in the above section, but there are important points to take away from comparing OsloAeroSec to OsloAero$_{imp}$ as well. Note that OsloAero$_{imp}$ has the same updates to oxidants and nucleation rate as OsloAeroSec, but does not have the sectional scheme. Also, remember that OsloAero$_{imp}$ has much lower NPF efficiency than OsloAero$_{def}$, but compared to OsloAeroSec it is more similar, but depends on the region. In

general OsloAeroSec produces more NPF particles in pristine regions, while OsloAero$_{imp}$ produces more particles in regions with higher aerosol concentrations.

When comparing only OsloAeroSec and OsloAero$_{def}$, it is not possible to separate the effect that increased NPF efficiency in remote regions has from decreased NPF efficiency in high-aerosol regions with respect to the ERF$_{aci}$. It is perhaps tempting to think that the reduction in NPF efficiency is alone responsible for the overall effect, and that the increase in NPF efficiency in remote regions is negligible. If so, any scheme which reduced NPF efficiency would have the same effect. The OsloAero$_{imp}$ simulation however, represents exactly such another scheme which reduces the NPF efficiency compared to OsloAero$_{def}$, with roughly the same amount as OsloAeroSec, though without the increases in NPF efficiency in remote regions. However, OsloAero$_{imp}$ does not weaken ERF$_{aci}$ like OsloAeroSec does, but rather slightly strengthens it. In essence, this shows that it is the combination of decreasing NPF efficiency in high aerosol regions and increasing NPF efficiency in low-aerosol regions which together gives the weakened ERF$_{aci}$ in OsloAeroSec.

5.7 Summary of hypothesis

We now summarize and relate the results back to the hypothesis presented in section 5.2.

1 **Smaller $\Delta_{\text{PD-PI}}\text{N}_a$:** While it is true that N$_a$ increases less from PI to PD with OsloAeroSec than OsloAero$_{def}$ (and OsloAero$_{imp}$), this can only explain the results in remote regions. Furthermore, OsloAero$_{imp}$ offers as a counter argument against this hypothesis: it also has a $\Delta_{\text{PD-PI}}\text{N}_a$ than OsloAero$_{def}$, but contrary to OsloAeroSec, OsloAero$_{imp}$ has a stronger negative ERF$_{aci}$ than OsloAero$_{def}$. In sum, this hypothesis does not explain well the differences in ERF$_{aci}$.

2 **Higher N$_a$ in PI:** OsloAeroSec mostly produces fewer particles than OsloAero$_{def}$ in the PI simulations and this is thus only true in remote regions. This hypothesis can therefore not explain the resulting ERF$_{aci}$.

3 **Higher cloud droplet activation in PI:** We found that OsloAeroSec has higher CDNC than the other model versions in the PI simulations both due to more efficient NPF in remote regions where NPF enhances cloud droplet activation (small activation diameter) and due to less efficient NPF in regions where NPF inhibits cloud droplet activation (large activation diameter). In these last areas, OsloAeroSec indeed has a higher concentration of larger particles than OsloAero$_{def}$ and OsloAero$_{imp}$, due to the condensate being distributed to fewer particles in OsloAeroSec. This hypothesis therefore explains well the part of the change in ERF$_{aci}$ originating from difference in NCRE$_{Ghan}$ in the PI simulations.

4 **Lower cloud droplet activation in PD:** We found this hypothesis to play an important role in the northern high latitudes, especially the North Pacific, were sulphate emissions are high in the PD simulations. Due to higher hygroscopicity in the PD simulations compared to the PI, the NPF particles are more likely to activate (smaller activation diameter) and thus the number of particles (which is lower in OsloAeroSec) is more important than the particles sizes. This hypothesis therefore is important to explain the changes in the PD simulations.

Additionally, after the analysis of the results, we may add two more explanations:

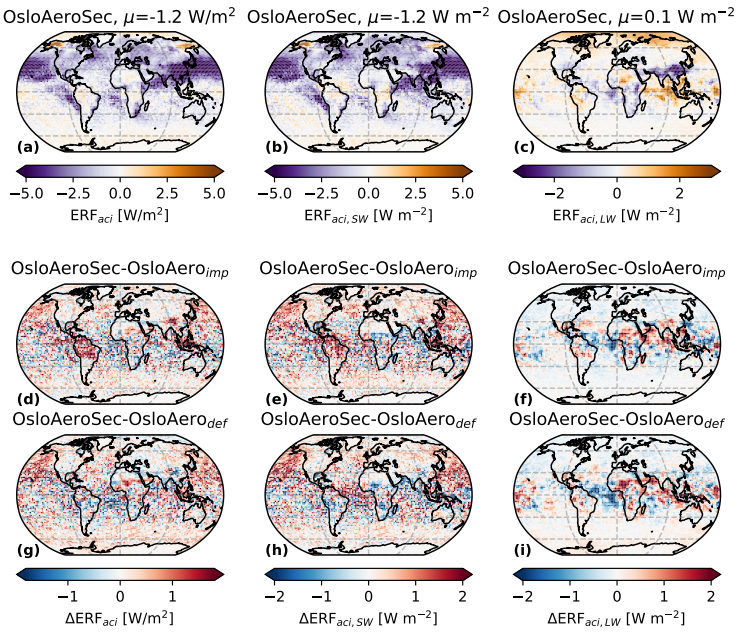

Figure 12. Annual averages of the ERF$_{aci}$ (left column), the short wave component of ERF$_{aci}$, ERF$_{aci,SW}$ (middle column) and the long wave component of the ERF$_{aci}$, ERF$_{aci,LW}$ (right column). The top panel shows the the absolute values for OsloAeroSec while the second and third row shows the difference OsloAero$_{imp}$ minus OsloAeroSec (second row) and OsloAero$_{def}$ minusOsloAeroSec (third row).

5 **Hygroscopicity:** As explained for hypothesis 4 above, the change in hygroscopicity from PI to PD, results in larger areas in the northern pristine latitudes having a NPF enhanced cloud droplet activation regime in the PD simulations, compared to the PI. This results in stronger NCRE$_{Ghan}$ with OsloAero$_{def}$ than OsloAeroSec in the PD simulations which further leads to a stronger ERF$_{aci}$ in OsloAero$_{def}$ than OsloAeroSec.

6 **Regional differences:** The comparison with OsloAero$_{def}$ shows that regional differences in NPF matter significantly. For reasons discussed above, OsloAeroSec gives higher CDNC in the PI simulation in regions with susceptible clouds and large ERF$_{aci}$, which dominates the global average.

6 Implications and discussion

The results in this paper go in line with previous work which shows both that the ERF$_{aci}$ is sensitive to the PI aerosol characteristics, e.g. Carslaw et al. (2013), and that changes the NPF parameterization can highly influence ERF$_{aci}$ (e.g. Gordon et al., 2016). However, the reduction in ERF$_{aci}$ found with OsloAeroSec in our simulations, is not a result of increased NPF

in under PI conditions alone. Rather the increase in CDNC and NCRE$_{Ghan}$ in the PI simulation originates from increased NPF efficiency where the NPF enhances cloud droplet activation, and decreased NPF efficiency where NPF inhibits particle activation. Additionally, we find that the modelled increase in hygroscopicity from PI to PD from increased sulphate emissions, results in a lower activation diameter and thus that more of the NPF particles contribute to CDNC.

The effect of NPF inhibition on cloud droplet activation, was also found by Sullivan et al. (2018), where they modelled the NPF effect on clouds over the mid-western USA using WRF-Chem v3.6.1 and using a 20 bin sectional aerosol scheme (Model for Simulating Aerosol Interactions and Chemistry, MOSAIC). As in this study, they find that the growth of the larger particles are inhibited by the increased condensation sink from the NPF particles. That fact that the same effect is seen in simulations with a completely differently structured aerosol model, shows it to be unlikely that this is an artifact of the OsloAero model. However, their study uses the same activation scheme, Abdul-Razzak and Ghan (2000), and we cannot exclude that this scheme for example overestimates the supersaturation adjustment effect.

As mentioned in the section 2, the sectional scheme, OsloAeroSec, has a higher contribution from organics to the growth from 5 nm than OsloAero$_{def}$ and OsloAero$_{imp}$ (only ELVOC in OsloAero). One could argue that the factor may be the driving factor of all these results, but in fact this is not the case. We did a test run where organics were treated in the same way in OsloAeroSec as in OsloAero$_{def}$ and OsloAero$_{imp}$ and the result in terms on particle number changes very little (see Fig. S20 and Fig. S21).

Furthermore, note that we have not discussed CCN concentrations in this discussion. There are two reasons for this: Firstly, these are not yet available as standard output for CAM6-Nor. Secondly, the CCN concentrations at a given supersaturation matters only when this supersaturation is actually achieved, so focusing on CDNC gives a more complete picture which is closer related to the actual climatic impact of the particles in question.

These results also illustrate the importance of adequately representing activation when investigating the effect of NPF on climate, and not simply considering CCN at fixed supersaturation as this will omit not only regional changes in updraft velocities, but also supersaturation adjustment by the aerosol population.

7 Conclusions

In this study, we have shown that including a sectional scheme (OsloAeroSec) for the growth of particles from nucleation and up to the original modal scheme, reduces the estimated ERF$_{aci}$ by between 0.13-0.14 Wm^{-2}. The reduction originates from higher CDNC and NCRE$_{Ghan}$ in the PI simulation, together with a smaller increase from PI to PD. By comparing model versions with different NPF parameterization in the pre-industrial and present day atmosphere respectively, we find that NPF in fact inhibits cloud droplet activation in parts of the atmosphere and leads to lower CDNC, due to reducing the growth of the larger, primary particles. The overall ERF$_{aci}$ therefore, depends on in which regions NPF is high/low both in the PI and in the PD simulations. The reduction in ERF$_{aci}$ with OsloAeroSec originates partly from higher NPF efficiency in PI areas where NPF enhances cloud droplet activation and lower NPF efficiency in PI areas where NPF inhibits cloud droplet activation. Furthermore, we find that the increase in sulphate from the PI to the PD simulation increases the hygroscopicity of the particles

and thus allows more NPF particles to activate. This expands the areas where NPF enhances cloud droplet activation in the PD simulations which also contributes to a weaker ERF_{aci} for OsloAeroSec than OsloAero_{def}.

Roughly speaking, we can say that the results in ERF_{aci} originate from OsloAeroSec is adding particles where the NPF particles are likely to act as CCN and removing them where they are unlikely to activate directly and rather act to diminish the size of the other particles.

Overall, this study shows that a more physical representation of the early growth of particles results in a lower ERF_{aci} and that adequately representing early growth on a regional scale is important when estimates of ERF_{aci}.

Code and data availability. The model code of NorESM2, release 2.0.1, is available at https://doi.org/10.5281/zenodo.3760870 (Seland et al., 2020a). The code modifications in OsloAeroSec are available at https://doi.org/10.5281/zenodo.4265057 (Blichner, 2020), see Blichner et al. (2020) for details. The post-processing code and the data from the model simulations will be made available before publication

Author contributions. SMB did the model code development and performed the simulations with NorESM. SMB did the data analysis and wrote the manuscript. SMB, MKS and TKB contributed with discussions regarding the experimental design and data analysis. All contributors have contributed to the discussions regarding the manuscript.

Competing interests. There are no competing interests.

Acknowledgements. Many thanks to Dirk Oliviè and Alf Kirkevåg at Meteorologisk institutt for answering so many questions. Special thanks to Dirk Oliviè who let us use his simulations as initialization for simulations. Thanks to Diego Aliaga for helping to design the schematic in figure 5. This work was funded under the LATICE strategic research initiative funded by the Faculty of Mathematics and Natural Sciences at the University of Oslo. This work has been financed by the Research Council of Norway (RCN) through the NOTUR/Norstore project NN2806K and NS9066K.

References

Abdul-Razzak, H. and Ghan, S. J.: A Parameterization of Aerosol Activation: 2. Multiple Aerosol Types, Journal of Geophysical Research: Atmospheres, 105, 6837–6844, https://doi.org/10.1029/1999JD901161, 2000.

Bellouin, N., Quaas, J., Gryspeerdt, E., Kinne, S., Stier, P., Watson-Parris, D., Boucher, O., Carslaw, K. S., Christensen, M., Daniau, A.-L., Dufresne, J.-L., Feingold, G., Fiedler, S., Forster, P., Gettelman, A., Haywood, J. M., Lohmann, U., Malavelle, F., Mauritsen, T., McCoy, D. T., Myhre, G., Mülmenstädt, J., Neubauer, D., Possner, A., Rugenstein, M., Sato, Y., Schulz, M., Schwartz, S. E., Sourdeval, O., Storelvmo, T., Toll, V., Winker, D., and Stevens, B.: Bounding Global Aerosol Radiative Forcing of Climate Change, Reviews of Geophysics, 58, e2019RG000 660, https://doi.org/10.1029/2019RG000660, 2020.

Bentsen, M., Bethke, I., Debernard, J. B., Iversen, T., Kirkevåg, A., Seland, Ø., Drange, H., Roelandt, C., Seierstad, I. A., Hoose, C., and Kristjánsson, J. E.: The Norwegian Earth System Model, NorESM1-M – Part 1: Description and Basic Evaluation of the Physical Climate, Geoscientific Model Development, 6, 687–720, https://doi.org/10.5194/gmd-6-687-2013, 2013.

Blichner, S. M.: Sarambl/OAS-Code-Setup: Pre-Publication Release, Zenodo, https://doi.org/10.5281/zenodo.4265057, 2020.

Blichner, S. M., Sporre, M. K., Makkonen, R., and Berntsen, T. K.: Implementing a Sectional Scheme for Early Aerosol Growth from New Particle Formation in the Norwegian Earth System Model v2: Comparison to Observations and Climate Impacts, Geoscientific Model Development Discussions, pp. 1–45, https://doi.org/10.5194/gmd-2020-357, 2020.

Bogenschutz, P. A., Gettelman, A., Morrison, H., Larson, V. E., Craig, C., and Schanen, D. P.: Higher-Order Turbulence Closure and Its Impact on Climate Simulations in the Community Atmosphere Model, Journal of Climate, 26, 9655–9676, https://doi.org/10.1175/JCLI-D-13-00075.1, 2013.

Bogenschutz, P. A., Gettelman, A., Hannay, C., Larson, V. E., Neale, R. B., Craig, C., and Chen, C.-C.: The Path to CAM6: Coupled Simulations with CAM5.4 and CAM5.5, Geoscientific Model Development, 11, 235–255, https://doi.org/10.5194/gmd-11-235-2018, 2018.

Boucher, O., Randall, D., Artaxo, P., Bretherton, C., Feingold, G., Forster, P., Kerminen, V.-M., Kondo, Y., Liao, H., Lohmann, U., Rasch, P., Satheesh, S., Sherwood, S., Stevens, B., and Zhang, X.: Clouds and Aerosols, in: Climate Change 2013: The Physical Science Basis. Contribution of Working Group I to the Fifth Assessment Report of the Intergovernmental Panel on Climate Change, edited by Stocker, T., Qin, D., Plattner, G.-K., Tignor, M., Allen, S., Boschung, J., Nauels, A., Xia, Y., Bex, V., and Midgley, P., pp. 571–658, Cambridge University Press, Cambridge, United Kingdom and New York, NY, USA, 2013.

Carslaw, K. S., Lee, L. A., Reddington, C. L., Pringle, K. J., Rap, A., Forster, P. M., Mann, G. W., Spracklen, D. V., Woodhouse, M. T., Regayre, L. A., and Pierce, J. R.: Large Contribution of Natural Aerosols to Uncertainty in Indirect Forcing, Nature, 503, 67–71, https://doi.org/10.1038/nature12674, 2013.

Danabasoglu, G., Lamarque, J.-F., Bacmeister, J., Bailey, D. A., DuVivier, A. K., Edwards, J., Emmons, L. K., Fasullo, J., Garcia, R., Gettelman, A., Hannay, C., Holland, M. M., Large, W. G., Lauritzen, P. H., Lawrence, D. M., Lenaerts, J. T. M., Lindsay, K., Lipscomb, W. H., Mills, M. J., Neale, R., Oleson, K. W., Otto-Bliesner, B., Phillips, A. S., Sacks, W., Tilmes, S., van Kampenhout, L., Vertenstein, M., Bertini, A., Dennis, J., Deser, C., Fischer, C., Fox-Kemper, B., Kay, J. E., Kinnison, D., Kushner, P. J., Larson, V. E., Long, M. C., Mickelson, S., Moore, J. K., Nienhouse, E., Polvani, L., Rasch, P. J., and Strand, W. G.: The Community Earth System Model Version 2 (CESM2), Journal of Advances in Modeling Earth Systems, 12, e2019MS001 916, https://doi.org/10.1029/2019MS001916, 2020.

Emmons, L. K., Walters, S., Hess, P. G., Lamarque, J.-F., Pfister, G. G., Fillmore, D., Granier, C., Guenther, A., Kinnison, D., Laepple, T., Orlando, J., Tie, X., Tyndall, G., Wiedinmyer, C., Baughcum, S. L., and Kloster, S.: Description and Evaluation of the Model for Ozone and

Related Chemical Tracers, Version 4 (MOZART-4), Geoscientific Model Development, 3, 43–67, https://doi.org/10.5194/gmd-3-43-2010, 2010.

Forster, P. M., Richardson, T., Maycock, A. C., Smith, C. J., Samset, B. H., Myhre, G., Andrews, T., Pincus, R., and Schulz, M.: Recommendations for Diagnosing Effective Radiative Forcing from Climate Models for CMIP6, Journal of Geophysical Research: Atmospheres, 121, 12,460–12,475, https://doi.org/10.1002/2016JD025320, 2016.

Gettelman, A. and Morrison, H.: Advanced Two-Moment Bulk Microphysics for Global Models. Part I: Off-Line Tests and Comparison with Other Schemes, Journal of Climate, 28, 1268–1287, https://doi.org/10.1175/JCLI-D-14-00102.1, 2015.

Ghan, S. J.: Technical Note: Estimating Aerosol Effects on Cloud Radiative Forcing, Atmos. Chem. Phys., 13, 9971–9974, https://doi.org/10.5194/acp-13-9971-2013, 2013.

Gordon, H., Sengupta, K., Rap, A., Duplissy, J., Frege, C., Williamson, C., Heinritzi, M., Simon, M., Yan, C., Almeida, J., Tröstl, J., Nieminen, T., Ortega, I. K., Wagner, R., Dunne, E. M., Adamov, A., Amorim, A., Bernhammer, A.-K., Bianchi, F., Breitenlechner, M., Brilke, S., Chen, X., Craven, J. S., Dias, A., Ehrhart, S., Fischer, L., Flagan, R. C., Franchin, A., Fuchs, C., Guida, R., Hakala, J., Hoyle, C. R., Jokinen, T., Junninen, H., Kangasluoma, J., Kim, J., Kirkby, J., Krapf, M., Kürten, A., Laaksonen, A., Lehtipalo, K., Makhmutov, V., Mathot, S., Molteni, U., Monks, S. A., Onnela, A., Peräkylä, O., Piel, F., Petäjä, T., Praplan, A. P., Pringle, K. J., Richards, N. A. D., Rissanen, M. P., Rondo, L., Sarnela, N., Schobesberger, S., Scott, C. E., Seinfeld, J. H., Sharma, S., Sipilä, M., Steiner, G., Stozhkov, Y., Stratmann, F., Tomé, A., Virtanen, A., Vogel, A. L., Wagner, A. C., Wagner, P. E., Weingartner, E., Wimmer, D., Winkler, P. M., Ye, P., Zhang, X., Hansel, A., Dommen, J., Donahue, N. M., Worsnop, D. R., Baltensperger, U., Kulmala, M., Curtius, J., and Carslaw, K. S.: Reduced Anthropogenic Aerosol Radiative Forcing Caused by Biogenic New Particle Formation, Proceedings of the National Academy of Sciences, 113, 12 053–12 058, https://doi.org/10.1073/pnas.1602360113, 2016.

Gordon, H., Kirkby, J., Baltensperger, U., Bianchi, F., Breitenlechner, M., Curtius, J., Dias, A., Dommen, J., Donahue, N. M., Dunne, E. M., Duplissy, J., Ehrhart, S., Flagan, R. C., Frege, C., Fuchs, C., Hansel, A., Hoyle, C. R., Kulmala, M., Kürten, A., Lehtipalo, K., Makhmutov, V., Molteni, U., Rissanen, M. P., Stozkhov, Y., Tröstl, J., Tsagkogeorgas, G., Wagner, R., Williamson, C., Wimmer, D., Winkler, P. M., Yan, C., and Carslaw, K. S.: Causes and Importance of New Particle Formation in the Present-Day and Preindustrial Atmospheres: CAUSES AND ROLE OF NEW PARTICLE FORMATION, Journal of Geophysical Research: Atmospheres, 122, 8739–8760, https://doi.org/10.1002/2017JD026844, 2017.

Hansen, J., Sato, M., Ruedy, R., Nazarenko, L., Lacis, A., Schmidt, G. A., Russell, G., Aleinov, I., Bauer, M., Bauer, S., Bell, N., Cairns, B., Canuto, V., Chandler, M., Cheng, Y., Genio, A. D., Faluvegi, G., Fleming, E., Friend, A., Hall, T., Jackman, C., Kelley, M., Kiang, N., Koch, D., Lean, J., Lerner, J., Lo, K., Menon, S., Miller, R., Minnis, P., Novakov, T., Oinas, V., Perlwitz, J., Perlwitz, J., Rind, D., Romanou, A., Shindell, D., Stone, P., Sun, S., Tausnev, N., Thresher, D., Wielicki, B., Wong, T., Yao, M., and Zhang, S.: Efficacy of Climate Forcings, Journal of Geophysical Research: Atmospheres, 110, https://doi.org/10.1029/2005JD005776, 2005.

Hoesly, R. M., Smith, S. J., Feng, L., Klimont, Z., Janssens-Maenhout, G., Pitkanen, T., Seibert, J. J., Vu, L., Andres, R. J., Bolt, R. M., Bond, T. C., Dawidowski, L., Kholod, N., Kurokawa, J.-i., Li, M., Liu, L., Lu, Z., Moura, M. C. P., O'Rourke, P. R., and Zhang, Q.: Historical (1750–2014) Anthropogenic Emissions of Reactive Gases and Aerosols from the Community Emissions Data System (CEDS), Geoscientific Model Development, 11, 369–408, https://doi.org/10.5194/gmd-11-369-2018, 2018.

Iversen, T., Bentsen, M., Bethke, I., Debernard, J. B., Kirkevåg, A., Seland, Ø., Drange, H., Kristjansson, J. E., Medhaug, I., Sand, M., and Seierstad, I. A.: The Norwegian Earth System Model, NorESM1-M – Part 2: Climate Response and Scenario Projections, Geoscientific Model Development, 6, 389–415, https://doi.org/10.5194/gmd-6-389-2013, 2013.

Jacobson, M. Z.: Development and Application of a New Air Pollution Modeling System — Part III. Aerosol-Phase Simulations, Atmospheric Environment, 31, 587–608, https://doi.org/10.1016/S1352-2310(96)00201-4, 1997.

Jacobson, M. Z.: Fundamentals of Atmospheric Modeling: Second Edition, Cambridge University Press, Cambridge, second edn., https://doi.org/10.1017/CBO9781139165389, 2005.

Karset, I. H. H.: Enhancing the Confidence in Estimates of Effective Radiative Forcing by Aerosol through Improved Global Modelling, Ph.D. thesis, University of Oslo, Oslo, 2020.

Karset, I. H. H., Berntsen, T. K., Storelvmo, T., Alterskjær, K., Grini, A., Olivié, D., Kirkevåg, A., Seland, Ø., Iversen, T., and Schulz, M.: Strong Impacts on Aerosol Indirect Effects from Historical Oxidant Changes, Atmospheric Chemistry and Physics, 18, 7669–7690, https://doi.org/10.5194/acp-18-7669-2018, 2018.

Kerminen, V.-M. and Kulmala, M.: Analytical Formulae Connecting the "Real" and the "Apparent" Nucleation Rate and the Nuclei Number Concentration for Atmospheric Nucleation Events, Journal of Aerosol Science, 33, 609–622, https://doi.org/10.1016/S0021-8502(01)00194-X, 2002.

Kerminen, V.-M., Chen, X., Vakkari, V., Petäjä, T., Kulmala, M., and Bianchi, F.: Atmospheric New Particle Formation and Growth: Review of Field Observations, Environ. Res. Lett., 13, 103 003, https://doi.org/10.1088/1748-9326/aadf3c, 2018.

Kirkevåg, A., Iversen, T., Seland, Ø., Hoose, C., Kristjánsson, J. E., Struthers, H., Ekman, A. M. L., Ghan, S., Griesfeller, J., Nilsson, E. D., and Schulz, M.: Aerosol–Climate Interactions in the Norwegian Earth System Model – NorESM1-M, Geosci. Model Dev., 6, 207–244, https://doi.org/10.5194/gmd-6-207-2013, 2013.

Kirkevåg, A., Grini, A., Olivié, D., Seland, Ø., Alterskjær, K., Hummel, M., Karset, I. H. H., Lewinschal, A., Liu, X., Makkonen, R., Bethke, I., Griesfeller, J., Schulz, M., and Iversen, T.: A Production-Tagged Aerosol Module for Earth System Models, OsloAero5.3 – Extensions and Updates for CAM5.3-Oslo, Geoscientific Model Development Discussions, pp. 1–72, https://doi.org/10.5194/gmd-2018-46, 2018.

Kooperman, G. J., Pritchard, M. S., Ghan, S. J., Wang, M., Somerville, R. C. J., and Russell, L. M.: Constraining the Influence of Natural Variability to Improve Estimates of Global Aerosol Indirect Effects in a Nudged Version of the Community Atmosphere Model 5, Journal of Geophysical Research: Atmospheres, 117, https://doi.org/10.1029/2012JD018588, 2012.

Lawrence, D. M., Fisher, R. A., Koven, C. D., Oleson, K. W., Swenson, S. C., Bonan, G., Collier, N., Ghimire, B., van Kampenhout, L., Kennedy, D., Kluzek, E., Lawrence, P. J., Li, F., Li, H., Lombardozzi, D., Riley, W. J., Sacks, W. J., Shi, M., Vertenstein, M., Wieder, W. R., Xu, C., Ali, A. A., Badger, A. M., Bisht, G., van den Broeke, M., Brunke, M. A., Burns, S. P., Buzan, J., Clark, M., Craig, A., Dahlin, K., Drewniak, B., Fisher, J. B., Flanner, M., Fox, A. M., Gentine, P., Hoffman, F., Keppel-Aleks, G., Knox, R., Kumar, S., Lenaerts, J., Leung, L. R., Lipscomb, W. H., Lu, Y., Pandey, A., Pelletier, J. D., Perket, J., Randerson, J. T., Ricciuto, D. M., Sanderson, B. M., Slater, A., Subin, Z. M., Tang, J., Thomas, R. Q., Martin, M. V., and Zeng, X.: The Community Land Model Version 5: Description of New Features, Benchmarking, and Impact of Forcing Uncertainty, Journal of Advances in Modeling Earth Systems, 11, 4245–4287, https://doi.org/10.1029/2018MS001583, 2019.

Lee, S.-H., Gordon, H., Yu, H., Lehtipalo, K., Haley, R., Li, Y., and Zhang, R.: New Particle Formation in the Atmosphere: From Molecular Clusters to Global Climate, Journal of Geophysical Research: Atmospheres, 124, 7098–7146, https://doi.org/10.1029/2018JD029356, 2019.

Lee, Y. H., Pierce, J. R., and Adams, P. J.: Representation of Nucleation Mode Microphysics in a Global Aerosol Model with Sectional Microphysics, Geoscientific Model Development, 6, 1221–1232, https://doi.org/10.5194/gmd-6-1221-2013, 2013.

Lehtinen, K. E. J., Dal Maso, M., Kulmala, M., and Kerminen, V.-M.: Estimating Nucleation Rates from Apparent Particle Formation Rates and Vice Versa: Revised Formulation of the Kerminen–Kulmala Equation, Journal of Aerosol Science, 38, 988–994, https://doi.org/10.1016/j.jaerosci.2007.06.009, 2007.

Myhre, G., Shindell, D., Bréon, F.-M., Collins, W., Fuglestvedt, J., Huang, J., Koch, D., Lamarque, J.-F., Lee, D., Mendoza, B., Nakajima, T., Robock, A., Stephens, G., Takemura, T., and Zhang, H.: Anthropogenic and Natural Radiative Forcing, in: Climate Change 2013: The Physical Science Basis. Contribution of Working Group I to the Fifth Assessment Report of the Intergovernmental Panel on Climate Change, edited by Stocker, T., Qin, D., Plattner, G.-K., Tignor, M., Allen, S., Boschung, J., Nauels, A., Xia, Y., Bex, V., and Midgley, P., pp. 659–740, Cambridge University Press, Cambridge, United Kingdom and New York, NY, USA, 2013.

Neale, R. B., Gettelman, A., Park, S., Chen, C.-c., Lauritzen, P. H., Williamson, D. L., Conley, A. J., Kinnison, D., Marsh, D., Smith, A. K., Vitt, F., Garcia, R., Lamarque, J.-f., Mills, M., Tilmes, S., Morrison, H., Cameron-smith, P., Collins, W. D., Iacono, M. J., Easter, R. C., Liu, X., Ghan, S. J., Rasch, P. J., and a Taylor, M.: Description of the NCAR Community Atmosphere Model (CAM 5.0). NCAR Technical Notes., Ncar/Tn-464+Str, p. 214, https://doi.org/10.5065/D6N877R0., 2012.

Olenius, T. and Riipinen, I.: Molecular-Resolution Simulations of New Particle Formation: Evaluation of Common Assumptions Made in Describing Nucleation in Aerosol Dynamics Models, Aerosol Science and Technology, 51, 397–408, https://doi.org/10.1080/02786826.2016.1262530, 2017.

Paasonen, P., Nieminen, T., Asmi, E., Manninen, H. E., Petäjä, T., Plass-Dülmer, C., Flentje, H., Birmili, W., Wiedensohler, A., Hõrrak, U., Metzger, A., Hamed, A., Laaksonen, A., Facchini, M. C., Kerminen, V.-M., and Kulmala, M.: On the Roles of Sulphuric Acid and Low-Volatility Organic Vapours in the Initial Steps of Atmospheric New Particle Formation, Atmos. Chem. Phys., 10, 11 223–11 242, https://doi.org/10.5194/acp-10-11223-2010, 2010.

Seland, Ø., Bentsen, M., Olivié, D., Toniazzo, T., Gjermundsen, A., Graff, L. S., Debernard, J. B., Gupta, A. K., He, Y., Kirkevåg, A., Schwinger, J., Tjiputra, J., Aas, K. S., Bethke, I., Fan, Y., Gao, S., Griesfeller, J., Grini, A., Guo, C., Ilicak, M., Karset, I. H. H., Landgren, O., Liakka, J., Moree, A., Moseid, K. O., Nummelin, A., Spensberger, C., Tang, H., Zhang, Z., Heinze, C., Iversen, T., and Schulz, M.: NorESM2 Source Code as Used for CMIP6 Simulations, Zenodo, https://doi.org/10.5281/zenodo.3760870, 2020a.

Seland, Ø., Bentsen, M., Seland Graff, L., Olivié, D., Toniazzo, T., Gjermundsen, A., Debernard, J. B., Gupta, A. K., He, Y., Kirkevåg, A., Schwinger, J., Tjiputra, J., Schancke Aas, K., Bethke, I., Fan, Y., Griesfeller, J., Grini, A., Guo, C., Ilicak, M., Hafsahl Karset, I. H., Landgren, O., Liakka, J., Onsum Moseid, K., Nummelin, A., Spensberger, C., Tang, H., Zhang, Z., Heinze, C., Iverson, T., and Schulz, M.: The Norwegian Earth System Model, NorESM2 – Evaluation of theCMIP6 DECK and Historical Simulations, Geoscientific Model Development Discussions, pp. 1–68, https://doi.org/10.5194/gmd-2019-378, 2020b.

Semeniuk, K. and Dastoor, A.: Current State of Aerosol Nucleation Parameterizations for Air-Quality and Climate Modeling, Atmospheric Environment, 179, 77–106, https://doi.org/10.1016/j.atmosenv.2018.01.039, 2018.

Smith, C. J., Kramer, R. J., Myhre, G., Alterskjær, K., Collins, W., Sima, A., Boucher, O., Dufresne, J.-L., Nabat, P., Michou, M., Yukimoto, S., Cole, J., Paynter, D., Shiogama, H., O'Connor, F. M., Robertson, E., Wiltshire, A., Andrews, T., Hannay, C., Miller, R., Nazarenko, L., Kirkevåg, A., Olivié, D., Fiedler, S., Lewinschal, A., Mackallah, C., Dix, M., Pincus, R., and Forster, P. M.: Effective Radiative Forcing and Adjustments in CMIP6 Models, Atmospheric Chemistry and Physics, 20, 9591–9618, https://doi.org/10.5194/acp-20-9591-2020, 2020.

Sullivan, R. C., Crippa, P., Matsui, H., Leung, L. R., Zhao, C., Thota, A., and Pryor, S. C.: New Particle Formation Leads to Cloud Dimming, npj Climate and Atmospheric Science, 1, 1–9, https://doi.org/10.1038/s41612-018-0019-7, 2018.

Twomey, S.: The Nuclei of Natural Cloud Formation Part II: The Supersaturation in Natural Clouds and the Variation of Cloud Droplet Concentration, Geofisica pura e applicata, 43, 243–249, https://doi.org/10.1007/BF01993560, 1959.

Twomey, S.: Aerosols, Clouds and Radiation, Atmospheric Environment. Part A. General Topics, 25, 2435–2442, https://doi.org/10.1016/0960-1686(91)90159-5, 1991.

van Marle, M. J. E., Kloster, S., Magi, B. I., Marlon, J. R., Daniau, A.-L., Field, R. D., Arneth, A., Forrest, M., Hantson, S., Kehrwald, N. M., Knorr, W., Lasslop, G., Li, F., Mangeon, S., Yue, C., Kaiser, J. W., and van der Werf, G. R.: Historic Global Biomass Burning Emissions for CMIP6 (BB4CMIP) Based on Merging Satellite Observations with Proxies and Fire Models (1750–2015), Geoscientific Model Development, 10, 3329–3357, https://doi.org/10.5194/gmd-10-3329-2017, 2017.

Vehkamäki, H., Kulmala, M., Napari, I., Lehtinen, K. E. J., Timmreck, C., Noppel, M., and Laaksonen, A.: An Improved Parameterization for Sulfuric Acid–Water Nucleation Rates for Tropospheric and Stratospheric Conditions, Journal of Geophysical Research: Atmospheres, 107, 4622, https://doi.org/10.1029/2002JD002184, 2002.

Zhang, G. J. and McFarlane, N. A.: Sensitivity of Climate Simulations to the Parameterization of Cumulus Convection in the Canadian Climate Centre General Circulation Model, Atmosphere-Ocean, 33, 407–446, https://doi.org/10.1080/07055900.1995.9649539, 1995.

Zhang, K., Wan, H., Liu, X., Ghan, S. J., Kooperman, G. J., Ma, P.-L., Rasch, P. J., Neubauer, D., and Lohmann, U.: Technical Note: On the Use of Nudging for Aerosol–Climate Model Intercomparison Studies, Atmospheric Chemistry and Physics, 14, 8631–8645, https://doi.org/10.5194/acp-14-8631-2014, 2014.

Supplementary for: Reduced effective radiative forcing from cloud-aerosol interactions (ERF_{aci}) with improved treatment of early aerosol growth in an Earth System Model

Sara M. Blichner[1], **Moa K. Sporre**[2], **and Terje K. Berntsen**[1]

[1]Department of Geosciences, University of Oslo, Oslo, Norway
[2]Department of Physics, Lund University, Lund, Sweden

Correspondence: Sara Marie Blichner (s.m.blichner@geo.uio.no)

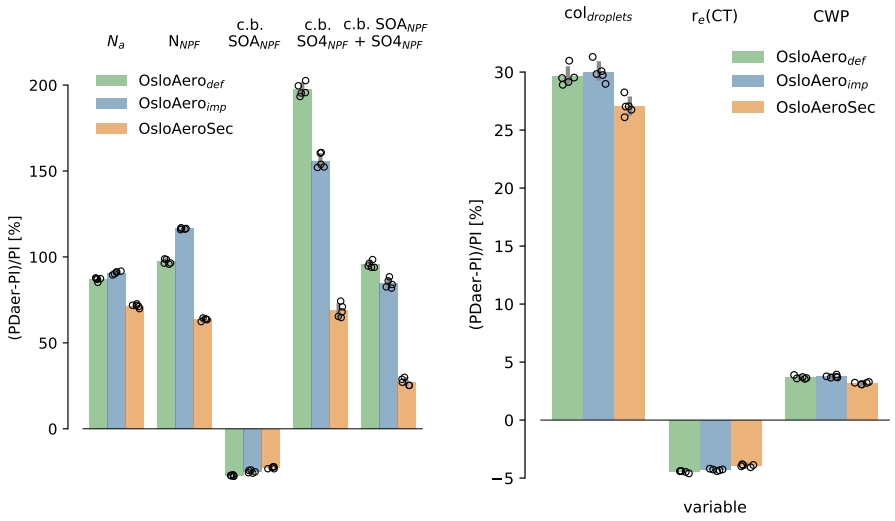

Figure S1. Globally averaged change in aerosol and cloud properties. N_{NPF} and N_a values are averaged up to 850 hPa and weighted by pressure difference of the grid cell.

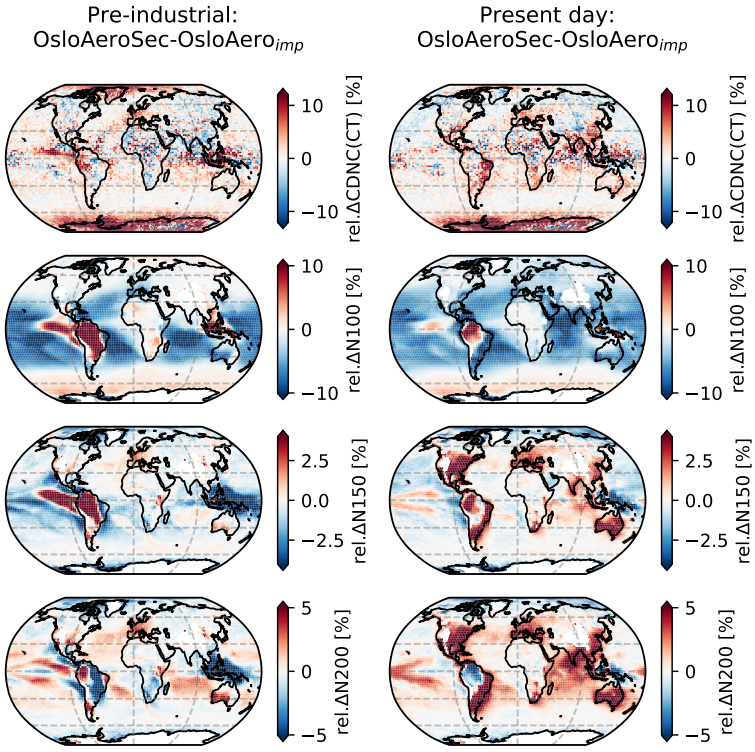

Figure S2. Top row: Difference in average cloud droplet number concentrations (CDNC) at cloud top between OsloAeroSec and OsloAero$_{def}$. Row 2–3: difference in average particle number concentration for particles larger than 100 nm (row 2), 150 nm (row 3) and 200 nm (row 4). The left column shows the difference for the pre-industrial atmosphere and the right column shows the difference for the present day atmosphere. The average particle concentrations are calculated averaging up to 850 hPa and averaging by pressure difference.

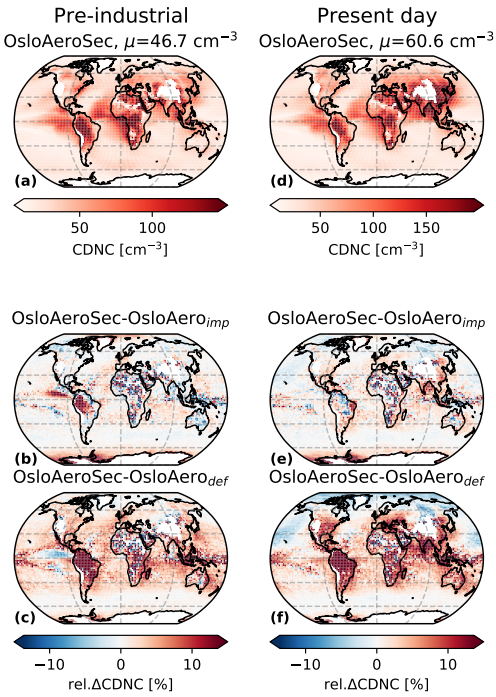

Figure S3. Top row: Near surface CDNC in OsloAeroSec for PI and PD atmosphere. Row 2 and 3 show the difference between OsloAeroSec and OsloAero$_{imp}$ and OsloAero$_{def}$ respectively. The average is calculated for grid boxes up to 850 hPa and averaging by pressure difference.

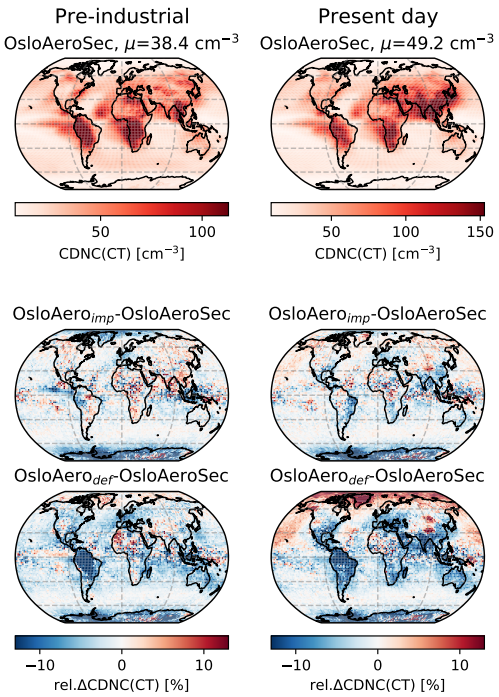

Figure S4. Top row: Cloud top CDNC in OsloAeroSec for PI and PD atmosphere. Row 2 and 3 show the difference between OsloAeroSec and OsloAero$_{imp}$ and OsloAero$_{def}$ respectively.

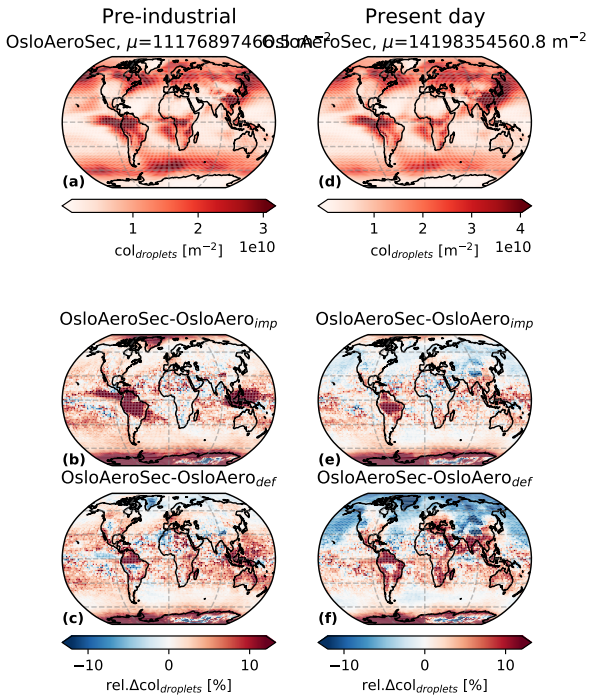

Figure S5. Top row: Column integrated droplet number in OsloAeroSec for PI and PD atmosphere. Row 2 and 3 show the difference between OsloAeroSec and OsloAero$_{imp}$ and OsloAero$_{def}$ respectively.

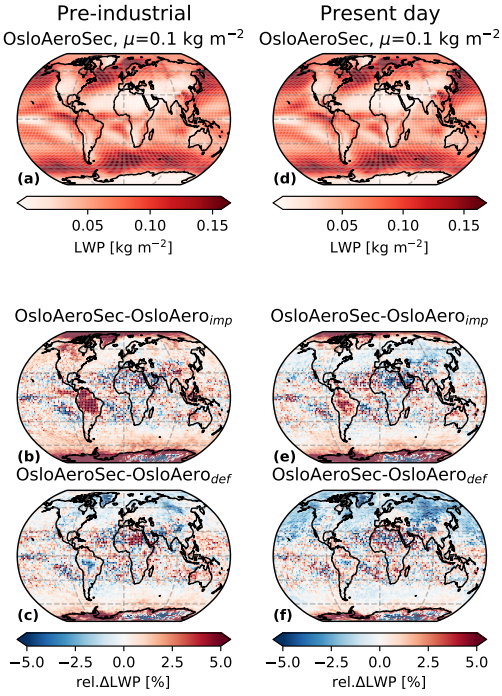

Figure S6. Top row: Liquid water path (LWP) OsloAeroSec for PI and PD atmosphere. Row 2 and 3 show the difference between OsloAeroSec and OsloAero$_{imp}$ and OsloAero$_{def}$ respectively.

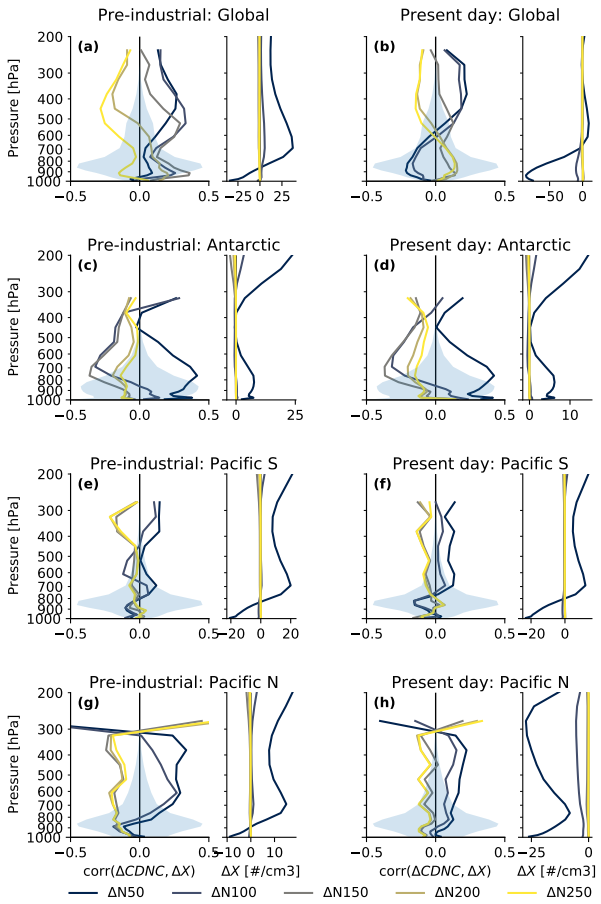

Figure S7. Left panel of each subplot: Correlations by pressure level between the change between OsloAero$_{def}$ and OsloAeroSec in cloud droplet number concentration (ΔCDNC) and the change in number of particles above 50, 100, 150,200 and 250 nm for different regions. The blue shaded signifies the relative fractional occurrence of liquid cloud and is included to give an idea of where the aerosols may actually have a noticeable impact on clouds. The right panel of each subplot shows the change in the aerosol concentration for the relevant region.

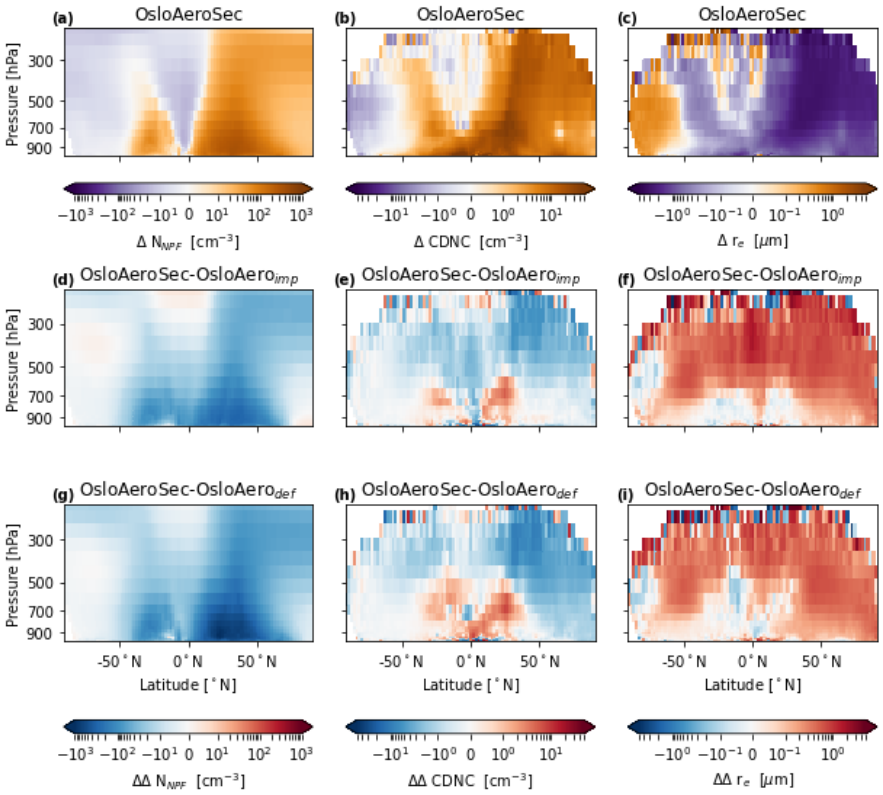

Figure S8. Zonally averaged values for N_{NPF}, cloud droplet number concentration (CDNC) and effective droplet radius (r_e). The top panel shows the PD - PI for OsloAeroSec while the second and third row shows the of this value to the value with OsloAero$_{imp}$ (second row) and OsloAero$_{def}$ (third row).

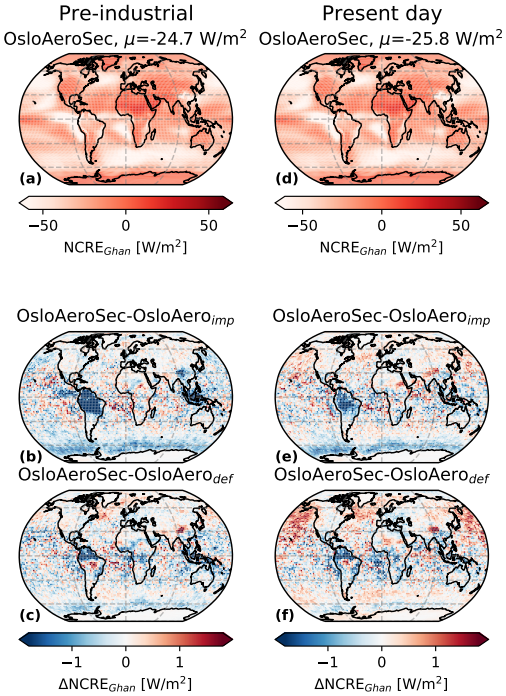

Figure S9. Top row: NCRE$_{Ghan}$ in OsloAeroSec for PI and PD atmosphere. Row 2 and 3 show the difference between OsloAeroSec and OsloAero$_{imp}$ and OsloAero$_{def}$ respectively.

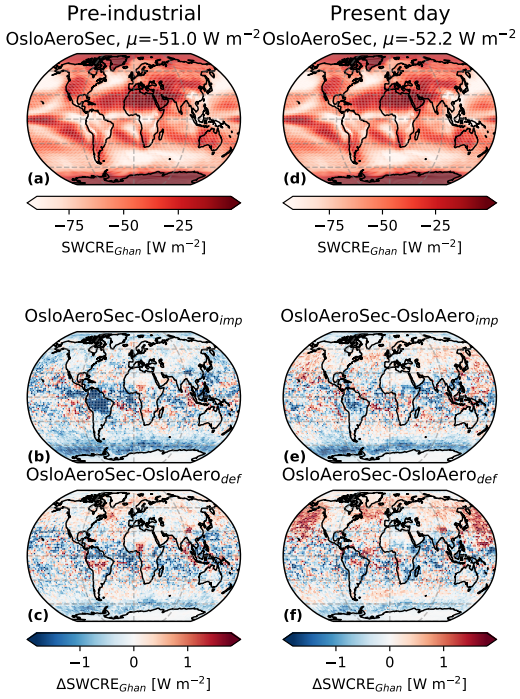

Figure S10. Top row: Short wave CRE in OsloAeroSec for PI and PD atmosphere. Row 2 and 3 show the difference between OsloAeroSec and OsloAero$_{imp}$ and OsloAero$_{def}$ respectively.

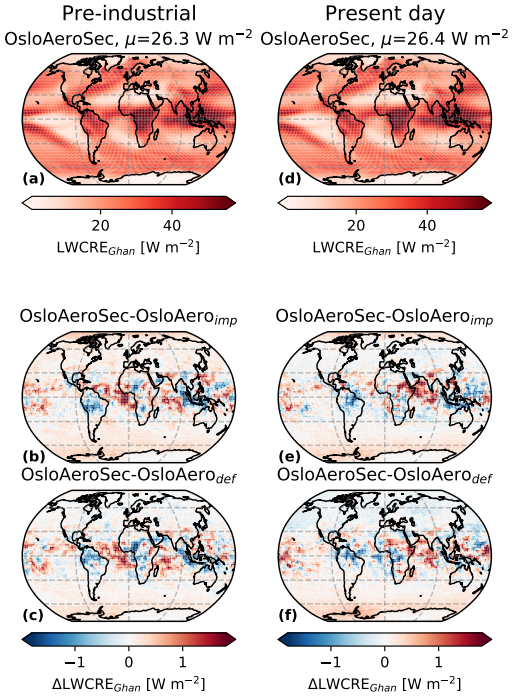

Figure S11. Top row: Long wave CRE in OsloAeroSec for PI and PD atmosphere. Row 2 and 3 show the difference between OsloAeroSec and OsloAero$_{imp}$ and OsloAero$_{def}$ respectively.

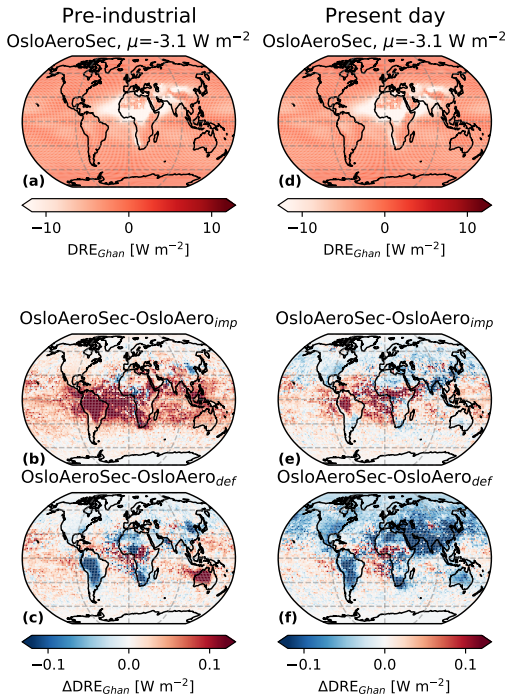

Figure S12. Top row: The direct radiative effect in OsloAeroSec for PI and PD atmosphere. Row 2 and 3 show the difference between OsloAeroSec and OsloAero$_{imp}$ and OsloAero$_{def}$ respectively.

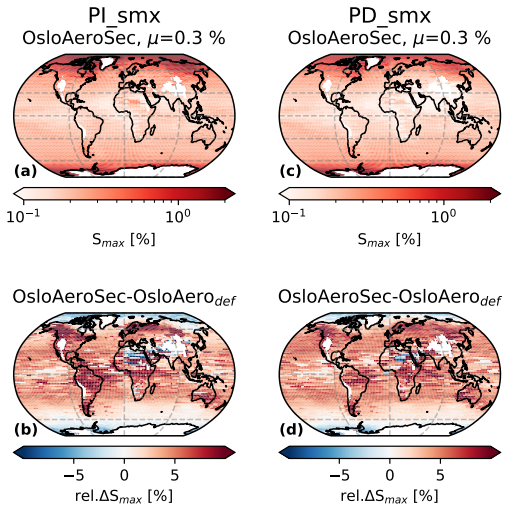

Figure S13. Top row:Average values of maximum supersaturation (S$_{max}$) for OsloAeroSec for PI (left) and PD (right). Row 2–3: the relative difference between OsloAeroSec and OsloAero$_{imp}$ (row 2) and OsloAero$_{def}$ (row 3) for PI (left) and PD(right). All values are averaged up to 850 hPa and weighted by pressure difference of the grid cell. Furthermore, only values where S$_{max}$ is larger than zero are counted towards the average.

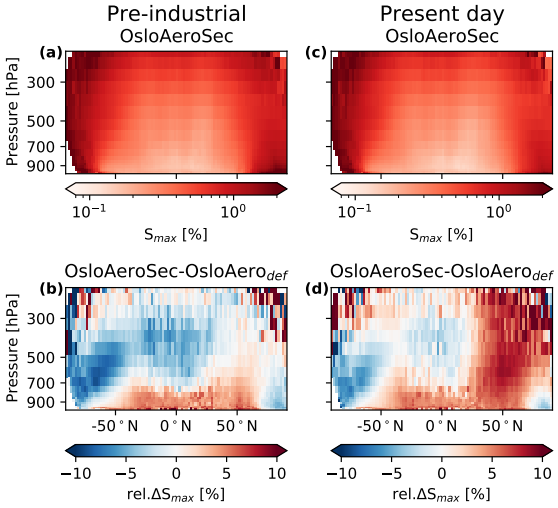

Figure S14. Top row:Average values of maximum supersaturation (S_{max} for OsloAeroSec for PI (left) and PD (right). Bottom row: the relative difference between OsloAeroSec and OsloAero$_{def}$ for PI (left) and PD(right). Only values where S_{max} is larger than zero are counted towards the average.

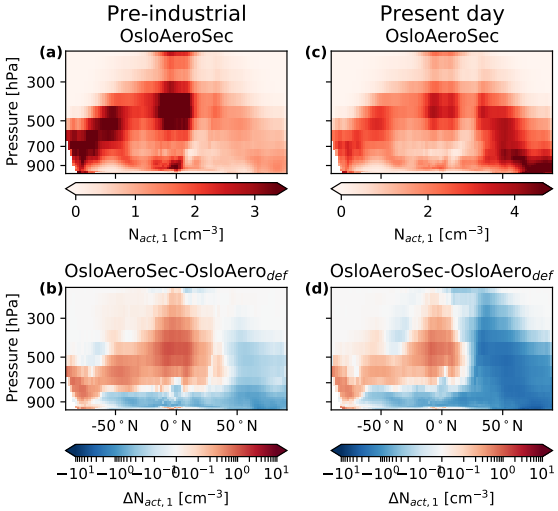

Figure S15. Top row: Average values of the averaged activation of particles from the NPF mode (mix number 1) for OsloAeroSec for PI (left) and PD (right). Bottom row: the relative difference between OsloAeroSec and OsloAero$_{def}$ for PI (left) and PD(right). The values are an approximation in the sense that they are calculated by multiplying the separately calculated monthly mean output of the number concentration in the mode and the activation fraction from that mode (see Fig. S17).

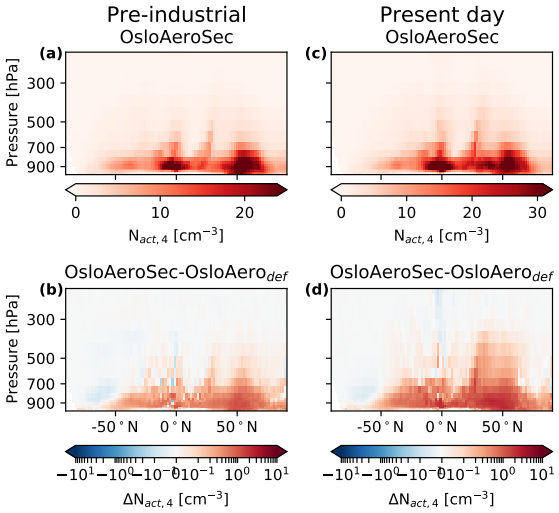

Figure S16. Top row: Average values of the averaged activation of particles from mode number 4 (mix number 4) for OsloAeroSec for PI (left) and PD (right). Bottom row: the relative difference between OsloAeroSec and OsloAero$_{def}$ for PI (left) and PD(right). The values are an approximation in the sense that they are calculated by multiplying the separately calculated monthly mean output of the number concentration in the mode and the activation fraction from that mode (see Fig. S18).

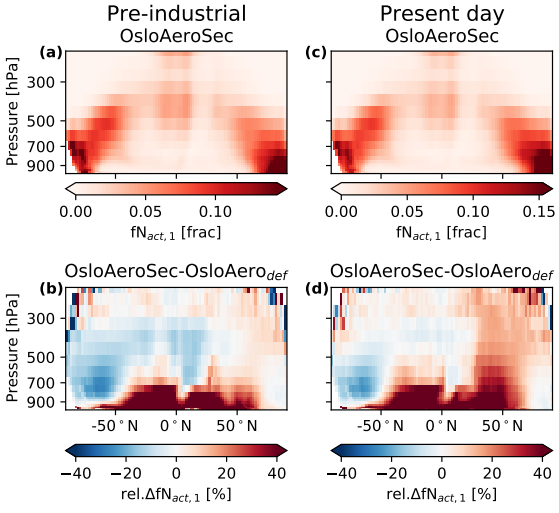

Figure S17. Top row: Average values of the activated fraction of particles from the NPF mode (mix number 1) for OsloAeroSec for PI (left) and PD (right). Bottom row: the relative difference between OsloAeroSec and OsloAero$_{def}$ for PI (left) and PD(right). The values are an approximation in the sense that they are calculated by multiplying the separately calculated monthly mean output of the number concentration in the mode and the activation fraction from that mode.

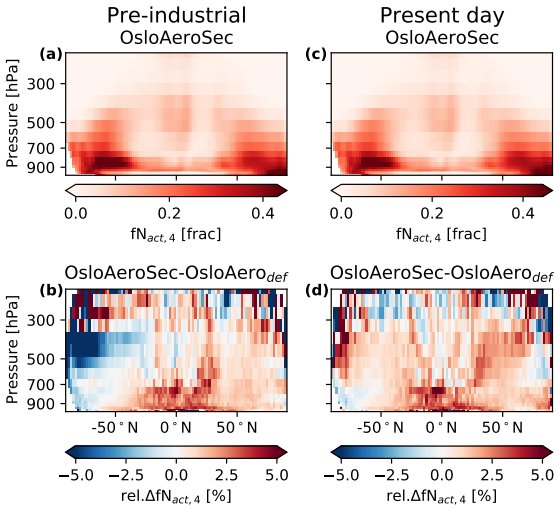

Figure S18. Top row: Average values of the activated fraction of particles from mode number 4 (mix number 4) for OsloAeroSec for PI (left) and PD (right). Bottom row: the relative difference between OsloAeroSec and OsloAero$_{def}$ for PI (left) and PD(right).

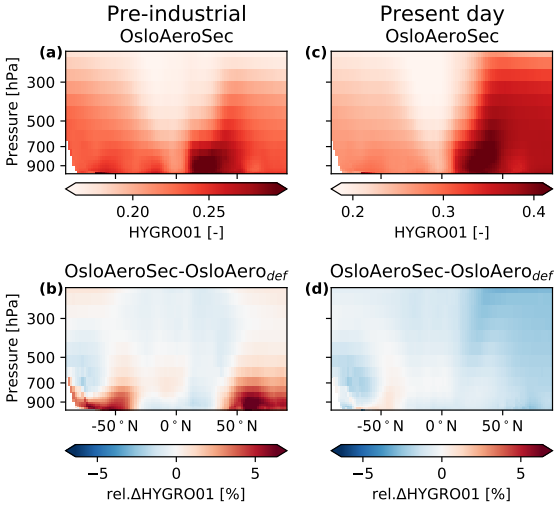

Figure S19. Top row: Average values of the hygroscopicity particles from mode number 1 (mix number 1) for OsloAeroSec for PI (left) and PD (right). Bottom row: the relative difference between OsloAeroSec and OsloAero$_{def}$ for PI (left) and PD(right).

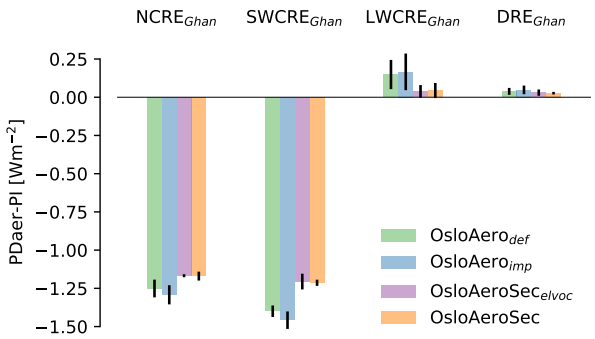

Figure S20. Globally averaged ERF for 1 year (plus one spin-up year) of simulations. The OsloAeroSec$_{elvoc}$ case is a sensitivity simulation were only 50% of ELVOC is allowed to condense onto the particles in the sectional scheme. The simulation was run to test the influence of this factor on the overall results in the paper.

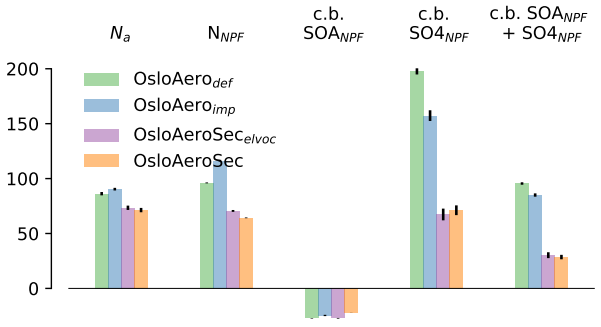

Figure S21. Globally averaged aerosol properties for 1 year (plus one spin-up year) of simulations. The OsloAeroSec$_{elvoc}$ case is a sensitivity simulation were only 50% of ELVOC is allowed to condense onto the particles in the sectional scheme. The simulation was run to test the influence of this factor on the overall results in the paper.

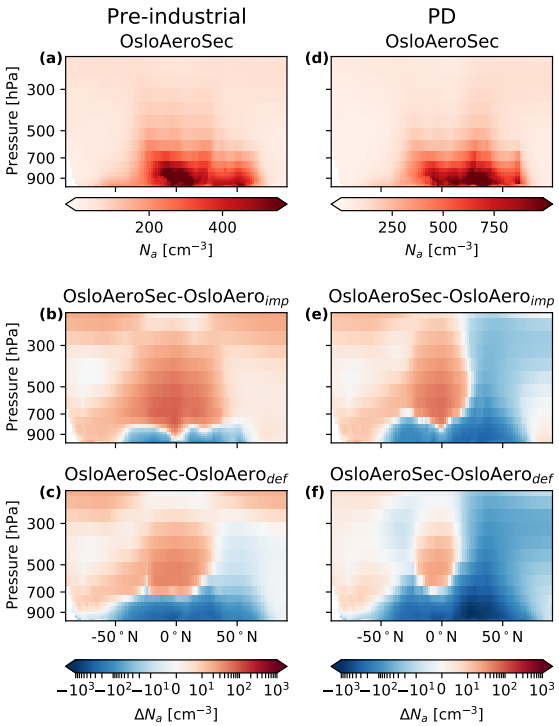

Figure S22. Zonally averaged values for N$_a$. The top panel shows the absolute values in the Pre-industrial (left) and Present day (right) atmosphere) PD - PI for OsloAeroSec while the second and third row shows the of this value to the value with OsloAero$_{imp}$ (second row) and OsloAero$_{def}$ (third row).

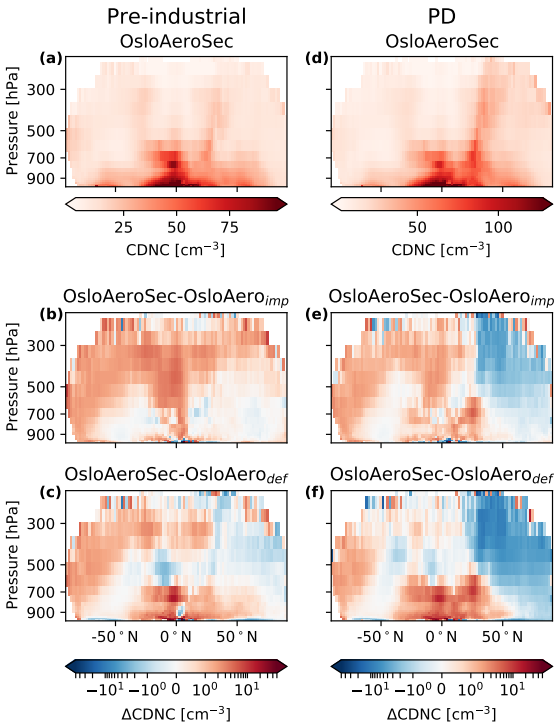

Figure S23. Zonally averaged values for cloud droplet number concentrations. The top panel shows the absolute values in the Pre-industrial (left) and Present day (right) atmosphere) PD - PI for OsloAeroSec while the second and third row shows the of this value to the value with OsloAero$_{imp}$ (second row) and OsloAero$_{def}$ (third row).